THE UNIVERSITY
of EDINBURGH

Performance Analysis of Spectrum Sensing Techniques for Future Wireless Networks

Yibo He

A thesis submitted for the degree of Doctor of Philosophy.
The University of Edinburgh.
October 2017

Abstract

In this thesis, spectrum sensing techniques are investigated for cognitive radio (CR) networks in order to improve the sensing and transmission performance of secondary networks. Specifically, the detailed exploration comprises of three areas, including single-node spectrum sensing based on eigenvalue-based detection, cooperative spectrum sensing under random secondary networks and full-duplex (FD) spectrum sensing and sharing techniques.

In the first technical chapter of this thesis, eigenvalue-based spectrum sensing techniques, including maximum eigenvalue detection (MED), maximum minimum eigenvalue (MME) detection, energy with minimum eigenvalue (EME) detection and the generalized likelihood ratio test (GLRT) eigenvalue detector, are investigated in terms of total error rates and achievable throughput. Firstly, in order to consider the benefits of primary users (PUs) and secondary users (SUs) simultaneously, the optimal decision thresholds are investigated to minimize the total error rate, i.e. the summation of missed detection and false alarm rate. Secondly, the sensing-throughput trade-off is studied based on the GLRT detector and the optimal sensing time is obtained for maximizing the achievable throughput of secondary communications when the target probability of detection is achieved.

In the second technical chapter, the centralized GLRT-based cooperative sensing technique is evaluated by utilizing a homogeneous Poisson point process (PPP). Firstly, since collaborating all the available SUs does not always achieve the best sensing performance under a random secondary network, the optimal number of cooperating SUs is investigated to minimize the total error rate of the final decision. Secondly, the achievable ergodic capacity and throughput of SUs are studied and the technique of determining an appropriate number of cooperating SUs is proposed to optimize the secondary transmission performance based on a target total error rate requirement.

In the last technical chapter, FD spectrum sensing (FDSS) and sensing-based spectrum sharing (FD-SBSS) are investigated. There exists a threshold pair, not a single threshold, due to the self-interference caused by the simultaneous sensing and transmission. Firstly, by utilizing the derived expressions of false alarm and detection rates, the optimal decision threshold pair is obtained to minimize total error rate for the FDSS scheme. Secondly, in order to further improve the secondary transmission performance, the FD-SBSS scheme is proposed and the collision and spectrum waste probabilities are studied. Furthermore, different antenna partitioning methods are proposed to maximize the achievable throughput of SUs under both FDSS and FD-SBSS schemes.

Declaration of originality

I hereby declare that the research recorded in this thesis and the thesis itself was composed and originated entirely by myself in the Institute for Digital Communications at The University of Edinburgh.

Yibo He

Acknowledgements

I would like to thank my supervisor, Prof. John Thompson and Prof. T. Ratnarajah, who provided me the opportunity to conduct this interesting research and complete my PhD study. Meanwhile, I would like to appreciate all the constructive discussions with my colleagues. Dr. Jiang Xue, who is research fellow in my group, deserves my big thanks. Dr. Xue always inspires me on research works and produces fruitful discussions on technical issues. Besides, I would also present my most sincere respect and thanks to my parents and my girlfriend Miss. Zhao, who support me all the time.

Contents

List of figures

List of tables

Acronyms and abbreviations

AND	Logic-AND
ARQ	Automatic Repeat Request
AWGN	Additive White Gaussian Noise
BEP	Bit Error Probability
CDF	Cumulative Distribution Function
CDR	Constant False Alarm Rate
CDT	Constant Decision Threshold
CFAR	Constant Detection Rate
CLT	Central Limit Theorem
CR	Cognitive Radio
CSA	Concurrent Spectrum Access
ED	Energy Detector
EGC	Equal-Gain Combination
EME	Energy with Minimum Eigenvalue
FC	Fusion Center
FCC	Federal Communications Commission
FD	Full-duplex
FDSS	Full-duplex Spectrum Sensing
FD-SBSS	Full-duplex Sensing-Based Spectrum Sharing
FECC	Forward Error Correction Coding
GLRT	Generalized Likelihood Ratio Test
HD	Half-duplex
i.i.d.	Independently and Identically Distributed
INR	Self-interference-to-Noise Ratio
MED	Maximum Eigenvalue Detection
MIMO	Multi-Input-Multi-Output
MME	Maximum Minimum Eigenvalue Detection

MRT	Maximal Ratio Transmission
MRC	Maximal Ratio Combining
MTM-SVD	Multitaper-Method Singular-Value-Decomposition
OR	Logic-OR
PDF	Probability Density Function
PPP	Poisson Point Process
PU	Primary User
ROC	Receiver Operating Characteristic
RRH	Remote Radio Head
RSI	Residual Self-Interference
SINR	Signal-to-Interference-plus-Noise Ratio
SIS	Self-Interference Suppression
SNR	Signal-to-Noise Ratio
SU-Tx	Secondary Transmitter
SU-Rx	Secondary Receiver
SU	Secondary User
UE	User Equipments
UHF	Ultra High Frequency
WRAN	Wireless Regional Area Network

Nomenclature

${}_1F_1\left(.;.;.\right)$	matrix-variate confluent hypergeometric function
${}_2F_1(.,.;.;.)$	Gaussian hypergeometric function
γ	Average received SNR of the PU's signals at the SU in HD sensing system
γ_i	Average received SNR measured at the ith SU
γ^{s0}	Received SNR measured at SU-Rx for secondary communications with absent PU
γ^{s1}	Received SINR measured at SU-Rx for secondary communications with present PU
ε	Path loss exponent factor
χ	SIS factor
μ_i^{fc}	Decision on the status of PU made by the ith SU seen at the FC
μ_i^{su}	Decision on the status of PU made by the ith SU seen at the SU
$\Gamma(\cdot)$	Gamma function
$\gamma(\cdot,\cdot)$	Lower incomplete Gamma function
$\Gamma(\cdot,\cdot)$	Upper incomplete Gamma function
μ	Noise uncertainty factor
ν	Space dimension
τ	Sensing time duration
$\tau_{\min}$	Minimum sensing time which can make total error rate achieve desired value
$\phi(A)$	Point measure on space A
$\Phi(\cdot)$	Error function
$\Lambda(A)$	Intensity measure on space A
$\delta_x(A)$	Dirac measure on a set X and any set $A \in X$
$\Theta(\cdot)$	Lebesgue measure operator
ρ	Density in a homogeneous PPP
θ	Angle variable
ω_i	Rayleigh fading gain between PU and the ith SU-Tx
α	Rayleigh fading channel gain in each secondary communication link
β	Rayleigh fading channel gain between PU and SU-Rx

$\lambda_{\rm on}$	Expectation of $t_{\rm on}$
$\lambda_{\rm off}$	Expectation of $t_{\rm off}$
λ_i	The i-th actual eigenvalue of covariance matrix of received signals
$\hat{\lambda}_i$	The i-th eigenvalue of sample covariance matrix of received signals
$\lambda_{\rm max}$	Actual maximum eigenvalue of covariance matrix of received signals
$\hat{\lambda}_{\rm max}$	Maximum eigenvalue of sample covariance matrix of received signals
$\lambda_{\rm min}$	Actual minimum eigenvalue of covariance matrix of received signals
$\hat{\lambda}_{\rm min}$	Minimum eigenvalue of sample covariance matrix of received signals
σ_v^2	Noise power
σ^2	Noise power at SU-Rx
B	Upper bound (in dB) of the noise uncertainty
$\mathcal{CN}(\cdot,\cdot)$	Complex normal distribution
$\mathcal{CW}(\cdot,\cdot)$	Complex Wishart distribution
$C_{\rm ac}$	Achievable capacity of each secondary link in cooperative sensing system
$C_{\rm ac0}$	Achievable capacity with the absence of PU
$C_{\rm ac1}$	Achievable capacity with the presence of PU
$\overline{C_{\rm ac}}$	Achievable ergodic capacity of each secondary link
$\overline{C_{\rm ac0}}$	Achievable ergodic capacity with the absence of PU
$\overline{C_{\rm ac1}}$	Achievable ergodic capacity with the presence of PU
$\overline{C_{\rm c}}$	Achievable ergodic capacity of secondary network
$C_{\rm at}$	Achievable throughput of each secondary link considering coverage probability
$C_{\rm cov0}$	Achievable throughput with coverage probability and the absence of PU
$C_{\rm cov1}$	Achievable throughput with coverage probability and the presence of PU
$C_{\rm th}$	Achievable throughput of secondary network considering coverage probability
$\det(\cdot)$	Determinant operator
d	Distance variable
d_i	Distance between PU and the ith nearest SU
D	Distance between PU and origin of the coverage area of FC
$\mathbb{E}$	Expectation operator
$f_0(t)$	PDF of $T_{\rm SS}$ under the hypotheses $\mathcal{H}_0$
$f_1(t)$	PDF of $T_{\rm SS}$ under the hypotheses $\mathcal{H}_1$

f_{MME0}	Exact PDF of test statistic T_{MME} under $\mathcal{H}_0$
f_{MME1}	Exact PDF of test statistic T_{MME} under $\mathcal{H}_1$
f_{EME0}	Exact PDF of test statistic T_{EME} under $\mathcal{H}_0$
f_{EME1}	Exact PDF of test statistic T_{EME} under $\mathcal{H}_1$
f_{GLRT0}	Exact PDF of test statistic T_{GLRT} under $\mathcal{H}_0$
f_{GLRT1}	Exact PDF of test statistic T_{GLRT} under $\mathcal{H}_1$
f^0_{GLRT}	Asymptotic PDF of test statistic T_{GLRT} under $\mathcal{H}_0$
f^1_{GLRT}	Asymptotic PDF of test statistic T_{GLRT} under $\mathcal{H}_1$
f_{s}	Sampling frequency
F^0_{GLRT}	Asymptotic CDF of test statistic T_{GLRT} under $\mathcal{H}_0$
F^1_{GLRT}	Asymptotic CDF of test statistic T_{GLRT} under $\mathcal{H}_1$
h	Channel gain
$\mathbf{h}$	Channel gain vector between PU and SU
$\mathcal{H}_0$	Hypothesis that PU is absent
$\mathcal{H}_1$	Hypothesis that PU is present
$\mathbf{I}_m$	Identity matrix with size $m \times m$
$I^{-1}(.,.,.)$	Inverse regularised incomplete Beta function
k	Number of cooperating SUs
k_{opt}	Optimal number of cooperating SUs
L	Distance between each SU-Tx and SU-Rx
m	Number of receive antennas in HD spectrum sensing
M_{s}	Number of sensing antennas in FD spectrum sensing
M_{t}	Number of transmission antennas in FD spectrum sensing
n	Number of receive samples in HD time-slotted spectrum sensing
$n_{\min}$	Minimum sample size that enables $P_{\mathrm{te}}(n, r_{\mathrm{opt}}) \leq \xi$
N	Sample number of received signals in FD spectrum sensing
$\mathcal{N}(a, b)$	Normal distribution with expectation a and variance b
P_{b}	Bit error probability
P_{d}	Probability of detection
$P^{\mathrm{su}}_{\mathrm{d},i}$	Probability of detection seen at the i SU
$P_{\mathrm{d},i}$	Probability of detection of the i SU seen at FC

P_{d}^{*}	Target probability of detection
$P_{\mathrm{d},i}^{*}$	Target probability of detection of the ith SU
$\bar{P}_{\mathrm{d}}$	Expected probability of detection
P_{fa}	Probability of false alarm
$P_{\mathrm{fa},i}^{\mathrm{su}}$	Probability of false alarm seen at the i SU
$P_{\mathrm{fa},i}$	Probability of false alarm of the i SU seen at FC
P_{fa}^{*}	Target probability of false alarm
$P_{\mathrm{fa},i}^{*}$	Target probability of false alarm of the ith SU
$\bar{P}_{\mathrm{fa}}$	Expected probability of false alarm
P_i	Received signal power at the ith SU
P_{m}	Probability of missed detection
P_{te}	Total error rate
P_{T}	PUs signal power
P_{ST}	SUs transmit power in HD spectrum sensing
P_{c}	Collision probability
P_{w}	Probability of spectrum waste
$Q(\cdot)$	Q-function
$Q^{-1}(\cdot)$	Inverse Q-function
r	Decision threshold
r_i	Decision threshold of the ith cooperating SU
r_{opt}	Optimal decision threshold
R	Coverage radius of FC
R_{b}	Data rate of the reporting channel
$R(r,\tau)$	Achievable throughput of secondary network in terms of threshold and sensing time
$R_0(r,\tau)$	Achievable throughput of secondary network when PU is absent
$R_1(r,\tau)$	Achievable throughput of secondary network when PU is present
$\mathbf{R}_{yy}$	Covariance matrix of received signals
$\hat{\mathbf{R}}_{yy}$	Sample covariance matrix of received signals
$\mathbb{R}^{\nu}$	Euclidean space with ν dimension
$\mathbf{s}$	Transmit signal vector of PU
$s(t)$	Transmit signal of PU at time slot t

t_{on}	Duration of PUs ON state
t_{off}	Duration of PUs OFF state
$\mathrm{tr}(\cdot)$	Trace of a matrix
T	One periodic spectrum sensing frame in single-node spectrum sensing
T_{f}	One periodic spectrum sensing frame in cooperative sensing
T_{s}	Sensing slot
T_{r}	Decision reporting slot
T_{t}	Data transmission slot
T_{ED}	Test statistic of ED
T_{EME}	Test statistic of EME
T_{GLRT}	Test statistic of GLRT
T_{MED}	Test statistic of MED
T_{MME}	Test statistic of MME
T_{SS}	Test statistic
$v(t)$	Additive white Gaussian noise at time slot t
$\mathbf{V}$	Additive white Gaussian noise matrix
Var	Variance operator
$\mathbf{W}$	Wishart matrix
$y(t)$	Received signal at time slot t
$\mathbf{Y}$	Received signal matrix

Chapter 1
Introduction

In recent decades, the explosive growth of wireless data traffic has led to spectrum scarcity due to ever-increasing demands for additional spectrum to provide new wireless services and applications. Under the rigid spectrum regulation policy, fixed spectrum resources are allocated to certain licensed wireless users and unlicensed users are banned from accessing these licensed frequency bands. However, there are many underutilized spectral resources in frequency, time and space, which are called spectrum holes, as shown in Fig. 1.1. The conflict between the existence of spectrum holes and the rigid spectrum regulations provides the potential to reuse these underutilized resources. Therefore, cognitive radio (CR) has been put forward as one of the promising solutions to the spectrum scarcity. Unlike the current spectrum allocation policy, CR allows unlicensed users to access idle licensed spectral resources without introducing harmful interference to licensed users. These unlicensed users are also referred to as secondary users (SUs) and licensed users are also known as primary users (PUs).

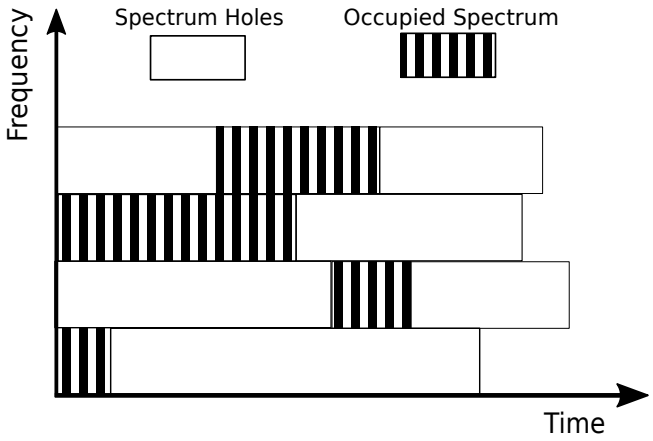

Figure 1.1: *Spectrum occupations*

1.1 Motivations

In CR networks, PUs have higher priority than SUs in terms of licensed spectrum access. Therefore, the occupation of frequency bands has to be ascertained before SUs are granted to access, so that severe interference to PUs caused by SUs can be mitigated. There exist different techniques to identify the status of PUs, including spectrum sensing, database lookup and transmission of beacons [2]. However, due to the advantage of lower infrastructure cost and the demand for further investigation on spectrum sensing, this thesis focuses on spectrum sensing techniques. Furthermore, a spectrum sensing procedure is required to sense spectrum holes before accessing the licensed frequency bands in sensing-based CR networks, e.g. interweave paradigm. It is worth mentioning that there are two other CR paradigms other than the interweave method, which will be introduced in detail in the next chapter.

In order to cope with the hidden terminal problem in spectrum sensing and improve the sensing performance, cooperative spectrum sensing is proposed and lots of sensing information fusion techniques are investigated in the literature [3, 4]. However, the performance gain achieved through cooperative spectrum sensing in the literature are based on a fixed secondary network with identical distances between the PU and all SUs. Obviously, this assumption is not valid in practice. The randomness of SUs can be modeled by utilizing the homogenous Poisson point process (PPP) [5]. The aforementioned points motivate this thesis to exploit the performance of collaborating spectrum sensing when SUs follow a homogenous PPP with a constant density across the plane of interest.

In the literature, various spectrum sensing methods have been proposed and studied, such as feature detectors, cyclostationarity detection and energy detector (ED) and so on [6]. Among these diverse detectors, eigenvalue-based spectrum sensing methods can be robust to noise uncertainty brought by inaccurate noise power estimation and offer excellent sensing performance without much prior knowledge about PUs. In contrast, although ED is non-robust to noise unceitainty, it is easy to implement in practice. So this thesis mainly focuses on ED and eigenvalue-based spectrum sensing techniques.

The main purpose of spectrum sensing is to determine the status of PUs and decide whether to grant the access of SUs to licensed bands of interest. Therefore, finding an appropriate

decision threshold to identify the activity of PUs is one of the key steps of spectrum sensing. The decision threshold can be obtained under two different requirements, including constant false alarm rate (CFAR) and constant detection rate (CDR) schemes. Specifically, under the CFAR requirement, the decision threshold is calculated based on a desired false alarm rate, which is considered from the perspective of SUs. Since a low probability of false alarm can create more chances to access spectrum holes. On the contrary, the CDR requirement emphasizes the interests of PUs, since a higher probability of detection can protect PUs better from the harmful interference brought by collisions of concurrent primary and secondary transmissions.

The existing works have mainly focused on the CFAR scheme [7–11], which guarantees the benefits of SUs preferentially. Thus, this may lead to poor detection probability, which is unfair to PUs. In order to make both false alarm and detection rates achieve acceptable levels, the interests of PUs and SUs are considered at the same time and this motivates me to investigate the total error rate of spectrum sensing, where the total error rate is defined to be the summation of false alarm and missed detection rates. Meanwhile, the optimal decision threshold which minimizes the total error rate is studied as well.

In a conventional half-duplex (HD) spectrum sensing system, each periodical secondary duration comprises two slots, including spectrum sensing and secondary transmission. The spectrum sensing and secondary transmission are alternate and consecutive. In this way, both the sensing and transmission performance of SUs are limited by corresponding time durations assigned. In detail, a long sensing duration helps to accumulate large numbers of samples of received signals, which benefits the spectrum sensing performance. However, a long sensing duration would reduce the time allocated to secondary transmission, which affects the secondary transmission performance. Therefore, in order to get rid of this limitation caused by the HD sensing system, FD spectrum sensing is investigated in this thesis, which realizes simultaneous spectrum sensing and secondary transmission [12, 13]. Specifically, in FD sensing systems, SUs can use the whole secondary period for spectrum sensing and secondary transmission at the same time.

1.2 Contributions and Thesis Organizations

Based on the motivations mentioned in the last section, this thesis investigates spectrum sensing techniques from three perspectives, including the performance analysis of eigenvalue-based spectrum sensing, cooperative spectrum sensing analysis under random secondary networks and the FD spectrum sensing analysis. The detailed contributions of this thesis are explained as follows:

- Firstly, the eigenvalue-based spectrum sensing techniques are investigated in terms of sensing and secondary transmission performance. Specifically, the detectors discussed in this part include maximum eigenvalue detection (MED), maximum minimum eigenvalue (MME) detection, energy with minimum eigenvalue (EME) detection and the generalized likelihood ratio test (GLRT) eigenvalue-based detector. With regard to sensing performance analysis, the total error rates of these eigenvalue-based detectors are studied and corresponding optimal decision thresholds that can minimize the total error rates are obtained as well. Therefore, the benefits of PUs and SUs can be considered simultaneously. It is worth mentioning that the total error rate is not a common metric to evaluate the spectrum sensing performance in the literature, however it is still a useful metric to consider the interests of PUs and SUs together so that the unfair treatments between PUs and SUs can be alleviated to some extent. In fact, the total error rate has been studied in [14] for cooperative spectrum sensing, where an optimal voting rule and decision threshold are both obtained to minimize the total error rate.

  Meanwhile, in terms of the secondary transmission, the trade-off between sensing and transmission performance is investigated and the optimal sensing time duration is obtained to maximize the throughput when the target probability of detection is achieved. So the benefits of SUs are maximized when the interests of PUs are guaranteed.

- Secondly, the cooperative spectrum sensing techniques are explored by using a homogeneous PPP. In previous works [14], it is proved that more SUs involved in the collaborating spectrum sensing can improve sensing performance. However, this result holds only when the distances between all the SUs and PU are identical [15]. In practice, SUs are distributed randomly, which means that the locations of SUs may vary

greatly in the distances between the PU and them. Therefore, this thesis investigates cooperative spectrum sensing performance under a random secondary network and the achievable ergodic capacity and throughput of the secondary network are discussed as well.

In detail, when a homogeneous PPP is employed for modeling the randomness of the secondary network, this thesis derives the probability density function (PDF) of the distance between the i-th nearest SU and PU. Besides, it has been demonstrated that cooperation between an optimal number of SUs, not all the SUs, can achieve the best sensing performance and an efficient cooperative sensing is proposed in this thesis as well. The simulation results have shown that the obtained optimal number of cooperating SUs can minimize the sensing errors. Besides, different cooperative strategies are proposed to achieve the best transmission performance when the total error rates are controlled below the desired value.

- Finally, the FD spectrum sensing and sharing are investigated in this thesis in order to improve the sensing and transmission performance. FD spectrum sensing (FDSS) and FD sensing-based spectrum sharing (FD-SBSS) schemes are proposed and investigated respectively. In terms of the FDSS scheme, the optimal decision threshold pair is studied based on the ED with multiple sensing antennas. The closed-form asymptotic expressions of sensing error rates are then derived. It is worth mentioning that there exists a decision threshold pair, including two separate decision thresholds under the absence and presence of secondary transmissions, because of self-interference. With regard to the FD-SBSS scheme, the collision and spectrum waste probabilities are investigated and the obtained results have demonstrated the improvement of the achievable throughput of FD-SBSS scheme compared with FDSS scheme. In addition, antenna partitioning is analyzed in order to maximize the achievable throughput under FDSS and FD-SBSS schemes respectively.

The remaining part of this thesis is organized as follows: Chapter 2 provides the background knowledge related to the work in the thesis, such as CR technology, spectrum sensing techniques, stochastic geometry and FD wireless communications. In Chapter 3, the total error rate of eigenvalue-based spectrum sensing are investigated and the sensing-throughput trade-

off is analyzed based on the GLRT detector. The randomness of secondary networks is considered in Chapter 4 and the optimal number of collaborating SUs is obtained. In Chapter 5, the FDSS and FD-SBSS schemes are proposed and the corresponding sensing and transmission performances are discussed as well. Finally, Chapter 6 concludes this thesis and the limitations of this thesis are indicated. Meanwhile, possible future work is described in Chapter 6 as well.

Chapter 2

Background

In this chapter, the related background knowledge is provided, which helps to understand the technical content in the subsequent chapters. Firstly, the cognitive radio mechanism is introduced, which is the basic framework of the thesis. Then an overview of spectrum sensing techniques is presented and this introduces the main research topic of the thesis. Finally, full-duplex wireless communications is also presented for its application in CR networks which is further studied in Chapter 5. In addition, basic concepts of the stochastic geometry are briefly illuminated for a better understanding of the work in Appendix A.

2.1 Cognitive Radio Technology

In this section, the basic idea and paradigms of CR networks are presented. As mentioned in the last chapter, CR is put forward to cope with the spectrum scarcity. The fixed spectrum access policy is widely adopted currently, so that certain frequency bands are exclusively assigned to licensed users. Under this rigid resource allocation regime, means unlicensed users are banned from accessing these licensed spectrum resources. In contrast, a dynamic spectrum access policy allows unlicensed users to access the licensed bands with a lower priority compared with the licensed users. In this way, the utilization efficiency of spectrum resources can be improved. In the dynamic spectrum access scheme, the licensed users with higher priority are called PUs and the unlicensed users are named as SUs. In order to realize dynamic spectrum access scheme, SUs have to be equipped with the capability of acquiring radio environment knowledge and these SUs are also defined to be cognitive radio users [16–18]. The main characters of CR mechanism are cognitive and reconfigurable capabilities. The two features are introduced in the following subsections.

2.1.1 Cognitive Capability

The cognitive capability of wireless devices means the ability of capturing the information on radio environments and adapting accordingly through appropriate communication parameters. The detailed steps for realizing this cognitive capability are incorporated into cognitive cycle [19] which is summarized as follows:

- **Spectrum sensing**: In this stage, the activity in frequency bands of interest are monitored periodically by cognitive users. Spectrum holes [1] are detected by applying proper spectrum sensing techniques so that available frequency bands can be found.
- **Spectrum analysis**: After spectrum holes are detected, cognitive devices are capable of evaluating the characteristics of the spectrum holes, e.g., interference, path loss, wireless link errors, link layer delay and holding time [19].
- **Spectrum decision**: Based on the estimated features of spectrum holes and requirements of secondary transmissions, cognitive users should select the most suitable spectrum holes to transmit. Generally, related reference information for this decision consists of interference temperature, transmission bandwidth and data rates, etc.

2.1.2 Reconfigurable Capability

The reconfigurable capability of a cognitive devices refers to the ability of adjusting communication parameters in order to adapt to dynamic radio environments. Meanwhile, this adaptation is accomplished through a programmable radio without any changes to hardware of devices. Certain reconfigurable parameters in CR [20] are introduced as follows:

- **Modulation schemes**: cognitive users are able to reconfigure modulation scheme according to system performance requirements and dynamic environments. For instance, different modulation schemes should be chosen for delay-sensitive and loss-sensitive communication systems. Specifically, the delay-sensitive application requires high data rate, e.g. voice and video traffics. As contrast, a low error rate is more significant to a loss-sensitive system, e.g. the local area network (LAN) data traffic.

- **Transmit power**: It is also required to be reconfigurable for a cognitive device in terms of transmit power in order to fulfil various targets. For example, increasing transmit power within the acceptable interference level to PUs helps to advance transmission rates. Alternatively, in order to reduce energy consumption, transmit power could be reduced through reconfigurable capability when a high data rate is unnecessary to a system.

- **Operating frequency**: In order to adapt to radio environments dynamically, it is necessary for a cognitive user to have reconfigurable ability on operating frequency. For instance, when the frequency band occupied by cognitive users is retrieved by licensed users, cognitive users have to vacate immediately and resume transmission in another available band. In this case, cognitive users may have to change operating frequency to cope with changes in the radio environment.

2.1.3 Cognitive Radio Paradigms

From the perspective of information theory, CR is defined as a wireless communication system that can share spectrum resources with other systems by intelligently using the side information of existing users, including channel conditions, activities or codebooks and so on [21]. Therefore, CR networks can be classified into three main categories: underlay, overlay and interweave. Table 2.1 summarizes characteristics of the three CR paradigms briefly.

2.1.3.1 Underlay Paradigm

The main idea of underlay paradigm is spectrum sharing between the primary and secondary networks as long as the interference caused by the SUs is tolerable to the PUs. Specifically, within the underlay paradigm, SUs can access the licensed spectrum assigned to PUs originally when the PUs' communications are not affected seriously. In other words, when the interference caused by spectrum sharing is lower than the pre-set threshold, sensing or detection is not required to confirm whether the frequency bands are occupied.

There exist many different techniques to weaken the interference generated by secondary

Underlay	**Overlay**	**Interweave**
SUs can transmit with PUs simultaneously as long as the interference brought by this concurrent transmission is under a predefined threshold.	SUs use partial power to transmit their own messages and the remaining power to relay PUs' information, so SUs and PUs can transmit simultaneously and the interference caused by this can be mitigated as well.	SUs can occupy the licensed frequency bands when SUs detect spectrum holes correctly or missed detection occurs.
Side information: SUs know the fading gain between the secondary transmitter and the primary receiver.	Side information: SUs know codebooks and messages of PUs.	Side information: SUs know the activity of PUs through spectrum sensing or some other ways.

Table 2.1: *Overlay, underlay and interweave CR paradigms*

transmissions in order to guarantee the primary transmission performance. For instance, firstly, the beamforming method can be applied at the secondary transmitter by using the strengths of multiple antennas so that the received interference at primary receivers can be reduced accordingly [22]. Secondly, a wide bandwidth can be assigned to secondary users so that the secondary transmit signal can be spread. By doing so, the signal power over unit bandwidth can be quite low and the interference to primary receiver would be alleviated [23, 24]. Lastly, Secondary transmitters can set a limit to their own transmit power according to the predefined interference threshold. But in this case, the service range of secondary transmitter would be confined because of the restricted transmit power. The underlay paradigm allows simultaneous spectrum access between PUs and SUs, so it is also called concurrent spectrum access (CSA) mode [23, 24].

2.1.3.2 Overlay Paradigm

In overlay paradigms [25, 26], SUs can access spectrum concurrently with PUs and help to improve the primary transmission performance by overhearing. Specifically, the codebooks

used by primary networks are known by SUs and even the messages from primary transmitters are also known by SUs. Therefore,one case of overlay paradigms is that secondary transmitters can relay the messages of primary transmitters to the primary receiver when the information received from the primary transmitters can not be directly decoded at the primary receiver because of deep fading, etc. One instance of this is the frequency modulation (FM) broadcast signal is lost when the vehicle stops at traffic lights. Based on this reciprocal scheme, secondary transmitters may use certain power to transmit their own messages and the remaining power is assigned for retransmitting primary users' signals. Specifically, from the perspective of PUs, the interference caused by the concurrent spectrum sharing between PUs and SUs could be counteracted due to the signal-to-noise power ratio (SNR) improvement brought by the secondary relaying. Thus, the transmission performance of primary network can be guaranteed as expected. Meanwhile, from the perspective of SUs, SUs obtain extra bandwidths and the interference caused by primary transmission could be mitigated by using the available codebooks or messages of PUs.

2.1.3.3 Interweave Paradigm

In the interweave paradigm [27], SUs have to implement spectrum sensing in order to detect spectrum holes before accessing licensed frequency bands. For a specific frequency band, when the PUs' activity is detected as absent, SUs are granted access. Once the PU is active or reactivated, SUs are banned access or have to vacate this frequency band immediately. Therefore, SUs have to monitor their occupied spectrum continually and exploit spectrum holes opportunistically. This is why interweave paradigm is also referred to as the opportunistic spectrum access (OSA) model. Unlike underlay and overlay schemes, the interweave method does not allow concurrent transmission between primary and secondary networks which only occurs when missed detection happens. Thus no interference caused by secondary transmission would be introduced to primary network when the presence of PUs is detected correctly. Therefore, in order to combine virtues of the above three different CR paradigms, certain hybrid CR paradigms are proposed [28]. For instance, sensing-based spectrum sharing incorporates the merits of underlay and interweave schemes. The main investigated paradigm throughput this thesis is the interweave method, so that spectrum sensing becomes main re-

search direction, which is an essential part of the interweave paradigm.

2.1.4 Cognitive Radio Applications

After the idea of CR was proposed by Mitola in 1999 [16], CR has attracted much attention from communications regulators, academia and industrial organizations. The United States Federal Communications Commission (FCC) looked for feedback on the commercial applications of CR through a notice of proposed rulemaking and order published by them in 2003. In November 2004, IEEE 802.22 Working Group took a lead in exploring the CR applications and defined a CR-based wireless access standard which is titled IEEE 802.22 Wireless Regional Area Network (WRAN) [29–31]. Specifically, IEEE 802.22 standard is proposed for the wireless broadband access system in large areas, eg. rural regions, that operates in ultra high frequency (UHF) TV bands [32]. Meanwhile, the specific spectrum sensing performance requirements are presented for WRAN as well. In detail, the detection probability should be not less than 90% and the maximum probability of false alarm is required at 10% [33]. According to the 802.22 standard, the cognitive device is able to sense spectrum holes even under a quite low received SNR down to -22 dB and capable of vacating the reactivated frequency bands within 2 seconds.

Subsequently, in 2008, FCC carried out a test on the devices with spectrum sensing capability that are provided by certain research institutes and companies. The purpose of this testing is to understand the actual effects of spectrum sensing on protecting the interests of PUs. After this, in late 2008, wireless devices were approved for serving in TV band white spaces, which promoted the further research and development on CR systems to some extent.

In addition to sensing-based dynamic spectrum access, a geolocation database solution [34] is also proposed and preferred for TV white-space occupation. Under this mechanism, a database is required to update the status of PUs' activities so that SUs can acquire the information on spectrum holes in a timely manner. However, for some other types of primary signals, it might be difficult for database suppliers to obtain the availability information of spectrum holes, eg. wireless microphone signals [24]. Therefore, under this condition, spectrum sensing is still necessary for capturing the status of licensed users. Alternatively, spectrum

sensing could be adopted by database suppliers as the approach of providing spectrum-hole-availability information.

2.2 Overview of Spectrum Sensing

As mentioned in the previous section, this thesis mainly focuses on the interweave paradigm. In interweave and sensing-based hybrid CR schemes, detecting the activities of PUs is an essential part which can be realized through spectrum sensing. Spectrum sensing is aimed at monitoring the usage of licensed frequency bands periodically and helps to decide if access requests of SUs should be granted. In this section, the basic idea and various spectrum sensing techniques are introduced, especially eigenvalue-based spectrum sensing techniques.

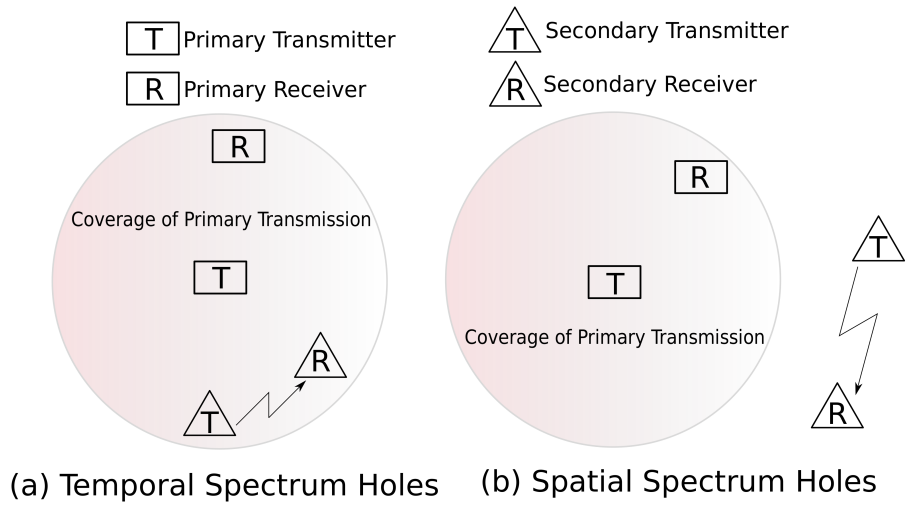

Figure 2.1: *Spectrum holes (following [1])*

2.2.1 Spectrum Holes

In order to understand spectrum sensing, it is necessary to know spectrum holes first. Spectrum holes are defined as the idle licensed frequency bands which are available for SUs [1]. Overall, spectrum holes consist of two distinct categories, including temporal and spatial spectrum holes. Their characteristics are shown in Fig. 2.1 and stated as follows:

- **Temporal spectrum holes**: Temporal spectrum holes refer to the idle frequency bands that are unoccupied within a certain time duration. Therefore, the SUs located in same cell with PUs can access these spectrum holes after sensing the absence of PUs. In this case, spectrum sensing is relatively easy because of high received SNRs at the SUs, because SUs only need to be with similar detection sensitivity as the primary receivers. Meanwhile, detecting the status of primary transmiters is easier than demodulating and decoding the primary signals.

- **Spatial spectrum holes**: When the frequency bands of interest are occupied by PUs only in a confined area, SUs can utilize these spectrum resources without causing harmful interference to primary transmissions. Specifically, secondary transmissions over licensed frequency bands are granted when the interference caused by SUs is tolerable to the primary receiver or the PUs are absent. However, spectrum sensing is relatively difficult to detect spatial spectrum holes because of low received SNRs [1].

2.2.2 Single-node Spectrum Sensing

Spectrum sensing, in general, can be divided into two categories, including direct and indirect sensing methods. Direct spectrum sensing refers to detecting the activities of primary receiver, which is obviously the most efficient way of spectrum sensing. For one-way communication systems, e.g. TV and radio broadcasting systems, the only way of implementing direct spectrum sensing is to detect the leakage signals of the primary receiver [35]. In terms of two-way communication systems, spectrum sensing is based on the interactions between the primary receiver and transmitter. For instance, a proactive spectrum sensing method is proposed for realizing direct sensing [36–38]. Specifically, a sounding signal is sent and then the primary signal is observed for probable change caused by closed-loop power control. However, in practice, the channel between primary transmitter and receiver is quite difficult to measure, therefore indirect sensing methods attract more attention from academic research. This thesis also focuses on indirect spectrum sensing which senses the status of primary transmitters.

Indirect spectrum sensing techniques decide the status of PUs by utilizing the primary signals

received at the SUs, therefore indirect spectrum sensing is also called primary transmitter detection. a basic system model for primary transmitter detection is shown as

$$y(t) = v(t) \qquad \mathcal{H}_0, \tag{2.1}$$

$$y(t) = hs(t) + v(t) \qquad \mathcal{H}_1, \tag{2.2}$$

where $s(t)$ is the transmit signal from primary transmitter and $v(t)$ denotes the additive white Gaussian noise (AWGN). h represents the channel gain between the primary transmitter and secondary transceiver. $y(t)$ denotes the received signal measured at the secondary transceivers. $\mathcal{H}_0$ defines the null hypothesis which refers to the case that there is no PUs operating in licensed frequency bands of interest. On the contrary, $\mathcal{H}_1$ indicates the alternative hypothesis that the licensed spectrum is occupied.

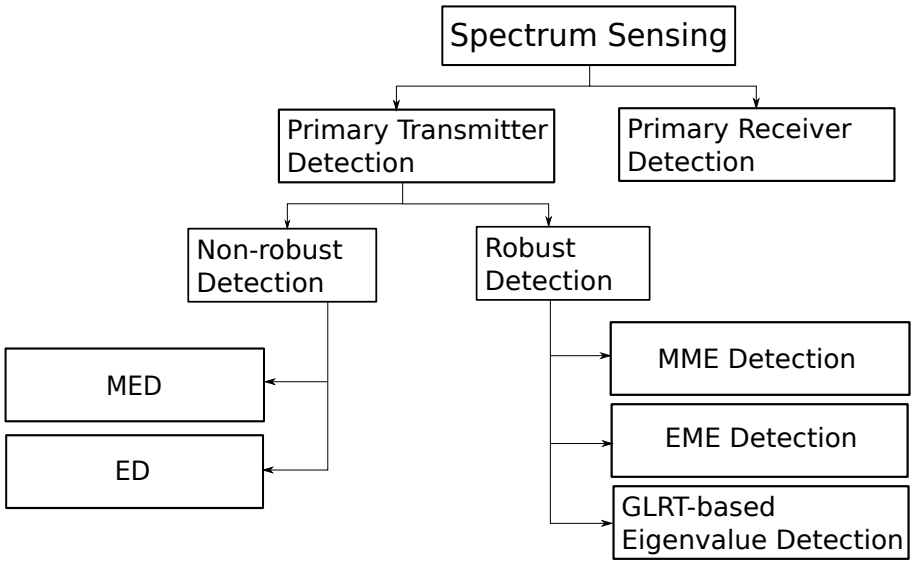

Figure 2.2: *Classifications of spectrum sensing methods*

Different spectrum sensing techniques have a different test statistic T_{SS} which is the detection metric for spectrum sensing. Assuming r is a predetermined decision threshold, the spectrum sensing results are obtained by comparing T_{SS} and r. In detail, sensing results state the licensed frequency bands are occupied when $T_{\mathrm{SS}} > r$. On the contrary, the spectrum of interest is regarded as idle when $T_{\mathrm{SS}} \leq r$. The key performance metrics for the spectrum sensing technique design are probabilities of false alarm and detection. Specifically, on the

one hand, probability of false alarm indicates the possibility that sensing results claim the presence of PUs when the licensed bands are idle in fact. On the other hand, probability of detection is the probability that SUs detect the presence of PUs successfully when PUs are actually present. Therefore, the probability of false alarm P_{fa} and the probability of detection P_{d} are defined as

$$P_{\mathrm{fa}}(r) = Prob\big[T_{\mathrm{SS}} > r|\mathcal{H}_0\big] = \int_r^{\infty} f_0(t)\,\mathrm{d}t, \tag{2.3}$$

$$P_{\mathrm{d}}(r) = Prob\big[T_{\mathrm{SS}} > r|\mathcal{H}_1\big] = \int_r^{\infty} f_1(t)\,\mathrm{d}t, \tag{2.4}$$

where $f_0(t)$ and $f_1(t)$ denote the probability density functions (PDFs) of the test statistic T_{SS} under the hypotheses $\mathcal{H}_0$ and $\mathcal{H}_1$ respectively.

Based on above definitions and explanations, the objective of a spectrum sensing technique design is maintaining a high probability of detection but a low probability of false alarm at the same time. A low false alarm rate can create more chances for SUs to access the idle frequency bands and a high detection rate helps to protect PUs better. In the literature, lots of different spectrum sensing methods have been proposed and investigated, including matched filter detection, energy detection and cyclostationary detection, etc. [39–43]. This thesis mainly investigates energy detection and eigenvalue-based spectrum sensing techniques. According to their sensitivity to noise uncertainty, these sensing techniques can be classified into robust and non-robust spectrum sensing techniques. As shown in Fig. 2.2, ED and MED are non-robust detection methods. MME, EME and GLRT eigenvalue-based spectrum sensing techniques are robust. Since the test statistics of the ED and MED include the noise power, but the noise power is difficult to estimate very accurately. This gap between the actual and estimate values of noise power affects the sensing performance. On the contrary, the MME, EME and GLRT eigenvalue-based detection do not require the noise power so that they are robust to noise uncertainty. Next, we are going to introduce these detection methods in detail and multiple antennas at SUs are assumed.

Non-robust spectrum sensing techniques:

(1) ED: ED determines the activity of PUs based on the received energy measured at SUs

[44] and the corresponding test statistic is given by

$$T_{\mathrm{ED}} = \sum_{k=1}^{K} \|\mathbf{y}(k)\|^2, \tag{2.5}$$

where $\|\cdot\|$ denotes the norm of a vector. When the number of samples, K, is large enough, the PDF of the test statistic T_{ED} can be approximated by a normal distribution [45]. So the corresponding decision threshold can be calculated through the derived expressions of false alarm and detection rates based on different system requirements. The specific criteria are stated as follows

$$T_{\mathrm{ED}} > \sigma_v^2 r: \quad \text{PU is identified as present}, \tag{2.6}$$

$$T_{\mathrm{ED}} \leq \sigma_v^2 r: \quad \text{PU is identified as absent}, \tag{2.7}$$

where σ_v^2 is the noise power and r represents the decision threshold.

The main merits and shortcomings are summarized as follows.
Advantages:

- When the exact noise power is known, ED is the most promising detection method for independently and identically distributed (i.i.d.) signals [46].
- ED is quite easy to realize in practical systems, so it is a popular detection method for spectrum sensing due to the simplicity.

Disadvantages:

- The ED is non-robust to noise uncertainty so that the sensing performance of ED is seriously affected by the inaccurate estimation of the noise power. It can be seen from Eq. (2.6) and (2.7) that sensing results of ED depend on the value of noise power. However, noise power is difficult to estimate accurately, which leads to the noise uncertainty.

(2) MED: The sensing results of MED are obtained based on the maximum eigenvalue of the covariance matrix of the received signals $\lambda_{\max}$ [47]. Specifically, the test statistic of MED is

given by

$$T_{\mathrm{MED}} = \lambda_{\max}. \tag{2.8}$$

Thus, the detailed decision criteria are given by

$$T_{\mathrm{MED}} > \sigma_v^2 r: \quad \text{PU is identified as present}, \tag{2.9}$$

$$T_{\mathrm{MED}} \leq \sigma_v^2 r: \quad \text{PU is identified as absent}. \tag{2.10}$$

The merits and defects of this detector are stated as below.
Advantages:

- MED has the best sensing performance among the eigenvalue-based spectrum sensing techniques studied in this thesis.

Disadvantages:

- MED is non-robust to noise uncertainty, which means its sensing performance would be degraded seriously by noise uncertainty. From Eq. (2.9) and (2.10), MED also requires prior knowledge of the noise power which is difficult to estimate very accurately.

Robust Spectrum Sensing Techniques:
(1) MME: MME [48] detection is a blind spectrum sensing approach which does not require prior knowledge. The MME detection identifies the activity of the PUs by comparing the maximum and minimum eigenvalue of the received signals' covariance matrix. In detail, the test statistic is given by

$$T_{\mathrm{MME}} = \frac{\lambda_{\max}}{\lambda_{\min}}. \tag{2.11}$$

So the decision criteria are stated as follows

$$\lambda_{\max} > \lambda_{\min} r: \quad \text{PU is identified as present}, \tag{2.12}$$

$$\lambda_{\max} \leq \lambda_{\min} r: \quad \text{PU is identified as absent}, \tag{2.13}$$

where $\lambda_{\min}$ is the minimum eigenvalue of the received signals' covariance matrix. The virtues and shortcomings are detailed as below.
Advantages:

- MME detection is a robust spectrum sensing detector which is not influenced by the noise uncertainty. It can be seen from Eq. (2.12) and (2.13) that the detection decisions of MME do not require accurate value of noise power [9]. So the corresponding sensing results are not related to noise power.
- MME detection can still maintain a good sensing performance even when the signal samples are highly related [49]. This is the reason why MME detection has been adopted by IEEE 802.22 draft standards.

Disadvantages:

- MME detection has a higher computational complexity because of the eigenvalue-decomposition.

(2) EME: EME detection [50] is also a blind spectrum sensing approach. It compares the summation of all the eigenvalues of the covariance matrix, e.g. the received signal energy, and the minimum eigenvalue. The corresponding test statistic is given by

$$T_{\mathrm{EME}} = \frac{\sum_{i=1}^{M} \lambda_i}{\lambda_{\min}}, \tag{2.14}$$

where M is the number of receive antennas at each SU. So the decision criteria of MME detection are given by

$$\sum_{i=1}^{M} \lambda_i > \lambda_{\min} r : \quad \text{PU is identified as present}, \tag{2.15}$$

$$\sum_{i=1}^{M} \lambda_i \leq \lambda_{\min} r : \quad \text{PU is identified as absent}. \tag{2.16}$$

The pros and cons are detailed as below.
Advantages:

- Similar to MME detection, EME detection is also robust to noise uncertainty since it does not need noise power information either, which can be observed from Eq. (2.15) and (2.16).

Disadvantages:

- Compared with MME and GLRT-based eigenvalue detections, the sensing performance of EME detection is not as good as the other blind eigenvalue-based spectrum sensing techniques.

(3) GLRT: The GLRT-based eigenvalue detector investigated in this thesis is a blind spectrum sensing approach, which means that it does not require any knowledge of primary signal and channel information. The sensing results are obtained by comparing the maximum eigenvalue of the covariance matrix of the received signal and the received signal energy. In mathematical terms, the test statistic of the GLRT-based eigenvalue detector is given by

$$T_{\mathrm{GLRT}} = \frac{\lambda_{\max}}{\sum_{i=1}^{M} \lambda_i}. \tag{2.17}$$

Thus the decision criteria of GLRT-based spectrum sensing are stated as follows.

$$\lambda_{\max} > \sum_{i=1}^{M} \lambda_i r : \quad \text{PU is identified as present}, \tag{2.18}$$

$$\lambda_{\max} \leq \sum_{i=1}^{M} \lambda_i r : \quad \text{PU is identified as absent}, \tag{2.19}$$

where λ_i denotes the ith eigenvalue of the received covariance matrix. The advantages and disadvantages of the GLRT-based eigenvalue detector are summarized briefly as below [10, 11].

Advantages:

- Compared with the other three blind eigenvalue-based spectrum sensing techniques, the GLRT detector has the best sensing performance.

- The GLRT-based detector can maintain good sensing performance no matter what type of signal is transmitted from PUs.
- Similarly, based on Eq. (2.18) and (2.19), when SUs make decisions by employing the GLRT detector, an estimate of the noise power value is not necessary so that the GLRT detector is robust to noise uncertainty as well [10].

Disadvantages:

- The excellent sensing performance is achieved at the price of high computational complexity. This is caused by the eigenvalue-decomposition [51].

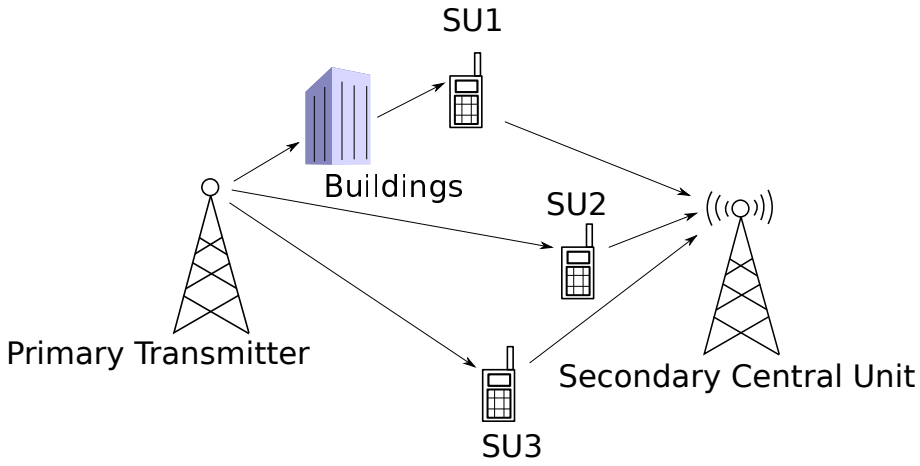

Figure 2.3: *Centralized cooperative spectrum sensing and hidden terminal problem*

2.2.3 Cooperative Spectrum Sensing

When performing single-node spectrum sensing, the hidden terminal problem may cause serious performance degradation, which would cause missed detections. The hidden terminal problem is revealed in Fig. 2.3. From this figure, the sensing channel between PU and SU 1 is blocked by a building so that the local sensing performance would be affected seriously and hidden terminal problem occurs. The hidden terminal problem is a result of sensing performance degradation caused by deep multipath fading or shadowing between the PU

and SUs. In order to cope with the hidden terminal problem in CR networks, cooperative spectrum sensing is proposed, in which multiple SUs collaborate to implement spectrum sensing together [42]. Existing work has demonstrated that cooperative sensing techniques can improve the sensing performance for combatting fading channels [52].

Generally, there exist two fashions called centralized and decentralized collaborations. In a decentralized CR system, there is no central access point. Instead, SUs make their own final decisions through sharing sensing information with each other. So one advantage of a decentralized system is reduced overhead on the core infrastructure [53]. Decentralized cooperative sensing has been investigated in many papers and some novel collaborating approaches are proposed [54–56]. For instance, a decentralized CR system is combined with the amplify-and-forward (AF) protocol in [57, 58]. In this AF decentralized sensing scheme, when SU 1 transmits sensing information to SU 2, SU 3 can work as an AF relay for SU 1.

On the contrary, a centralized cooperative spectrum sensing system has a common central unit for collecting and processing local sensing data or decisions, which is shown as Fig. 2.3. The cooperating SUs will be notified about the occupation status of targeted spectrum after the central unit combines the collected sensing information and makes a final decision. The combination at the fusion center can be accomplished in a soft or hard way:

- **soft combination**: In this soft combination mode [59], collaborating SUs send their own observations directly to the fusion center. Therefore, all the original sensing data from every SU is sent to the central unit without further processing. The received sensing data at the fusion center will be processed by data fusion techniques [4]. Many different data fusion approaches have been studied in the literature, such as multitaper-method singular-value-decomposition (MTM-SVD) and equal-gain combination (EGC) [4, 18], etc. Soft combination has a superb sensing performance comparing with the hard combination scheme. However, the excellent performance of data fusion is achieved at the price of the high overhead on bandwidth of control channels.

- **hard combination**: In order to reduce the required bandwidth of control channels, hard combination is proposed and studied [52]. Under the hard combination scheme, SUs send quantized sensing information to the central unit for conducting decision

fusion. The popular and simplest hard combination approach is 1-bit decision fusion. Specifically, all the cooperative SUs send their own 1-bit decision after they make local decisions on the availability of licensed spectrum. Then the common central unit makes a final decision based on these received 1-bit sensing information and an appropriate decision fusion rules, such as logic-AND, logic-OR and K-out-of-M fusion rules and so on [60, 61]. Indeed, hard combination scheme has information loss because of the quantization of sensing information. However, this method saves the overhead on local sensing information feedback to fusion center, which improves the spectral efficiency of control channels.

In addition, a 2-bit decision fusion method is proposed in [4] and it has been proven that the sensing performance of 2-bit decision fusion can be comparable with the EGC data fusion scheme. In 1-bit decision fusion, the sensing information is quantized to be 1-bit data based on a single decision threshold. Different from 1-bit hard combination, in a 2-bit scheme, individual SUs divided received sensing information into 4 regions based on three thresholds and then quantize this information to 2-bit data. In this way, the local sensing information has more information compared with the 1-bit scheme. This thesis focuses on cooperative spectrum sensing with 1-bit decision fusion and the optimal number of collaborating SUs is investigated in order to achieve the best sensing performance.

2.3 Full-duplex Wireless Communications

In order to satisfy the increasing requirement on data rates, the spectral efficiency has to be further improved. In current wireless networks, half-duplex (HD) modes are employed, which restricts the improvement of spectrum efficiency. Specifically, in HD wireless systems, the transmission and reception of signals are implemented in time-division or frequency-division modes. However, FD systems can realize the simultaneous transmission and reception in the same frequency bands. Therefore, FD communication is proposed to advance the utilization efficiency of spectral resource by overcoming the disadvantages brought by HD operation. Many research papers have demonstrated that FD systems are feasible in practical applica-

tions [62].

2.3.1 Benefits and Shortcomings Brought by FD Communications

Compared with the HD mode, FD systems have advantages in terms of throughput and delay and so on. But FD mode still has some disadvantages as well. So the merits and shortcomings are discussed in this subsection.
Advantages:

- In single-hop communication link, FD wireless communications has the potential to double the throughput compared with the HD mode.
- In multi-user communications, the FD technique can help to solve the hidden node problem. In HD wireless systems, when a user is transmitting to the base station, the base station would broadcast 'ACK' repetitively in order to avoid the collisions caused by hidden terminal problems.
- In a topology wireless system, FD techniques can reduce the capacity loss caused by the congestion. Since the congested node can only effect one function between transmission and reception, which will affect the capacity performance.
- Compared with the store-and-forward mode employed by HD systems, FD systems can decrease the delay between two ends, especially for multi-hop systems. In FD mode, every FD node can launch transmissions after partial data is received.
- In CR networks, FD technology can realize the simultaneous spectrum sensing and secondary transmissions, which can help to improve the secondary throughput and protect the PUs' interests at the same time [63].

Disadvantages:

- The performance gain brought by FD techniques is degraded by the residual self-interference. The self-interference is inevitable in FD systems because of the natu-

ral features in FD mode and the power of self-interference is much stronger than the received signal with information before self-interference cancellation.

- Compared with the HD node, the FD node has to cope with more packets due to the simultaneous transmission and reception. Therefore, the FD node would have a higher packet loss ratio. Otherwise, a large buffer is necessary in order to reduce the packet loss ratio in FD systems [64].

2.3.2 Self-interference Cancellation

As mentioned in the last subsection, self-interference is a major issue in the implementation of FD wireless communications. Therefore, many self-interference cancellation methods are proposed in order to realize simultaneous transmission and reception in the same frequency band without introducing strong self-interference. Generally, the self-interference cancellation techniques can be classified into three categories, including passive, analog and digital self-interference cancellations.

- *Passive self-interference cancellation*: Passive self-interference cancellation refers to the suppression of self-interference brought by physical separation between the transmit and receive antennas of FD node [65]. In this way, the electromagnetic coupling between the transmit and receive antennas of the FD node decreases or the path loss between them increases. Therefore, the power of the self-interference can be suppressed before it is received at the receive antennas of the FD node. The methods include antenna separation, antenna cancellation and beamforming, etc.

- *Analog cancellation*: Generally, if the introduced self-interference is not cancelled completely by the passive suppression techniques, the analog cancellation [66] has to be applied before the contaminated signal is digitized. Specifically, the detailed steps of implementing analog cancellation are presented as follows: Firstly, a self-interference inverse signal should be generated by inverting the its phase. Secondly, the attenuation and delay have to be applied in the created self-interference inverse signal according to the attenuation and delay experienced by the self-interference. Lastly, the gener-

ated self-interference inverse signal in previous steps can be combined with the self-interference together. The ideal result of this combination is a zero self-interference output, but there will be still some residual self-interference after the analog cancellation component because of the imperfect hardware.

- *Digital cancellation*: After the received signal at receive antennas of FD nodes is quantized through the analog-to-digital converter, the digital cancellation techniques will proceed in order to mitigate the residual interference output from the analog step [64]. In detail, the self-interference is extracted and remodulated so that it can be removed from the contaminated signal.

In this thesis, FD techniques are employed in CR networks and help to improve the spectrum sensing and secondary transmission performance. The FD spectrum sensing work is explored under the residual self-interference.

Chapter 3
Eigenvalue-based Detections and Total Error Rates

3.1 Introduction

This chapter mainly addresses the eigenvalue-based detectors. Among many spectrum sensing techniques, eigenvalue-based spectrum sensing does not require much prior knowledge about the primary signal and can detect spectrum holes with high accuracy. Various eigenvalue-based detection techniques have been considered in the literature, including MED [8], MME detection [9], EME detection [7] and the GLRT eigenvalue detector [10, 67]. In order to analyse the total error rate and sensing-throughput trade-off, the closed form expressions for probabilities of false alarm and detection are required. However, previous studies, e.g., [7–10, 67], have mainly focused on the probability of false alarm. This is attributed to the difficulty and complexity of obtaining the expressions for the probability of detection for eigenvalue-based detectors. For example, in reviewing the literature, it is found that the exact PDF of T_{GLRT} assuming the alternate hypothesis, i.e., the presence of PUs, was derived in [10] for the GLRT detector. However, this result in [10] is only valid for the special case of 2 receive antennas. Also, the exact expression of probability of false alarm provided in [10] is very complex. Therefore, the aforementioned issues form our major motivation to investigate sensing performance of various eigenvalue-based detections.

In detail, exact optimal decision thresholds are investigated for different eigenvalue-based detections in order to minimize total error rates. Besides, the optimization of the GLRT detector is investigated in terms of asymptotic optimal decision threshold and minimum sensing time. The purpose of this optimality investigation is to accelerate the spectrum sensing process while maintaining a superior sensing performance. Furthermore, based on the trade-off relationship between the probabilities of false alarm and detection, the achievable sensing-throughput tradeoff is formulated for the secondary network. The sensing-throughput trade-

off for ED was addressed in [68], but only special cases of eigenvalue-based detection, with only 2 receive antennas, were studied in [11]. Hence, in this chapter, we study the optimal sensing time for the sensing-throughput trade-off based on the general case of GLRT detector and compare the results among GLRT detection, MED and ED.

In this chapter, the investigations are summarized as follows:

- This chapter derives the generalized asymptotic closed form expressions of the PDF and cumulative distribution function (CDF) of the test statistic for the general case of the GLRT detector (with an arbitrary number of receive antennas). In addition, the expressions of the decision threshold with regard to the probabilities of false alarm and detection are also derived. Furthermore, taking noise uncertainty into consideration, the expressions of the probabilities of false alarm and detection are also presented.

- The optimization of the studied detectors is conducted from two aspects, including exact and asymptotic analyses. In terms of exact analysis, we investigate optimal decision thresholds for different eigenvalue-based detections, including MED, MME, EME and GLRT detections. A main purpose of spectrum sensing is finding out a sensing threshold to achieve a high probability of detection and a low probability of false alarm. On the one hand, a high probability of detection serves the interests of PUs, which makes PUs well protected. On the other hand, a low probability of false alarm benefits SUs only, which enables SUs to get more chances to access the idle licensed frequency bands. Therefore, it is necessary to minimize the total error rate so that both the interests of PUs and SUs can be considered simultaneously. In terms of asymptotic analysis, we first investigate the optimal decision threshold based on the general case of the GLRT detector. Second, for a given transmit signal, a longer sensing time can provide a larger sample size, which can improve the performance of the detector [51]. However, a long sensing time affects the speed of spectrum sensing. Thus, we also propose a method to determine the minimum sensing time which can satisfy the desired total error rate requirement.

- In addition, the optimal sensing time is determined to maximize the achievable throughput of the secondary network when the PU's benefits are guaranteed simultaneously.

For a fixed periodic spectrum sensing duration, a longer sensing time can improve the sensing performance but it will reduce the data transmission time which is closely related to the achievable throughput of the secondary network. Two scenarios are considered in this chapter for the achievable throughput, including the absence and presence of the noise uncertainty, and the cases of the ED are also presented for comparison.

The remainder of this chapter is organized as follows. Section 3.2 describes the considered system model. Section 3.3 focuses on the exact analysis for various eigenvalue-based detectors and the corresponding optimal decision thresholds are obtained to minimize the total error rate. Section 3.4 investigates the asymptotic analyses for the GLRT detector. Meanwhile, the sensing-throughput trade-off is studied as well in this section. Simulation results are presented in Section 3.5 and Section 3.6 summarizes this chapter.

3.2 System Model

Let us consider a spectrum sensing scenario which consists of m receive antennas. The PU is assumed to be equipped with a single antenna, and the transmitted signal is assumed to have a length of n samples, where $n > m$. Let $\mathcal{H}_0$ (PU is absent) and $\mathcal{H}_1$ (PU is present) denote the null and the alternate hypotheses respectively. During the sensing period, the matrix of received signal samples, $\mathbf{Y} \in \mathbb{C}^{m\times n}$, by the secondary user is

$$\mathcal{H}_0 : \mathbf{Y} = \mathbf{V}, \tag{3.1}$$

$$\mathcal{H}_1 : \mathbf{Y} = \mathbf{h}\mathbf{s}^{\dagger} + \mathbf{V}, \tag{3.2}$$

where $\mathbf{V} \in \mathbb{C}^{m\times n}$ represents the samples from a circular symmetric complex AWGN, where $\mathbf{V} \sim \mathcal{CN}\left(\mathbf{0}, \sigma_v^2\mathbf{I}_m \otimes \mathbf{I}_n\right)$ and $\otimes$ denotes the Kronecker product. $(\cdot)^{\dagger}$ denotes the conjugate transpose of a matrix. $\mathbf{s} \in \mathbb{C}^{n\times 1}$ consists of the transmitted signal samples which are assumed to be circularly symmetric complex Gaussian variables, where $\mathbf{s} \sim \mathcal{CN}(\mathbf{0}, P_{\mathrm{T}}\mathbf{I}_n)$. Finally, $\mathbf{h} \in \mathbb{C}^{m\times 1}$ is the channel vector. Henceforth, the covariance matrix of $\mathbf{Y}$, $\mathbf{R}_{yy} \triangleq \mathbb{E}[\mathbf{Y}\mathbf{Y}^{\dagger}]$, is

given by

$$\mathcal{H}_0 : \quad \mathbf{R}_{yy} = \sigma_v^2 \mathbf{I}_m, \tag{3.3}$$

$$\mathcal{H}_1 : \quad \mathbf{R}_{yy} = P_{\mathrm{T}} \mathbf{h}\mathbf{h}^\dagger + \sigma_v^2 \mathbf{I}_m. \tag{3.4}$$

Within the sensing duration of n samples, the sample covariance matrix estimated from $\mathbf{Y}$ is

$$\widehat{\mathbf{R}}_{yy} = \frac{1}{n} \mathbf{Y}\mathbf{Y}^\dagger. \tag{3.5}$$

Let $\mathbf{W} \in \mathbb{C}^{m \times m}$ be the complex Wishart matrix that is given by $\mathbf{W} = n\widehat{\mathbf{R}}_{yy} = \mathbf{Y}\mathbf{Y}^\dagger$. Also, let $\hat{\lambda}_m < \cdots < \hat{\lambda}_1$ be the eigenvalues, in ascending order, estimated from $\widehat{\mathbf{R}}_{yy}$, i.e., the maximum eigenvalue is $\hat{\lambda}_{\max} = \hat{\lambda}_1$ and the minimum eigenvalue is $\hat{\lambda}_{\min} = \hat{\lambda}_m$. Hence, the test statistics for MED, MME detection, EME detection and GLRT detection are given by:

- the test statistic of MED detector: $T_{\mathrm{MED}} = \hat{\lambda}_{\max}$,
- the test statistic of MME detector: $T_{\mathrm{MME}} = \frac{\hat{\lambda}_{\max}}{\hat{\lambda}_{\min}}$,
- the test statistic of EME detector: $T_{\mathrm{EME}} = \frac{\sum_{i=1}^{m} \hat{\lambda}_i}{\hat{\lambda}_{\min}}$,
- the test statistic of GLRT detector: $T_{\mathrm{GLRT}} = \frac{\hat{\lambda}_{\max}}{\sum_{i=1}^{m} \hat{\lambda}_i}$.

For a given sampling frequency f_{s}, let τ denote the sensing time such that the received number of samples by each receive antenna is $n = \tau f_{\mathrm{s}}$.

Many detectors assume that the exact noise power is known precisely. However, in practice, the precise value of the noise power is difficult to be obtained because of many involved factors. Noise uncertainty is mainly caused by fluctuations of noise power due to nonlinearity of receiver components and the time-varying thermal noise in these components, as well as the transmissions of other users [6, 69]. Thus, the performance of detection methods, that require the exact noise power, can be significantly affected by noise uncertainty, e.g., the ED [70]. Let the estimated noise power be $\hat{\delta}_v^2 = \mu\sigma_v^2$, where μ is the noise uncertainty factor and

the upper bound (in dB) of the noise uncertainty is defined as [6, 71]

$$B = \sup\left\{10\log_{10}\mu\right\}. \tag{3.6}$$

Assuming that noise uncertainty (in dB) is uniformly distributed within the interval $[-B, B]$, then the variation in noise power ranges between $10^{-B/10}$ and $10^{B/10}$.

3.3 Exact Analysis for Eigenvalue-based Detectors

In this section, we investigate the exact optimal sensing thresholds for MED (with an arbitrary number of receive antennas), MME, EME and GLRT detectors (with 2 receive antennas). In order to find the optimal decision threshold $r_{\rm opt}$ and the total error rate $P_{\rm te}$ of the studied eigenvalue-based detectors, the exact CDF (or the PDF) of the corresponding test statistic is required for both cases of $\mathcal{H}_0$ and $\mathcal{H}_1$. Meanwhile, the total error rate $P_{\rm te}$ is given by [14]

$$P_{\rm te} = P_{\rm fa} + P_{\rm m}, \tag{3.7}$$

where $P_{\rm m} = 1 - P_{\rm fa}$.

3.3.1 Optimal Threshold for MED

In this subsection, we present the exact expression of the total error rate $P_{\rm te}$ for MED assuming an arbitrary number of receive antennas. Also, the corresponding optimal decision threshold is analysed by using the derivative of the total error rate. However, in order to get the derivative of $P_{\rm te}$, we have to solve the issue of finding the derivative of a confluent hypergeometric function with a matrix argument. This case was not studied in the literature and only the derivative of the confluent hypergeometric function with a scalar argument is studied before.

Firstly, let us start with the case of $\mathcal{H}_0$, where in this case $\boldsymbol{W} \sim \mathcal{CW}_m(n, \sigma_v^2\boldsymbol{I_m})$. Hence, by making use of the CDF of the maximum eigenvalues of an uncorrelated complex central

Wishart matrix, the probability of false alarm is given by [72]

$$P_{\text{fa}}(x) = 1 - \frac{C\Gamma_m(m)}{C\Gamma_m(n+m)} x^{mn}\ {}_1F_1(n; n+m; -x\sigma_v^2 \boldsymbol{I}), \tag{3.8}$$

where ${}_1F_1\left(.;.;.\right)$ is the matrix-variate confluent hypergeometric function and

$$C\Gamma_m(a) = \pi^{\frac{m(m-1)}{2}} \prod_{k=1}^{m} \Gamma(a-k+1),$$

where $\Gamma(.)$ is the gamma function, $\Re(a) > (m-1) + k_1$, $k = k_1 + k_2 + \cdots + k_m$ and $k_1 \geq \cdots \geq k_m \geq 0$. On the other hand, considering the hypothesis $\mathcal{H}_1$, $\boldsymbol{W} \sim \mathcal{CW}_m(n, \boldsymbol{\Sigma_m})$ and $\boldsymbol{\Sigma_m} = \sigma_x^2 \boldsymbol{h}\boldsymbol{h}^\dagger + \sigma_v^2 \boldsymbol{I_m}$. Therefore, the probability of missed detection is given by [72]

$$P_{\text{m}}(x) = \frac{C\Gamma_m(m) x^{mn}\ {}_1F_1(n; n+m; -x{\boldsymbol{\Sigma_m}}^{-1})}{C\Gamma_m(n+m)(\det \boldsymbol{\Sigma_m})^n}. \tag{3.9}$$

Henceforth, the total error rate P_{te} for MED with an arbitrary number of receive antennas can be obtained by using (3.7). It can be seen from the performance curves shown in Fig. 3.1 that $P_{\text{te}}(x)$ has a global minimum value for x. Also, this implies that there exists one and only one value of x which minimizes $P_{\text{te}}(x)$. Therefore, the optimal decision threshold r_{opt} is given by

$$r_{\text{opt}} = \arg\min_x \ P_{\text{te}}(x), \tag{3.10}$$

which can be achieved when the derivative of the total error rate is $\frac{\mathrm{d}P_{\text{te}}(x)}{\mathrm{d}x} = 0$. The corresponding derivative is obtained as

$$\begin{aligned}
&\frac{\mathrm{d}P_{\text{te}}(x)}{\mathrm{d}x} \\
&= \frac{C\Gamma_m(m)\ {}_1F_1(n; n+m; -x{\boldsymbol{\Sigma_m}}^{-1})}{C\Gamma_m(n+m)(\det \boldsymbol{\Sigma_m})^n} \times \left(mnx^{mn-1} + x^{mn}\Big(\operatorname{tr}(\boldsymbol{C}) - \operatorname{tr}(\boldsymbol{D})\Big)\right) \\
&- \frac{C\Gamma_m(m)\ {}_1F_1(n; n+m; -x\sigma_v^2 \boldsymbol{I_m})}{C\Gamma_m(n+m)} \times \left(mnx^{mn-1} + x^{mn}\Big(\operatorname{tr}(\boldsymbol{A}) - \operatorname{tr}(\boldsymbol{B})\Big)\right),
\end{aligned} \tag{3.11}$$

where the matrices $\boldsymbol{A}, \boldsymbol{B}, \boldsymbol{C}, \boldsymbol{D}$ are given by

$$\begin{aligned}
\boldsymbol{A} &= \Big((-x\sigma_v^2)^{k_j+m-j}\Big)^{-1}\Big(\sigma_v^2(-k_j-m+j)(-\sigma_v^2 x)^{k_j+m-j-1}\Big),\\
\boldsymbol{B} &= \Big((-x\sigma_v^2)^{m-j}\Big)^{-1}\Big(\sigma_v^2(j-m)(-\sigma_v^2 x)^{m-j-1}\Big),\\
\boldsymbol{C} &= \Big((x\beta_i)^{k_j+m-j}\Big)^{-1}\Big(\beta_i(k_j+m-j)(\beta_i x)^{k_j+m-j-1}\Big),\\
\boldsymbol{D} &= \Big((x\beta_i)^{m-j}\Big)^{-1}\Big(\beta_i(m-j)(\beta_i x)^{m-j-1}\Big),
\end{aligned}$$

where $\beta_1, ..., \beta_m$ are the eigenvalues of the matrix $-{\boldsymbol{\Sigma_m}}^{-1}$. The solution to $\frac{\mathrm{d}P_{\mathrm{te}}(x)}{\mathrm{d}x} = 0$ can be evaluated numerically and represents the desired optimal decision threshold.

3.3.2 Optimal Threshold for MME

In this subsection, we derive the exact expression of the total error rate for the MME detector assuming $m = 2$ and show the required steps to obtain the optimal decision threshold. Assuming $\mathcal{H}_0$, the PDF of the test statistic T_{MME} for the case of $m = 2$ is given by[9]

$$f_{\mathrm{MME0}}(x) = \frac{\Gamma(2n)}{\Gamma(n)\Gamma(n-1)}\left(1-\frac{1}{x}\right)^2\left(\frac{1}{x}\right)^n\left(1+\frac{1}{x}\right)^{-2n}. \tag{3.12}$$

By making use of the previous equation (3.12), we derive the probability of false alarm as

$$P_{\mathrm{fa}}(x) = \frac{\Gamma(2n)}{\Gamma(n)\Gamma(n-1)}\Big[\Delta_1(2n, n-1, x) - 2\Delta_1(2n, n, x) + \Delta_1(2n, n+1, x)\Big], \tag{3.13}$$

where $\Delta_1(a, b, y) = \frac{y^{-b}}{b}\,{}_2F_1(a, b; b+1, -y^{-1})$, and ${}_2F_1(.,.;.;.)$ is the Gaussian hypergeometric function. Assuming $\mathcal{H}_1$, $\boldsymbol{W} \sim \mathcal{CW}_2(n, \boldsymbol{\Sigma_2})$, and making use of the results in [72] yields the PDF of the test statistic T_{MME} associated with $\boldsymbol{W}$ as given by

$$\begin{aligned}
f_{\mathrm{MME1}}(x) = {}& \frac{(\delta_1\delta_2)^{1-n}}{(n-1)!(n-2)!(\delta_2-\delta_1)}\\
&\times\Big(\Delta_2(n-1, n-1, 1/\delta_1, 1/\delta_2, x) - \Delta_2(n-2, n, 1/\delta_1, 1/\delta_2, x)\\
&- \Delta_2(n-1, n-1, 1/\delta_2, 1/\delta_1, x) + \Delta_2(n-2, n, 1/\delta_2, 1/\delta_1, x)\Big), \quad x > 1
\end{aligned} \tag{3.14}$$

where

$$\Delta_2(a,b,c,d,y) = -(b-1)!\sum_{k=0}^{b-1}\frac{(a+k)!y^{k-1}(kd-c(a+1)y)}{k!c^{b-k}(cy+d)^{a+k+2}},$$

and $\delta_1 > \delta_2$ are the non-zero ordered eigenvalues of $\mathbf{\Sigma_2}$. The probability of missed detection of the MME detector can then be obtained by

$$P_{\mathrm{m}}(x) = \frac{(\delta_1\delta_2)^{1-n}}{(n-1)!(n-2)!(\delta_2-\delta_1)}\Big(S(x)-S(1)\Big), \tag{3.15}$$

where $x > 1$, and $S(y)$ is given by

$$\begin{aligned} S(y) &= \Delta_3(n-1,n-1,1/\delta_1,1/\delta_2,y) - \Delta_3(n-2,n,1/\delta_1,1/\delta_2,y) \\ &\quad - \Delta_3(n-1,n-1,1/\delta_2,1/\delta_1,y) + \Delta_3(n-2,n,1/\delta_2,1/\delta_1,y) \end{aligned} \tag{3.16}$$

and Δ_3 is given by

$$\Delta_3(a,b,c,d,y) = (b-1)!\times\left(\frac{a!}{c^b d^{a+1}} - \sum_{k=0}^{b-1}\frac{(a+k)!y^k}{k!c^{b-k}(cy+d)^{a+k+1}}\right).$$

Thus, the exact expression of the total error rate P_{te} can be directly obtained from summing (3.13) and (3.15). In order to obtain the optimal decision threshold r_{opt}, the derivative $\frac{\mathrm{d}P_{\mathrm{te}}(x)}{\mathrm{d}x}$ is

$$\frac{\mathrm{d}P_{\mathrm{te}}(x)}{\mathrm{d}x} = \frac{\mathrm{d}(P_{\mathrm{fa}}(x)+P_{\mathrm{m}}(x))}{\mathrm{d}x} = f_{\mathrm{MME1}}(x) - f_{\mathrm{MME0}}(x).$$

The solution to $f_{\mathrm{MME1}}(x) - f_{\mathrm{MME0}}(x) = 0$ can be evaluated numerically and is the desired optimal decision threshold.

3.3.3 Optimal Threshold for EME

In this subsection, the case of the EME detector is considered assuming 2 receive antennas. Since under $\mathcal{H}_0$, $\boldsymbol{W} \sim \mathcal{CW}_2(n, \sigma_v^2\boldsymbol{I_m})$ then the PDF of the test statistic T_{EME} is given by [73]

$$f_{\mathrm{EME0}}(x) = \frac{\Gamma(2n)x^{-2n}(x-1)^{n-2}(x-2)^2}{\Gamma(n)\Gamma(n-1)}, x \geq 2. \tag{3.17}$$

Hence, we derive the probability of false alarm $P_{\rm fa}$ as

$$P_{\rm fa}(x) = 1 - \frac{\Gamma(2n)}{\Gamma(n)\Gamma(n-1)} \sum_{k=0}^{n-2} \binom{n-2}{k} (-1)^{n-2-k} \times \Big(\frac{x^{k-2n+3} - 2^{k-2n+3}}{k-2n+3} - 4\frac{x^{k-2n+2} - 2^{k-2n+2}}{k-2n+2} + 4\frac{x^{k-2n+1} - 2^{k-2n+1}}{k-2n+1} \Big). \quad (3.18)$$

Assuming $\mathcal{H}_1$, and using [74], the PDF of the threshold $T_{\rm EME}$, that is associated with the dual correlated complex central Wishart matrix $\boldsymbol{W} \sim \mathcal{CW}_2(n, \boldsymbol{\Sigma_2})$ is given by

$$f_{\rm EME1}(x) = \frac{\Gamma(2n-1)(\delta_1\delta_2)^{1-n}(x-2)}{\Gamma(n)\Gamma(n-1)(\delta_1-\delta_2)}(x-1)^{n-2} \times \Big(\Delta_4(\delta_1, \delta_2, x)^{1-2n} - \Delta_4(\delta_2, \delta_1, x)^{1-2n} \Big), \quad (3.19)$$

where $x \geq 2$, $\Delta_4(\delta_1, \delta_2, x) = \frac{x-1}{\delta_1} + \frac{1}{\delta_2}, \Delta_4(\delta_2, \delta_1, x) = \frac{x-1}{\delta_2} + \frac{1}{\delta_1}$ and δ_1 and δ_2 are the non-zero ordered eigenvalues of $\boldsymbol{\Sigma_2}$, where $\delta_1 > \delta_2$. Hence, using the CDF in [74] , $P_{\rm m}$ is given by

$$P_{\rm m}(x) = \frac{\Gamma(2n-1)(\delta_1\delta_2)^{1-n}}{\Gamma(n)\Gamma(n-1)(\delta_1-\delta_2)} \times \Big\{ \Delta_5\left(\frac{\delta_1-\delta_2}{\delta_1}, \frac{\delta_2}{\delta_1}, \delta_2, x\right) - \Delta_5\left(\frac{\delta_2-\delta_1}{\delta_2}, \frac{\delta_1}{\delta_2}, \delta_1, x\right) - \Delta_5\left(\frac{\delta_1-\delta_2}{\delta_1}, \frac{\delta_2}{\delta_1}, \delta_2, 2\right) + \Delta_5\left(\frac{\delta_2-\delta_1}{\delta_2}, \frac{\delta_1}{\delta_2}, \delta_1, 2\right) \Big\}, \quad (3.20)$$

where $x \geq 2$, and

$$\Delta_5(a, b, c, x) = \Big(\frac{c}{a}\Big)^{2n-1} \sum_{k=0}^{n-2} \binom{n-2}{k} (-1)^k \times \Big\{ P(n-k-1, b, a, 2n-1, x) - 2P(n-k-2, b, a, 2n-1, x) \Big\}, \quad (3.21)$$

$$P(n, b, a, m, x) = \frac{x^{n+1}}{n+1}\, {}_2F_1\left(m, n+1; n+2; -x\frac{b}{a}\right). \quad (3.22)$$

Thus, the derivative of the total error rate $P_{\rm te}$ is $\frac{{\rm d}P_{\rm te}(x)}{{\rm d}x} = \frac{{\rm d}(P_{\rm fa}(x)+P_{\rm m}(x))}{{\rm d}x} = f_{\rm EME1}(x) - f_{\rm EME0}(x)$ and the solution to $f_{\rm EME1}(x) - f_{\rm EME0}(x) = 0$ is the desired optimal decision threshold.

3.3.4 Optimal Threshold for GLRT

This subsection investigates the case of the optimal threshold for the GLRT detector with 2 receive antennas. Starting with the null hypothesis, and since in this case $\boldsymbol{W} \sim \mathcal{CW}_2(n, \sigma_v^2 \boldsymbol{I_m})$, then using the PDF and CDF in [10], the PDF of the test statistic T_{GLRT} and the probability of false alarm are given by

$$f_{\mathrm{GLRT0}}(x) = \frac{\Gamma(2n)(2x-1)^2}{\Gamma(n)\Gamma(n-1)\left(x(1-x)\right)^{2-n}}, \tag{3.23}$$

$$P_{\mathrm{fa}}(x) = 1 - \frac{\Gamma(2n)\left(\Delta_6(n,x) - \Delta_6(n,\frac{1}{2})\right)}{\Gamma(n)\Gamma(n-1)}, \tag{3.24}$$

where $\frac{1}{2} \leq x \leq 1$ and

$$\Delta_6(n,y) = \sum_{k=0}^{n-2} \begin{pmatrix} n-2 \\ k \end{pmatrix} (-1)^{n-2-k} \times \left\{ \frac{y^{2n-k-3}}{2n-k-3} - 4\frac{y^{2n-k-2}}{2n-k-2} + 4\frac{y^{2n-k-1}}{2n-k-1} \right\}. \tag{3.25}$$

Assuming $\mathcal{H}_1$, we have $\boldsymbol{W} \sim \mathcal{CW}_2(n, \boldsymbol{\Sigma_2})$, and therefore the PDF of T_{GLRT} is given by [10]

$$f_{\mathrm{GLRT1}}(x) = \frac{\left(x\delta_2 + (1-x)\delta_1\right)^{1-2n} - \left(x\delta_1 + (1-x)\delta_2\right)^{1-2n}}{\Gamma(n)\Gamma(n-1)(\delta_1 - \delta_2)\left(x(1-x)\right)^{2-n}} \Gamma(2n-1)(\delta_1\delta_2)^n(2x-1), \tag{3.26}$$

where $\frac{1}{2} \leq x \leq 1$ and $\delta_1 > \delta_2$ are the non-zero ordered eigenvalues of $\boldsymbol{\Sigma_2}$. By applying the binomial expansion and then integrating we derive the probability of missed detection as given by

$$\begin{aligned} P_{\mathrm{m}}(x) = C_{\mathrm{g}} \sum_{k=0}^{n-2} \binom{n-2}{k} (-1)^k \\ \times \Bigg[2\Bigg(\Delta_7\left(\delta_1, 2n-1, k+n, \delta_1-\delta_2, x\right) - \Delta_7\left(\delta_1, 2n-1, k+n, \delta_1-\delta_2, \frac{1}{2}\right) \Bigg) \\ - 2\Bigg(\Delta_7\left(\delta_2, 2n-1, k+n, \delta_2-\delta_1, x\right) - \Delta_7\left(\delta_2, 2n-1, k+n, \delta_2-\delta_1, \frac{1}{2}\right) \Bigg) \\ - \Bigg(\Delta_7(\delta_1, 2n-1, n+k-1, \delta_1-\delta_2, x) - \Delta_7\left(\delta_1, 2n-1, n+k-1, \delta_1-\delta_2, \frac{1}{2}\right) \Bigg) \\ + \Bigg(\Delta_7(\delta_2, 2n-1, n+k-1, \delta_2-\delta_1, x) - \Delta_7\left(\delta_2, 2n-1, n+k-1, \delta_2-\delta_1, \frac{1}{2}\right) \Bigg) \Bigg], \end{aligned} \tag{3.27}$$

where $\frac{1}{2} \leq x \leq 1$ and

$$C_{\mathrm{g}} = \frac{\Gamma(2n-1)(\delta_1\delta_2)^n}{\Gamma(n)\Gamma(n-1)(\delta_1-\delta_2)},$$
$$\Delta_7(a,b,c,d,t) = \frac{a^{-b}t^c}{c}\,{}_2F_1(b,c;1+c;\frac{d}{a}t). \tag{3.28}$$

Therefore, the derivative of the total error rate can be obtained as $\frac{\mathrm{d}P_{\mathrm{te}}(x)}{\mathrm{d}x} = \frac{\mathrm{d}(P_{\mathrm{fa}}(x)+P_{\mathrm{m}}(x))}{\mathrm{d}x} = f_{\mathrm{GLRT1}}(x) - f_{\mathrm{GLRT0}}(x)$ and the solution to $f_{\mathrm{GLRT1}}(x) - f_{\mathrm{GLRT0}}(x) = 0$ is the desired optimal decision threshold.

3.4 Asymptotic Performance Analysis of the GLRT Detector

This section investigates the asymptotic performance analysis of the general case of the GLRT detector. Specifically, expressions of false alarm and detection rates are derived and optimal decision thresholds are obtained as well. Besides, the minimum sensing time is studied for speeding up spectrum sensing and optimal sensing time is investigated to maximize the secondary transmission performance. In addition, the sensing and transmission performance of MED and ED are presented for comparison.

3.4.1 Performance Using GLRT Detector

Considering the GLRT eigenvalue detector, in this subsection we investigate the generalized asymptotic statistical distributions of the decision statistic T_{GLRT}, assuming an arbitrary number of receive antennas. For both hypotheses of $\mathcal{H}_0$ and $\mathcal{H}_1$, the PDF and the CDF of T_{GLRT} are necessary to quantify the performance of the detector and to investigate other performance measures such as the achievable throughput. This is also necessary to obtain optimized versions of the detector such as investigation of the optimal sensing threshold that minimizes the total error rate and the analysis of the minimum sensing time which can make spectrum sensing efficient. Hence, in this part we derive the generalized asymptotic PDF and CDF of T_{GLRT} when $n \gg m$.

3.4.1.1 Statistical Distributions Under Hypothesis $\mathcal{H}_0$

Considering the null hypothesis $\mathcal{H}_0$, an asymptotic expression for the PDF of the test statistic T_{GLRT} is presented in this subsection. The test statistic T_{GLRT} can be rewritten as

$$T_{\mathrm{GLRT}} = \frac{1}{m}\frac{m\hat{\lambda}_{\max}}{\sum_{i=1}^{m}\hat{\lambda}_i} = x. \tag{3.29}$$

Let $z = \frac{m\hat{\lambda}_{\max}}{\sum_{i=1}^{m}\hat{\lambda}_i}$ and $f_z(z)$ denote the PDF of z, therefore $x = g(z) = \frac{z}{m}$ and the PDF of T_{GLRT} can be calculated by

$$f^0_{\mathrm{GLRT}}(x) = \left.\frac{f_z(z)}{\left|\frac{\mathrm{d}}{\mathrm{d}z}\left(g(z)\right)\right|}\right|_{z=mx}, \tag{3.30}$$

where the expression of $f_{\mathrm{z}}(z)$ is referred in [75] and given as

$$f_{\mathrm{z}}(z) = \frac{\Gamma(mn)c^{1-mn}}{m\Gamma(mn-d)\Gamma(d)}\left(\frac{z}{m}\right)^{d-1}\left(c-\left(\frac{z}{m}\right)\right)^{mn-d-1}, \tag{3.31}$$

where c and d are given by

$$c = \frac{0.8132b^2}{a-1.7711b}, \quad d = \frac{(a-1.7711b)^2}{0.8132b^2}, \tag{3.32}$$

where a and b are defined as

$$a = (\sqrt{m}+\sqrt{n})^2, \quad b = (\sqrt{m}+\sqrt{n})\left(\sqrt{\frac{1}{m}}+\sqrt{\frac{1}{n}}\right)^{\frac{1}{3}}. \tag{3.33}$$

Then, by substituting (3.31) and $z = mx$ into (3.30), the expression of the PDF of T_{GLRT} can be obtained as the following proposition.

Proposition 1. *Given the complex central uncorrelated Wishart matrix $\mathbf{W} \sim \mathcal{CW}_m(n, \sigma_v^2\mathbf{I}_m)$, where $m \ll n$, then the PDF of $T_{\mathrm{GLRT}} = \frac{\hat{\lambda}_{\max}}{\sum_{i=1}^{m}\hat{\lambda}_i}$ under the hypothesis $\mathcal{H}_0$ is given by*

$$f^0_{\mathrm{GLRT}}(x) = \frac{\Gamma(mn)c^{1-mn}}{\Gamma(mn-d)\Gamma(d)}x^{d-1}(c-x)^{mn-d-1}, \quad \frac{1}{m} \le x \le 1. \tag{3.34}$$

It is worth mentioning that the parameters a, b, c and d are related to the Tracy-Widom distribution of order 2. Specifically, it is known from [76] that $\frac{\hat{\lambda}_{\max}-a}{b}$ converges to the Tracy-Widom distribution of

order 2 under $\mathcal{H}_0$, when $m \ll n$ and n is large enough. Therefore, the expectation and variance of $\hat{\lambda}_{\max}$ is given as

$$\mathbb{E}[\hat{\lambda}_{\max}] = a - 1.7711b, \quad \mathrm{Var}[\hat{\lambda}_{\max}] = 0.8132b^2, \tag{3.35}$$

where -1.7711 and 0.8132 are the statistical expectation and variance of the Tracy-Widom distribution of order 2. Meanwhile, $\hat{\lambda}_{\max}$ can be approximated well by the Gamma distribution with scale and shape parameters c, d so that

$$\mathbb{E}[\hat{\lambda}_{\max}] = cd, \quad \mathrm{Var}[\hat{\lambda}_{\max}] = c^2 d. \tag{3.36}$$

By using the equations 3.35 and 3.36, the expressions of parameters c and d can be obtained.

By integrating the PDF of the test statistic derived as (3.34) and conducting further manipulations, the asymptotic expression of the CDF of the test statistic T_{GLRT} under the hypothesis $\mathcal{H}_0$ is given by the following corollary.

Corollary 1. *Given the complex central uncorrelated Wishart matrix $\mathbf{W} \sim \mathcal{CW}_m(n, \sigma_v^2 \mathbf{I}_m)$, where $m \ll n$, then the CDF of the test statistic T_{GLRT} under the hypothesis $\mathcal{H}_0$ is given by*

$$F^0_{\mathrm{GLRT}}(x) = \frac{\Gamma(mn)(mc)^{-d}}{d\Gamma(mn-d)\Gamma(d)} \left(\boldsymbol{\Xi}(x) - \boldsymbol{\Xi}\left(\frac{1}{m}\right) \right), \quad \frac{1}{m} \le x \le 1, \tag{3.37}$$

where $\boldsymbol{\Xi}(\cdot)$ is defined by

$$\boldsymbol{\Xi}(y) = {}_2F_1\left(d, 1+d-mn; d+1; \frac{y}{c}\right)(my)^d. \tag{3.38}$$

Using the result from the previous corollary and the definition in (2.3), the probability of false alarm P_{fa} is obtained as

$$P_{\mathrm{fa}}(x) = 1 - F^0_{\mathrm{GLRT}}(x), \quad \frac{1}{m} \le x \le 1. \tag{3.39}$$

Hence, for a complex Gaussian signal, the decision threshold r with respect to the probability of false alarm can be calculated from

$$r = cI^{-1}\left(\frac{\Gamma(mn)(mc)^{-d}}{d\Gamma(mn-d)\Gamma(d)} \left(\boldsymbol{\Xi}\left(\frac{1}{m}\right) + (1-P_{\mathrm{fa}}) \frac{d\Gamma(mn-d)\Gamma(d)}{\Gamma(mn)(mc)^{-d}} \right), d, mn-d \right), \tag{3.40}$$

where $I^{-1}(.,.,.)$ represents the inverse regularised incomplete Beta function [77]. See the provided Appendix for full proof.

Under the assumption of AWGN, the expression of the average probability of false alarm $\overline{P}_{\rm fa}$ is still the same as the expression of the probability of false alarm without considering noise uncertainty, therefore

$$\overline{P}_{\rm fa}(x) = P_{\rm fa}(x). \tag{3.41}$$

3.4.1.2 Statistical Distributions Under Hypothesis $\mathcal{H}_1$

In this part, the asymptotic expressions of the distributions of the ratio $T_{\rm GLRT}$ are derived assuming the alternate hypothesis $\mathcal{H}_1$. In this case, we have $\mathbf{W} \sim \mathcal{CW}_m(n, \mathbf{\Sigma}_m)$. The PDF of the test statistic $T_{\rm GLRT}$ under the hypothesis $\mathcal{H}_1$ is given in the following theorem.

Theorem 1. *Given the complex central correlated Wishart matrix $\mathbf{W} \sim \mathcal{CW}_m(n, \mathbf{\Sigma}_m)$, the PDF of the test statistic $T_{\rm GLRT}$ for GLRT detector under the hypothesis $\mathcal{H}_1$ is derived as*

$$\begin{aligned} f^1_{\rm GLRT}(x) = & \frac{(m-1)\left(1-\frac{1+m\gamma}{mn\gamma}\right)}{\sqrt{\frac{2\pi}{n}}(1+m\gamma)(1-x)^2} \\ & \times \exp\left(-\frac{n}{2}\left[\frac{x(m-1)}{1-x}\left(\frac{1}{1+m\gamma}-\frac{1}{mn\gamma}\right)-\left(1+\frac{m-1}{mn\gamma}\right)\right]^2\right), \end{aligned} \tag{3.42}$$

where γ is the average received SNR of the PU's signals at the secondary user, which is given by

$$\gamma \triangleq \frac{P_{\rm T}\|\mathbf{h}\|^2}{m\sigma_v^2}. \tag{3.43}$$

Proof. The largest eigenvalue $\hat{\lambda}_{\max}$ of the sample covariance matrix follows a Gaussian distribution [78] under the hypothesis $\mathcal{H}_1$, which is given as follows

$$\hat{\lambda}_{\max} \sim \mathcal{N}\left(\lambda_{\max} + \frac{(m-1)\lambda_{\max}\sigma_v^2}{n(\lambda_{\max}-\sigma_v^2)}, \frac{\lambda_{\max}^2}{n}\right), \tag{3.44}$$

where $\lambda_{\max}$ is the maximum eigenvalue of the covariance matrix $\mathbf{R}_{yy}$ under the hypothesis $\mathcal{H}_1$. Since the determinant of the covariance matrix $\det(\mathbf{R}_{yy}) = (\sigma_v^2)^{m-1}(P_{\rm T}\|\mathbf{h}\|^2 + \sigma_v^2)$ and $\lambda_{\max} = \lambda_1 > \lambda_2 = \lambda_3 = \cdots = \lambda_m$, it can be deduced that $\lambda_{\max} = P_{\rm T}\|\mathbf{h}\|^2 + \sigma_v^2$.

The summation of the eigenvalues of the sample covariance matrix $\widehat{\mathbf{R}}_{\mathrm{yy}}$ excluding the maximum eigenvalue can be approximated as [79]

$$\sum_{i=2}^{m} \hat{\lambda}_i \approx (m-1)\left(\sigma_v^2 - \frac{\sigma_v^2 \lambda_{\max}}{(\lambda_{\max} - \sigma_v^2)n}\right) = \psi. \tag{3.45}$$

The test statistic of the GLRT detector can be rewritten as

$$T_{\mathrm{GLRT}} = \frac{\hat{\lambda}_{\max}}{\sum_{i=1}^{m} \hat{\lambda}_i} = \frac{\hat{\lambda}_{\max}}{\hat{\lambda}_{\max} + \sum_{i=2}^{m} \hat{\lambda}_i} = x. \tag{3.46}$$

Thus, it can be obtained that $\hat{\lambda}_{\max} = \frac{x\psi}{1-x}$. Let $\hat{\lambda}_{\max} = z$ and $f_{\hat{\lambda}_{\max}}(z)$ denote the PDF of $\hat{\lambda}_{\max}$, then the generalized PDF of the test statistic T_{GLRT} under $\mathcal{H}_1$ can be derived through

$$f^1_{\mathrm{GLRT}}(x) = \left.\frac{f_{\hat{\lambda}_{\max}}(z)}{\left|\frac{\mathrm{d}}{\mathrm{d}z}\left(\frac{z}{z+\psi}\right)\right|}\right|_{z=\frac{x\psi}{1-x}}, \tag{3.47}$$

after further manipulation, the expression of the PDF of T_{GLRT} can be derived as (3.42). □

Hence, by making use of the result from the previous theorem, the asymptotic expression of the CDF of the test statistic T_{GLRT} is given in the following corollary.

Corollary 2. *Given the complex central correlated Wishart matrix $\mathbf{W} \sim \mathcal{CW}_m(n, \mathbf{\Sigma}_m)$, the CDF of the test statistic T_{GLRT} for the GLRT detector under the hypothesis $\mathcal{H}_1$ is expressed as*

$$F^1_{\mathrm{GLRT}}(x) = \frac{1}{2}\left[\Phi\left(\alpha\sqrt{\beta} + \frac{x}{2\sqrt{\beta}(1-x)}\right) - \Phi\left(\alpha\sqrt{\beta} + \frac{1}{2(m-1)\sqrt{\beta}}\right)\right], \tag{3.48}$$

where $\Phi(y) \triangleq \frac{2}{\sqrt{\pi}} \int_0^y e^{-t^2} \mathrm{d}t$ denotes the error function, α and β are given by

$$\alpha = n(m-1)\left(\frac{1}{mn\gamma} - \frac{1}{1+m\gamma}\right)\left(1 + \frac{m-1}{mn\gamma}\right), \tag{3.49}$$

$$\beta = \frac{1}{2n(m-1)^2}\left(\frac{1}{1+m\gamma} - \frac{1}{mn\gamma}\right)^{-2}. \tag{3.50}$$

Hence, the probability of detection can be expressed as

$$P_{\mathrm{d}}(x) = 1 - F^1_{\mathrm{GLRT}}(x), \quad \frac{1}{m} \leq x \leq 1. \tag{3.51}$$

Besides, we also derive the expression for calculating the decision threshold in terms of the probability of detection, which is given by

$$r=\left(\frac{1}{2}\left(\sum_{k=0}^{\infty}\frac{C_k\sqrt{\beta}}{2k+1}\left[\frac{\sqrt{\pi}}{2}\Phi\left(\alpha\sqrt{\beta}+\frac{1}{2(m-1)\beta}\right)+\sqrt{\pi}(1-P_{\mathrm{d}})\right]^{2k+1}-\alpha\beta\right)^{-1}+1\right)^{-1}, \tag{3.52}$$

where the coefficient $C_k=\begin{cases}1, & k=0,\\ \sum_{i=0}^{k-1}\frac{C_iC_{k-1-i}}{(i+1)(2i+1)}, & otherwise.\end{cases}$

Furthermore, taking noise uncertainty into account, the expected probability of detection $\overline{P}_{\mathrm{d}}$ can be obtained by

$$\overline{P}_{\mathrm{d}}(x)=\int_{10^{-B/10}}^{10^{B/10}}\left(1-\frac{1}{2}\left[\Phi\left(\breve{\alpha}\sqrt{\breve{\beta}}+\frac{x}{2\sqrt{\breve{\beta}}(1-x)}\right)-\Phi\left(\breve{\alpha}\sqrt{\breve{\beta}}+\frac{1}{2(m-1)\sqrt{\breve{\beta}}}\right)\right]\right)\frac{5}{Bt\ln(10)}\mathrm{d}t, \tag{3.53}$$

where $\breve{\alpha}$ and $\breve{\beta}$ are given by

$$\breve{\alpha}=n(m-1)\left(\frac{1}{mnt\gamma}-\frac{1}{1+mt\gamma}\right)\left(1+\frac{m-1}{mnt\gamma}\right), \tag{3.54}$$

$$\breve{\beta}=\frac{1}{2n(m-1)^2\left(\frac{1}{1+mt\gamma}-\frac{1}{mnt\gamma}\right)^2}. \tag{3.55}$$

3.4.2 Performance Using MED

The test statistic of the maximum eigenvalue detection is defined as the largest eigenvalue of the sample covariance matrix $\widehat{\mathbf{R}}_{yy}$, Meanwhile, the maximum eigenvalue of $n\widehat{\mathbf{R}}_{yy}$ under the hypothesis $\mathcal{H}_0$ was approximated tightly by using Gamma distribution in [75], hence the probability of false alarm for MED in the absence of noise uncertainty can be easily obtained as

$$P_{\mathrm{fa}}(x)=1-\frac{\gamma\left(d,\frac{nx}{c\sigma_v^2}\right)}{\Gamma(d)}, \tag{3.56}$$

where $\gamma(\cdot,\cdot)$ denotes the lower incomplete Gamma function and c,d are defined in (3.32). Meanwhile, the largest eigenvalue $\hat{\lambda}_{\max}$ of the sample covariance matrix $\widehat{\mathbf{R}}_{yy}$ follows a Gaussian distribution [78]

under the hypothesis $\mathcal{H}_1$, therefore the probability of detection for MED in the absence of noise uncertainty can be given by

$$P_{\mathrm{d}}(x) = Q\left(\frac{\frac{x}{\sigma_v^2} - m\gamma - 1 - \frac{(m-1)(m\gamma+1)}{mn\gamma}}{m\gamma+1}\sqrt{n}\right). \tag{3.57}$$

Based on the above expressions, the expected probabilities of false alarm $\overline{P}_{\mathrm{fa}}$ and detection $\overline{P}_{\mathrm{d}}$ for MED in the presence of noise uncertainty are derived as

$$\overline{P}_{\mathrm{fa}}(x) = \int_{10^{-B/10}}^{10^{B/10}} \left(1 - \frac{\gamma\left(d, \frac{nxt}{c\sigma_v^2}\right)}{\Gamma(d)}\right) \frac{5}{Bt\ln(10)}\mathrm{d}t, \tag{3.58}$$

$$\overline{P}_{\mathrm{d}}(x) = \int_{10^{-B/10}}^{10^{B/10}} Q\left(\frac{\frac{xt}{\sigma_v^2} - m\gamma t - 1 - \frac{(m-1)(m\gamma t+1)}{mn\gamma t}}{m\gamma t+1}\sqrt{n}\right) \frac{5}{Bt\ln(10)}\mathrm{d}t. \tag{3.59}$$

3.4.3 Performance Using ED

The statistical distributions of the test statistic of the energy detector were derived in [80] and assuming noise uncertainty in [11]. Considering the system model employed in this chapter, the decision statistic T_{ED} is the average power at the end of the sensing period which is given by

$$T_{\mathrm{ED}} = \frac{1}{n}\sum_{i=1}^{m} w_i \sum_{j=1}^{n} |y_i(j)|^2, \tag{3.60}$$

where w_i is the weighting factor and the equal gain combining scheme is employed for ED such that $w_i = \frac{1}{m}$. Detection of PUs is performed by comparing the average received power with the noise power when the noise power is assumed to be known. Without noise uncertainty, the probability of false alarm P_{fa} and the probability of detection P_{d} for the ED are given by

$$P_{\mathrm{fa}}(x) = Q\Big((x-1)\sqrt{mn}\Big), \tag{3.61}$$

$$P_{\mathrm{d}}(x) = Q\left((x-1-\gamma)\left(\frac{m\gamma^2+2\gamma+1}{mn}\right)^{-\frac{1}{2}}\right). \tag{3.62}$$

Based on the equations of P_{fa} and P_{d} for ED above, we can obtain the expressions to calculate the decision thresholds in terms of the probabilities of false alarm and detection respectively, which are

given as follows

$$r = \frac{Q^{-1}(P_{\mathrm{fa}})}{\sqrt{mn}} + 1, \tag{3.63}$$

$$r = \sqrt{\frac{m\gamma^2 + 2\gamma + 1}{mn}} Q^{-1}(P_{\mathrm{d}}) + 1 + \gamma, \tag{3.64}$$

where $Q^{-1}(\cdot)$ stands for the inverse Q-function. For the case in which the noise uncertainty is assumed, the expected probabilities of false alarm $\overline{P}_{\mathrm{fa}}$ and detection $\overline{P}_{\mathrm{d}}$ for ED are obtained as[11]

$$\overline{P}_{\mathrm{fa}}(x) = \int_{10^{-B/10}}^{10^{B/10}} Q\left((xt-1)\sqrt{mn}\right) \frac{5}{Bt\ln(10)} \mathrm{d}t, \tag{3.65}$$

$$\overline{P}_{\mathrm{d}}(x) = \int_{10^{-B/10}}^{10^{B/10}} Q\left(\frac{xt-1-\gamma t}{\sqrt{\frac{m\gamma^2 t^2 + 2\gamma t + 1}{mn}}}\right) \frac{5}{Bt\ln(10)} \mathrm{d}t. \tag{3.66}$$

3.4.4 Optimization of Spectrum Sensing Based on GLRT Detector

In this subsection, we consider optimization of the GLRT eigenvalue detector based on two criteria. In the previous work, only the constant false alarm rate scenario was considered, which only considered the interests of SUs, so that the benefits of PUs were neglected. In this part, we investigate the optimal decision threshold that can make the total error rate achieve the minimum value with constraints of target probabilities of false alarm and missed detection. Therefore, the benefits of PUs and SUs can be guaranteed simultaneously. Moreover, the minimum sensing time is analysed, which enables the minimum total error rate to achieve the desired value speedily. According to the IEEE 802.22 standard for WRANs, the SUs have to vacate the licensed frequency bands as soon as possible once the PUs are active in order to avoid the harmful interference to PUs. Therefore, it is of significance to the CR system to complete the spectrum sensing process within the shortest sensing time while guaranteeing the target total error rate.

3.4.4.1 Optimal Decision Threshold Analysis

In this part, the optimal decision threshold is investigated. The optimal decision threshold can minimize the total error rate P_{te} with the constraints of target P_{fa} and P_{m}. Let us assume that the number of the receive antennas m, the width of the sensing windows n, and the average received SNR of the PU's signals measured at the secondary user γ are known. Hence, the optimal decision threshold r_{opt}

can be determined. The total error rate is defined as the summation of the probabilities of false alarm and missed detection, .i.e,

$$P_{\mathrm{te}}(r) = P_{\mathrm{fa}}(r) + P_{\mathrm{m}}(r), \tag{3.67}$$

where

$$P_{\mathrm{m}}(r) = 1 - P_{\mathrm{d}}(r). \tag{3.68}$$

It can be seen that the total error rate $P_{\mathrm{te}}(r)$ decreases first and then increases monotonically and this implies that there exists one and only one value of r which minimizes $P_{\mathrm{te}}(r)$ under the constraints of target probabilities of false alarm and missed detection. Therefore, the optimal decision threshold r_{opt} with constraints is given by

$$r_{\mathrm{opt}} = \arg\min_{x} \; P_{\mathrm{te}}(x), \tag{3.69}$$

$$\text{s.t.} \quad P_{\mathrm{fa}}(x) \leq \xi_{\mathrm{fa}}, \tag{3.70}$$

$$P_{\mathrm{m}}(x) \leq \xi_{\mathrm{m}}, \tag{3.71}$$

where ξ_{fa} and ξ_{m} are the desired values of P_{fa} and P_{m} respectively. An appropriate decision threshold r can achieve the desired value of probability of false alarm P_{fa}, but the corresponding probability of missed detection P_{m} may not meet an acceptable value concurrently. Therefore, in practical applications, it is essential to find an optimal decision threshold r_{opt} that minimizes the total error rate with constraints. This can lead to the minimum total error rate and also make both P_{fa} and P_{m} meet the acceptable values simultaneously.

In order to make sure there exist feasible solutions to the above optimization issue, it is necessary to check whether the solutions to the two constraints have intersections. Specifically, the solution to $P_{\mathrm{fa}}(x) = \xi_{\mathrm{fa}}$ has to be smaller than the solution to $P_{\mathrm{m}}(x) = \xi_{\mathrm{m}}$, otherwise, there is no feasible solution. The appearance of this unsolvable case indicates that at least one of the two target error rates ξ_{fa} and ξ_{m} is assigned an excessively low value. One of the possible ways to guarantee the feasible solutions under the excessively low ξ_{fa} and ξ_{m} is increasing the number of sensing antennas and the sample size. However, this thesis does not consider this optimization issue with too low individual error rate targets, but this could be further studied as a possible future research direction.

The total error rate function is a quasi-convex function, so only one global minimum exists and no

local minimum exists. The derivative of the objective function P_{te} is given by

$$\begin{aligned}\frac{\mathrm{d}P_{\mathrm{te}}(x)}{\mathrm{d}x} =& \frac{(m-1)\left(1-\frac{1+m\gamma}{mn\gamma}\right)}{\sqrt{\frac{2\pi}{n}}(1+m\gamma)(1-x)^2}\exp\left(-\frac{n}{2}\left[\frac{x(m-1)}{1-x}\left(\frac{1}{1+m\gamma}-\frac{1}{mn\gamma}\right)-\left(1+\frac{m-1}{mn\gamma}\right)\right]^2\right) \\ &- \frac{\Gamma(mn)c^{1-mn}}{\Gamma(mn-d)\Gamma(d)}x^{d-1}(c-x)^{mn-d-1}, \quad \frac{1}{m}\leq x\leq 1. \end{aligned} \tag{3.72}$$

On the defined interval $x\in\left[\frac{1}{m},1\right]$, the above function is not monotonic. However, one necessary and sufficient condition of convex functions is the first order derivative has to be non-decreasing within an interval [81]. Thus, the objective function P_{te} is non-convex. Based on the definition of total error rate, P_{te} is the summation of the CDF of decision threshold under $\mathcal{H}_1$ and the complementary CDF under $\mathcal{H}_0$, so that the total error rate decreases initially and then increases with the increasing decision threshold [14]. Therefore, it can be deduced that, for $\forall t\in[0,1]$, all the solutions to $P_{\mathrm{te}}(x)\leq t$ are in a convex set, which implies that the function P_{te} is a quasi-convex function within the defined interval [82].

According to the discussion above, the optimal decision threshold r_{opt} can be obtained numerically by utilizing the Karush-Kuhn-Tucker (KKT) conditions [83, 84], then the optimization of the decision threshold can be reformulated as follows

$$(1+\eta_2)f^1_{\mathrm{GLRT}}(x)-(1+\eta_1)f^0_{\mathrm{GLRT}}(x)=0, \tag{3.73}$$

$$P_{\mathrm{fa}}(x)\leq\xi_{\mathrm{fa}}, \tag{3.74}$$

$$P_{\mathrm{m}}(x)\leq\xi_{\mathrm{m}}, \tag{3.75}$$

$$\eta_1\left(P_{\mathrm{fa}}(x)-\xi_{\mathrm{fa}}\right)=0, \tag{3.76}$$

$$\eta_2\left(P_{\mathrm{m}}(x)-\xi_{\mathrm{m}}\right)=0, \tag{3.77}$$

$$\eta_1,\eta_2\geq 0, \tag{3.78}$$

where η_1 and η_2 are the KKT multipliers. Specifically, this converted optimization issue can be solved by utilizing the CVX toolbox for dual problem in MATLAB and the optimal decision threshold can be obtained [85, 86]. Since the primal objective function P_{te} is quasi-convex, not convex, there may exist a gap between the factual optimal point and the solution obtained through the KKT conditions. However, the objective function $P_{\mathrm{te}}(x)$ and the constraints $P_{\mathrm{fa}}(x)-\xi_{\mathrm{fa}}$, $P_{\mathrm{m}}(x)-\xi_{\mathrm{m}}$ are all twice differential. Thus, the global optimality of the solution from the KKT conditions can be checked through the Second-order Sufficient Optimality Conditions (SSOC) [87].

3.4.4.2 Minimum Sensing Time Analysis

In this part, the minimum sensing time duration is investigated. Generally, a longer sensing time provides a larger number of received samples, which is helpful to achieve a better sensing performance to some extent. However, in real time, very long sensing periods may affect the speed of the spectrum sensing process. In order to address this issue, we propose a method to get the minimum sensing time which can make the total error rate achieve the desired value. Assuming that the average received SNR γ and the optimal decision threshold $r_{\rm opt}$ are known, the minimum sensing time $\tau_{\rm min}$ can be determined, which can satisfy the desired total error rate, i.e., $P_{\rm te} \leq \xi$.

For a given transmit signal, the sampling frequency is known, thus the minimum number of samples should be determined first in order to obtain the minimum sensing time. Let us define the objective function as a function of the number of samples n as

$$F(n, r_{\rm opt}) = P_{\rm te}(n, r_{\rm opt}) - \xi, \tag{3.79}$$

where $r_{\rm opt}$ is as defined in last subsection. The desired minimum number of samples $n_{\rm min}$ should satisfy the conditions

$$F(n_{\rm min}, r_{\rm opt}) \leq 0, \tag{3.80}$$

$$F(n_{\rm min} - 1, r_{\rm opt}) > 0, \tag{3.81}$$

where $n_{\rm min}$ is the minimum sample size that enables $P_{\rm te}(n, r_{\rm opt}) \leq \xi$. In order to obtain $n_{\rm min}$, it is necessary to find the first zero-crossing point of the curve $F(n, r_{\rm opt})$ with respect to n which is denoted by n^*. Specifically, n^* can be obtained by solving $F(n_{\rm min}, r_{\rm opt}) = 0$. It is probable that the obtained n^* is not an integer, however $n_{\rm min}$ has to be computed through ceiling operator in order to satisfy the conditions in (3.80) and (3.81). Meanwhile, this manipulation can be given by

$$n_{\rm min} = \lceil n^* \rceil. \tag{3.82}$$

By utilizing the relation between the sample size n and the sensing time, the desired sensing time can be obtained as $\tau_{\rm min} = n_{\rm min}/f_{\rm s}$. Therefore, the minimum sensing time $\tau_{\rm min}$ can be used for a spectrum sensing process so that the speed of spectrum sensing can be improved and the target total error rate can be also guaranteed at the same time.

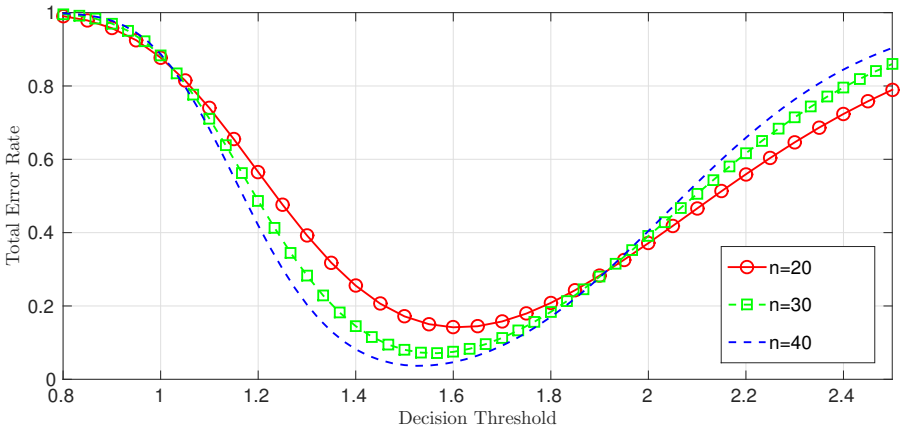

Figure 3.1: *The total error rate of MED (m=2, SNR=0 dB) v.s. decision threshold*

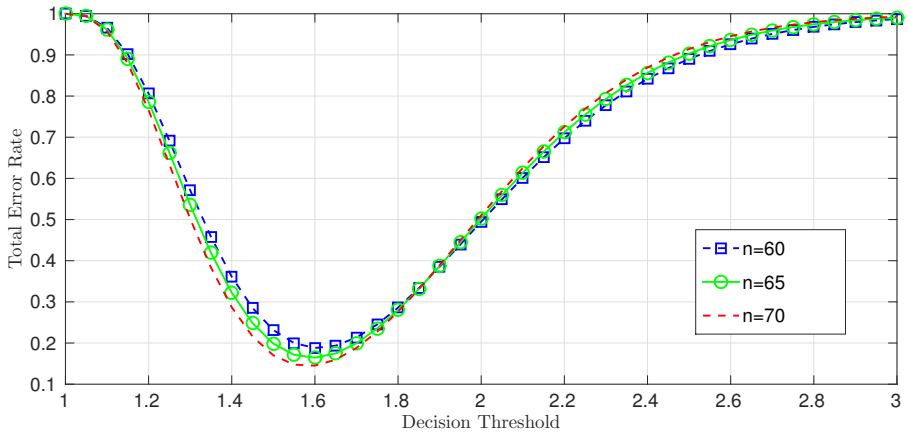

Figure 3.2: *The total error rate of MME detector (m=2, SNR=-5 dB) v.s. decision threshold*

3.4.5 Sensing-throughput Trade-off Analysis

The achievable throughput of the secondary network for the GLRT detector is analysed in this subsection. We focus on the optimal sensing time which enables the achievable throughput of the secondary network to achieve the maximum value while the PUs are protected sufficiently. Two scenarios are considered in this investigation, including the absence and the presence of noise uncertainty. For a cognitive radio network, one periodic spectrum sensing frame T consists of two parts which are the sensing period τ and the data transmission slot $(T - \tau)$. The secondary users can access the unlicensed frequency bands and transmit data in two cases. In detail, one case occurs when the primary user is inactive and the secondary user detects its absence correctly. The other case occurs when the primary user is active but the secondary user fails to detect its presence. The optimization issue of the

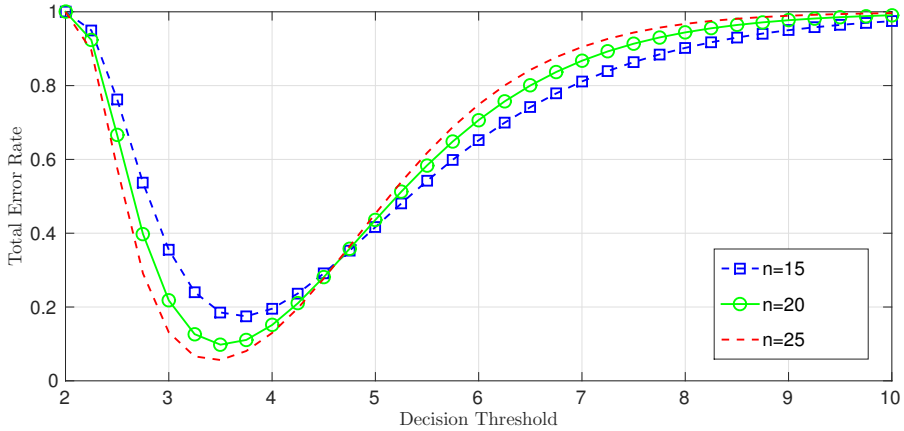

Figure 3.3: *The total error rate of EME detector (m=2, SNR=0 dB) v.s. decision threshold*

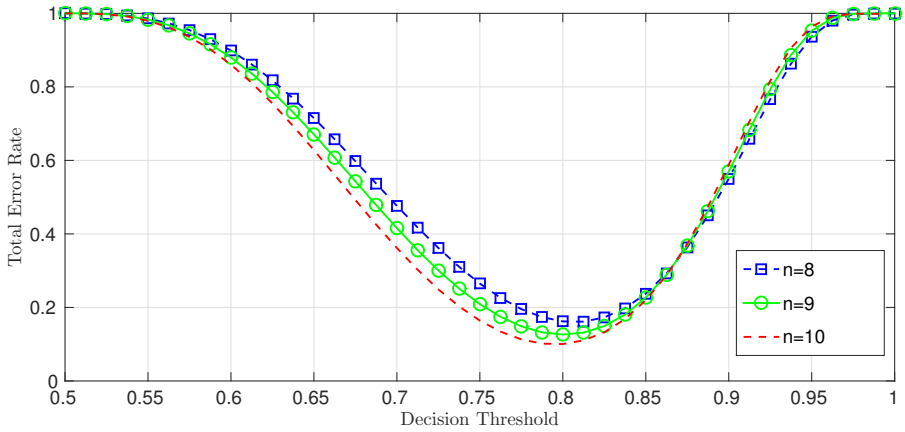

Figure 3.4: *The total error rate of GLRT detector (m=2, SNR=0 dB) v.s. decision threshold*

achievable throughput of the secondary network can be formulated as

$$\max_{\tau} \quad R(r,\tau) = R_0(r,\tau) + R_1(r,\tau) \tag{3.83}$$

$$\text{s.t.} \quad P_{\mathrm{d}}(r,\tau) \geq P_{\mathrm{d}}^{*}, \tag{3.84}$$

where $R_0(r,\tau)$ and $R_1(r,\tau)$ represent the achievable throughput when the primary users are absent and present, respectively. P_{d}^{*} is the desired probability of detection which can make the primary users have sufficient protection.

Suppose both the primary user's signal and the secondary user's signal are Gaussian and they are independent of each other. The SNR of the secondary link is defined as $SNR_s = \frac{\mathcal{P}_{\mathrm{s}}}{\mathcal{P}_{\mathrm{n}}}$, where $\mathcal{P}_{\mathrm{s}}$

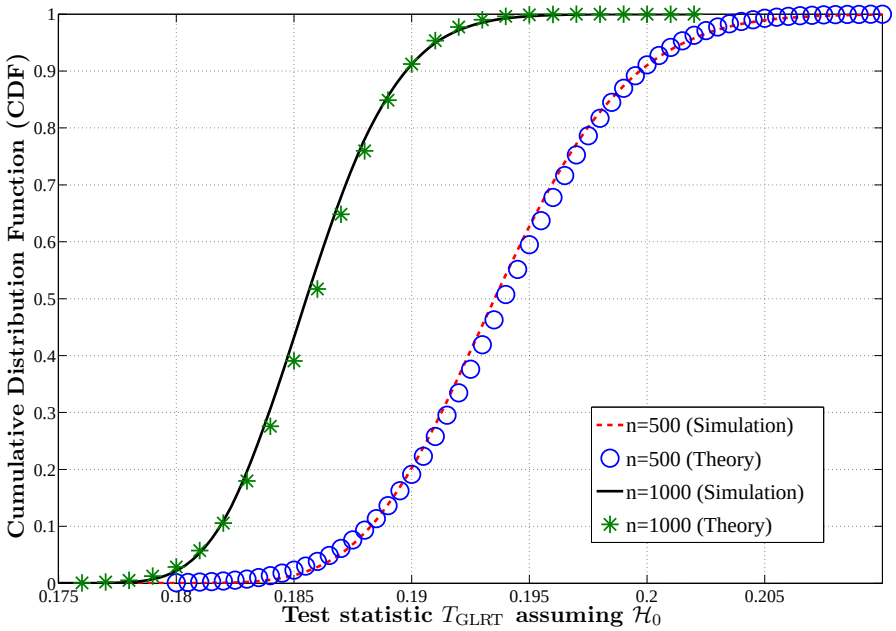

Figure 3.5: *The CDF of the GLRT detector under the hypothesis* $\mathcal{H}_0$ *with* $m = 6$.

denotes the average power of the secondary transmitter that is received at the secondary receiver, and $\mathcal{P}_{\mathrm{n}}$ denotes the noise power. Meanwhile, as noted in the previous section, γ denotes the received SNR at the secondary receiver, which can also be expressed as $\gamma = \frac{\mathcal{P}_{\mathrm{p}}}{\mathcal{P}_{\mathrm{n}}}$, where $\mathcal{P}_{\mathrm{p}}$ denotes the average power of the primary transmitter that is measured at the secondary receiver. Henceforth, the throughput of the secondary network in the absence of the PU is $C_0 = \log_2(1 + \frac{\mathcal{P}_{\mathrm{s}}}{\mathcal{P}_{\mathrm{n}}}) = \log_2(1 + SNR_s)$ and the throughput of the secondary network in the presence of the PU is $C_1 = \log_2(1 + \frac{\mathcal{P}_{\mathrm{s}}}{\mathcal{P}_{\mathrm{p}}+\mathcal{P}_{\mathrm{n}}}) = \log_2(1 + \frac{SNR_{\mathrm{s}}}{1+\gamma})$. It is obvious that $C_0 > C_1$.

Let $P(\mathcal{H}_0)$ and $P(\mathcal{H}_1)$ be the probabilities that the PU is absent and present respectively. We can obtain the achievable sensing throughput of the secondary network with the absence and presence of the primary user respectively as

$$R_0(r,\tau) = \frac{T-\tau}{T} C_0 \left(1 - P_{\mathrm{fa}}(r,\tau)\right) P(\mathcal{H}_0), \tag{3.85}$$

$$R_1(r,\tau) = \frac{T-\tau}{T} C_1 \left(1 - P_{\mathrm{d}}(r,\tau)\right) P(\mathcal{H}_1). \tag{3.86}$$

where $P(\mathcal{H}_1) + P(\mathcal{H}_0) = 1$ and the expressions of $P_{\mathrm{fa}}(r,\tau)$ and $P_{\mathrm{d}}(r,\tau)$ can be obtained easily by replacing n and x of $P_{\mathrm{fa}}(x)$ and $P_{\mathrm{d}}(x)$ by τf_{s} and r, respectively. Generally, it is reasonable to suppose that the presence probability of the primary user $P(\mathcal{H}_1)$ is small based on the fact that

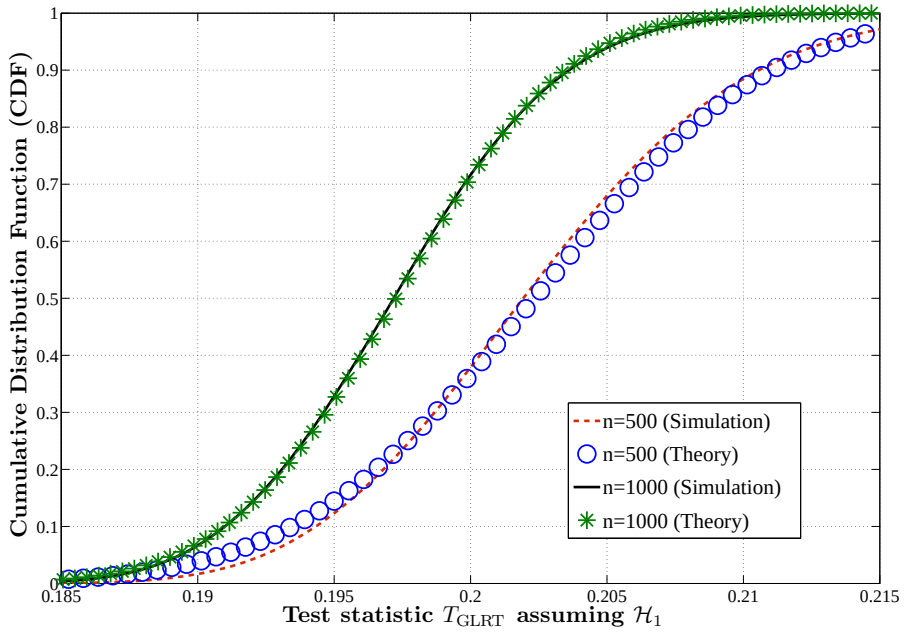

Figure 3.6: *The CDF of the GLRT detector under the hypothesis* $\mathcal{H}_1$ *with* $m = 6$ *and* $\gamma = -15\mathrm{dB}$.

spectrum resource is highly underutilized at some locations and time slots, since a very high $P(\mathcal{H}_1)$ will lead to a very low probability to access the unlicensed frequency band for the secondary user. Based on these assumptions, it can be found that $R_0 \gg R_1$. Thus, the achievable throughput of the secondary network in (3.83) and (3.84) can be simplified as

$$\max_{\tau} \; R(r,\tau) = R_0(r,\tau) \tag{3.87}$$

$$\text{s.t.} \quad P_{\mathrm{d}}(r,\tau) \geq P_{\mathrm{d}}^{*}. \tag{3.88}$$

In order to optimize the sensing time for the achievable throughput, the optimum decision threshold should be determined first. It can be proven that the optimal decision threshold solution to (3.87) and (3.84) is achieved when the equality constraint in (3.84) is satisfied, which means that the chosen decision threshold r_{d} should satisfy $P_{\mathrm{d}}(r_{\mathrm{d}},\tau) = P_{\mathrm{d}}^{*}$. Since, for a given sensing time τ, both $P_{\mathrm{d}}(r,\tau)$ and $P_{\mathrm{fa}}(r,\tau)$ are monotonically decreasing functions. If the arbitrary decision threshold r_{a} satisfies $P_{\mathrm{d}}(r_{\mathrm{a}},\tau) > P_{\mathrm{d}}^{*}$, then $r_{\mathrm{a}} < r_{\mathrm{d}}$ and $P_{\mathrm{fa}}(r_{\mathrm{a}},\tau) > P_{\mathrm{fa}}(r_{\mathrm{d}},\tau)$. From equation (3.87), it can be obtained that $R(r_{\mathrm{a}},\tau) < R(r_{\mathrm{d}},\tau)$. Thus, the optimal solution to the formulation in (3.87) and (3.84) should be achieved with the equality constraint in (3.84). Similarly, it can also be demonstrated that the optimal

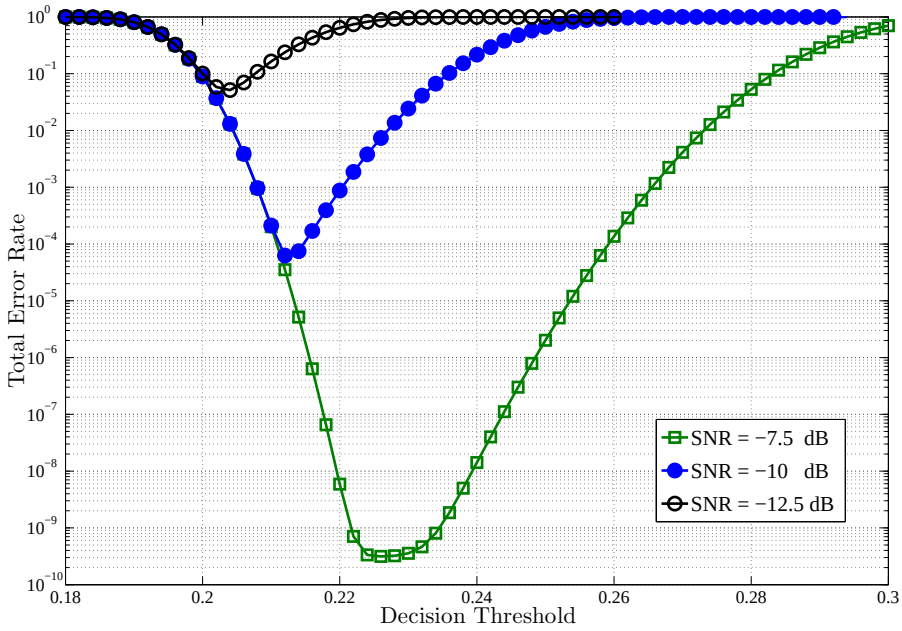

Figure 3.7: *The total error rate of the GLRT detector with multiple antennas ($m = 6$ and $n = 500$) under different received SNRs.*

solution to (3.83) and (3.84) is achieved when the equality constraint in (3.84) is fulfilled.

When the noise uncertainty is not considered, the achievable throughput of the secondary network can be calculated as follows.

- (1) First, the optimum decision threshold r_{d} can be obtained by computing the equality constraint in (3.84) for a target probability of detection P_{d}^{*}.
- (2) Second, the corresponding value of $P_{\mathrm{fa}}(r,\tau)$ can be determined by substituting the value of r_{d} obtained in the first step.
- (3) Finally, the achievable throughput of the secondary network can be calculated by substituting the value of $P_{\mathrm{fa}}(r,\tau)$ obtained in the second step into (3.87).

Similarly, considering noise uncertainty, the achievable throughput of the secondary network can be calculated by using $\overline{P}_{\mathrm{fa}}(r,\tau)$ and $\overline{P}_{\mathrm{d}}(r,\tau)$ instead of $P_{\mathrm{fa}}(r,\tau)$ and $P_{\mathrm{d}}(r,\tau)$ during the above calculation steps, respectively. Meanwhile, the expressions of $\overline{P}_{\mathrm{fa}}(r,\tau)$ and $\overline{P}_{\mathrm{d}}(r,\tau)$ can be obtained easily through replacing n and x of $\overline{P}_{\mathrm{fa}}(x)$ and $\overline{P}_{\mathrm{d}}(x)$ by τf_{s} and r, respectively.

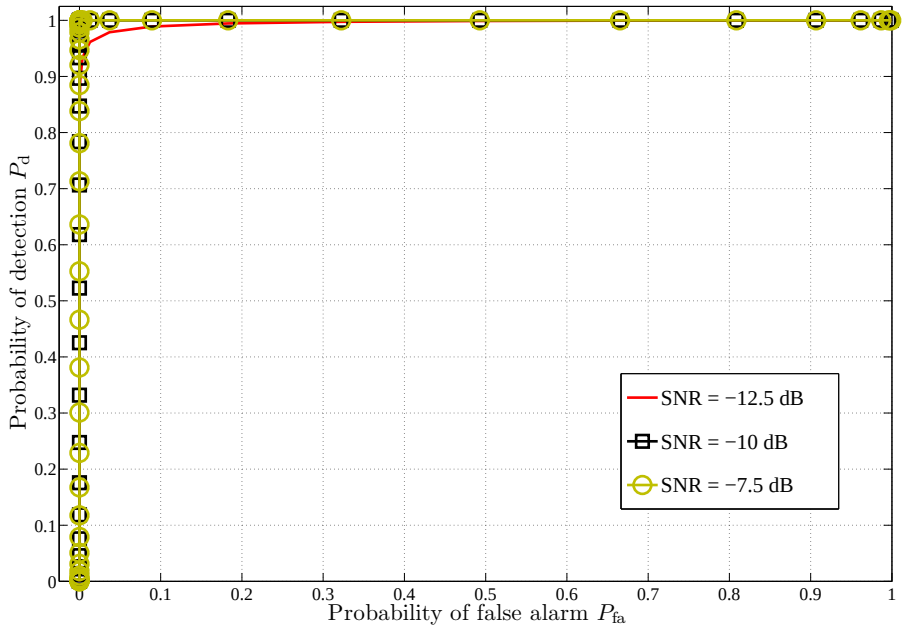

Figure 3.8: *The ROC curves of the GLRT detector with multiple antennas ($m = 6$ and $n = 500$) under different received SNRs.*

3.5 Simulation Results

In this section, simulation results are provided to validate the obtained results throughout this chapter. Meanwhile, more insights will be provided into the optimal decision threshold, the minimum sensing time and the achievable sensing throughput trade-off analysis.

3.5.1 Exact Optimal Decision Threshold

Exact optimal decision thresholds are presented in this subsection for various eigenvalue-based detectors. The calculation of the matrix-variate confluent complex hypergeometric function utilizes MATLAB code provided by [88]. Starting with the case of MED, Fig. 3.1 depicts the total error rate versus the decision threshold. The results are plotted for different sample sizes $n = \{20, 30, 40\}$ while SNR$= 0$dB and $\boldsymbol{\Sigma_m} = \left(\begin{smallmatrix} 2 & 0 \\ 0 & 1.3 \end{smallmatrix}\right)$. The results show the corresponding optimal decision thresholds are $r_{\rm opt} = \{1.60, 1.57, 1.53\}$ which make total error rate at $P_{\rm te} = \{0.14, 0.07, 0.04\}$.

Fig. 3.2 shows the total error rate of MME detection versus the threshold. The simulation parameters are $n = \{60, 65, 70\}$, SNR $= -5$dB and $\boldsymbol{\Sigma_m} = \left(\begin{smallmatrix} 1.7 & -0.3+0.2i \\ -0.3-0.2i & 1.2 \end{smallmatrix}\right)$. Here we can indicate the

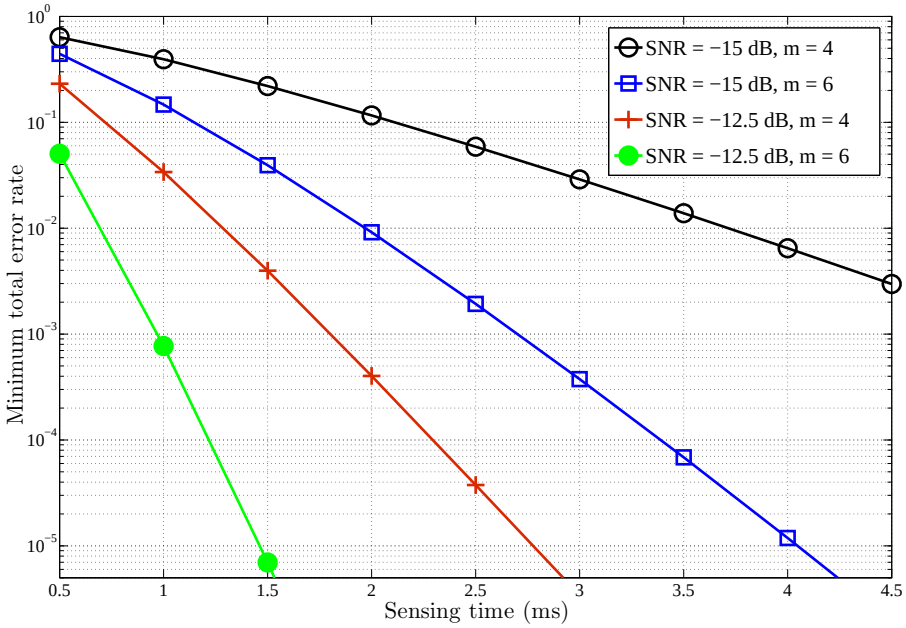

Figure 3.9: *The minimum total error rate versus sensing time of the GLRT detector with multiple antennas ($m = 4$, $m = 6$) under different values of the received SNR ($\gamma = -15$dB, $\gamma = -12.5$dB).*

optimal decision threshold is $r_{\text{opt}} = 1.6$, where $P_{\text{te}} = \{0.19, 0.16, 0.15\}$. Fig. 3.3 illustrates the total error rate of EME detection versus the threshold using $n = \{15, 20, 25\}$ when $\text{SNR} = 0\text{dB}$ and $\boldsymbol{\Sigma_m} = \left(\begin{smallmatrix} 3.3 & -0.9+0.7i \\ -0.9-0.7i & 1.6 \end{smallmatrix}\right)$. Here we can find the optimal decision threshold is $r_{\text{opt}} = 3.75$ for $n = 15$ and $r_{\text{opt}} = 3.5$ for $n = \{20, 25\}$. The corresponding total error rates are $P_{\text{te}} = \{0.17, 0.09, 0.06\}$. Finally, Fig. 3.4 shows the total error rate of the GLRT detector versus the threshold, assuming $n = \{8, 9, 10\}$ when $\text{SNR} = 0\text{dB}$ and $\boldsymbol{\Sigma_m} = \left(\begin{smallmatrix} 1.9 & 0.55+2.1i \\ 0.55-2.1i & 6.2 \end{smallmatrix}\right)$. Here it is found that the optimal decision threshold is $r_{\text{opt}} = 0.82$ for $n = 8$ and $r_{\text{opt}} = 0.80$ for $n = \{9, 10\}$, where the corresponding total error rates are $P_{\text{te}} = \{0.17, 0.13, 0.10\}$. For all the exact cases, it is clear that the proposed optimal decision thresholds minimize the total error rates, which considers the interests of PUs and SUs simultaneously.

3.5.2 Asymptotic Optimal Decision Threshold for GLRT Detector

The total error rate P_{te} and the optimal decision threshold r_{opt} for the GLRT detector with multiple antennas are presented in this subsection. Meanwhile, the derived expressions of CDF of the test statistic are verified as well under the hypotheses $\mathcal{H}_0$ and $\mathcal{H}_1$. Specifically, The CDF given by (3.37) is

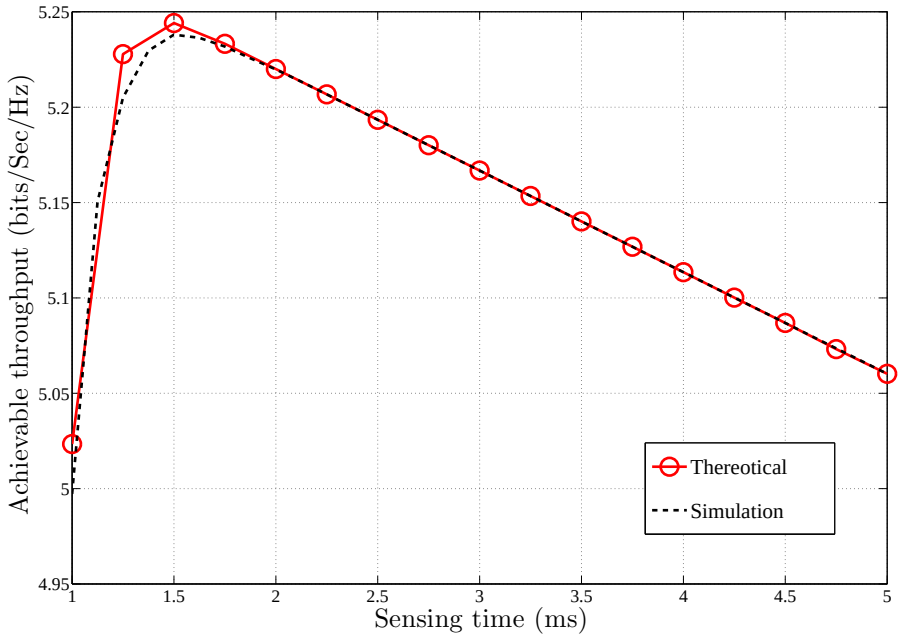

Figure 3.10: *The achievable throughput of the secondary network for the GLRT detector with* $m = 6$, $f_{\mathrm{s}} = 1\mathrm{MHz}$ *and* $\gamma = -15\mathrm{dB}$.

verified in Fig. 3.5. The theoretical and empirical CDF curves in Fig. 3.5 are plotted for various cases of the number of received samples n, and it can be observed that the asymptotic and empirical results are identical. Fig. 3.6 illustrates the CDF curves obtained from the derived CDF expression for the case of $\mathcal{H}_1$ versus Monte Carlo simulations for various received sample sizes $n = \{500, 1000\}$. It can be found that the theoretical results match the simulation results, which demonstrates our analytical expression is consistent with the empirical data. The specific assignments of the simulation parameters are detailed in Table 3.1.

We are interested in the value of the optimal decision threshold and the performance of total error rate in different cases of low SNR. Fig. 3.7 shows the performance of the total error rate for the GLRT detector with 6 receive antennas and sample size of 500 samples, i.e., $m = 6, n = 500$, under different values of the received SNR, γ, from -12.5 dB to -7.5 dB. From Fig. 3.7, it can be observed that the minimum values of the total error rate are very low when the received SNR is $\gamma \geq -12.5$ dB. This indicates that the probability of false alarm and missed detection are also very low. The values of the optimal decision thresholds which minimize the total error rate with constraints can be obtained numerically. Specifically, the corresponding optimal decision thresholds r_{opt} are $\{0.2034, 0.2127, 0.2259\}$ for the different SNR values that are given by $\gamma = \{-12.5, -10, -7.5\}$ dB,

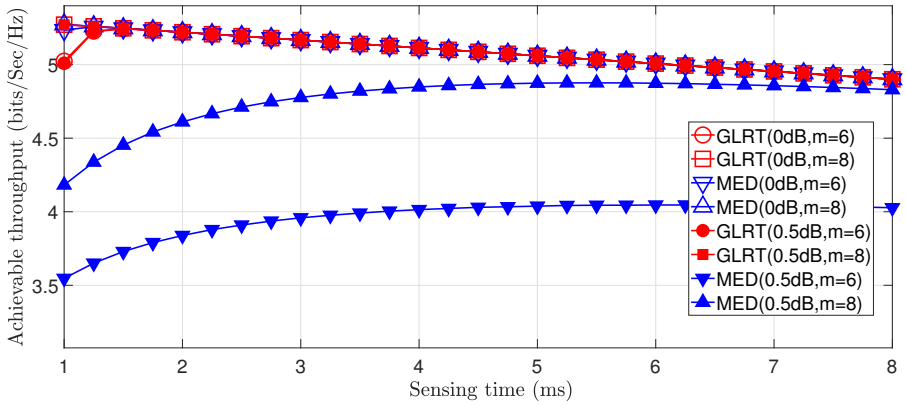

Figure 3.11: *The achievable throughput of the secondary network for the GLRT detector and MED with and without the noise uncertainty ($f_{\mathrm{s}} = 1\mathrm{MHz}$, $\gamma = -15\mathrm{dB}$ and noise uncertainty is $0.5\mathrm{dB}$).*

Parameters	**Values**
Received SNR at SUs γ	-15 dB, -12.5 dB, -10 dB, -7.5 dB
SNR of the secondary link SNR_{s}	20 dB
Number of SU antennas m	$4, 6, 8$
Number of spectrum sensing samples n	500, 1000
Sampling frequency f_{s}	1 MHz
Probability of the absence of the PU $P(\mathcal{H}_0)$	0.8
Duration of single sensing frame T	100 ms
Noise uncertainty B	0.5 dB

Table 3.1: *Simulation parameters for the performance of the GLRT detector*

respectively. The corresponding values employed for the constraints of target probabilities of false alarm and missed detection ξ_{fa} and ξ_{m} are given by $\xi_{\mathrm{fa}} = \xi_{\mathrm{m}} = 0.1$. All these obtained optimal decision thresholds minimize the total error rate. Meanwhile, the SUs can achieve a high probability of accessing an unlicensed band and the PUs are protected from the consequences of missed detections concurrently. In order to observe the performance in terms of the probability of false alarm P_{fa} and the probability of detection P_{d}, the receiver operating characteristic (ROC) curves are depicted in Fig. 3.8.

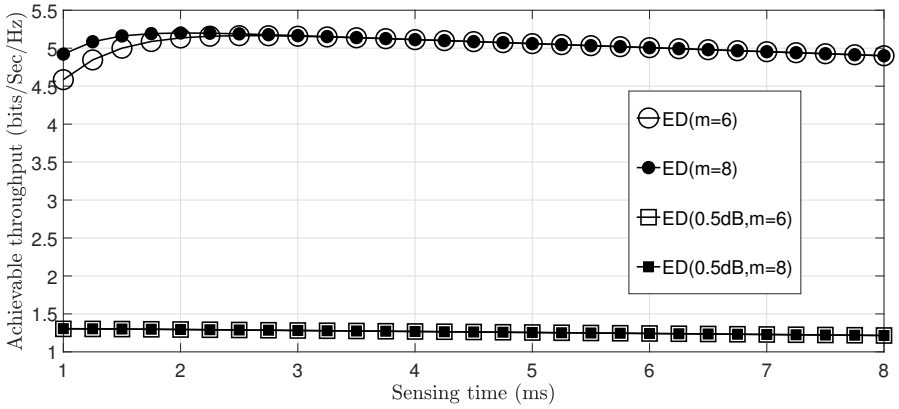

Figure 3.12: *The achievable throughput of the secondary network for the ED with and without the noise uncertainty ($f_{\rm s} = 1$MHz, $\gamma = -15$dB and noise uncertainty is 0.5dB).*

3.5.3 Minimum Sensing Time for GLRT Detector

The minimum sensing time $\tau_{\min}$ and the total error rate $P_{\rm te}$ for the GLRT detector with multiple antennas are presented in this subsection. We are interested in the values of the minimum sensing time and the minimum total error rates in the low SNR regime. Fig. 3.9 shows the minimum total error rates with regard to different values of the sensing time for the GLRT detector with multiple antennas $m = \{4, 6\}$ under low SNR values of $\gamma = \{-15, -12.5\}$ dB. It is found that the performance of the minimum total error rate tends to be better by increasing the number of receive antennas and the sensing time. When the desired minimum total error rate is set at 0.01, for $\gamma = -15$ dB, it is found that the corresponding minimum sensing time should be 4.0 ms and 2.0 ms for $m = 4$ and $m = 6$, respectively, and for $\gamma = -12.5$ dB, the corresponding minimum sensing time can be obtained at 1.5 ms and 1.0 ms for $m = 4$ and $m = 6$, respectively. All these results for the obtained values of the minimum sensing time enable the minimum total error rates to achieve the target of minimum total error rate speedily and efficiently.

3.5.4 Achievable Throughput of Secondary Network

In this part, the results for the achievable throughput of the secondary network and the optimal sensing time which can maximize the throughput are considered and discussed. We assume that the SNR of the PU's signals measured at the secondary receiver is $\gamma = -15$ dB. The SNR of the secondary link between the secondary transmitter and receiver is set to be $SNR_{\rm s} = 20$ dB and the sampling

frequency used for simulations is 1 MHz. Meanwhile, the probability of the absence of the PU is assumed as $P(\mathcal{H}_0) = 0.8$, and the duration of single spectrum sensing frame is $T = 100$ ms. Besides, the predefined target probability of detection is $P_{\mathrm{d}}^{*} = 0.9$. Also, the comparison of the achievable throughput of the secondary network with and without noise uncertainty is also presented in this subsection.

First, Fig. 3.10 shows the theoretical and Monte Carlo simulation results of the achievable throughput of the secondary network for the GLRT detector with 6 receive antennas, i.e., $(m = 6)$. In this figure, it can be seen that the theoretical results match the simulation results well. In addition, these results reveal that the optimal sensing times obtained from the theoretical and simulation curves are both 1.5 ms, which indicates that our proposed expressions in the previous section for calculating the achievable throughput of the GLRT detector with multiple antennas are correct. Thus, we will only show the theoretical results in the following figures.

Second, the achievable throughput of the secondary network is provided in Fig. 3.11 and Fig. 3.12 for different detectors, including the GLRT detector, MED and ED. Both the absence and presence of the noise uncertainty are considered in these two figures. Simulations assume the received SNR sourced from the PU's signal is $\gamma = -15$ dB. In these two figures, the achievable throughput using the three different detector models are illustrated for different numbers of receive antennas. Also, the values of the optimal sensing time which maximize the achievable throughput of the secondary network can be obtained. Specifically, from Fig. 3.11, when the noise uncertainty is absent, the optimal sensing time for the GLRT detector with 6 and 8 receive antennas are 1.50 ms and 1.00 ms, respectively. The optimal sensing time for the MED with 6 and 8 receive antennas are 1.25 ms and 1.00 ms respectively. Meanwhile, it can be seen that when the noise uncertainty is present, the performance of the GLRT detector is not affected so that the optimal sensing times are unchanging. However, the performance of the MED is affected. Specifically, for MED, the corresponding optimal sensing times are changed to be 6.00 ms and 5.50 ms for the cases with 6 and 8 receive antennas respectively.

From Fig. 3.12, when the noise uncertainty is absent, the optimal values of the sensing time for the ED with 6 and 8 receive antennas are 2.50 ms and 2.00 ms, respectively. As contrast, when the noise uncertainty is present, the performance of the ED is affected seriously. In detail, the corresponding optimal sensing times for 6 and 8 receive antennas both change to be 1.00 ms. Besides, for all the investigated detection methods, it is obvious that the optimal sensing time will be shorter if the detector has more receive antennas. The simulation results shown in Fig. 3.11 and Fig. 3.12 have demonstrated that the GLRT eigenvalue-based detector is robust to the noise uncertainty, but MED and the ED

is non-robust. Nevertheless, the ED has the advantage of easy implementation in practice and still widely adopted in many research works. Both the GLRT and MED detections require eigenvalue-decomposition so that GLRT and MED have higher computational costs than the ED.

3.6 Summary

In this chapter, optimal decision thresholds and the sensing-throughput trade-off were investigated for eigenvalue-based spectrum sensing techniques. Specifically, these investigations were conducted from two aspects, including exact and asymptotic analyses. In terms of exact analysis, we focused on the MED with arbitrary number of receive antennas, as well as MME, EME and GLRT detectors with 2 receive antennas. For the cases of both the MME and EME detectors we presented accurate expressions for the probability of false alarm. Furthermore, for the case of the GLRT detector we derived an accurate expression for the probability of missed detection. By using these expressions of sensing performance metrics, we formulated the exact total error rate $P_{\rm te}$ expressions and presented the equations to numerically obtain the optimal decision thresholds for four detection methods which can minimize the total error rate.

In terms of asymptotic analysis, this chapter studied the general case of the GLRT eigenvalue detector. Initially, we derived the asymptotic expressions of the probabilities of false alarm and detection when the sample size from each primary user was large enough compared with the number of receive antennas. Unlike the asymptotic expression of the probability of false alarm given in the previous work which was difficult to obtain the derivative, the expressions derived in this chapters were mathematically traceable. Furthermore, the optimal decision threshold was studied for the GLRT detector and the results showed that the proposed optimization model for the decision threshold could minimize the total error rate under different received SNR regimes. Moreover, the chapter provided a fast spectrum sensing method which only required a short sensing time to satisfy the target of the minimum total error rate. Thus, the sensing time could be reduced while maintaining a desired total error rate and the chosen optimal decision thresholds were also applied during this process. Finally, by analysing the achievable sensing-throughput trade-off for the secondary network, the optimal sensing time which maximized the achievable throughput was found. It is worth noticing that both cases of the absence and presence of noise uncertainty were considered and a comparison was also provided between the GLRT detector, MED and conventional ED. The results revealed that the investigated GLRT eigenvalue detector outperformed the MED and ED in the presence of noise uncertainty.

Chapter 4

Cooperative Spectrum Sensing Based on Random Secondary Network

4.1 Introduction

The objective of spectrum sensing is to determine whether the PU is present so that the SU can decide when to access the licensed frequency bands. Generally, spectrum sensing techniques utilize single node or cooperative spectrum sensing. Cooperative spectrum sensing can improve the performance of the spectrum sensing system [3] by making a final decision on the status of the PU in a centralized or distributed manner. Many different combining techniques, fusion strategies and sensing techniques have been proposed to improve the accuracy and efficiency of cooperative spectrum sensing [9, 89–96]. The sensor selection method was investigated in [97] in order to obtain spatially independent sensors. In [68], the sensing throughput trade-off of the secondary network was studied based on ED. The performance of cooperative spectrum sensing with ED was investigated in [15] based on the CDR and the CFAR requirements when the SUs were distributed randomly. Besides, the optimization of cooperative spectrum sensing with ED was studied in [14], but the locations of SUs were assumed to be identical and fixed.

Meanwhile, the stochastic geometry approach using PPP has been used to analyze the performance of random wireless networks and CR networks [98–101]. In [102], the spectrum-sharing transmission capacity was investigated by applying stochastic geometry in overlay and underlay CR networks and the optimal spatial density was derived in order to achieve the maximum sum spectrum-sharing transmission capacity. Khoshkholgh *et al.* [103] analyzed the outage performance and mean spatial throughput of the primary network in CR networks by utilizing stochastic geometry. Peng *et al.* [104] derived the ergodic capacity achieved by the single nearest and Nth-nearest remote radio head (RRH) association strategies in cloud radio access networks and investigated the impact of RRH density and number of antennas per RRH on the ergodic capacity gain. In [105], the interference in CR networks was investigated when the PPP of PUs and the Poisson hole process of the SUs were dependent and

the interference was estimated well by utilizing a Poisson cluster process to model the Poisson hole process.

Besides, in the existing works, a multi-channel CR network has been exploited [106–109]. For instance, the total transmit capacity over all the subchannels for the secondary network was studied in [107] under transmit power and interference power constraints. In order to improve the sensing reliability, a spatial-spectral joint detection approach was proposed in [108] for multi-channel spectrum sensing. However, we focus on narrowband spectrum sensing in this chapter, since the single-channel spectrum sensing performance with the homogeneous PPP still needs further exploration and the results in this chapter are also valid for wideband spectrum sensing when the subchannel is sensed in a sequential manner.

This chapter investigates the cooperative spectrum sensing with the GLRT eigenvalue based detector in interweave CR networks while assuming that the SUs follow a homogeneous PPP and this is motivated by multiple factors. Firstly, it is more practical to assume SUs follow a homogeneous PPP compared with the traditional assumption in the literature. Most of the previous works assumed that the received SNRs at SUs were identical, but in practice the received SNRs could vary depending on the locations of SUs. Secondly, cooperative spectrum sensing with PPP is a challenging topic and still needs further investigation. Specifically, a new strategy is required to cope with the diversity of the received SNRs in the PPP model, which has not been studied in the literature. Thirdly, existing works are mainly based on ED when the stochastic geometry is employed, but one of the limitations of the ED based methods is the sensitivity to the noise uncertainty. Therefore, the robust GLRT detector [110] is employed to evaluate the cooperative spectrum sensing and secondary transmission performance. Lastly, a minimum total error rate considers the benefits of PUs and SUs simultaneously, but the previous works such as [75],[10] mainly focused on the probability of false alarm due to the lack of generalized closed-form expression of the detection probability, which only considered the interests of SUs. A low probability of false alarm allows SUs more opportunities to access the spectrum holes, however, the benefits of PUs may not be guaranteed. Therefore, the aforementioned issues motivate us to investigate the total error rate performance and the optimality of cooperative spectrum sensing system with the GLRT detector by applying stochastic geometry, which considers the benefits of PU and SUs concurrently.

The main contributions of this chapter can be summarized as follows.

- Firstly, an efficient GLRT-based cooperative spectrum sensing technique is proposed by using

stochastic geometry, which can utilize only a few, not always all, SUs to achieve the minimum total error rate. Meanwhile, the optimal number of the cooperating SUs is also studied, which enables the total error rate to achieve the minimum value. Therefore, the speed and accuracy of cooperative spectrum sensing is improved compared to the cooperation among all SUs, when sending local decisions in different time slots is chosen for decision combining.

- Secondly, in order to maximize the achievable ergodic capacity and throughput of the random secondary network, effective methods are proposed for different fusion rules to determine the appropriate number of cooperating SUs when the target total error rate is not exceeded.

The remainder of this chapter is organized as follows. Section 4.2 describes the system model of cooperative spectrum sensing based on the GLRT detector. Section 4.3 investigates the optimal number of collaborating SUs by employing the GLRT detector. The achievable ergodic capacity and throughput of the secondary network are analyzed in section 4.4. Section 4.5 presents the simulation results and discussions and section 4.6 concludes this chapter briefly.

4.2 System Model

We consider a centralized cooperative spectrum sensing system with decision fusion, shown in Fig. 4.1. The fusion center (FC) is used to collect the decisions made by the SUs to make a final decision. The SUs which are used to sense the status of PUs comprise RRHs or user equipment (UE). During the cooperative spectrum sensing process, each SU within the coverage radius of the FC detects the status of the PU independently and then sends the detection result to the FC. After that, the FC gives a final decision on the status of the PU through an appropriate voting rule. The PU is assumed to be equipped with single antenna and each SU has multiple antennas.

A practical assumption is that the SUs are uniformly distributed on a 2-dimensional plane $\mathbb{R}^2$ based on a homogenous PPP with density ρ. According to Palm theory [111], the SUs located within the coverage radius of the FC follow the same PPP. The coverage radius of the FC is denoted by R and the distance between the PU and the secondary receiver located at the origin of the coverage area of the FC is represented by D. Since only the SUs within the coverage radius of the corresponding FC can collaborate together to detect the status of the PU, we only consider the SUs that are located within the area of interest in this work. Assuming the transmitted signals between the PU and secondary network

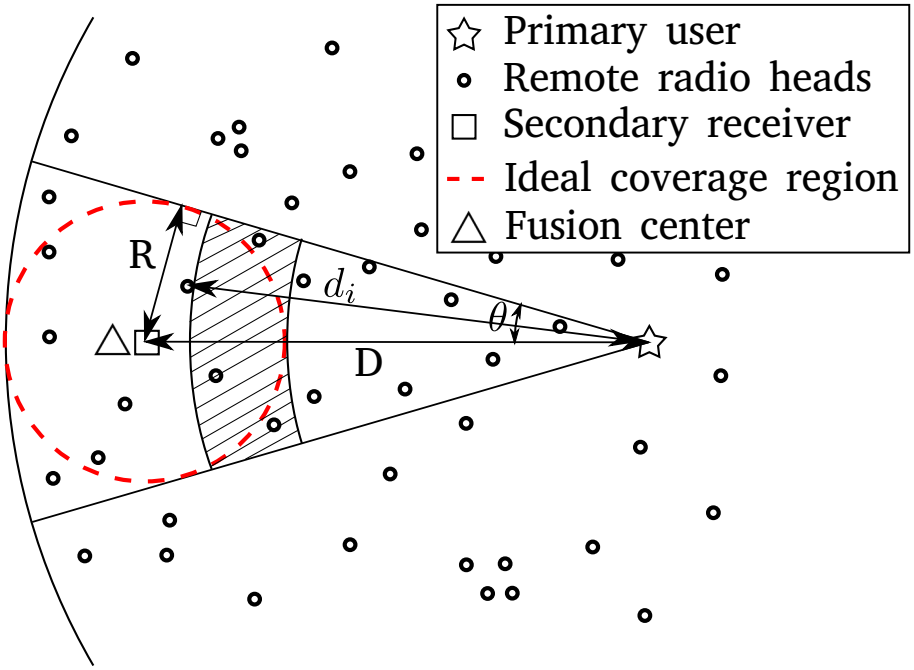

Figure 4.1: *The system model of cooperative spectrum sensing based on PPP.*

experience path loss and Rayleigh fading, the received signal power at the ith SU can be given as

$$P_i = \frac{P_{\mathrm{T}}}{d_i^{\varepsilon}}\omega_i, \tag{4.1}$$

where ω_i denotes the Rayleigh fading gain and follows the Gamma distribution when maximal ratio combining (MRC) is used to achieve full diversity gain, i.e., $\omega_i \sim \Gamma(m, 1)$, m is the number of receive antennas of each SU, P_{T} denotes the PU's signal power, d_i means the distance between the PU and the ith nearest SU from the PU and ε is the path loss exponent factor. The shadowing area in Fig. 4.1 is defined as the region whose distance is equal or greater than $D - R$ but less than $d_i - D + R$. The PDF of ω_i can be written as

$$f_{\omega_i}(\omega) = \frac{\omega^{m-1}e^{-\omega}}{(m-1)!}. \tag{4.2}$$

The spectrum sensing between each SU and the PU is assumed to be a GLRT-based sensing system with m receive antennas. Let $\mathcal{H}_0$ (PU is absent) and $\mathcal{H}_1$ (PU is present) denote the null and the alternate hypotheses. During the sensing period, the matrix of received signal samples, $\mathbf{Y} \in \mathbb{C}^{m\times n}$,

at the SU is

$$\mathcal{H}_0 : \mathbf{Y} = \mathbf{V}, \tag{4.3}$$

$$\mathcal{H}_1 : \mathbf{Y} = \mathbf{h}\mathbf{s}^\dagger d^{-\frac{\varepsilon}{2}} + \mathbf{V}, \tag{4.4}$$

where n is the sample number, $\mathbf{V} \in \mathbb{C}^{m\times n}$ represents the samples from a circularly symmetric complex AWGN process, where $\mathbf{V} \sim \mathcal{CN}\left(\mathbf{0}, \sigma_v^2\mathbf{I}_m \otimes \mathbf{I}_n\right)$, and $\mathbf{s} \sim \mathcal{CN}\left(\mathbf{0}, P_{\mathrm{T}}\mathbf{I}_n\right) \in \mathbb{C}^{n\times 1}$ is the transmit signal of the PU. Finally, $\mathbf{h} \in \mathbb{C}^{m\times 1}$ is the channel vector. Henceforth, the covariance matrix of $\mathbf{Y}$, $\mathbf{R}_{yy} = \mathbb{E}[\mathbf{Y}\mathbf{Y}^\dagger]$, is given by

$$\mathcal{H}_0 : \quad \mathbf{R}_{yy} = \sigma_v^2\mathbf{I}_m, \tag{4.5}$$

$$\mathcal{H}_1 : \quad \mathbf{R}_{yy} = P_{\mathrm{T}} d^{-\varepsilon}\mathbf{h}\mathbf{h}^\dagger + \sigma_v^2\mathbf{I}_m. \tag{4.6}$$

Within the sensing duration of n samples, the sample covariance matrix estimated from $\mathbf{Y}$ is $\widehat{\mathbf{R}}_{yy} = \frac{1}{n}\mathbf{Y}\mathbf{Y}^\dagger$. Thus $\mathbf{W} = n\widehat{\mathbf{R}}_{yy} = \mathbf{Y}\mathbf{Y}^\dagger \in \mathbb{C}^{m\times m}$ is a complex Wishart matrix. Also, let $\hat{\lambda}_{\min} = \hat{\lambda}_m < \cdots < \hat{\lambda}_1 = \hat{\lambda}_{\max}$ be the eigenvalues, in ascending order, estimated from $\widehat{\mathbf{R}}_{yy}$. The decision statistic for the GLRT-based eigenvalue detector is given by

$$T_{\mathrm{GLRT}} = \frac{\hat{\lambda}_{\max}}{\sum_{l=1}^{m}\hat{\lambda}_l}. \tag{4.7}$$

Nowadays, there exists many wideband signals in practical applications, eg. the orthogonal-frequency-division-multiplexing (OFDM) encoding signals, multi-tone transmit signals and signals over consecutive block-fading channels. The spectrum sensing techniques for these wideband signals have been proposed and studied in the literature, such as using the variational message passing algorithm or wavelet transform to estimate the power spectral density of wideband signals. However, the results presented in this chapter are still valid for wideband spectrum sensing, when the subchannel is sensed in a sequential manner. One potential solution is the radio frequency front-end is equipped with a tunable narrowband bandpass filter [112]. So one narrow frequency band can be searched at a time and existing narrowband spectrum sensing techniques can be applied. This is a way to extend our current work to a practical system with wideband primary signals.

4.3 Sensing Performance Analysis Based on Stochastic Geometry

In this section, an efficient cooperative spectrum sensing technique is proposed while achieving the minimum total error rate of the final decision. Firstly, collaborating all the possible SUs to implement cooperative spectrum sensing can not always achieve the best performance due to the diversity of the SNRs received at SUs. An SU with very low received SNR can be classified as an unreliable node and may degrade the cooperative sensing performance. Secondly, combining all the local spectrum sensing decisions concurrently at the fusion center can lead to the high design complexity and the waste of bandwidth, such as sending local decisions on orthogonal frequency bands. Hence, sending different local decisions in different time slots is chosen in this work, but this may affect the sensing speed. However, according to the IEEE 802.22 standard for Wireless Regional Area Networks (WRANs) [113], the SUs have to vacate the licensed frequency bands as soon as possible once the PU is active. Therefore, in order to address the two issues mentioned above, an efficient cooperative spectrum sensing technique using different time slots to receive local decisions is proposed to guarantee the accuracy and speed of the sensing process. Furthermore, the statistical optimal number of the cooperating SUs $k_{\rm opt}$ is studied, which can make the total error rate achieve the minimum value when the number of available SUs is large enough.

4.3.1 Sensing Performance without Reporting Errors

Both the probabilities of detection and false alarm of an individual SU are required to investigate the total error rate and transmission performance of the secondary network in CR networks. Therefore, we present the probability of detection $P_{{\rm d},i}^{\rm su}$ and probability of false alarm $P_{{\rm fa},i}^{\rm su}$ seen at the ith SU in this subsection. Due to the imperfection of the reporting channel between the SUs and the FC, a reporting error may occur during the decision reporting frame of the spectrum sensing process [114]. The sensing error probabilities seen at the FC will be discussed in the next subsection when considering decision reporting errors. The closed-form expression of the probability of false alarm seen at the ith SU using the GLRT detector with m receive antennas, i.e., $P_{{\rm fa},i}^{\rm su}$, is given by

$$P_{{\rm fa},i}^{\rm su}(r_i) = 1 - \frac{\Gamma(mn)(m\eta)^{-\xi}}{\xi\Gamma(mn-\xi)\Gamma(\xi)} \left(\mathbf{\Xi}(r_i) - \mathbf{\Xi}\left(\frac{1}{m}\right) \right), \tag{4.8}$$

where $\frac{1}{m} \leq r_i \leq 1$ denotes the decision threshold of ith SU and $\boldsymbol{\Xi}(\cdot)$ is defined by

$$\boldsymbol{\Xi}(y) = {}_2F_1\left(\xi, 1+\xi-mn; \xi+1; \frac{y}{\eta}\right)(my)^{\xi}, \tag{4.9}$$

where η and ξ are given by

$$\eta = \frac{0.8132b^2}{a-1.7711b}, \quad \xi = \frac{(a-1.7711b)^2}{0.8132b^2}, \tag{4.10}$$

and a, b are defined as

$$a = (\sqrt{m}+\sqrt{n})^2, \quad b = (\sqrt{m}+\sqrt{n})\left(\sqrt{\frac{1}{m}}+\sqrt{\frac{1}{n}}\right)^{\frac{1}{3}}. \tag{4.11}$$

Hence, for a complex Gaussian signal, the decision threshold r_i with respect to the individual probability of false alarm seen at the ith SU can be calculated by

$$r_i = \eta I^{-1}\left(\frac{\Gamma(mn)(m\eta)^{-\xi}}{\xi\Gamma(mn-\xi)\Gamma(\xi)}\left(\boldsymbol{\Xi}\left(\frac{1}{m}\right)+(1-P_{\mathrm{fa},i}^{\mathrm{su}})\frac{\xi\Gamma(mn-\xi)\Gamma(\xi)}{\Gamma(mn)(m\eta)^{-\xi}}\right), \xi, mn-\xi\right). \tag{4.12}$$

This expression is used to calculate the required decision threshold for a desired false alarm rate, which is necessary for the individual and cooperative spectrum sensing under the CFAR requirement.

In the meantime, the detection probability $P_{\mathrm{d},i}^{\mathrm{su}}$ seen at the ith SU using the GLRT detector is presented as

$$P_{\mathrm{d},i}^{\mathrm{su}}(r_i) = 1 - \frac{1}{2}\left[\Phi\left(\tau_i\sqrt{\varphi_i}+\frac{r_i}{2\sqrt{\varphi_i}(1-r_i)}\right)-\Phi\left(\tau_i\sqrt{\varphi_i}+\frac{1}{2(m-1)\sqrt{\varphi_i}}\right)\right], \tag{4.13}$$

where τ_i and φ_i are given by

$$\tau_i = n(m-1)\left(\frac{1}{mn\gamma_i}-\frac{1}{1+m\gamma_i}\right)\left(1+\frac{m-1}{mn\gamma_i}\right), \tag{4.14}$$

$$\varphi_i = \frac{1}{2n(m-1)^2}\left(\frac{1}{1+m\gamma_i}-\frac{1}{mn\gamma_i}\right)^{-2}, \tag{4.15}$$

and γ_i denotes the average received SNR at the ith SU. It is worth noting that γ_i depends on the homogeneous PPP model in this chapter and the corresponding closed-form expression is derived as Eq. (4.26) in Section 4.3.3.

Meanwhile, the expression of decision threshold in terms of $P_{\mathrm{d},i}^{\mathrm{su}}$ is given by

$$r_i = \left(\frac{1}{2} \left(\sum_{t=0}^{\infty} \frac{C_t \sqrt{\varphi_i}}{2t+1} \left[\frac{\sqrt{\pi}}{2} \Phi \left(\tau_i \sqrt{\varphi_i} + \frac{1}{2(m-1)\varphi_i} \right) + \sqrt{\pi}(1 - P_{\mathrm{d},i}^{\mathrm{su}}) \right]^{2t+1} - \tau_i \varphi_i \right)^{-1} + 1 \right)^{-1}, \tag{4.16}$$

where the coefficient $C_t = 1$ for $t = 0$, otherwise $C_t = \sum_{q=0}^{t-1} \frac{C_q C_{t-1-q}}{(q+1)(2q+1)}$. The proof of (4.16) is given in the Appendix B.

4.3.2 Cooperative Sensing with Reporting Errors

In the cooperative spectrum sensing system, the final decision on the status of the PU can be made through different techniques, including decision fusion and data fusion. In this work, we apply decision fusion to investigate the performance of the system. During a decision fusion process, each SU processes the data individually and makes a local decision that is represented by a single bit ($1/0$ represents the presence/absence of the PU) independently. Then, the final decision is made by fusing these individual decisions through a voting rule. Assuming the reporting channel bit error probability (BEP) under $\mathcal{H}_0$ and $\mathcal{H}_1$ are represented by $P_{\mathrm{b},i}^0$ and $P_{\mathrm{b},i}^1$ for the ith reporting channel, the probability of false alarm of the ith SU seen at the FC $P_{\mathrm{fa},i}$ with the presence of reporting errors is given by

$$\begin{aligned} P_{\mathrm{fa},i} &= \mathbf{P}\left(u_i^{\mathrm{fc}} = 1 \mid \mathcal{H}_0\right) \\ &= \mathbf{P}\left(u_i^{\mathrm{fc}} = 1 \mid u_i^{\mathrm{su}} = 1\right) \mathbf{P}\left(u_i^{\mathrm{su}} = 1 \mid \mathcal{H}_0\right) + \mathbf{P}\left(u_i^{\mathrm{fc}} = 1 \mid u_i^{\mathrm{su}} = 0\right) \mathbf{P}\left(u_i^{\mathrm{su}} = 0 \mid \mathcal{H}_0\right) \\ &= (1 - P_{\mathrm{b},i}^0) P_{\mathrm{fa},i}^{\mathrm{su}} + P_{\mathrm{b},i}^0 (1 - P_{\mathrm{fa},i}^{\mathrm{su}}), \end{aligned} \tag{4.17}$$

where u_i^{fc} and u_i^{su} denote the decision on the status of the PU made by the ith SU seen at the FC and SU respectively. Similarly, the probability of detection of the ith SU seen at the FC with the presence of reporting errors is given by

$$\begin{aligned} P_{\mathrm{d},i} &= \mathbf{P}\left(u_i^{\mathrm{fc}} = 1 \mid \mathcal{H}_1\right) \\ &= \mathbf{P}\left(u_i^{\mathrm{fc}} = 1 \mid u_i^{\mathrm{su}} = 1\right) \mathbf{P}\left(u_i^{\mathrm{su}} = 1 \mid \mathcal{H}_1\right) + \mathbf{P}\left(u_i^{\mathrm{fc}} = 1 \mid u_i^{\mathrm{su}} = 0\right) \mathbf{P}\left(u_i^{\mathrm{su}} = 0 \mid \mathcal{H}_1\right) \\ &= (1 - P_{\mathrm{b},i}^1) P_{\mathrm{d},i}^{\mathrm{su}} + P_{\mathrm{b},i}^1 (1 - P_{\mathrm{d},i}^{\mathrm{su}}). \end{aligned} \tag{4.18}$$

Generally, the BEP depends on the modulation scheme and the SNR or signal-to-interference-plus-noise ratio (SINR) between the SU and the FC. In order to confine the interference to the PU caused by the missed detection, the FC has to be far away from the PU in practice. Therefore, $P_{\mathrm{b},i}^{0}$ and $P_{\mathrm{b},i}^{1}$ are quite close so that the approximation relation $P_{\mathrm{b},i}^{0} = P_{\mathrm{b},i}^{1}$ can be obtained. Furthermore, the BEPs can be controlled within a very low and similar value for different SUs by applying error rate control techniques, including increasing transmit power, utilizing the diversity in space, time and frequency domains, retransmitting the echoed back information, applying automatic repeat request (ARQ) method and employing forward error correction coding (FECC). Thus, the difference of BEPs between different SUs is quite small after employing appropriate error rate control techniques, so that it has little influence on the sensing error rate of the final decision in practice.

Based on the above conditions in practice, a simplified and reasonable assumption is that reporting processes of different SUs are independent and the BEPs are identical for different SUs, which indicates that $P_{\mathrm{b},i}^{0} = P_{\mathrm{b},i}^{1} = P_{\mathrm{b}}$. This approximation would not affect the analyses on sensing and transmission performance in this chapter, since the difference of BEPs between different SUs is quite small and has little influence on performance of the system after employing error rate control techniques.

Specifically, voting rules Logic-OR (OR) and Logic-AND (AND) are used in this work in order to find out the optimal number of the collaborating SUs conveniently. Assuming there are k cooperating SUs, the properties of the OR and AND rules are as follows:

- (1) OR rule: When at least one local decision among the k local decisions indicates the PU is present, the final decision declares the PU is present. The probabilities of detection and false alarm of the final decision are given by

$$P_{\mathrm{d}} = 1 - \prod_{i=1}^{k}(1 - P_{\mathrm{d},i}), \tag{4.19}$$

$$P_{\mathrm{fa}} = 1 - \prod_{i=1}^{k}(1 - P_{\mathrm{fa},i}). \tag{4.20}$$

- (2) AND rule: Only when all local decisions indicate the PU is present, the final decision declares the PU is present. The corresponding probabilities of detection P_{d} and false alarm P_{fa}

of the final decision are given by

$$P_{\mathrm{d}} = \prod_{i=1}^{k} P_{\mathrm{d},i}, \tag{4.21}$$

$$P_{\mathrm{fa}} = \prod_{i=1}^{k} P_{\mathrm{fa},i}. \tag{4.22}$$

The total error rate of the final decision is defined to be the summation of the false alarm and missed detection rates of the final decision, which is given by

$$P_{\mathrm{te}} = P_{\mathrm{fa}} + P_{\mathrm{m}}, \tag{4.23}$$

where the probability of missed detection of the final decision P_{m} is defined as

$$P_{\mathrm{m}} = 1 - P_{\mathrm{d}}. \tag{4.24}$$

4.3.3 Optimal Number of Cooperating SUs to Minimize the Total Error Rate

The optimization of the cooperative spectrum sensing can be considered from three perspectives. Firstly, it can be considered under the CDR requirement, which aims to minimize the probability of false alarm for a given probability of detection. This guarantees the benefits of PU preferentially. Secondly, the probability of detection can be minimized for a desired CFAR, which gives priority to the interests of the SUs. Thirdly, this issue can be considered to minimize the total error rate for a given constant decision threshold (CDT), which considers the interests of PU and SUs concurrently. In this subsection, the optimization of cooperative spectrum sensing is investigated from all the three requirements.

From (4.13), it can be found that a higher received SNR helps to achieve a higher individual probability of detection $P_{\mathrm{d},i}$. Therefore, the SUs with higher received SNRs should be chosen first to implement the cooperative spectrum sensing under all the three different system requirements. In order to study the received SNR at the ith nearest SU, the Euclidean distance d_i between the PU and the ith nearest SU within the coverage radius of FC (shown as Fig. 4.1) needs to be investigated. The PDF of d_i is derived as the following theorem.

Theorem 2. *In a PPP with density ρ on a 2-dimensional plane, the PDF of the distance d_i between the ith nearest SU within the coverage radius of the FC from the PU and the PU outside the region of interest is given by*

$$f_{d_i}(d) = \frac{2\rho\theta(D-R)e^{-2\rho\theta(D-R)(d-D+R)}}{\Gamma(i)\big(2\rho\theta(D-R)(d-D+R)\big)^{1-i}}, \tag{4.25}$$

where $\theta = \sin^{-1}\left(\frac{R}{D}\right)$ and $D \gg R$.

Proof. The proof is provided in the Appendix B. □

Hence, the average received SNR γ_i at the ith nearest SU can be derived as

$$\begin{aligned}\gamma_i &= \int_{D-R}^{\infty}\int_{0}^{\infty} \frac{P_{\mathrm{T}}\omega}{\sigma_v^2 d^{\varepsilon}} f_{\omega_i}(\omega) f_{d_i}(d) \quad \mathrm{d}\omega\mathrm{d}d \\ &= \frac{P_{\mathrm{T}} m e^{2\rho\theta(D-R)^2}}{\sigma_v^2\big(2\rho\theta(D-R)\big)^{-\varepsilon}} \sum_{j=0}^{i-1} \binom{i-1}{j} \frac{\Gamma\left(i-j-\varepsilon, 2\rho\theta(D-R)^2\right)}{\Gamma(i)\left(-2\rho\theta(D-R)^2\right)^{-j}},\end{aligned} \tag{4.26}$$

where $\Gamma(\cdot,\cdot)$ denotes the upper incomplete Gamma function and the above expression is obtained by averaging the small scale fading ω and distance d. Therefore, by using the above result, $P_{\mathrm{fa},i}$ and $P_{\mathrm{d},i}$ can be computed under the CDT requirement. Also, the total error rate P_{te} can be obtained under specific decision fusion rules.

According to the above expression of the received SNR measured at the ith nearest SU under the homogeneous PPP model, the received SNR decreases with increasing i. With the increase of the number of the SUs involved in the cooperative sensing k, the local decision made by the SU with very low received SNR may be included in the final decision so that the sensing performance would be affected. Thus, there exists an optimal number of cooperating SUs k_{opt} that can minimize the total error rate of the final decision. Therefore, the optimization issue can be formulated as follow:

$$k_{\mathrm{opt}} = \arg\min_{k} P_{\mathrm{te}}(k). \tag{4.27}$$

Since the total number of available SUs follows Poisson distribution, the optimal solution k_{opt} is difficult to obtain. Therefore, the exhaustive search approach is applied in our work to find the solution to the above optimization issue.

There exist many benefits when k_{opt} SUs cooperate to perform spectrum sensing rather than collab-

orating all the available SUs all the time. Specifically, firstly, only considering a few, not always all, the SUs to implement spectrum sensing, the sensing performance (i.e., the total error rate of the final decision in this chapter) can be improved which can be seen from Fig. 4.3. Secondly, compared with the traditional approach, fewer SUs reduces energy consumption since the unemployed SUs are silent during the sensing and reporting durations. Finally, it is obvious that fewer SUs can reduce the reporting time in the time division mode so that the spectrum sensing process can be accelerated. Therefore, for a fixed periodic spectrum sensing frame, the SUs have more time for data transmission, which helps to enhance the achievable ergodic capacity or throughput of the secondary network.

4.3.3.1 Constant Decision Threshold Scheme

Under the CDT requirement, the decision threshold is fixed and identical for every individual spectrum sensing period. Therefore, the individual probability of false alarm $P_{\mathrm{fa},i}$ for each SU is constant. However, the individual probability of detection varies depending on γ_i. When an additional SU is added into the cooperative spectrum sensing, the additional SU has the worst individual probability of detection, i.e. $P_{\mathrm{d},k}$, among the cooperating SUs. However, the individual probability of false alarm of the additional SU $P_{\mathrm{fa},k}$ is identical with other cooperating SUs. Meanwhile, the additional SU does not affect the performance of the other SUs.

OR rule The total error rate of the final decision P_{te} under OR rule can be given by

$$P_{\mathrm{te}} = 1 - \prod_{i=1}^{k}(1 - P_{\mathrm{fa},i}) + \prod_{i=1}^{k}(1 - P_{\mathrm{d},i}). \tag{4.28}$$

Because of the properties of $P_{\mathrm{fa},i}$ and $P_{\mathrm{m},i}$ mentioned above, it can be seen from (4.19) that the probability of false alarm of the final decision P_{fa} increases with the increase of the number of cooperating SUs k, but the probability of missed detection of the final decision P_{m} reduces. Due to the monotonicity of P_{m} and P_{fa}, it can be seen from (3.69) that using all the SUs in the secondary network is not always the best option. The performance of the total error rate is determined by the absolute values of the slope of P_{fa} and P_{m} with the increase of k. Therefore, under two cases, using all the available SUs may not achieve the minimum total error rate. Firstly, when the absolute values of the slope of P_{fa} and P_{m} are similar, the total error rate of the final decision will reduce initially and rise later with the increase of k. Secondly, when the absolute value of the slope of P_{fa} is larger than the value of P_{m}, the total error rate increases with the increasing k. By utilizing (4.8), (4.13), (4.17), (4.18) and (4.28), the

total error rate can be calculated and the optimal number of the cooperating SUs k_{opt} can be obtained.

AND rule Under the AND rule, the total error rate is given by

$$P_{\mathrm{te}} = 1 - \prod_{i=1}^{k} P_{\mathrm{d},i} + \prod_{i=1}^{k} P_{\mathrm{fa},i}. \tag{4.29}$$

Compared with the OR rule, it can be seen from (4.21) that P_{fa} is a decreasing function and P_{m} is an increasing function with regard to the number of the cooperating SUs k under the AND rule. From (3.69), the trend of the total error rate of the final decision is also decided by the absolute values of the slope of P_{fa} and P_{m}. Hence, using all the SUs in the network may not guarantee that the total error rate achieves the minimum value. By utilizing (4.8), (4.13), (4.17), (4.18) and (4.29), the total error rate when using AND rule under CDT requirement can be computed and the optimal number of the cooperating SUs can be obtained when the number of available SUs is large.

4.3.3.2 Constant Detection Rate Scheme

The CDR requirement is considered from the perspective of the PU, which fixes the probability of detection at a desired value. We assume the targeted individual probability of detection $P^*_{\mathrm{d},i}$ of each SU is identical and P^*_{d} denotes the targeted probability of detection of the final decision. In order to calculate the corresponding $P_{\mathrm{fa},i}$ under different cases which consist of different numbers of collaborating SUs, the corresponding decision threshold r_i can be computed as follows:

- Firstly, the target individual probability of detection can be obtained from (4.30) and (4.32);
- Secondly, the target individual detection rate seen at the SU $P^{\mathrm{su}}_{\mathrm{fa},i}$ can be computed based on (4.18);
- Finally, the corresponding decision threshold would be obtained by (4.16).

From (4.8), (4.16) and (4.17), it can be deduced that a higher received SNR leads to a lower $P_{\mathrm{fa},i}$, thus the SUs with a high received SNRs should be chosen first to implement the cooperative spectrum sensing. Under the CDR requirement, the trend of P_{te} is same with P_{fa} in this scenario since P_{d} is constant.

OR rule Under the OR rule, the targeted individual probability of detection of each SU under CDR requirement can be given by

$$P_{\mathrm{d},i}^{*} = 1 - \sqrt[k]{1 - P_{\mathrm{d}}^{*}}, \quad i = 1, \ldots, k. \tag{4.30}$$

When an additional SU is added into the cooperation, it is obvious from the above equation that $P_{\mathrm{d},i}^{*}$ will reduce because of the increase of k. Since $P_{\mathrm{fa},i}$ and $P_{\mathrm{d},i}$ are both decreasing functions with regard to decision threshold r_i, the individual false alarm rates of the other cooperating SUs (i.e. $P_{\mathrm{fa},1}, \ldots, P_{\mathrm{fa},k-1}$) should decrease. Meanwhile, the additional SU with the lowest SNR has a corresponding individual false alarm rate $P_{\mathrm{d},k}$ that should be the highest among k cooperating SUs. Under the CDR requirement, the total error rate of the final decision is given by

$$P_{\mathrm{te}} = 1 - \prod_{i=1}^{k}(1 - P_{\mathrm{fa},i}) + P_{\mathrm{d}}^{*}, \tag{4.31}$$

from the above expression, P_{te} is an increasing function with both $P_{\mathrm{fa},i}$ and k. However, $P_{\mathrm{fa},i}$ decreases with an increasing k, which means that, when more SUs are involved in cooperative sensing, P_{te} should decrease with the decrease of $P_{\mathrm{fa},i}$, but increase with the increasing k at the same time. Thus, it can be deduced that P_{te} does not always decrease with the increasing k and this trend depends on the degree of the changes caused by $P_{\mathrm{fa},i}$ and k. In other words, it is very possible that the total error rate of the final decision P_{te} will decrease first because of the rapid decrease of $P_{\mathrm{fa},i}$. However, P_{te} will then go up since P_{te} is an increasing function with regard to k.

AND rule When using AND rule, the targeted individual probability of detection of each SU under the CDR requirement can be given by

$$P_{\mathrm{d},i}^{*} = \sqrt[k]{P_{\mathrm{d}}^{*}}, \quad i = 1, \ldots, k. \tag{4.32}$$

When an additional SU is involved in the cooperative system, this additional SU has the lowest received SNR among the cooperating SUs so that the individual false alarm rate of the additional SU must be highest among these cooperating SUs. Both $P_{\mathrm{fa},i}$ and $P_{\mathrm{d},i}$ are decreasing functions with regard to the decision threshold r. Meanwhile, from (4.32), target individual detection rate $P_{\mathrm{d},i}^{*}$ increases with the increase of k. Therefore, the individual false alarm rates of the other cooperating SUs (i.e. $P_{\mathrm{fa},1}, \ldots, P_{\mathrm{fa},k-1}$) will go up with the increase of k. However, the total error rate of the final decision

P_{te} is a decreasing function with regard to k, but an increasing function with regard to $P_{\mathrm{fa},i}$. This property can be revealed from the expression of total error rates under the AND rule which is given by

$$P_{\mathrm{te}} = \prod_{i=1}^{k} P_{\mathrm{fa},i} + P_{\mathrm{d}}^{*}. \tag{4.33}$$

The trend of P_{te} is determined by the changing degree of $P_{\mathrm{fa},i}$ and k. So, based on the above analysis, it is likely that the total error rate may decreases first due to the increasing k and then increase because of the increase of $P_{\mathrm{fa},i}$. Beside, total error rate may also increase or decrease monotonically as well. When more cooperating SUs are involved, more unreliable SUs (i.e. the SUs with low received SNR) will be used to detect the PU. As a consequence, the accuracy of the final decision will reduce.

4.3.3.3 Constant False Alarm Rate Scheme

Under CFAR requirement, the probability of false alarm is fixed at a targeted value which is denoted by P_{fa}^{*}. This is considered from the perspective of the SUs, so that the chance of occupying the spectrum holes for the SUs can be guaranteed. The remaining work is to maximize the probability of detection P_{d} to achieve the best performance of the cooperative spectrum sensing. The targeted individual probability of false alarm $P_{\mathrm{fa},i}^{*}$ of each SU is assumed to be identical. In order to calculate the corresponding probability of detection for a desired false alarm rate, the corresponding decision threshold has to be determined first. Based on the above assumptions, the corresponding decision threshold can be computed as follows:

- Firstly, the targeted individual false alarm rate seen at the FC can be calculated by (4.34) and (4.36);
- Secondly, the targeted individual false alarm rates seen at the SUs can be obtained based on (4.17).
- Finally, the corresponding decision thresholds can be obtained through (4.12).

Besides, the trend of P_{te} is consistent with P_{d} because P_{fa} is constant in this scenario.

OR rule Under OR rule, the targeted individual probability of false alarm of each SU $P^*_{\mathrm{fa},i}$ can be given by

$$P^*_{\mathrm{fa},i} = 1 - \sqrt[k]{1 - P^*_{\mathrm{fa}}}, \quad i = 1, \ldots, k. \tag{4.34}$$

It is obvious that $P^*_{\mathrm{fa},i}$ decreases with the increase of k. It can be deduced that the corresponding individual probability of detection $P_{\mathrm{d},i}$ also decreases because of the same monotonicity of $P_{\mathrm{d},i}$ and $P_{\mathrm{fa},i}$. Under the OR rule and CFAR requirement, the total error rate of the final decision is given by

$$P_{\mathrm{te}} = 1 - \prod_{i=1}^{k}(1 - P_{\mathrm{d},i}) + P^*_{\mathrm{fa}}. \tag{4.35}$$

From the above expression, on the one hand, when k is increasing, the individual detection rates $P_{\mathrm{d},i}$ will decrease so that the total error rate P_{te} will decrease as well. On the other hand, P_{te} is an increasing function with the increase of k. Therefore, the actual trend of P_{te} is determined by how fast the change of $P_{\mathrm{d},i}$ is, which indicates there exists an optimal number of the cooperating SUs k_{opt} which enables P_{te} to achieve the minimum value. It is worth noting that k_{opt} can be, but not always, equal to the total number of the available SUs. From (4.13), the individual probability of detection $P_{\mathrm{d},i}$ decreases with the decrease of the received SNRs at the SUs γ_i. A higher γ_i brings about a higher $P_{\mathrm{d},i}$, thus the SUs with higher γ_i should collaborate first to implement cooperative spectrum sensing. Under the CFAR requirement and OR rule, when an additional SU is involved in the cooperation, the individual probability of detection of the additional SU, i.e. $P_{\mathrm{d},k}$, will have the lowest detection rate among these cooperating SUs and the other individual probabilities of detection, i.e. $P_{\mathrm{d},1}, \ldots, P_{\mathrm{d},k-1}$, will also reduce.

AND rule Considering the AND rule under the CFAR requirement, the targeted individual false alarm rate of each SU seen at FC can be given by

$$P^*_{\mathrm{fa},i} = \sqrt[k]{P^*_{\mathrm{fa}}}, \quad i = 1, \ldots, k. \tag{4.36}$$

From the above expression, when an additional SU, i.e. kth SU, is included in the cooperative spectrum sensing, $P^*_{\mathrm{fa},i}$ will increase so that the individual detection rate $P_{\mathrm{d},0}, \cdots, P_{\mathrm{d},k-1}$ will go up. Besides, the additional SU will have the lowest individual detection rate ($P_{\mathrm{d},k}$) among the cooperating SUs. The detection rate of the final decision P_{d} is a decreasing function with the increase of k, meanwhile, P_{d} is an increasing function with the increase of $P_{\mathrm{d},i}$. Under the CFAR requirement, the total error

rate P_{te} has the same monotonicity as P_{d} and can be given by

$$P_{\mathrm{te}} = \prod_{i=1}^{k} P_{\mathrm{d},i} + P_{\mathrm{fa}}^{*}. \tag{4.37}$$

Thus P_{te} may decrease first because of the increase of k and then increase due to the rapid increase of $P_{\mathrm{d},i}$. Meanwhile, it has to be admitted that P_{te} may increase or decrease monotonically in some cases under CFAR requirement. In these cases, the trend of P_{te} is dominated by only one factor between k and $P_{\mathrm{d},i}$ all the time. Therefore, no matter how P_{te} changes with the increase of the number of cooperating SUs, there has to exist an optimal number of cooperating SUs to minimize the total error rate under the CFAR requirement and AND decision fusion rule. When more cooperating SUs are involved in the sensing period, the number of unreliable SUs may increase accordingly and the final sensing performance could be degraded.

4.4 Achievable Ergodic Capacity and Outage Throughput

In this section, the achievable ergodic capacity and throughput of the CR network are investigated in order to capture the performance of the sensing-based secondary links. As shown in Fig. 4.1, the RRHs are the secondary transmitters (SU-Txs) and the secondary receiver (SU-Rx) is located at the origin of the secondary network region. As defined in the section 4.2, each SU-Tx is equipped with multiple antennas and the SU-Rx is with single antenna. The path loss and Rayleigh fading between the SU-Tx and SU-Rx are considered in this chapter. When the PU is absent, the received SNR at the SU-Rx sourced from each SU-Tx is given as

$$\gamma^{\mathrm{s0}} = \frac{P_{\mathrm{ST}}}{L^{\varepsilon}\sigma^{2}}\alpha, \tag{4.38}$$

where P_{ST} denotes the transmitted signal power from the SU-Tx, σ^2 is the additive noise power at the SU-Rx, L is the distance between each SU-Tx and SU-Rx, ε is the path loss factor and α denotes the Rayleigh fading channel gain in each secondary link. When maximal ratio transmission (MRT) is applied, the PDF of α is given as

$$f_{\alpha}(\alpha) = \frac{\alpha^{m-1}e^{-\alpha}}{(m-1)!}, \tag{4.39}$$

and the PDF of L is given by

$$f_L(L) = \frac{2L}{R^2}. \tag{4.40}$$

Meanwhile, when the PU is present, the interference from the PU's signal is considered and the received SINR is given by

$$\gamma^{\mathrm{s1}} = \frac{P_{\mathrm{ST}} L^{-\varepsilon} \alpha}{\sigma^2 + P_{\mathrm{T}} D^{-\varepsilon} \beta}, \tag{4.41}$$

where β denotes the Rayleigh fading gain between the PU and the SU-Rx and β follows the exponential distribution with mean 1, i.e.,

$$f_\beta(\beta) = \exp(-\beta). \tag{4.42}$$

For a CR network, one periodic spectrum sensing frame T_{f} consists of three parts, including the sensing slot T_{s}, decision reporting slot T_{r} and data transmission slot T_{t}. In the interweave method, the data transmission of the secondary links can be carried out under two situations, one is there is no false alarm when the PU is absent and the other one is missed detection occurs when the PU is present. Therefore, the achievable ergodic capacity and throughput of the secondary network also comprise these two parts.

4.4.1 Achievable Ergodic Capacity

Based on the structure of the CR system mentioned above, the achievable capacity of each secondary link in the CR system can be given by

$$C_{\mathrm{ac}} = C_{\mathrm{ac0}} + C_{\mathrm{ac1}}, \tag{4.43}$$

where C_{ac0} denotes the achievable capacity with the absence of the PU and C_{ac1} denotes the achievable capacity with the presence of the PU. Specifically, C_{ac0} and C_{ac1} can be obtained as follows

$$C_{\mathrm{ac0}} = \left(\frac{T_{\mathrm{f}} - T_{\mathrm{s}} - kT_{\mathrm{r}}}{T_{\mathrm{f}}}\right) \log_2(1+\gamma^{\mathrm{s0}})(1-P_{\mathrm{fa}})P(\mathcal{H}_0), \tag{4.44}$$

$$C_{\mathrm{ac1}} = \left(\frac{T_{\mathrm{f}} - T_{\mathrm{s}} - kT_{\mathrm{r}}}{T_{\mathrm{f}}}\right) \log_2(1+\gamma^{\mathrm{s1}})(1-P_{\mathrm{d}})P(\mathcal{H}_1), \tag{4.45}$$

where k is the number of the SUs involved in the cooperative sensing, $P(\mathcal{H}_0)$ and $P(\mathcal{H}_1)$ represent the probabilities that the PU is absent and present respectively.

4.4.1.1 Achievable Ergodic Capacity under $\mathcal{H}_0$

Proposition 2. *The achievable ergodic capacity of each secondary link when the PU is absent can be derived as*

$$\overline{C_{\mathrm{ac0}}} = \frac{2G_{4,3}^{2,3}\left(\frac{P_{\mathrm{ST}}R^{-\varepsilon}}{\sigma^2}\middle|\begin{matrix}1-m,1,1,\frac{2}{\varepsilon}+1\\ \frac{2}{\varepsilon},1,0\end{matrix}\right)}{\varepsilon(m-1)!\ln(2)}\left(\frac{T_{\mathrm{f}}-T_{\mathrm{s}}-kT_{\mathrm{r}}}{T_{\mathrm{f}}}\right)(1-P_{\mathrm{fa}})P(\mathcal{H}_0). \tag{4.46}$$

Proof. In order to derive the expression of $\overline{C_{\mathrm{ac0}}}$, we first obtain the statistical average of $\log_2(1+\gamma^{\mathrm{s0}})$. Let $C_{\mathrm{ec0}} = \log_2(1+\gamma^{\mathrm{s0}})$ and the statistical average $\overline{C_{\mathrm{ec0}}}$ can be calculated by

$$\begin{aligned}\overline{C_{\mathrm{ec0}}} &= \int_0^R\int_0^\infty \log_2\left(1+\frac{P_{\mathrm{ST}}}{L^\varepsilon\sigma^2}\alpha\right)f_\alpha(\alpha)f_L(L)\mathrm{d}\alpha\mathrm{d}L\\ &= \int_0^R\int_0^\infty \frac{\ln\left(1+\frac{P_{\mathrm{ST}}}{L^\varepsilon\sigma^2}\alpha\right)}{\ln(2)}\frac{\alpha^{m-1}e^{-\alpha}}{(m-1)!}\frac{2L}{R^2}\mathrm{d}\alpha\mathrm{d}L.\end{aligned} \tag{4.47}$$

By utilizing the equality relationship

$$\ln(1+ax) = G_{2,2}^{1,2}\left(ax\middle|\begin{matrix}1,1\\1,0\end{matrix}\right), \tag{4.48}$$

the calculation of $\overline{C_{\mathrm{ec0}}}$ can be rewritten as

$$\begin{aligned}\overline{C_{\mathrm{ec0}}} &= \int_0^R\int_0^\infty G_{2,2}^{1,2}\left(\frac{P_{\mathrm{ST}}\alpha}{\sigma^2L^\varepsilon}\middle|\begin{matrix}1,1\\1,0\end{matrix}\right)\frac{\alpha^{m-1}}{e^\alpha}\mathrm{d}\alpha\frac{2L/\ln(2)}{R^2(m-1)!}\mathrm{d}L\\ &= \int_0^R G_{3,2}^{1,3}\left(\frac{P_{\mathrm{ST}}}{\sigma^2L^\varepsilon}\middle|\begin{matrix}1-m,1,1\\1,0\end{matrix}\right)\frac{2L/\ln(2)}{(m-1)!R^2}\mathrm{d}L.\end{aligned} \tag{4.49}$$

Let $z = \left(\frac{R}{L}\right)^\varepsilon$, the equation above can be reorganized. After further manipulations with the aid of [115, (7.811.3)], the expression of $\overline{C_{\mathrm{ec0}}}$ can be derived and the expression (4.46) can be achieved. □

4.4.1.2 Achievable Ergodic Capacity under $\mathcal{H}_1$

The achievable ergodic capacity of each secondary link when the PU is present can be derived as

$$\begin{aligned}\overline{C_{\mathrm{ac1}}} =&(1-P_{\mathrm{d}})P(\mathcal{H}_1)\int_0^{\infty}\int_0^{R}\int_0^{\infty}\log_2\left(1+\frac{P_{\mathrm{ST}}L^{-\varepsilon}\alpha}{\sigma^2+P_{\mathrm{T}}D^{-\varepsilon}\beta}\right)f_{\alpha}(\alpha)f_L(L)f_{\beta}(\beta)\mathrm{d}\alpha\mathrm{d}L\mathrm{d}\beta\\ =&\int_0^{\infty}\frac{2G_{4,3}^{2,3}\left(\frac{P_{\mathrm{ST}}R^{-\varepsilon}}{\sigma^2+P_{\mathrm{T}}D^{-\varepsilon}\beta}\middle|\begin{matrix}1-m,1,1,\frac{2}{\varepsilon}+1\\ \frac{2}{\varepsilon},1,0\end{matrix}\right)}{\varepsilon(m-1)!\ln(2)}e^{-\beta}\mathrm{d}\beta\left(\frac{T_{\mathrm{f}}-T_{\mathrm{s}}-kT_{\mathrm{r}}}{T_{\mathrm{f}}}\right)(1-P_{\mathrm{d}})P(\mathcal{H}_1).\end{aligned} \tag{4.50}$$

By utilizing the expressions (4.46) and (4.50), the achievable ergodic capacity of each secondary link $\overline{C_{\mathrm{ac}}}$ can be obtained by

$$\overline{C_{\mathrm{ac}}} = \overline{C_{\mathrm{ac0}}} + \overline{C_{\mathrm{ac1}}}. \tag{4.51}$$

Therefore, considering all the secondary links, the achievable ergodic capacity of the secondary network[1] based on the homogeneous PPP is given by

$$\begin{aligned}\overline{C_{\mathrm{c}}} &= \sum_{K=1}^{\infty} K\overline{C_{\mathrm{ac}}}\mathbf{P}\{K \quad \text{SU-Txs within secondary network}\}\\ &= \sum_{K=1}^{\infty}\overline{C_{\mathrm{ac}}}e^{-4\rho\theta DR}\frac{(4\rho\theta DR)^K}{(K-1)!}.\end{aligned} \tag{4.52}$$

The value of $\overline{C_{\mathrm{c}}}$ converges with the increasing K, since the probability that there exists K secondary links approaches 0 with the increase of K.

4.4.2 Achievable Throughput

Similarly, the achievable throughput C_{at} of each secondary link can be defined as

$$C_{\mathrm{at}} = C_{\mathrm{at0}} + C_{\mathrm{at1}}, \tag{4.53}$$

[1]In this chapter, the achievable ergodic capacity of the secondary network means the summation of the achievable ergodic capacity of all the possible secondary links. Similarly, the achievable throughput of the secondary network is defined in the same way.

where C_{at0} and C_{at1} denote the achievable throughput of each secondary link when the PU is absent and present respectively. In detail, C_{at0} and C_{at1} can be calculated as

$$C_{\mathrm{at0}} = \left(\frac{T_{\mathrm{f}} - T_{\mathrm{s}} - kT_{\mathrm{r}}}{T_{\mathrm{f}}}\right) \log_2(1+T) P_{\mathrm{cov0}}(1 - P_{\mathrm{fa}}) P(\mathcal{H}_0), \tag{4.54}$$

$$C_{\mathrm{at1}} = \left(\frac{T_{\mathrm{f}} - T_{\mathrm{s}} - kT_{\mathrm{r}}}{T_{\mathrm{f}}}\right) \log_2(1+T) P_{\mathrm{cov1}}(1 - P_{\mathrm{d}}) P(\mathcal{H}_1), \tag{4.55}$$

where the coverage probabilities P_{cov0} and P_{cov1} are defined as the probability that the received SNR or SINR at the SU-Rx is larger than the preset threshold T when the PU is absent and present respectively.

4.4.2.1 Achievable Throughput under $\mathcal{H}_0$

Proposition 3. *Assuming that the path loss $L^{-\varepsilon}$ and Rayleigh fading are experienced by secondary signals and MRT is applied at the SU-Tx, the coverage probability P_{cov0} achieved by each secondary link when the PU is absent, i.e. under the hypothesis $\mathcal{H}_0$, can be derived as*

$$P_{\mathrm{cov0}} = \sum_{t=0}^{m-1} \frac{2T^{-\frac{2}{\varepsilon}} \left(\frac{P_{\mathrm{ST}}}{\sigma^2}\right)^{\frac{2}{\varepsilon}}}{\varepsilon R^2 t!} \gamma\left(t + \frac{2}{\varepsilon}, \frac{T\sigma^2}{P_{\mathrm{ST}}} R^{\varepsilon}\right), \tag{4.56}$$

where $\gamma(\cdot,\cdot)$ denotes the lower incomplete Gamma function.

Proof. According to the definition of the coverage probability, the coverage probability under the hypothesis $\mathcal{H}_0$ can be written as

$$\begin{aligned}
P_{\mathrm{cov0}} &= \Pr[\gamma^{\mathrm{s0}} \geq T] \\
&= \mathbb{E}\left[\Pr\left[\frac{P_{\mathrm{ST}}}{L^{\varepsilon}\sigma^2}\alpha \geq T\right] \middle| L\right] \\
&= \mathbb{E}\left[\Pr\left[\alpha \geq T\frac{L^{\varepsilon}\sigma^2}{P_{\mathrm{ST}}}\right] \middle| L\right] \\
&= \mathbb{E}\left[\int_{\frac{T\sigma^2}{P_{\mathrm{ST}}}L^{\varepsilon}}^{\infty} \frac{\alpha^{m-1}e^{-\alpha}}{(m-1)!} \mathrm{d}\alpha \middle| L\right] \\
&= \mathbb{E}\left[\frac{\Gamma\left(m, \frac{T\sigma^2}{P_{\mathrm{ST}}}L^{\varepsilon}\right)}{(m-1)!} \middle| L\right] \\
&= \int_0^R \sum_{t=0}^{m-1} \exp\left(-\frac{T\sigma^2}{P_{\mathrm{ST}}}L^{\varepsilon}\right) L^{\varepsilon t} \frac{T^t \sigma^{2t}}{{P_{\mathrm{ST}}}^t t!} \frac{2L}{R^2} \mathrm{d}L,
\end{aligned} \tag{4.57}$$

by utilizing the definition of the lower incomplete Gamma function and after further manipulations, the closed-form expression of the coverage probability under the hypothesis $\mathcal{H}_0$ can be obtained as equation (4.56). □

Therefore, the expression of the achievable throughput for each secondary link under the hypothesis $\mathcal{H}_0$ can be obtained by utilizing equation (4.54) and (4.56).

4.4.2.2 Achievable Throughput under $\mathcal{H}_1$

Proposition 4. *When the PU is present, the interference to the secondary network sourced from the PU is considered. Assuming that the path loss $L^{-\varepsilon}$ and Rayleigh fading are experienced by secondary signals and MRT is applied at the SU-Tx, the coverage probability of each secondary link under the hypothesis $\mathcal{H}_1$ is derived as*

$$P_{\text{cov1}} = \sum_{t=0}^{m-1} \sum_{w=0}^{\infty} \frac{2(-1)^w R^{\varepsilon(t+w)} e^{\frac{\sigma^2 D^{\varepsilon}}{P_{\text{T}}}}}{\varepsilon t! w! \left(t+w+\frac{2}{\varepsilon}\right) (P_{\text{T}} D^{-\varepsilon} T / P_{\text{ST}})^{-t-w}} \Gamma\left(t+w+1, \frac{\sigma^2 D^{\varepsilon}}{P_{\text{T}}}\right). \tag{4.58}$$

Proof. Based on the definition of the coverage probability, the coverage probability under the hypothesis $\mathcal{H}_1$ can be calculated as

$$\begin{aligned}
P_{\text{cov1}} &= \Pr[\gamma^{\text{s1}} \geq T] \\
&= \mathbb{E}\left[\Pr\left[\frac{P_{\text{ST}} L^{-\varepsilon}\alpha}{\sigma^2 + P_{\text{T}} D^{-\varepsilon}\beta} \geq T\right] \middle| \beta, L\right] \\
&= \mathbb{E}\left[\Pr\left[\alpha \geq \frac{\sigma^2 + P_{\text{T}} D^{-\varepsilon}\beta}{P_{\text{ST}} L^{-\varepsilon}} T\right] \middle| \beta, L\right] \\
&= \mathbb{E}\left[\frac{\Gamma\left(m, \frac{T(\sigma^2 + P_{\text{T}} D^{-\varepsilon}\beta)}{P_{\text{ST}}} L^{\varepsilon}\right)}{\Gamma(m)} \middle| \beta, L\right] \\
&= \int_0^{\infty} \int_0^{R} \exp\left(-\frac{T}{P_{\text{T}}}(\sigma^2 + P_{\text{T}} D^{-\varepsilon}\beta) L^{\varepsilon}\right) \sum_{t=0}^{m-1} \frac{T^t (\sigma^2 + P_{\text{T}} D^{-\varepsilon}\beta)^t}{{P_{\text{ST}}}^t t!} L^{\varepsilon t} f_L(L) f_{\beta}(\beta) \mathrm{d}L \mathrm{d}\beta \\
&= \int_0^{\infty} \sum_{t=0}^{m-1} \frac{2T^{-\frac{2}{\varepsilon}} \left(\frac{P_{\text{ST}}}{\sigma^2 + P_{\text{T}} D^{-\varepsilon}\beta}\right)^{\frac{2}{\varepsilon}}}{\varepsilon t! R^2} \gamma\left(t+\frac{2}{\varepsilon}, \frac{T}{P_{\text{ST}}}(\sigma^2 + P_{\text{T}} D^{-\varepsilon}\beta) R^{\varepsilon}\right) e^{-\beta} \mathrm{d}\beta,
\end{aligned} \tag{4.59}$$

let $z = \frac{T}{P_{\text{ST}}}(\sigma^2 + P_{\text{T}} D^{-\varepsilon}\beta)$, the integral above can be reorganized as

$$P_{\text{cov1}} = \int_{\frac{T\sigma^2}{P_{\text{ST}}}}^{\infty} \sum_{t=0}^{m-1} \frac{2 P_{\text{ST}} z^{-\frac{2}{\varepsilon}}}{\varepsilon t! R^2 P_{\text{T}} D^{-\varepsilon} T} \gamma\left(t+\frac{2}{\varepsilon}, R^{\varepsilon} z\right) \exp\left(-\frac{P_{\text{ST}} z - T\sigma^2}{P_{\text{T}} D^{-\varepsilon} T}\right) \mathrm{d}z. \tag{4.60}$$

By utilizing the power series expansion of the lower incomplete gamma function, the coverage probability under the hypothesis $\mathcal{H}_1$ can be rewritten as

$$P_{\text{cov1}} = \int_{\frac{T\sigma^2}{P_{\text{ST}}}}^{\infty} \sum_{t=0}^{m-1} \sum_{w=0}^{\infty} \frac{2(-1)^w P_{\text{ST}} R^{\varepsilon(t+w+2/\varepsilon)}}{P_{\text{T}} D^{-\varepsilon} T\varepsilon t! w! R^2 (t+w+2/\varepsilon)} z^{t+w} \exp\left(-\frac{P_{\text{ST}} z - T\sigma^2}{P_{\text{T}} D^{-\varepsilon} T}\right) \mathrm{d}z. \quad (4.61)$$

The above integral can be calculated with the aid of the definition of the upper incomplete gamma function and then the expression of (4.58) can be obtained. □

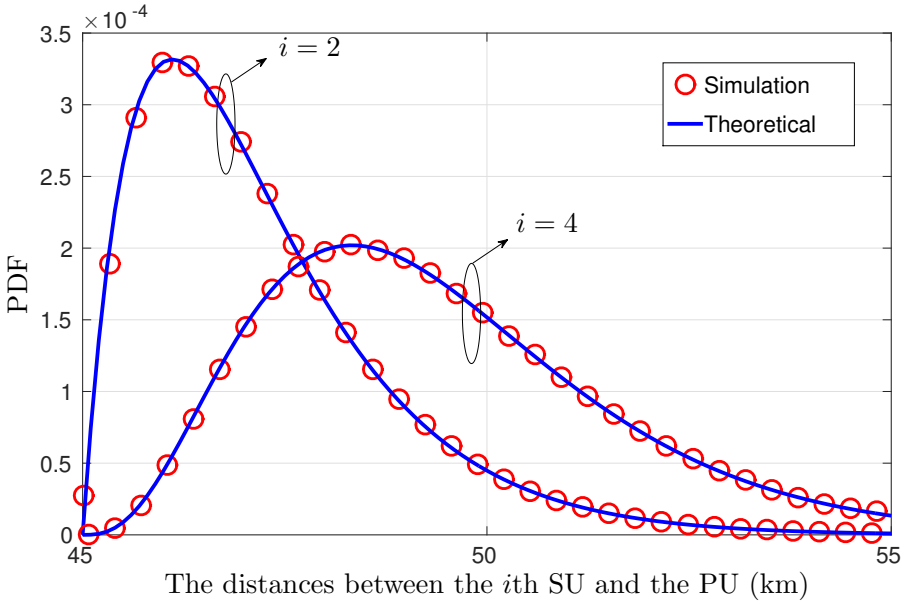

Figure 4.2: *The PDF of the distances between the ith SU within the area of interest and the PU.*

By using the Eq. (4.55) and the expression (4.58), the achievable throughput of each secondary link can be obtained in the presence of the PU.

After the expressions of the coverage probability under the hypothesis $\mathcal{H}_0$ and $\mathcal{H}_1$ are derived, the closed-form expressions of the achievable throughput under the absence and presence of the PU can be obtained by utilizing (4.54) and (4.55). Therefore, the achievable throughput C_{at} of each secondary link can be obtained by using (4.53).

Furthermore, considering all the available secondary links, the achievable throughput of the secondary

Parameters	**Values**
Transmit power of PU-Tx P_{T}	5W
Transmit power of SU-Tx P_{ST}	40mW
Additive noise power at SUs σ_v^2	-90 dBm
Antenna number of the SU m	$4, 6$
Sample size of spectrum sensing n	500, 600, 800
Sampling frequency f_{s}	6 MHz
Path loss exponent factor ε	3.1
Single periodic frame of the SU T_{f}	100 ms
Coverage radius of the FC R	5 km
Distance between the FC and PU D	50 km
BEP of the decision reporting channel P_{b}	0.01
Data rate of the reporting channel R_{b}	100 Kbps
Density in the PPP ρ	10^{-7} nodes/m^2

Table 4.1: *Simulation parameters of cooperative spectrum sensing with random secondary networks*

network based on the homogeneous PPP is given by

$$\begin{aligned} C_{\mathrm{th}} &= \sum_{K=1}^{\infty} KC_{\mathrm{at}}\mathbf{P}\{K \quad \text{SU-Txs within secondary network}\} \\ &= \sum_{K=1}^{\infty} C_{\mathrm{at}} e^{-4\rho\theta DR}\frac{(4\rho\theta DR)^K}{(K-1)!}. \end{aligned} \tag{4.62}$$

It is worth mentioning that the value of C_{th} converges with the increase of K, since the probability of having K secondary links approaches 0 when K is large enough.

4.5 Simulation Results and Discussions

In this section, simulation results are provided to validate the derived expressions and the analysis throughout this chapter. In the simulation results, it is assumed that the coverage radius of the FC is $R = 5$ km, the distance between the FC and PU is $D = 50$ km. The PU is assumed as a TV transmitter and the transmit power is 5 W, meanwhile, the additive noise power is assumed at -90 dBm [42]. In [42], the noise power level is assumed at -98 dBm, however, it still makes sense that we consider a higher noise power and 5 W as the transmit power in this chapter. Actually, what we care in this work is the ratio of the transmit power and noise level, which can be found in (4.26). Based

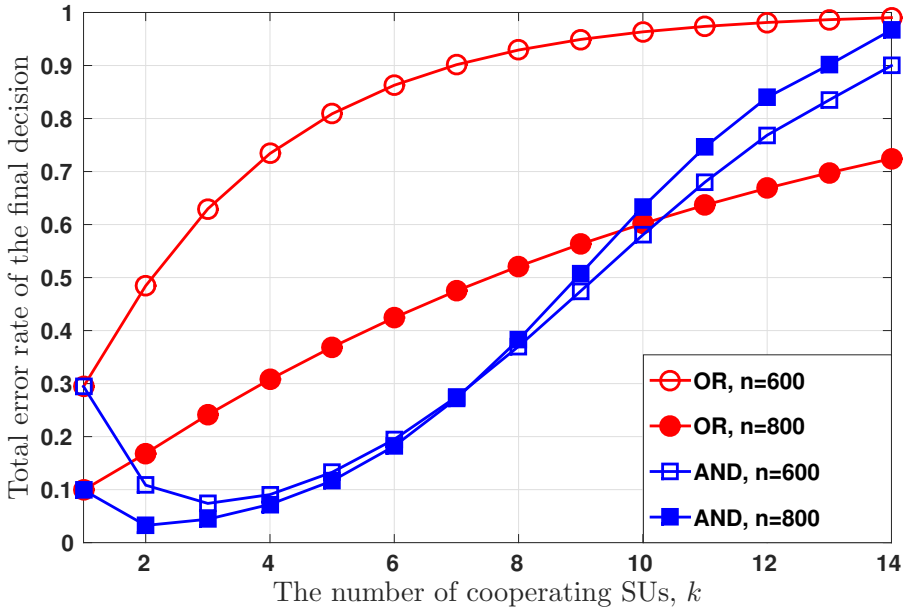

Figure 4.3: *The total error rate of the final decision versus the number of cooperating SUs k for various sample sizes n by using OR and AND fusion rules under the CDT requirement.*

on IEEE 802.22 standard, the SNR for spectrum sensing can be down to -22 dB, so the assumptions of 5 W transmit power and -90 dBm noise power help us to make the received SNR at the FC of the secondary network achieve around -15 dB. Many literatures made similar assumptions for simplifying the calculations, e.g. [108]. Besides, in a practical system, the interference measured at the receiver could be considered as noise as well and the transmit power can be adjusted for different objectives. Therefore, the assumptions of transmit and noise powers in this chapter are still reasonable. The path loss exponent factor is $\varepsilon = 3.1$. When employing error rate control methods, the BEP during the decision reporting process is assumed as $P_{\mathrm{b}} = 10^{-2}$. The sampling frequency of the signal $f_{\mathrm{s}} = 6$ MHz, the data rate of the reporting channel $R_{\mathrm{b}} = 100$ Kbps so that $T_{\mathrm{r}} = \frac{1}{R_{\mathrm{b}}}$. One periodic frame of the SU is $T_{\mathrm{f}} = 100$ ms and the density in the considered PPP is $\rho = 10^{-7}$ nodes/m^2. These simulation parameter are detailed in the Table 4.1 as well.

Fig. 4.2 validates the expression of the PDF of the distance between the ith nearest SU and the PU derived as (4.25) in this chapter. This figure represents the PDF of the Euclidean distance of the second and fourth nearest SU from the PU. It can be seen that the analytical results match with the Monte-Carlo results very well, which proves that the closed-form expression of the distance between the PU and its ith nearest neighbour located within the area of interest.

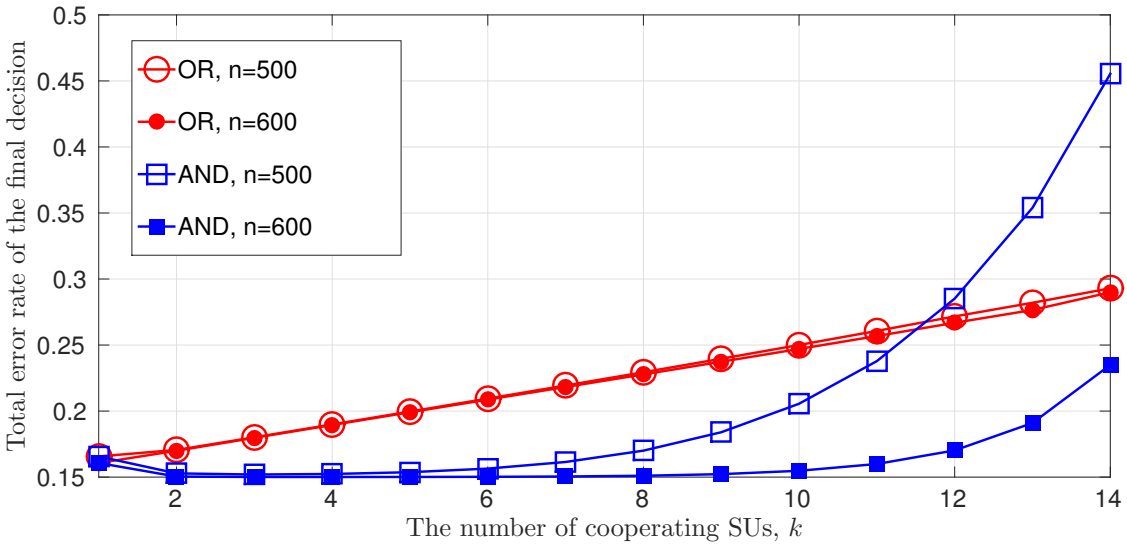

Figure 4.4: *The total error rate of the final decision versus the number of cooperating SUs k for various sample sizes n by using OR and AND fusion rules under the CDR requirement.*

Fig. 4.3 depicts the total error rate of the final decision versus the number of collaborating SUs under the CDT requirement by using OR and AND fusion rules, respectively. Due to the verifications in Fig. 3.5 and Fig. 3.6, only the analytical results are shown in this figure. In this figure, the preset decision threshold is 0.28, each SU is assumed with 4 receive antennas ($m = 4$) and the sample size of received signal is $n = \{600, 800\}$. The total error rate of the final decision can be calculated as described in Section III. Since the number of available SUs in PPP is random, it is impossible to show all the possible cases of different numbers of SUs. However, the probability of above a certain number of SUs within the coverage radius of FC can be calculated by using (B.13). For the PPP with the determined density ρ considered in this chapter, the probability of over 14 SUs located within the area of interest is under 0.05. Thus, Fig. 4.3 only shows the cases of the number of available SUs up to 14, which is enough for analysis.

It can be seen from Fig. 4.3 that the total error rate decreases first and then increases with the increase of the number of cooperating SUs, under the AND rule. The optimal numbers of cooperating SUs are $k_{\text{opt}} = \{3, 2\}$ which makes the total error rates achieve the minimum values $\{0.07, 0.03\}$ for the cases of $n = \{600, 800\}$, respectively. Under the OR rule, the total error rate increases with the increasing k. Hence, single node spectrum sensing based on the nearest SU can achieve the best

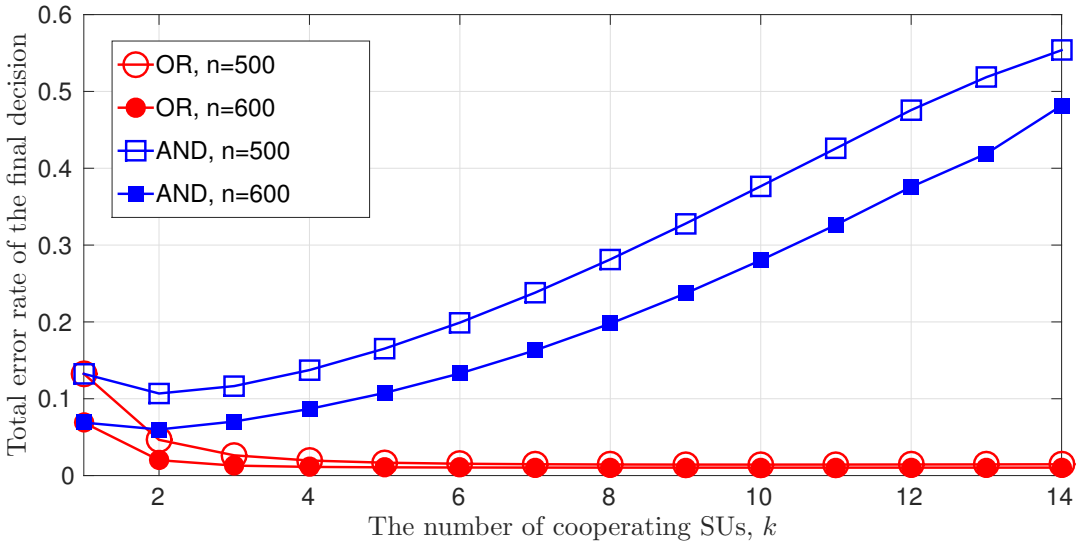

Figure 4.5: *The total error rate of the final decision versus the number of cooperating SUs k for various sample sizes n by using OR and AND fusion rules under the CFAR requirement.*

sensing performance. Therefore, it can be deduced that using all the available SUs is not always necessary to achieve the best sensing performance. When the SUs follow a homogeneous PPP and the number of available SUs is large, considering k_{opt} SUs (not always all the SUs) not only improves the accuracy of spectrum sensing, but also accelerates the cooperative spectrum sensing.

Similarly, Fig. 4.4 represents the total error rate of the final decision versus the number of collaborating SUs under the CDR requirement. These curves are obtained by employing OR and AND decision fusion rules respectively. As mentioned in the former section, the probability of detection of the final decision is constant under this CDR requirement and the desired detection rate is set at 0.85. Each SU is equipped with 4 antennas ($m = 4$) and the sample sizes are $n = 500, 600$. From this figure, it can be seen that the total error rate of the final decision is a monotonically increasing function with regard to k under the OR rule. Thus cooperating the single SU with highest received SNR is best choice to minimize the final total error rate for the OR cases shown in this figure. As contrast, the total error rate decreases with the increasing k under the AND rule. Specifically, the minimum total error rates are obtained when the numbers of cooperating SUs are 3 and 4 for $n = 500, 600$ respectively.

Besides, the total error rate performance of the final decision is also presented under the CFAR requirement as Fig. 4.5. In this plot, a constant false alarm rate of the final decision is predefined and

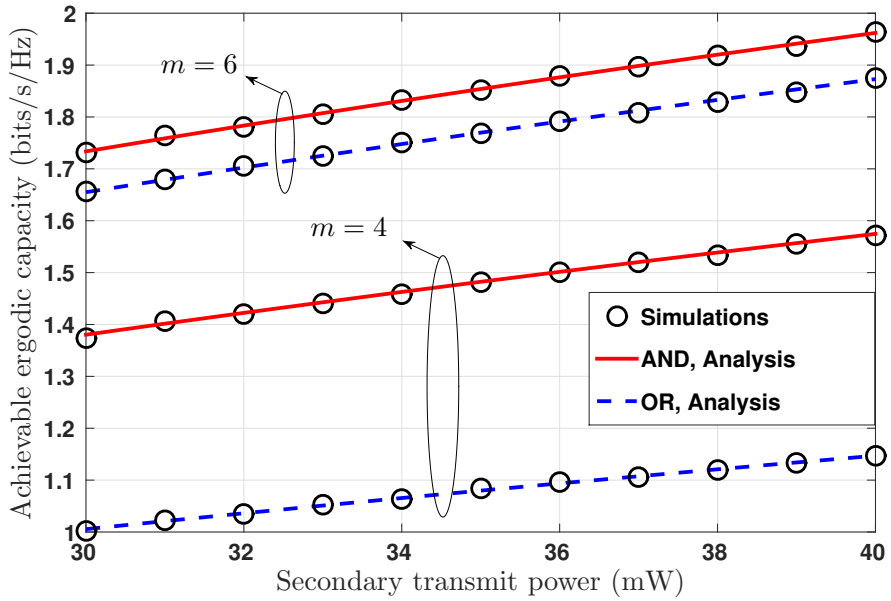

Figure 4.6: *The achievable ergodic capacity versus the secondary transmit power under different fusion rules, the antenna number at each SU-Tx is* $m = 4, 6$ *and the sample size is* $n = 600$.

this figure is 1%. This scenario is considered from the interests of SUs, since guaranteeing a low false alarm rate assures that SUs could get enough chances to access the licensed frequency bands. It can be observed from this figure that the final total error rates goes up first and then reduces under both OR and AND rules. It is worth noting that, under the OR rule, the final total error rate increases slightly after the initial decrease. Specifically, the optimal number of cooperative SUs is 2 for both $n = 500, 600$ under the AND rule. Meanwhile, under the OR rule, the optimal values are 10 and 11 for $n = 500, 600$ respectively.

Fig. 4.6 shows the achievable ergodic capacity of each secondary link versus the transmit power of the SU-Tx from 30 mW to 40 mW under the CDT requirement when achieving the minimum total error rate. The minimum total error rate can be obtained by utilizing the method proposed in section III. In this figure, various cases are presented under different numbers of SU-Tx antennas (i.e., $m = 4$, $m = 6$) and different decision fusion rules. The number of samples of the PU's signal is $n = 600$. Under the CDT requirement, a preset decision threshold is required. The definition area of the decision threshold is $[1/m, 1]$, which means the definition area of the decision thresholds can vary depending on the number of antennas at each SU-Tx. Therefore, the predefined decision thresholds are assumed to be 0.28 and 0.24 for the cases of $m = 4$ and $m = 6$ respectively. Furthermore, it can be seen

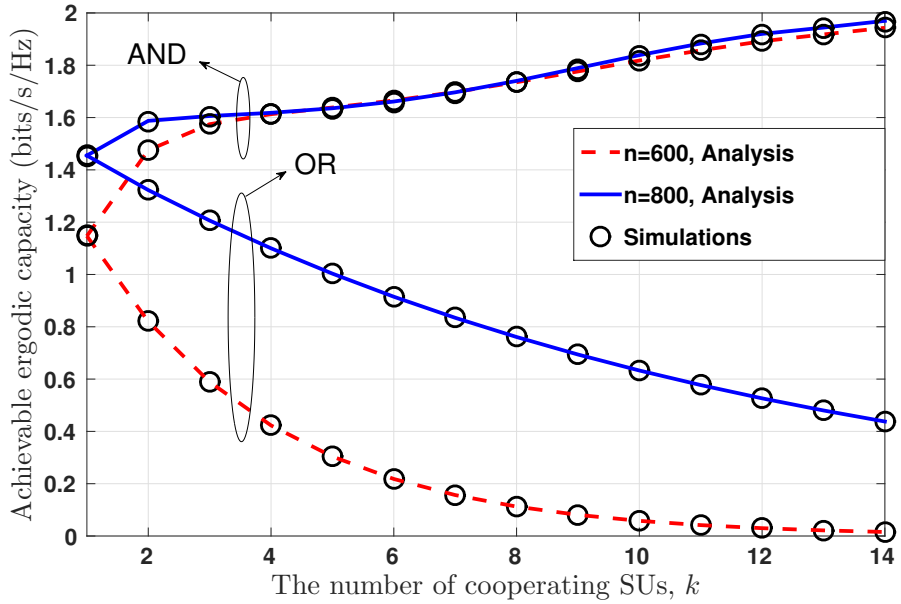

Figure 4.7: *The achievable ergodic capacity versus the number of cooperating SUs under different fusion rules, each SU-Tx is with* 4 *antennas and the sample size is* $n = 600, 800$.

that the achievable ergodic capacity of the secondary network rises monotonically with the increasing transmit power of the SU-Tx. When comparing the achievable ergodic capacity in terms of decision fusion rules, the AND rule outperforms the OR rule for a same number of SU-Tx antennas. Besides, it can be seen that the gap of the achievable ergodic capacity between the AND and OR fusion rules reduces with increasing m.

Fig. 4.7 represents the achievable ergodic capacity of each secondary link versus the number of the cooperating SUs under the CDT requirement when the SUs follow a PPP with density ρ. In this figure, each SU-Tx is equipped with 4 antennas and the number of samples of the PU's signal is $n = 600, 800$. The predefined decision threshold is 0.28 and the transmit power of the SU-Tx is $P_{\mathrm{ST}} = 40$ mW. The other parameter settings are the same as the previous part. Firstly, the achievable ergodic capacity by using the AND decision fusion rule is higher than the results by using the OR rule when each SU-Tx has the same number of antennas. Secondly, it can also be seen that a larger number of samples of the PU's signal can help to improve the achievable ergodic capacity of the secondary network. Furthermore, when the AND fusion rule is applied, the achievable ergodic capacity increases with increasing k. However, under the OR fusion rule, the achievable ergodic capacity decreases with increasing k. Under the CDT requirement, for the AND decision fusion rule, both P_{fa} and P_{d} are

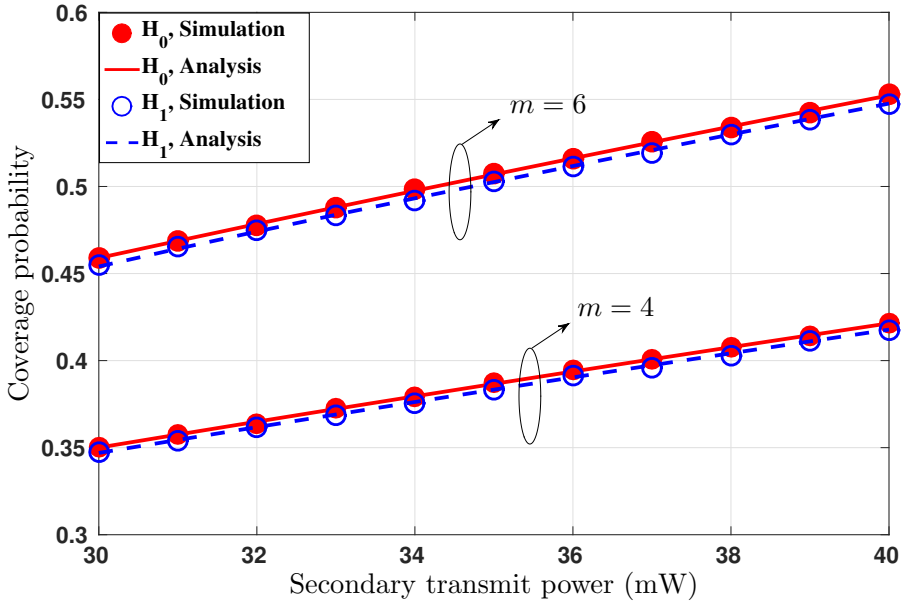

Figure 4.8: *The coverage probability versus the secondary transmit power under the hypothesis $\mathcal{H}_0$ and $\mathcal{H}_1$, the antenna number at each SU-Tx is $m = 4, 6$.*

decreasing functions with regard to k. However, when the OR fusion rule is applied, $P_{\rm fa}$ and $P_{\rm d}$ both increase with increasing k. Thus, for given primary and secondary transmit powers, it can be found from (4.43), (4.44) and (4.45) that the achievable ergodic capacity of the secondary network increases under the AND rule and decreases under the OR rule with the increase of k. Therefore, considering the total error rate of the final decision performance shown as Fig. 4.3 and the achievable ergodic capacity described in Fig. 4.7 together, the method of choosing the optimum number of cooperating SUs should be as follows:

In order to achieve a high achievable ergodic capacity and an acceptable total error rate concurrently, the eligible numbers of the cooperating SUs can be determined first for a target total error rate and then the optimum number of cooperating SUs which maximizes the achievable ergodic capacity can be selected among the eligible numbers obtained. Specifically, the achievable ergodic capacity is an increasing function with regard to k for the AND rule, but it is a decreasing function for the OR rule. Hence the largest number of the cooperating SUs which satisfies the desired total error rate requirement should be chosen to maximize the achievable ergodic capacity for the AND rule. On the contrary, the smallest number of the collaborating SUs that makes the total error rate under or equal to the targeted value is selected for the OR rule.

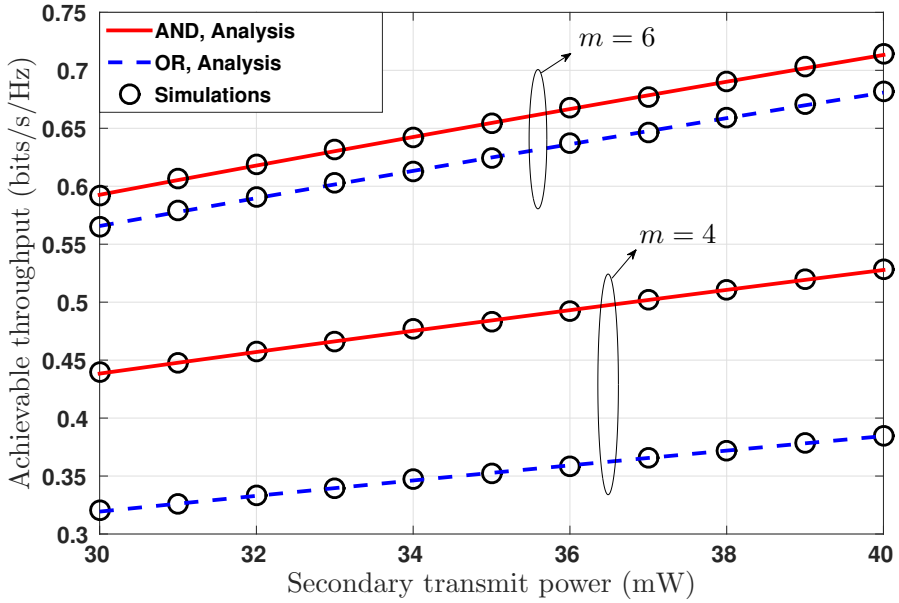

Figure 4.9: *The achievable throughput versus the secondary transmit power under different fusion rules, the antenna number at each SU-Tx is* $m = 4, 6$ *and the sample size is* $n = 600$.

Fig. 4.8 describes the coverage probability of each secondary link versus the transmit power of the SU-Tx from 30 mW to 40 mW under the hypotheses $\mathcal{H}_0$ and $\mathcal{H}_1$. The predefined threshold of the received SNR and SINR at the secondary receiver is assumed to be 3 dB. Two cases (i.e., $m = 4, m = 6$) are presented in this figure under the hypotheses $\mathcal{H}_0$ and $\mathcal{H}_1$ respectively. From this figure, the coverage probabilities under the hypotheses $\mathcal{H}_0$ and $\mathcal{H}_1$ both increase with the increasing secondary transmit power. Furthermore, it can also be observed that more antennas at each SU-Tx help to improve the coverage probability, which can also be inferred from the expressions (4.56) and (4.58).

Fig. 4.9 shows the achievable throughput performance of each secondary link with the increase of the secondary transmit power from 30 mW to 40 mW when the minimum total error rate is achieved. Multiple cases are represented for different numbers of antennas at each SU-Tx (i.e., $m = 4, m = 6$) and decision fusion rules. It can be seen that the achievable throughput increases with the increase of the secondary transmit power and the number of the antennas at each SU-Tx under both of the fusion rules. Besides, the AND fusion rule can achieve a better achievable throughput than the OR rule.

Fig. 4.10 presents the achievable throughput of each secondary link with the increase of the number of the cooperating SUs under the CDT requirement. The transmit power of the SU-Tx is 40 mW and the preset decision threshold is 0.28. Firstly, for a given sample size, the AND rule can achieve a

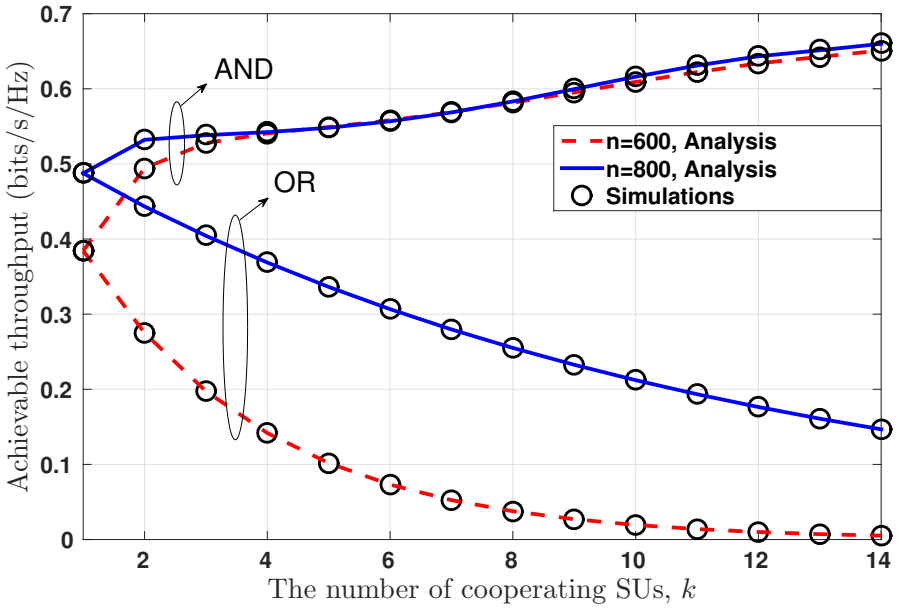

Figure 4.10: *The achievable throughput versus the number of cooperating SUs under different fusion rules, each SU-Tx is with* 4 *antennas and the sample size is* $n = 600, 800$.

higher achievable throughput of the secondary network than the OR rule under the CDT requirement. Secondly, a larger sample size helps to obtain a higher achievable throughput of the secondary network. Lastly, the achievable throughput of the secondary network increases with the number of cooperating SUs under the AND rule, however, it decreases with an increasing k under the OR rule. Therefore, considering the total error rate performance and the achievable throughput of the secondary network concurrently, different strategies should be used to determine the optimal number of cooperating SUs for different decision fusion rules. Specifically, under the AND rule, the chosen number of cooperating SUs should be as large as possible while not exceeding the target total error rate. On the contrary, under the OR rule, the chosen number of cooperating SUs should be as small as possible based on the target total error rate requirement.

4.6 Summary

This chapter investigated the efficient cooperative spectrum sensing in CR networks by using the GLRT detector when SUs follow a homogeneous PPP. The total error rate performance of the cooperative sensing system was analysed by utilizing the theoretical expressions of the individual proba-

bilities of false alarm and detection. The total error rate of the final decision was then investigated when cooperating different numbers of SUs under OR and AND fusion rules, respectively. It is worth mentioning that reporting errors were also considered in this chapter. The analytical results indicated that cooperation between all the SUs does not always achieve the best spectrum sensing performance and the obtained optimal numbers of cooperating SUs in this chapter minimized the total error rates of the final decisions. It is worth noting that the SUs with higher average received SNRs are preferentially chosen to implement cooperative spectrum sensing. Besides, the analytical expressions of the achievable ergodic capacity and throughput of the secondary network were derived. We also studied the impact of the number of cooperating SUs on the achievable ergodic capacity and throughput of the secondary network. Accordingly, different strategies were proposed to determine the optimum number of cooperating SUs in order to achieve the best transmission performance for different fusion rules while not exceeding the target total error rate.

Chapter 5
Full-duplex Spectrum Sensing and Sharing Analyses

5.1 Introduction

The spectrum sensing techniques and strategies investigated in the last two chapters are both based on the traditional HD spectrum sensing system. Under the HD spectrum sensing scenario, the sensing and transmission frames of the secondary network are separate. Therefore, the sensing-throughput trade-off has to be considered in order to maximize the throughput of the secondary network, which has been studied in Chapter 3 of this thesis. On the contrary, FD systems can conduct transmission and reception simultaneously in the same frequency bands, but self-interference will be introduced by the FD antennas. In order to cope with the strong self-interference generated by the FD antennas, various self-interference reduction techniques have been proposed and studied, such as a phase shifter, radio frequency analog cancellation and digital baseband interference cancellation, etc. Therefore, due to the recent advances on self-interference reduction techniques [65, 116, 117], the FD technique has been put forward to apply in CR networks to improve the sensing performance and spectral efficiency of the secondary network. In FD CR networks, the SU possesses FD capability and the antennas of the SU are partitioned into two parts, including the sensing and transmission antennas. Compared with the HD CR network within the same length of periodic spectrum sensing frame, FD CR systems can implement sensing and transmission during the whole frame so that more samples can be accumulated for spectrum sensing and longer data transmission time can be obtained for the secondary network.

In practical CR systems, the realization of the synchronization between the PUs and SUs is difficult since the types of the primary and secondary networks are different normally. However, in the previous works on CR networks, the system is usually assumed to be time-slotted which means that the PUs can only change their state (i.e., active or inactive) at the beginning of each time-slotted secondary frame. On the contrary, the PUs and SUs are asynchronous in the non-time-slotted network. Therefore, the non-time-slotted CR network is more practical and realistic. However, because of the complexity of the non-time-slotted model, most existing works on both HD and FD CR networks, e.g., [13, 68,

118, 119], have mainly focused on the time-slotted system where the PUs and SUs are assumed to be perfectly synchronized.

Motivated by the benefits of the FD technique and the practical significance of the non-time-slotted system, we investigate the FD spectrum sensing and sharing performance for multi-antenna non-time-slotted CR networks in this chapter. Most of the existing FD works for CR networks, e.g., [12, 13, 120], assumed that there was only a single antenna for sensing and another single antenna for transmission at the SU. Therefore multi-antenna ED is considered in this chapter. A low probability of false alarm creates more chances to access the spectrum holes for SUs, which benefits the SUs. Meanwhile, a low missed detection rate helps to protect the PUs from the harmful interference caused by the SUs, which considers the interests of PUs. Thus, the total error rate is investigated in order to consider the benefits of PUs and SUs concurrently. The investigations in this chapter consist of two parts, including the FDSS and FD-SBSS schemes, and the detailed contributions are as follows.

- In terms of the FDSS scenario, firstly, the generalized closed-form expressions of the probabilities of false alarm and missed detection of the multi-antenna ED are derived based on the non-time-slotted FD system. Secondly, the total error rate is investigated in order to consider the interests of PUs and SUs simultaneously. Furthermore, the optimal decision threshold pair is obtained, which can minimize the total error rate.

- In terms of the FD-SBSS scheme, firstly, the expressions of collision and spectrum waste probabilities are derived based on the proposed FD-SBSS scheme. Secondly, the antenna-partitioning is explored in order to maximize the achievable throughput of the SU. Furthermore, appropriate antenna-partitioning methods are proposed for both FD-SBSS and FDSS cases.

The remainder of this chapter is organized as follows. Section 5.2 describes the system model. In Section 5.3, the FDSS scheme is investigated and the closed-form expressions of the probabilities of false alarm and missed detection are derived. Meanwhile, optimal decision threshold pairs are studied to minimize the total error rate. The FD-SBSS scheme is proposed in Section 5.4 in order to improve the achievable throughput of the secondary network. Both the sensing and transmission performance are explored in this section. Section 5.5 provides the simulation results and related discussions. Finally, Section 5.6 concludes this chapter.

5.2 System Model

We consider the FD non-time-slotted CR network based on multi-antenna ED, which is shown in Fig. 5.1. The PU is assumed to be equipped with single antenna and the SU-Tx has multiple antennas. The antennas of SU-Tx comprise two parts, including the sensing and transmission antennas. Specifically, the sensing antennas perform spectrum sensing and the transmission antennas conduct the data transmission of the secondary network simultaneously. The SUs and PU share the licensed frequency bands with different transmit powers based on sensing results.

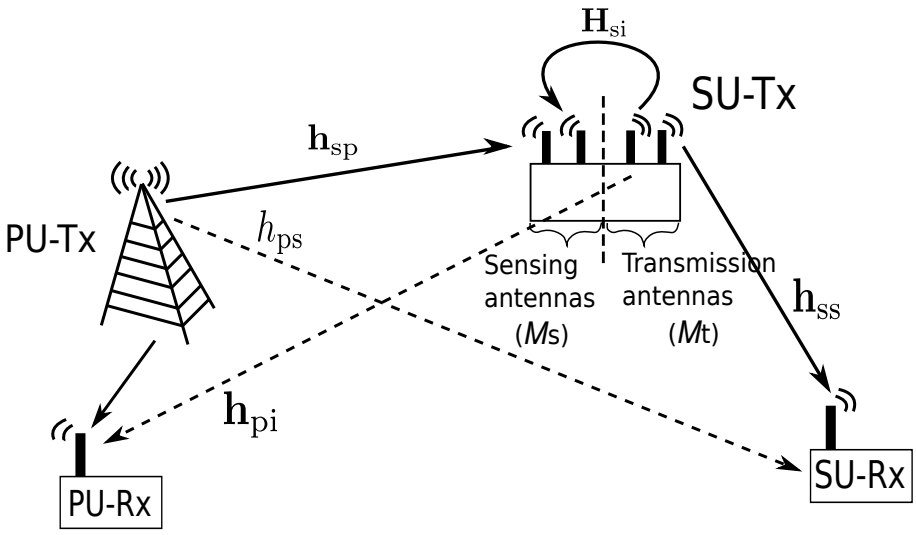

Figure 5.1: *The system model of FD spectrum sensing*

The considered non-time-slotted system is presented in Fig. 5.2 (a), where the PU's state may change at any time within the periodic spectrum sensing frame so that the PU can access and leave the licensed frequency bands randomly. For comparison, the traditional HD time-slotted spectrum sensing system is also illustrated as Fig. 5.2 (b). The activity of the PU is characterized as an alternating ON/OFF process. In practical applications, the state of the PU would not change frequently within one spectrum sensing frame, since each activity period of the PU is longer than each sensing/transmission period of the SU. Hence, without loss of generalization, we assume the PU may change its status up to once within one periodic spectrum sensing frame and the duration of either PU's state follows exponential distribution [121]. As shown in Fig. 5.2, $t_{\mathrm{on}}, t_{\mathrm{off}}$ denote the durations of PU's ON and OFF states,

thus the PDFs of $t_{\rm on}$ and $t_{\rm off}$ are given by

$$f_{\rm on}(t_{\rm on}) = \frac{1}{\lambda_{\rm on}} \exp\left(-\frac{t_{\rm on}}{\lambda_{\rm on}}\right), \tag{5.1}$$

$$f_{\rm off}(t_{\rm off}) = \frac{1}{\lambda_{\rm off}} \exp\left(-\frac{t_{\rm off}}{\lambda_{\rm off}}\right), \tag{5.2}$$

where $\lambda_{\rm on} = \mathbb{E}(t_{\rm on})$ and $\lambda_{\rm off} = \mathbb{E}(t_{\rm off})$ denote the expectations of $t_{\rm on}$ and $t_{\rm off}$. Therefore, the departure probability of PU within an arbitrary secondary sensing/transmission slot is given by

$$\mu_0 = \int_0^T f_{\rm on}(t_{\rm on})\, {\rm d}t_{\rm on} = 1 - \exp\left(-\frac{T}{\lambda_{\rm on}}\right), \tag{5.3}$$

where T is the duration of every secondary sensing/transmission time slot and $\lambda_{\rm off}, \lambda_{\rm on} \gg T$. Similarly, the arrival probability of PU within a secondary slot is given by

$$\mu_1 = \int_0^T f_{\rm off}(t_{\rm off})\, {\rm d}t_{\rm off} = 1 - \exp\left(-\frac{T}{\lambda_{\rm off}}\right). \tag{5.4}$$

ED is employed at the sensing antennas of the SU-Tx in this chapter, since the ED does not require the knowledge of the PU's signal and is easy to realize in hardware. Assuming the numbers of sensing and transmission antennas at the SU-Tx are denoted by $M_{\rm s}$ and $M_{\rm t}$ respectively and N is the total number of the samples of the received signals for each whole sensing period, the test statistic of the ED is given by

$$T_{\rm ED} = \frac{1}{M_{\rm s} N} \sum_{i=1}^{M_{\rm s}} \sum_{n=1}^{N} |y_i(n)|^2, \tag{5.5}$$

where $y_i(n)$ denotes the received signal of the nth sample observed at the ith sensing antenna of the SU. Also, a saturated traffic scenario is assumed, which means that the SUs always have data to transmit.

5.3 Performance Analysis of FD Spectrum Sensing

In this section, the performance of the multi-antenna ED based non-time-slotted spectrum sensing using the FD technique is investigated. In order to consider the interests of the PU and SUs simul-

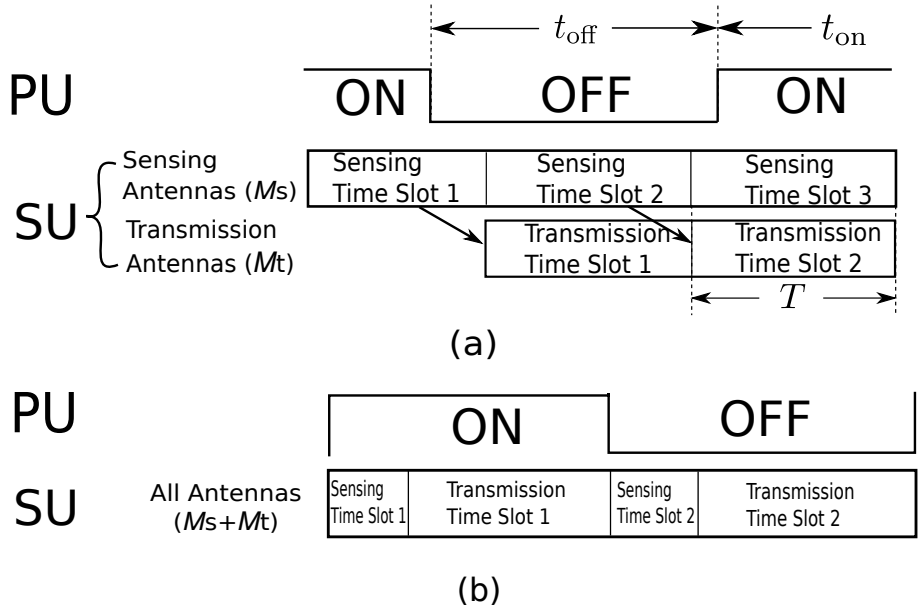

Figure 5.2: *(a) The FD non-time-slotted spectrum sensing system. (b) The HD time-slotted spectrum sensing system. (ON: The PU is active, OFF: The PU is inactive.)*

taneously, the total error rate of the spectrum sensing is studied and the optimal decision threshold pair is obtained. The total error rate $P_{\rm te}$ is defined by the probabilities of false alarm $P_{\rm fa}$ and missed detection $P_{\rm m}$. Therefore, the closed-form expressions of $P_{\rm fa}$ and $P_{\rm m}$ are required for the analyses of $P_{\rm te}$ and decision thresholds.

5.3.1 FD Spectrum Sensing Scheme

As introduced in the previous section, the spectrum sensing of the SU-Tx can be implemented with the FD technique under two cases: (1) The transmission antennas of the SU-Tx are transmitting data; (2) The transmission antennas are silent. When the transmission antennas of the SU-Tx are active, self-interference will be introduced to the spectrum sensing process at the sensing antennas. The self-interference can be reduced partly through existing self-interference reduction techniques [65, 116, 117], so the spectrum sensing can still be conducted with the residual self-interference. The capability of the self-interference reduction technique can be measured by the self-interference suppression (SIS) factor χ which is defined as

$$\chi^2 = \frac{\text{Power of the residual self-interference (RSI)}}{\text{SU's transmit power}}. \tag{5.6}$$

Considering the states of the PU and the SU jointly, the received signal observed at the sensing antennas of the SU-Tx is given by

$$\mathbf{y}(n) = \begin{cases} \chi \mathbf{H}_{\mathrm{si}} \mathbf{s}_{\mathrm{s}}(n) + \mathbf{u}(n), & \text{PU is inactive (0) and SU is active(1),} \\ \mathbf{u}(n), & \text{PU is inactive (0) and SU is inactive (0),} \\ \mathbf{h}_{\mathrm{sp}} s_{\mathrm{p}}(n) + \chi \mathbf{H}_{\mathrm{si}} \mathbf{s}_{\mathrm{s}}(n) + \mathbf{u}(n), & \text{PU is active (1) and SU is active (1),} \\ \mathbf{h}_{\mathrm{sp}} s_{\mathrm{p}}(n) + \mathbf{u}(n), & \text{PU is active (1) and SU is inactive (0),} \end{cases} \tag{5.7}$$

where $\mathbf{h}_{\mathrm{sp}}$ denotes the Rayleigh fading channel between the PU and the sensing antennas of SU-Tx, $\mathbf{H}_{\mathrm{si}} \in \mathbb{C}^{M_{\mathrm{s}} \times M_{\mathrm{t}}}$ is the self-interference channel between the transmission and sensing antennas at the SU-Tx, $s_{\mathrm{p}}(n) \sim \mathcal{CN}(0, \sigma_{\mathrm{p}}^2)$ represents the PU's circularly symmetric complex Gaussian signal, $\mathbf{s}_{\mathrm{s}}(n) \sim \mathcal{CN}(0, \sigma_{\mathrm{s}}^2 \mathbf{I}_{M_{\mathrm{t}}})$ denotes the transmit signal of the SU-Tx and $\mathbf{u}(n) \sim \mathcal{CN}(0, \sigma_{\mathrm{u}}^2 \mathbf{I}_{M_{\mathrm{s}}})$ represents the sample of a complex additive white Gaussian noise.

In the non-time-slotted FD spectrum sensing system, the state of the PU is defined as the state at the end of each periodic frame of the SU's activity. Therefore, there exists 4 different hypotheses in terms of the activities of the PU and the SU, which can be summarized as follows:

- $\mathcal{H}_{10}$: The SU is active (1), the PU is active for a samples and then turns to inactive (0) within the secondary periodic frame,
- $\mathcal{H}_{00}$: The SU is inactive (0), the PU is active for a samples and then turns to inactive (0) within the secondary periodic frame,
- $\mathcal{H}_{11}$: The SU is active (1), the PU is inactive for b samples and then turns to active (1) within the secondary periodic frame,
- $\mathcal{H}_{01}$: The SU is inactive (0), the PU is inactive for b samples and then turns to active (1) within the secondary periodic frame,

where $0 \leq a, b < N$ and a, b vary depending on the realistic situations, thus different cases are shown in simulation results for various a, b.

The PU can departure or arrive at any time in a secondary time slot, which means that a, b can be any integer between 0 and N. In practice, it is inevitable that some cases with large a and b would have unacceptable sensing performance, e.g. the probability of false alarm or missed detection is over 90%. Therefore, the decision threshold is determined by middle values of a and b rather than considering the

worst cases. Due to the influence of RSI, two sets of decision threshold pairs are required for spectrum sensing under the presence and absence of RSI. Therefore, under the FDSS scheme, we assume r_1, r_0 denote the decision thresholds with and without RSI respectively. Specifically, the FDSS protocol is proposed as described in the pseudocode for Protocol 1.

Protocol 1 Full-duplex Spectrum Sensing Scheme

```
The SU attempts or continues to occupy the licensed channel
if The SU-Tx is transmitting currently then
    The SU-Tx performs spectrum sensing based on decision threshold r_1
    if Received signal energy is above r_1 then
        The channel is reported as busy
        The SU-Tx stops transmitting in the next time slot
    else
        The channel is reported as idle
        The SU-Tx gets the permission to transmit in the next time slot
    end if
else {The SU-Tx is silent currently}
    The SU-Tx conducts spectrum sensing based on decision threshold r_0
    if Received signal energy is above r_0 then
        The transmission of SU-Tx is not allowed in the next time slot
    else
        The transmission of SU-Tx is granted in the next time slot
    end if
end if
```

5.3.2 Sensing Error Analysis

In order to evaluate the sensing performance of the system, two sets of sensing error probabilities have to be investigated in FD non-time-slotted CR networks, i.e., (1) the probability of false alarm with the active SU $P_{\mathrm{fa},1}$ and with the inactive SU $P_{\mathrm{fa},0}$; (2) the probability of missed detection with the active SU $P_{\mathrm{m},1}$ and with the inactive SU $P_{\mathrm{m},0}$. Assuming that the received signal samples at the sensing antennas of the SU-Tx are identical and independent distributed (i.i.d.) and the total sample number for the entire secondary frame N is relatively large, the statistical distributions of the test statistic for the ED T_{ED} can be obtained by applying the central limit theorem (CLT). Thus the related sensing error probabilities for the hypotheses mentioned above can be derived as follows.

Firstly, when the SU-Tx is active (under $\mathcal{H}_{10}$), the probability of false alarm $P_{\mathrm{fa},1}$ is derived as

$$P_{\mathrm{fa},1}(r_1) = \mathcal{Q}\left(\frac{M_{\mathrm{s}}^{\frac{1}{2}}\left(\frac{Nr_1}{\sigma_u^2} - a\gamma_{\mathrm{sp}} - N\chi^2\gamma_{\mathrm{in}} - N\right)}{\sqrt{a(\gamma_{\mathrm{sp}} + \chi^2\gamma_{\mathrm{in}} + 1)^2 + (N-a)(\chi^2\gamma_{\mathrm{in}} + 1)^2}}\right), \tag{5.8}$$

where $\gamma_{\mathrm{sp}} = \frac{\sigma_{\mathrm{p}}^2\|\mathbf{h}_{\mathrm{sp}}\|^2}{M_{\mathrm{s}}\sigma_u^2}$ is the received SNR, $\gamma_{\mathrm{in}} = \frac{\|\mathbf{H}_{\mathrm{si}}\mathbf{s}\|^2}{M_{\mathrm{s}}\sigma_u^2}$ denotes the self-interference-to-noise ratio (INR) measured at the sensing antennas, $\|\cdot\|^2$ is the Frobenius norm operator and $\mathcal{Q}(\cdot)$ denotes the complementary cumulative distribution function of the normal distribution. It is worth noting that different decision thresholds r_0, r_1 are required for the spectrum sensing because of the self-interference. Specifically, r_0 is the decision threshold under the absence of SU's transmission ($\mathcal{H}_{00}, \mathcal{H}_{01}$). r_1 denotes the decision threshold when the SU-Tx is transmitting ($\mathcal{H}_{10}, \mathcal{H}_{11}$).

Secondly, when the SU-Tx is inactive (under $\mathcal{H}_{00}$), the probability of false alarm $P_{\mathrm{fa},0}$ is given by

$$P_{\mathrm{fa},0}(r_0) = \mathcal{Q}\left(\frac{M_{\mathrm{s}}^{\frac{1}{2}}\left(\frac{Nr_0}{\sigma_u^2} - a\gamma_{\mathrm{sp}} - N\right)}{\sqrt{a\gamma_{sp}^2 + 2a\gamma_{\mathrm{sp}} + N}}\right). \tag{5.9}$$

Thirdly, based on the statistical distributions of T_{ED} under the hypothesis $\mathcal{H}_{11}$, the probability of missed detection under the presence of the secondary transmission $P_{\mathrm{m},1}$ is derived as

$$P_{\mathrm{m},1}(r_1) = 1 - \mathcal{Q}\left(\frac{M_{\mathrm{s}}^{\frac{1}{2}}\left(\frac{Nr_1}{\sigma_u^2} - (N-b)\gamma_{\mathrm{sp}} - N\chi^2\gamma_{\mathrm{in}} - N\right)}{\sqrt{(N-b)(\gamma_{sp} + \chi^2\gamma_{\mathrm{in}} + 1)^2 + b(\chi^2\gamma_{\mathrm{in}} + 1)^2}}\right). \tag{5.10}$$

Finally, the probability of missed detection when the SU is inactive, $P_{\mathrm{m},0}$, is given by

$$P_{\mathrm{m},0}(r_0) = 1 - \mathcal{Q}\left(\frac{M_{\mathrm{s}}^{\frac{1}{2}}\left(\frac{Nr_0}{\sigma_u^2} - (N-b)\gamma_{\mathrm{sp}} - N\right)}{\sqrt{(N-b)\gamma_{sp}^2 + 2(N-b)\gamma_{\mathrm{sp}} + N}}\right). \tag{5.11}$$

The closed-form expression of sensing errors mentioned above are derived for the multi-sensing-antenna ED based FD non-time-slotted system. Furthermore, it is worth noticing that these expressions can be simplified to be the probabilities of false alarm and missed detection for the time-slotted CR network, when $a = b = 0$. This reveals that the time-slotted spectrum sensing system is a special case of the non-time-slotted system and the model studied in this chapter is more generalized and practical.

The detailed proof for the above expressions is provided in the appendix.

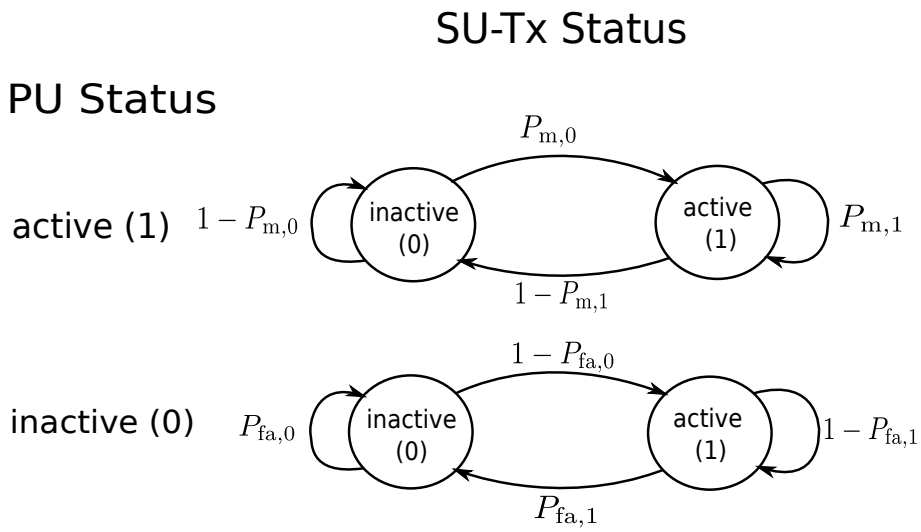

Figure 5.3: *The Markov chains of the activities of the PU and SU-Tx in FD spectrum sensing system*

In order to analyse the total error rate and the optimal decision threshold of the spectrum sensing system, both the probabilities of false alarm P_{fa} and missed detection P_{m} of the whole system are necessary. Therefore, the expressions of P_{fa} and P_{m} should be investigated based on equations (5.8), (5.9), (5.10) and (5.11). The transitions between the states of PU and SU can be modelled as the discrete-time Markov chains which is shown in Fig. 5.3. Note that the states of PU stand for *the statuses of the PU observed at the end of a secondary sensing frame*. Assuming P_{q_1,q_2} is the probability that the FD CR system remains at the state (q_1, q_2), where $q_1, q_2 = \{0, 1\}$ represent the states of the SU-Tx and the PU respectively, the relationship among various sensing error probabilities can be achieved by using the steady-state of the Markov chains as follows,

$$\begin{cases} P_{0,1}P_{\mathrm{m},0} = P_{1,1}(1-P_{\mathrm{m},1}), \\ P_{0,0}(1-P_{\mathrm{fa},0}) = P_{1,0}P_{\mathrm{fa},1}, \\ P_{0,0} + P_{1,0} = 1, \\ P_{0,1} + P_{1,1} = 1, \\ P_{\mathrm{m}} = P_{1,1}, \\ P_{\mathrm{fa}} = P_{0,0}. \end{cases} \tag{5.12}$$

By solving the above system of equations, the probability of false alarm of the whole system P_{fa} is

given by

$$P_{\mathrm{fa}}(r_0, r_1) = \frac{P_{\mathrm{fa},1}(r_1)}{1 - P_{\mathrm{fa},0}(r_0) + P_{\mathrm{fa},1}(r_1)}, \tag{5.13}$$

and the probability of missed detection of the whole system is given by

$$P_{\mathrm{m}}(r_0, r_1) = \frac{P_{\mathrm{m},0}(r_0)}{1 + P_{\mathrm{m},0}(r_0) - P_{\mathrm{m},1}(r_1)}. \tag{5.14}$$

5.3.3 Total Error Rate Analysis

In this subsection, the total error rate is investigated in order to consider the benefits of the PU and the SUs simultaneously. Since there exists two decision thresholds, i.e. r_0 and r_1, in the FD non-time-slotted spectrum sensing system, it is not easy to find the ideal combination of r_0 and r_1. An exercisable and simple way is to obtain the appropriate combination of decision thresholds (r_0, r_1) based on the given P_{fa} or P_{m} and this will not affect the validity of the theoretical analyses.

Firstly, let us start with the scenario with a given probability of missed detection of the whole system P_{m}. In practical applications, the probabilities of missed detection when the SU-Tx is silent $P_{\mathrm{m},0}$ and active $P_{\mathrm{m},1}$ should be guaranteed to be a similar value, so that there would be no gaps of the missed detection performance between the cases of active and inactive SU-Tx. According to this practical requirement, the probability of missed detection when the SU is transmitting is equal to the probability when the SU is silent, i.e., $P_{\mathrm{m},1} = P_{\mathrm{m},0}$. Then, from equation (5.14), it can be seen that $P_{\mathrm{m},1} = P_{\mathrm{m},0} = P_{\mathrm{m}}$.

Based on the above assumptions and analysis, the desired decision threshold r_1 for a given P_{m} (when the SU-Tx is active) can be derived as

$$r_1(P_{\mathrm{m}}) = \frac{\sigma_u^2}{N}\left(\mathcal{Q}^{-1}(1 - P_{\mathrm{m}})\alpha_1 + (N - b)\gamma_{\mathrm{sp}} + N\chi^2\gamma_{\mathrm{in}} + N\right), \tag{5.15}$$

where α_1 is given by

$$\alpha_1 = \sqrt{\frac{\left[(N - b)\gamma_{\mathrm{sp}}^2 + 2(N - b)\gamma_{\mathrm{sp}}(\chi^2\gamma_{\mathrm{in}} + 1) + N(\chi^2\gamma_{\mathrm{in}} + 1)^2\right]}{M_{\mathrm{s}}}}. \tag{5.16}$$

Thus, the corresponding false alarm rate $P_{\mathrm{fa},1}$ when the SU is transmitting with respect to the given

P_{m} can be obtained through (5.8) and (5.15) and is given by

$$P_{\mathrm{fa},1}(P_{\mathrm{m}}) = \mathcal{Q}\left(\frac{\mathcal{Q}^{-1}(1-P_{\mathrm{m}})\alpha_1 + (N-b-a)\gamma_{\mathrm{sp}}}{\beta_1}\right), \tag{5.17}$$

where β_1 is given by

$$\beta_1 = \sqrt{\frac{a\gamma_{\mathrm{sp}}^2 + 2a\gamma_{\mathrm{sp}}(\chi^2\gamma_{\mathrm{in}}+1) + N(\chi^2\gamma_{\mathrm{in}}+1)^2}{M_{\mathrm{s}}}}. \tag{5.18}$$

Meanwhile, when the SU-Tx is silent, the desired decision threshold r_0 for a given P_{m} can be obtained as

$$r_0(P_{\mathrm{m}}) = \frac{\sigma_u^2}{N}\left(\mathcal{Q}^{-1}(1-P_{\mathrm{m}})\alpha_0 + (N-b)\gamma_{\mathrm{sp}} + N\right), \tag{5.19}$$

where α_0 is given by

$$\alpha_0 = \sqrt{\frac{(N-b)\gamma_{\mathrm{sp}}^2 + 2(N-b)\gamma_{\mathrm{sp}} + N}{M_{\mathrm{s}}}}. \tag{5.20}$$

Thus, the corresponding probability of false alarm $P_{\mathrm{fa},0}$ can be derived through (5.9) and (5.19) and is given by

$$P_{\mathrm{fa},0}(P_{\mathrm{m}}) = \mathcal{Q}\left(\frac{\mathcal{Q}^{-1}(1-P_{\mathrm{m}})\alpha_0 + (N-b-a)\gamma_{\mathrm{sp}}}{\beta_0}\right), \tag{5.21}$$

where β_0 is given by

$$\beta_0 = \sqrt{\frac{a\gamma_{\mathrm{sp}}^2 + 2a\gamma_{\mathrm{sp}} + N}{M_{\mathrm{s}}}}. \tag{5.22}$$

Herein, for a given probability of missed detection of the whole system P_{m}, the desired decision threshold pair (r_0, r_1) can be obtained by equation (5.15) and (5.19) based on the above derivations.

Secondly, the scenario with a given probability of false alarm of the whole system P_{fa} is considered. Similarly, a practical assumption is $P_{\mathrm{fa},0} = P_{\mathrm{fa},1}$, so it can be seen from equation (5.13) that $P_{\mathrm{fa}} = P_{\mathrm{fa},0} = P_{\mathrm{fa},1}$. Therefore, when the SU-Tx is active, the desired decision threshold r_1 for a given P_{fa}

is given by

$$r_1(P_{\rm fa}) = \frac{\sigma_u^2}{N}\left(\mathcal{Q}^{-1}(P_{\rm fa})\beta_1 + a\gamma_{\rm sp} + N\chi^2\gamma_{\rm in} + N\right). \tag{5.23}$$

By using equation (5.10) and (5.23), the corresponding probability of missed detection $P_{\rm m,1}$ can be represented with regard to the desired $P_{\rm fa}$ and is given by

$$P_{\rm m,1}(P_{\rm fa}) = 1 - \mathcal{Q}\left(\frac{\mathcal{Q}^{-1}(P_{\rm fa})\beta_1 + (a+b-N)\gamma_{\rm sp}}{\alpha_1}\right). \tag{5.24}$$

When the SU-Tx is silent, the desired decision threshold r_0 for a given $P_{\rm fa}$ is derived as

$$r_0(P_{\rm fa}) = \frac{\sigma_u^2}{N}\left(\mathcal{Q}^{-1}(P_{\rm fa})\beta_0 + a\gamma_{\rm sp} + N\right). \tag{5.25}$$

Then, the closed-form expression of the corresponding probability of missed detection $P_{\rm m,0}$ with regard to $P_{\rm fa}$ can be derived with the aid of equation (5.11) and (5.25), which is shown as

$$P_{\rm m,0}(P_{\rm fa}) = 1 - \mathcal{Q}\left(\frac{\mathcal{Q}^{-1}(P_{\rm fa})\beta_0 + (a+b-N)\gamma_{\rm sp}}{\alpha_0}\right). \tag{5.26}$$

Therefore, in a multi-antenna ED based FD spectrum sensing system, the desired decision threshold pair (r_0, r_1) based on a given probability of false alarm of the whole system $P_{\rm fa}$ can be obtained through equations (5.23) and (5.25).

In order to consider the benefits of both the PU and SUs, the total error rate of the whole system $P_{\rm te}$ is defined as

$$P_{\rm te}(r_0, r_1) = P_{\rm fa}(r_0, r_1)P(\mathcal{H}_0) + P_{\rm m}(r_0, r_1)P(\mathcal{H}_1), \tag{5.27}$$

where $P(\mathcal{H}_0)$ denotes the probability that the PU is actually idle and $P(\mathcal{H}_1)$ represents the probability that the PU is actually busy. One significant step and objective during the FD spectrum sensing process is determining the decision threshold pair. The optimal decision threshold pair can minimize the total error rate of the system and is formulated as

$$(r_0, r_1)_{\rm opt} = \underset{r_0, r_1}{\arg\min}\, P_{\rm fa}(r_0, r_1) + P_{\rm m}(r_0, r_1). \tag{5.28}$$

This optimal decision threshold pair can be obtained by using the derived equations in this section. It should be noted that this optimization issue can be investigated under the two different scenarios mentioned above, including the cases of a given P_{m} and P_{fa}.

Remark 1. *Improved FD Spectrum Sensing System: The above FD spectrum sensing scheme can be further improved in terms of sensing performance. A simple way to realize this is utilizing all the antennas ($M_{\mathrm{s}}+M_{\mathrm{t}}$) of the FD BS to conduct spectrum sensing when the detection result is busy based on the data collect in the previous time slot. The benefit by doing this is the sensing performance would be advanced due to the increased number of sensing antennas, and the secondary transmission performance is not affected by this. In contrast, in the FD spectrum sensing scheme proposed above, there are M_{t} antennas exclusive to transmission so that these antennas are idle when the PU is detected as busy. Therefore, it is obvious that the improved system proposed here can improve the system performance without any negative effects. In addition, the corresponding test statistics and theoretical expressions of sensing performance metrics can be obtained conveniently by replacing M_{s} in eqs.* (5.5), (5.9) *and* (5.11) *with* $M_{\mathrm{s}}+M_{\mathrm{t}}$.

5.4 Performance Analysis of FD Sensing-based Spectrum Sharing System

In order to improve the spectrum efficiency of the FD cognitive network, the sensing-based spectrum sharing scheme is proposed in this section. Meanwhile, the sensing and transmission performance are investigated.

5.4.1 Sensing-based Spectrum Sharing Scheme

Under the sensing-based spectrum sharing scheme, when considering the states of the PU and the SU jointly, the received signal observed at the sensing antennas of the SU-Tx is given by

$$\mathbf{y}(n)=\begin{cases}\chi\mathbf{H}_{\mathrm{si}}\mathbf{s}_1(n)+\mathbf{u}(n), & \text{PU is inactive (0) and SU is transmitting with high power,}\\ \chi\mathbf{H}_{\mathrm{si}}\mathbf{s}_0(n)+\mathbf{u}(n), & \text{PU is inactive (0) and SU is transmitting with low power,}\\ \mathbf{h}_{\mathrm{sp}}s_{\mathrm{p}}(n)+\chi\mathbf{H}_{\mathrm{si}}\mathbf{s}_1(n)+\mathbf{u}(n), & \text{PU is active (1) and SU is transmitting with high power,}\\ \mathbf{h}_{\mathrm{sp}}s_{\mathrm{p}}(n)+\chi\mathbf{H}_{\mathrm{si}}\mathbf{s}_0(n)+\mathbf{u}(n), & \text{PU is active (1) and SU is transmitting with low power,}\end{cases} \tag{5.29}$$

where $\mathbf{s}_1(n) \sim \mathcal{CN}(0, \sigma_{\mathrm{s},1}^2 \mathbf{I}_{M_\mathrm{t}})$ and $\mathbf{s}_0(n) \sim \mathcal{CN}(0, \sigma_{\mathrm{s},0}^2 \mathbf{I}_{M_\mathrm{t}})$ denote the transmit signals of the SU-Tx with high power and low power respectively.

Therefore, there exist 4 different hypotheses in terms of the activities of the PU and the SU, which can be summarized as follows:

- $\mathcal{H}_{10}$: The SU is transmitting with high power, the PU is active for a samples and then turns to inactive (0) within the secondary periodic frame,
- $\mathcal{H}_{00}$: The SU is transmitting with low power, the PU is active for a samples and then turns to inactive (0) within the secondary periodic frame,
- $\mathcal{H}_{11}$: The SU is transmitting with high power, the PU is inactive for b samples and then turns to active (1) within the secondary periodic frame,
- $\mathcal{H}_{01}$: The SU is transmitting with low power, the PU is inactive for b samples and then turns to active (1) within the secondary periodic frame,

where $0 \leq a, b < N$.

In order to take full advantage of the spectrum resource, the FD-SBSS scheme is proposed. Due to the influence of RSI, two sets of decision threshold pairs are required for the spectrum sensing under the presence and absence of RSI. Therefore, under the FD-SBSS scheme, we assume r_1 and r_0 denote the decision thresholds under the strong and weak RSI. Specifically, the FD-SBSS protocol is proposed as described in the pseudocode for Protocol 2.

5.4.2 Collision and Spectrum Waste Analyses

In order to evaluate the sensing performance metrics of the FD-SBSS system, the CDFs of the test statistic have to be investigated under the 4 different hypotheses defined in previous subsection. Assuming that the received signal samples at the sensing antennas of the SU-Tx are i.i.d. and the total number of samples for the entire secondary frame N is relatively large, the statistical distributions of the test statistic for the ED T_{ED} can be obtained by applying the central limit theorem (CLT).

Firstly, the probability of false alarm $P_{\mathrm{fa},\varrho}$ ($\varrho = 0, 1$) when the SU-Tx is with high power ($\varrho = 1$,

Protocol 2 ***Full-duplex Sensing-based Spectrum Sharing Scheme***

The SU attempts or continues to occupy the licensed channel
if The SU-Tx is transmitting currently **then**
  The SU-Tx performs spectrum sensing based on decision threshold r_1
  if Received signal energy is above r_1 **then**
    The channel is reported as busy
    The SU-Tx is allowed to transmit with a low power in the next time slot
  else
    The channel is reported as idle
    The SU-Tx gets the permission to transmit with full power in the next time slot
  end if
else {The SU-Tx is silent currently}
  The SU-Tx conducts spectrum sensing based on decision threshold r_0
  if Received signal energy is above r_0 **then**
    The low power transmission of SU-Tx is scheduled in the next time slot
  else
    The full power transmission of SU-Tx is granted in the next time slot
  end if
end if

under $\mathcal{H}_{10}$) and low power ($\varrho = 0$, under $\mathcal{H}_{00}$) are derived as

$$P_{\mathrm{f},\varrho}(r_\varrho) = \mathcal{Q}\left(\frac{\frac{Nr_\varrho}{\sigma_u^2} - a\gamma_{\mathrm{sp}} - N\chi^2\gamma_{\mathrm{in},\varrho} - N}{\beta_\varrho}\right), \tag{5.30}$$

where $\gamma_{\mathrm{in},\varrho} = \frac{\|\mathbf{H}_{\mathrm{si}}\mathbf{s}_\varrho\|^2}{M_{\mathrm{s}}\sigma_u^2}$ denotes the INR measured at the sensing antennas for different transmit statuses of the SU-Tx, β_ϱ is given by

$$\beta_\varrho = \sqrt{\frac{a\gamma_{\mathrm{sp}}^2 + 2a\gamma_{\mathrm{sp}}(\chi^2\gamma_{\mathrm{in},\varrho} + 1) + N(\chi^2\gamma_{\mathrm{in},\varrho} + 1)^2}{M_{\mathrm{s}}}}, \tag{5.31}$$

where $\|\cdot\|^2$ is the Frobenius norm operator and $\mathcal{Q}(\cdot)$ denotes the complementary CDF of the normal distribution. It is worth noting that different decision thresholds r_0 and r_1 are required for the spectrum sensing because of the self-interference. Specifically, r_0 is the decision threshold under the low secondary transmission power ($\mathcal{H}_{00}, \mathcal{H}_{01}$). r_1 denotes the decision threshold when the SU-Tx is transmitting with a high power ($\mathcal{H}_{10}, \mathcal{H}_{11}$).

Secondly, based on the statistical distributions of T_{ED} under the hypothesis $\mathcal{H}_{11}$, the probability of

detection $P_{\mathrm{d},\varrho}$ under high ($\varrho = 1$) and low ($\varrho = 0$) secondary transmission power are derived as

$$P_{\mathrm{d},\varrho}(r_\varrho) = \mathcal{Q}\left(\frac{\frac{Nr_\varrho}{\sigma_u^2} - (N-b)\gamma_{\mathrm{sp}} - N\chi^2\gamma_{\mathrm{in},\varrho} - N}{\alpha_\varrho}\right), \tag{5.32}$$

where α_ϱ is given by

$$\alpha_\varrho = \sqrt{\frac{(N-b)\gamma_{\mathrm{sp}}^2 + 2(N-b)\gamma_{\mathrm{sp}}(\chi^2\gamma_{\mathrm{in},\varrho}+1) + N(\chi^2\gamma_{\mathrm{in},\varrho}+1)^2}{M_{\mathrm{s}}}}, \tag{5.33}$$

and the missed detection rate $P_{\mathrm{m},\varrho} = 1 - P_{\mathrm{d},\varrho}$.

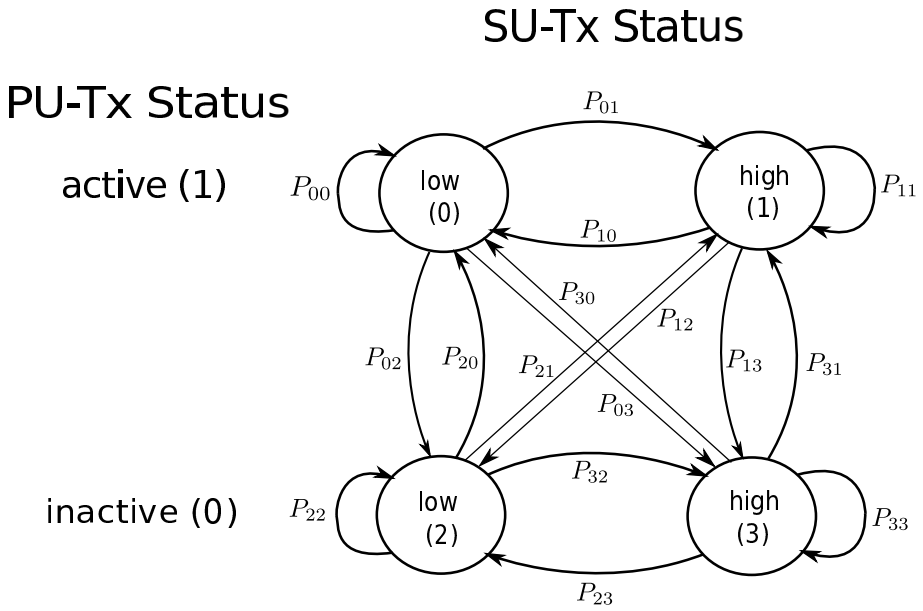

Figure 5.4: *The Markov chains of the activities of the PU and SU-Tx in FD sensing-based spectrum sharing system*

The transitions between the states of PU and SU can be modelled as a discrete-time Markov chain which is shown in Fig. 5.4. Assuming $P_{q_iq_j}$ is the probability that the FD CR system transfer from state q_i to q_j, where $q_i, q_j = \{q_0, q_1, q_2, q_3\}$ represent the states of this system, then the state transition

matrix is given by

$$\begin{aligned}\mathbf{\Phi} &= \begin{bmatrix} P_{00} & P_{10} & P_{20} & P_{30} \\ P_{01} & P_{11} & P_{21} & P_{31} \\ P_{02} & P_{12} & P_{22} & P_{32} \\ P_{03} & P_{13} & P_{23} & P_{33} \end{bmatrix} \\ &= \begin{bmatrix} P_{\mathrm{d},0}(1-\mu_0) & P_{\mathrm{d},1}(1-\mu_0) & P_{\mathrm{f},0}\mu_1 & P_{\mathrm{f},1}\mu_1 \\ P_{\mathrm{m},0}(1-\mu_0) & P_{\mathrm{m},1}(1-\mu_0) & (1-P_{\mathrm{f},0})\mu_1 & (1-P_{\mathrm{f},1})\mu_1 \\ P_{\mathrm{d},0}\mu_0 & P_{\mathrm{d},1}\mu_0 & P_{\mathrm{f},0}(1-\mu_1) & P_{\mathrm{f},1}(1-\mu_1) \\ P_{\mathrm{m},0}\mu_0 & P_{\mathrm{m},1}\mu_0 & (1-P_{\mathrm{f},0})(1-\mu_1) & (1-P_{\mathrm{f},1})(1-\mu_1) \end{bmatrix}, \end{aligned} \tag{5.34}$$

Assuming $\mathbf{p} = [P_0, P_1, P_2, P_3]$ represents the probability that the system stays at state q_i, P_i can be obtained by using the steady-state of Markov chains as follows

$$\begin{cases} \mathbf{\Phi p} = \mathbf{p} \\ \sum_{i=0}^{3} P_i = 1. \end{cases} \tag{5.35}$$

By solving the above system equations, the probability P_i is given as follows:

$$P_0 = \frac{\mu_1\Big\{(1-P_{\mathrm{m},1})\big[\phi(1-P_{\mathrm{f},0})+\mu_1\big] + P_{\mathrm{f},1}\big[\phi(1-P_{\mathrm{m},1})+\mu_0\big]\Big\}}{(\mu_0+\mu_1)\Big\{1-(P_{\mathrm{m},1}-P_{\mathrm{m},0})(1-\mu_0)+(P_{\mathrm{f},1}-P_{\mathrm{f},0})\big[1-\mu_1+(P_{\mathrm{m},1}-P_{\mathrm{m},0})\phi\big]\Big\}}, \tag{5.36}$$

$$P_1 = \frac{-\mu_1\Big\{(-1+P_{\mathrm{f},0})\mu_0 + P_{\mathrm{m},0}\big[-1+\mu_0+\phi(P_{\mathrm{f},0}-P_{\mathrm{f},1})\big]\Big\}}{(\mu_0+\mu_1)\Big\{1-(P_{\mathrm{m},1}-P_{\mathrm{m},0})(1-\mu_0)+(P_{\mathrm{f},1}-P_{\mathrm{f},0})\big[1-\mu_1+(P_{\mathrm{m},1}-P_{\mathrm{m},0})\phi\big]\Big\}}, \tag{5.37}$$

$$P_2 = \frac{\mu_0\Big\{(1-P_{\mathrm{m},1})\mu_1 + P_{\mathrm{f},1}\big[1-\mu_1+\phi(P_{\mathrm{m},0}-P_{\mathrm{m},1})\big]\Big\}}{(\mu_0+\mu_1)\Big\{1-(P_{\mathrm{m},1}-P_{\mathrm{m},0})(1-\mu_0)+(P_{\mathrm{f},1}-P_{\mathrm{f},0})\big[1-\mu_1+(P_{\mathrm{m},1}-P_{\mathrm{m},0})\phi\big]\Big\}}, \tag{5.38}$$

$$P_3 = \frac{\mu_0\Big\{1-\mu_1+P_{\mathrm{m},0}(1-\mu_0)-P_{\mathrm{m},1}\phi+P_{\mathrm{f},0}\big[-1+\mu_1+(P_{\mathrm{m},1}-P_{\mathrm{m},0})\phi\big]\Big\}}{(\mu_0+\mu_1)\Big\{1-(P_{\mathrm{m},1}-P_{\mathrm{m},0})(1-\mu_0)+(P_{\mathrm{f},1}-P_{\mathrm{f},0})\big[1-\mu_1+(P_{\mathrm{m},1}-P_{\mathrm{m},0})\phi\big]\Big\}}, \tag{5.39}$$

where $\phi = 1-\mu_0-\mu_1$.

The collision probability P_{c} is defined as the conditional probability that the SU transmits at a high power given that the PU is active actually, i.e., $P\{\text{SU transmits at a high power} \mid \text{PU is active}\}$. There-

fore, by using Bayes' rule, the collision probability in the SBSS scheme can be calculated as

$$P_{\mathrm{c}} = \frac{P\{\text{SU transmits at a high power, PU is active}\}}{P\{\text{PU is active}\}} = \frac{P_1}{\frac{\mu_1}{\mu_0+\mu_1}} = \frac{P_1(\mu_0+\mu_1)}{\mu_1}. \tag{5.40}$$

By contrast, the probability of spectrum waste P_{w} is defined as the conditional probability that the SUs conduct transmission at a low power when the PU is idle actually. Thus, the probability of spectrum waste in the SBSS scheme is expressed as

$$P_{\mathrm{w}} = \frac{P\{\text{SU transmits at a low power, PU is idle}\}}{P\{\text{PU is idle}\}} = \frac{P_2}{\frac{\mu_0}{\mu_0+\mu_1}} = \frac{P_2(\mu_0+\mu_1)}{\mu_0}. \tag{5.41}$$

5.4.3 Transmission Performance

In this section, the downlink transmission performance of the secondary network is investigated. As shown in Fig. 5.1, the secondary receiver (SU-Rx) and primary receiver (PU-Rx) are both equipped with a single antenna. $\mathbf{h}_{\mathrm{ss}}$ denotes the channel vector between the SU-Tx and SU-Rx. $\mathbf{h}_{\mathrm{pi}}$ is the interference channel vector between the SU-Tx and PU-Rx. The scalar h_{ps} denotes the channel between the PU-Tx and the SU-Rx. Thus, the achievable throughput of the secondary network can be given by

$$\begin{aligned} C\left(r_0, r_1, \sigma_{\mathrm{s},0}^2, \sigma_{\mathrm{s},1}^2\right) = &\left(P_0(r_0, r_1, \sigma_{\mathrm{s},0}^2, \sigma_{\mathrm{s},1}^2) + P_2(r_0, r_1, \sigma_{\mathrm{s},0}^2, \sigma_{\mathrm{s},1}^2)\right) \log_2\left(1 + \frac{\|\mathbf{h}_{\mathrm{ss}}\|^2 \sigma_{\mathrm{s},0}^2}{\sigma_{\mathrm{n}}^2}\right) \\ &+ \left(P_1(r_0, r_1, \sigma_{\mathrm{s},0}^2, \sigma_{\mathrm{s},1}^2) + P_3(r_0, r_1, \sigma_{\mathrm{s},0}^2, \sigma_{\mathrm{s},1}^2)\right) \log_2\left(1 + \frac{\|\mathbf{h}_{\mathrm{ss}}\|^2 \sigma_{\mathrm{s},1}^2}{\sigma_{\mathrm{n}}^2}\right), \end{aligned} \tag{5.42}$$

where σ_{n}^2 is the additive noise at the SU-Rx and the interference to the SU-Rx from the PU-Tx is neglected because of the long distance between the PU and SUs.

5.5 Simulation Results and Discussions

In this section, the simulation and theoretical results are provided to validate the derived expressions and analyses throughout this chapter. The comparison with the traditional HD sensing system is also provided based on the non-time-slotted model. In the simulation results of the FDSS scheme, the SU-Tx has 4 antennas, including the sensing antennas $M_{\mathrm{s}} = 2$ and the transmission antennas $M_{\mathrm{t}} = 2$.

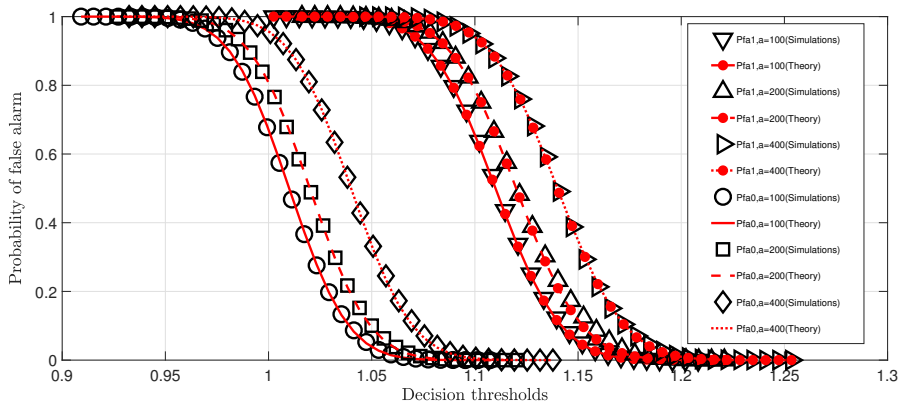

Figure 5.5: *The probabilities of false alarm under the presence and absence of secondary transmission.*

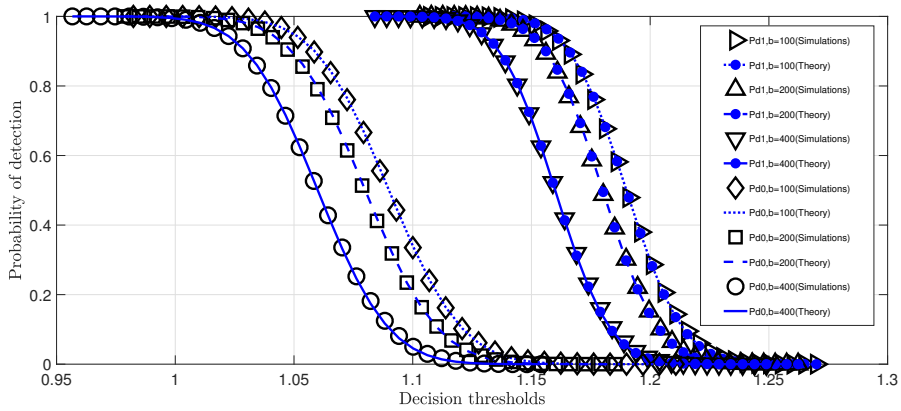

Figure 5.6: *The probabilities of detection under the presence and absence of secondary transmission.*

The total number of samples for one periodic secondary frame is $N = 1000$. Various values of a and b are assumed because of the non-time-slotted model. The SIS factor χ can vary from 0.1 to 0.3. The received SNR at the sensing antennas of the SU-Tx is $\gamma_{\rm sp} = -10{\rm dB}$ and the recieved INR is $\gamma_{\rm in} = 10{\rm dB}$.

Fig. 5.5 and Fig. 5.6 verify the derived expressions of sensing error rates under different hypotheses $\mathcal{H}_{10}, \mathcal{H}_{11}, \mathcal{H}_{01}, \mathcal{H}_{00}$. Specifically, this figure represents the probabilities of false alarm and missed detection when the SU-Tx is active and inactive under the condition $\chi = 0.1$. Note that $P_{\rm d,1} = 1 - P_{\rm m,1}, P_{\rm d,0} = 1 - P_{\rm m,0}$ are plotted instead of $P_{\rm m,1}, P_{\rm m,0}$ for the convenience of plotting. The Monte-Carlo simulation results match the theoretical results very well. Besides, comparing the results

under different a and b, it can be seen that the sensing performance will degrade with the increase of a and b for every hypothesis mentioned above. Since large values of a and b imply that the PU changes its state late within one periodic secondary frame, a large number of samples that affect the sensing performance would be received.

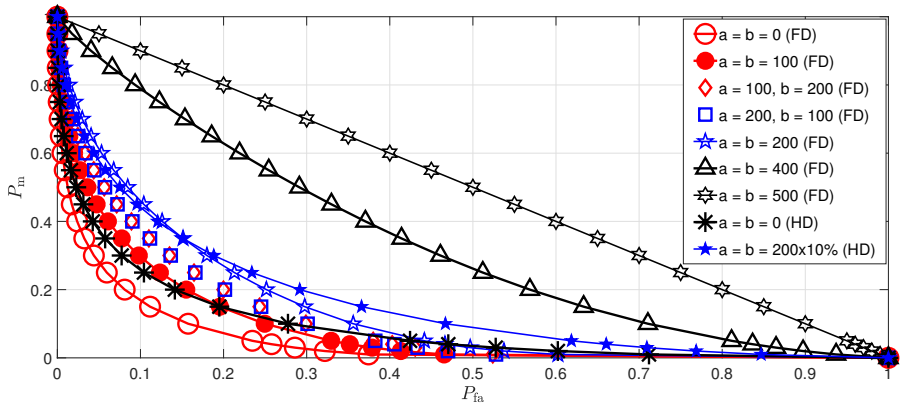

Figure 5.7: *The ROC curves of the FD spectrum sensing system and the comparison with the HD system.*

The ROC curves are depicted in Fig. 5.7 to show the sensing performance of the FD CR system under different conditions when $\chi = 0.3$. From this figure, it can be deduced that the sensing performance of the whole system will degrade with the increase of the summation of a and b, i.e., $a + b$. When $a + b = N$, i.e. $a = b = 500$ in the figure, the sensing performance has been extremely poor, which is caused by the quite late change of the PU's status within a sensing frame. Therefore, the sensing performance beyond this point, i.e. the cases of $a + b > N$, is not considered in this thesis. Besides, when $a + b$ is constant, the sensing performance of the FD non-time-slotted CR system is similar no matter what the specific values of a and b are. For instance, this system has a similar sensing performance when $a = 100, b = 200$ and $a = 200, b = 100$. In addition, it can be seen from the comparison with the HD spectrum sensing approach that the FD can achieve a better sensing performance based on the multi-sensing-antenna ED in the non-time-slotted CR network, since more received signal samples can be accumulated by employing the FD technique. In order to ensure a fair comparison, the parameter settings for the HD sensing system in this figure are as follows: the number of the antennas at the SU-Tx for the HD system is $M = M_{\mathrm{s}} + M_{\mathrm{t}} = 4$ and the ratio between the sensing time τ and one periodic secondary frame duration T is $\kappa = \frac{\tau}{T} = 10\%$, since a large κ would degrade the throughput of the secondary network severely in the HD system. Specifically, a reasonable comparison is between the sensing performances of $a = b = q$ for the FD system and $a = b = q \times \kappa$

for the HD system.

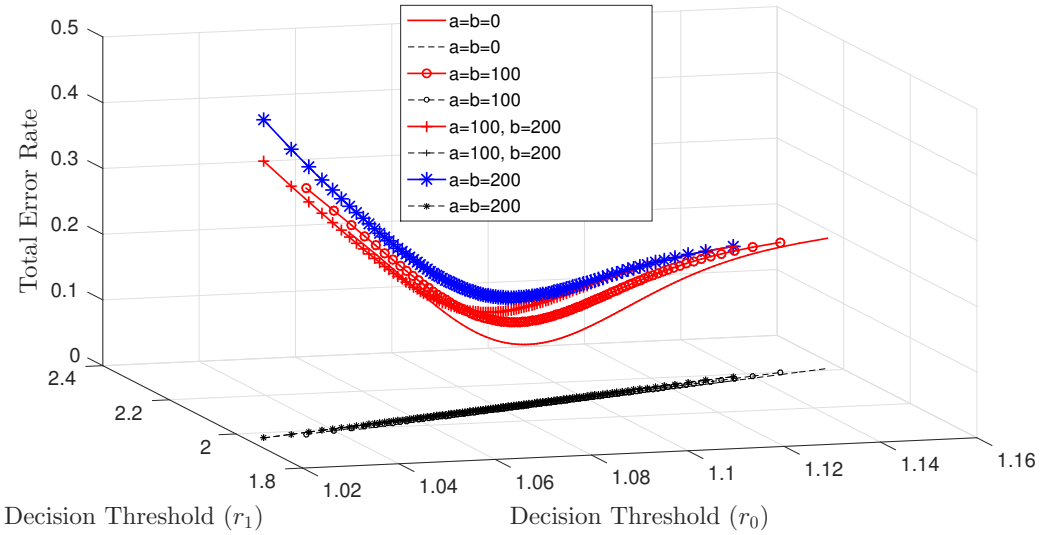

Figure 5.8: *The total error rate of the system P_{te} V.S. the decision threshold pair (r_0, r_1) (The dashed black lines on x-y plane are the projections of the total error rate curves).*

The total error rate of the system is presented in Fig. 5.8 versus the different decision threshold pairs under different system conditions. The scenario of a given probability of missed detection is considered and $\chi = 0.3$. The probabilities that the PU is absent and present are assumed as $P(\mathcal{H}_0) = 0.8$, $P(\mathcal{H}_1) = 0.2$, since the PU would not occupy the licensed frequency bands at a high probability in practical applications. The total error rate of the system increases with the increasing $a + b$, since more signal samples with negative effects are received for spectrum sensing. Meanwhile, it can be also seen from this figure that the total error rate of the system is a quasi-convex function with regard to the decision threshold pairs. This implies that there exists one and only one optimal decision threshold pair to minimize the total error rate. Therefore, the optimal decision threshold pair can be obtained by using the derived equations in the last section. Specifically, the optimal decision threshold pairs $(r_0, r_1)_{\text{opt}}$ are $(1.086, 1.974)$, $(1.084, 1.980)$, $(1.080, 1.980)$ and $(1.085, 1.990)$ for the cases of $(a = b = 0), (a = b = 100), (a = 100, b = 200)$ and $(a = b = 200)$, respectively. Meanwhile, the corresponding minimum total error rates are $0.09, 0.12, 0.14$ and 0.16.

The FD-SBSS scheme is also investigated in terms of sensing and transmission performance, assuming the sampling frequency is 6 MHz and $\lambda_{\text{off}} = 4$, $\lambda_{\text{on}} = 1$. The received INRs at the sensing antennas are $\gamma_{\text{in},0} = 15$ dB and $\gamma_{\text{in},1} = 25$ dB for the low and full power cases respectively. The numbers of sensing and transmit antennas at the FD SU-Tx are both assumed to be 4 and the RSI factor $\chi = 0.1$.

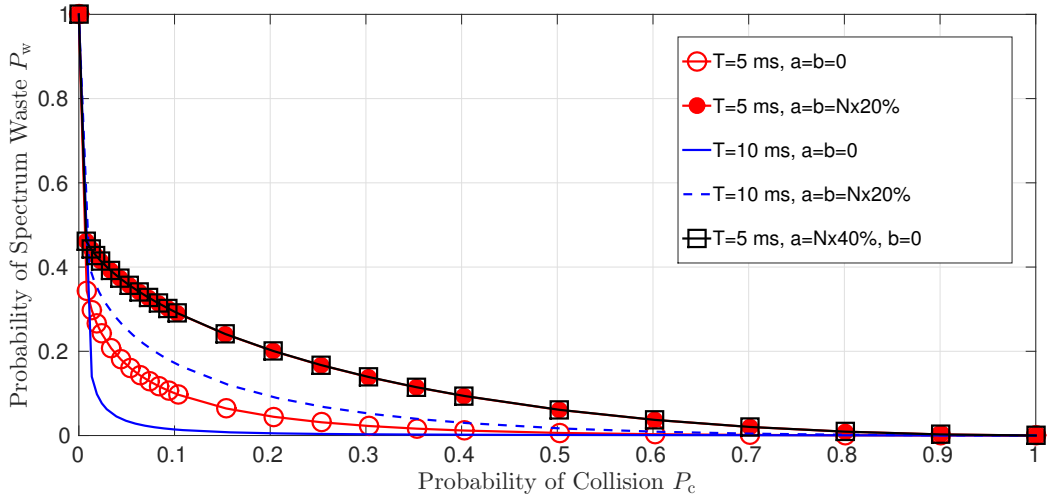

Figure 5.9: *The probability of collision v.s. the probability of spectrum waste under different conditions when* $P_{\mathrm{d},0} = P_{\mathrm{d},1}$.

In order to guarantee the same level of protection to PUs, it is reasonable to assume equal probability of detection under the high and low power of secondary transmissions, i.e. $P_{\mathrm{d},0} = P_{\mathrm{d},1}$. Therefore, the ROC curves on probabilities of collision and spectrum waste are depicted in Fig. 5.9. Different cases are presented for various sensing frame duration T and different a, b values. It can be seen from this figure that the probability of spectrum waste decreases with the increase of collision probability and a longer sensing frame duration helps to improve sensing performance due to more accumulated samples. Meanwhile, the FD-SBSS system has almost same sensing performance for same value of $a + b$. For instance, as shown in Fig. 5.9, the cases with $a = N \times 40\%, b = 0$ and $a = b = N \times 20\%$ have same performances on the collision and spectrum waste.

In order to have insight into the relationship between collision, spectrum waste and RSI factor, Fig. 5.10 shows the probabilities of collision and spectrum waste v.s. the RSI factor when CDR requirement is employed. The desired detection probabilities are 0.9 for both the low and high transmit power cases under the CDR requirement. The sensing frame duration is set at 10 ms. From this figure, it can seen that the probability of collision reduces slightly with the increase of the RSI factor. Meanwhile, the collision performance does change obviously for different values of a, b. On the contrary, the probability of spectrum waste goes up dramatically with the increasing RSI factor and a high a, b leads to a high spectrum waste probability.

In addition, in order to explore the effect of antenna partitioning on achievable throughput of the SU,

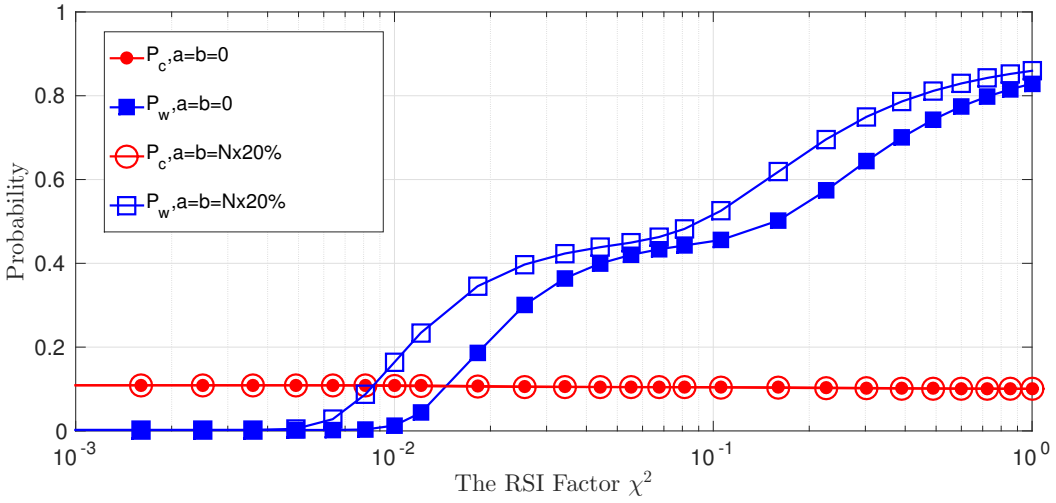

Figure 5.10: *The probabilities of collision and spectrum waste v.s. various RSI factors under different conditions when $P_{\mathrm{d},0} = P_{\mathrm{d},1}$ and CDR requirement is employed.*

the achievable throughput under the FD-SBSS scheme is investigated and shown in Fig. 5.11. By contrast, the achievable throughput under the FDSS scheme is also studied and presented in Fig. 5.12. These two figures both describe the achievable throughput of the SU v.s. the different received SNRs of the PU's signal from -20 dB to 5 dB. Assuming the FD SU-Tx is equipped with 8 antennas in total, various antenna partitioning cases are presented in the two figures, i.e., antenna partitioning pair $(M_{\mathrm{s}}, M_{\mathrm{t}}) = (6,2), (4,4), (2,6)$. The CDR requirement is also applied here in order to make sure the PU has enough protection from harmful interference and the desired detection rate is set as $P_{\mathrm{d},0} = P_{\mathrm{d},1} = 0.9$. Meanwhile, the received INR at the sensing antennas of the SU-Tx is assumed as $\frac{\|\mathbf{H}_{\mathrm{si}}\mathbf{s}_0\|^2}{M_{\mathrm{t}}M_{\mathrm{s}}\sigma_{\mathrm{u}}^2} = 15$ dB for the low transmit power case and $\frac{\|\mathbf{H}_{\mathrm{si}}\mathbf{s}_1\|^2}{M_{\mathrm{t}}M_{\mathrm{s}}\sigma_{\mathrm{u}}^2} = 25$ dB for the high transmit power case. Accordingly, the corresponding received SNR at the SU-Rx is $\frac{\|\mathbf{h}_{\mathrm{ss}}\|^2\sigma_{\mathrm{s},0}^2}{M_{\mathrm{t}}\sigma_{\mathrm{n}}^2} = 5$ dB for the low power transmission and $\frac{\|\mathbf{h}_{\mathrm{ss}}\|^2\sigma_{\mathrm{s},1}^2}{M_{\mathrm{t}}\sigma_{\mathrm{n}}^2} = 15$ dB for high power transmission.

When SU-Tx is with FD capability, the antenna partitioning at the SU-Tx is a factor that might influence the trade-off between the sensing and transmission performance of the secondary network. Generally, more sensing antennas at the FD SU-Tx helps to improve the spectrum sensing performance which can promote the achievable throughput of the secondary network. In the meantime, if the total number of antennas is fixed, the number of transmit antennas would reduce accordingly and this would lead to the decrease of the achievable throughout. Therefore, it can be deduced that there may exist an optimal antenna partitioning combination to maximize the achievable throughput of the secondary network. In fact, the existence of this optimal point depends on the slopes of probability

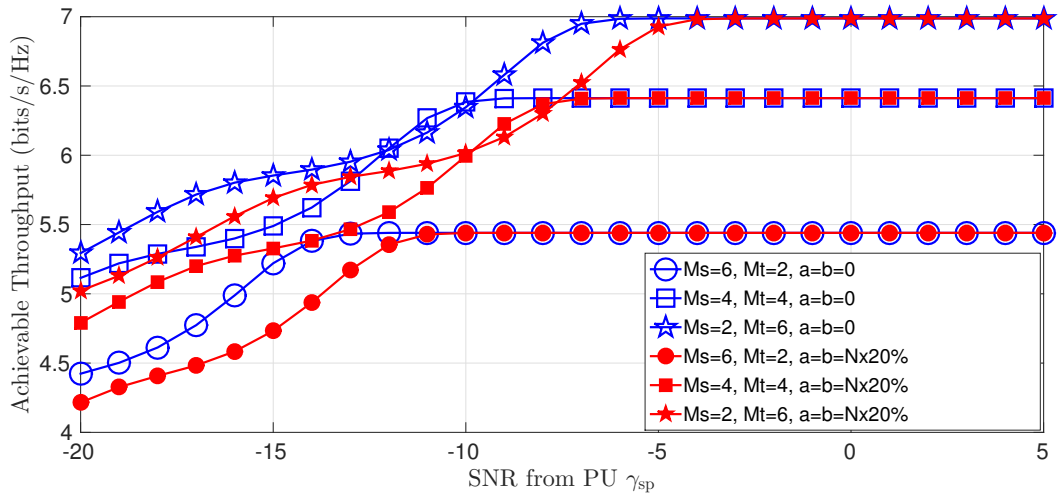

Figure 5.11: *The achievable throughput of the SU with different antenna partitioning v.s. the received SNR sourced from the PU (γ_{sp}) under the FD-SBSS scheme.*

terms, e.g. $(P_0 + P_2)$ and $(P_1 + P_3)$, and throughput terms.

Based on the practical parameter setting above, the achievable throughput under the FD-SBSS scheme increases with the increasing number of transmit antennas on the whole. The only exception is the antenna partitioning combination $(M_{\mathrm{s}}, M_{\mathrm{t}}) = (4, 4)$ achieves slightly better transmission performance than $(2, 6)$ between $\gamma_{\mathrm{sp}} = -12$ dB and -10 dB for $a = b = 0$ and between $\gamma_{\mathrm{sp}} = -10$ dB and -12.5 dB for $a = b = N \times 20\%$. It should be noted that the advantage mentioned above is quite limited. Therefore, it is reasonable to point out that assigning more transmit antennas could help to attain a better transmission performance over the whole range of γ_{sp}. On the contrary, under the FDSS scheme, more transmit antennas do not always improve the achievable throughput of the secondary network. Specifically, taking the performance for $a = b = 0$ as an example, employing 2 transmit and 6 sensing antennas achieves the best transmission performance over the range of γ_{sp} from -17 dB to -12 dB and $M_{\mathrm{s}} = M_{\mathrm{t}} = 4$ has the highest achievable throughput among the three different antenna partitioning combinations between -12 dB and -8 dB of γ_{sp}. For the remaining range of γ_{sp}, assigning 6 antennas for secondary transmission is the best choice for a superior transmission performance.

In addition, by comparing the achievable throughput in Fig. 5.11 and 5.12, the FD-SBSS scheme outperforms the FDSS technique. For instance, the achievable throughput gain can be up to 2.286 bits/s/Hz for the case with $(M_{\mathrm{s}}, M_{\mathrm{t}}) = (2, 6)$ and $a = b = 0$.

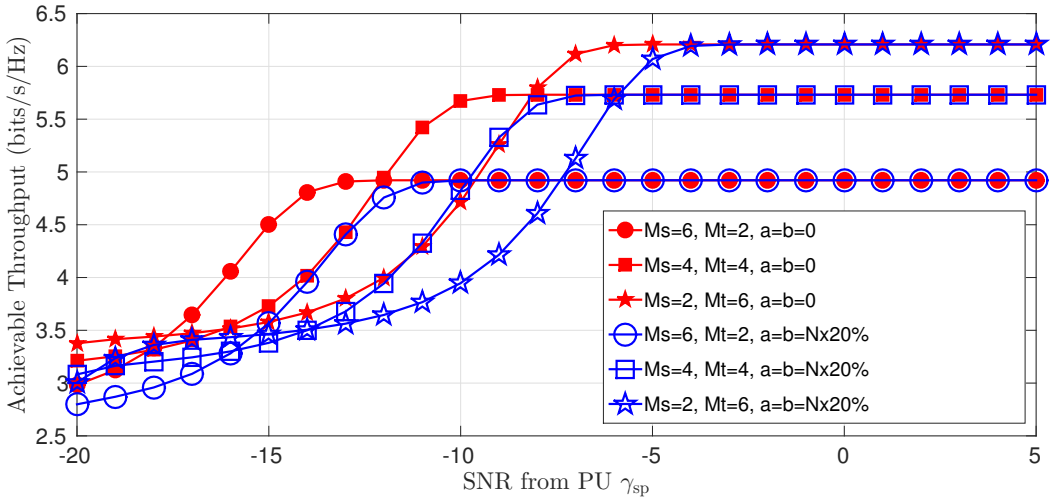

Figure 5.12: *The achievable throughput of the SU with different antenna partitioning v.s. the received SNR sourced from the PU (γ_{sp}) under the FD-SS scheme.*

Based on the performance indicated in Fig. 5.11 and 5.12 and the explanation in last paragraph, different antenna partitioning strategies should be applied for different sensing-based CR systems with FD capability when the total number of antennas is fixed and the CDR requirement is applied in order to guarantee the interests of PUs. The detailed strategy selection and reasons for this are stated as follows.

Under the FD-SBSS scheme, more antennas should be employed as transmit antennas, which could benefit the secondary transmission performance. Under this scheme and the above system setting, the sensing performance does not affect the achievable throughput seriously so that the final achievable throughput is dominated by the number of transmit antennas. This is attributed to the low power transmission when the presence of the PU is detected, which mitigates the negative effects of false alarms on the secondary throughput. However, under the FDSS scheme, different antenna partitioning combinations should be selected for different values of γ_{sp} in order to maximize the transmission performance. Specifically, for the extremely low or high received sensing SNR (≤ -18 dB or ≥ -8 dB for $a = b = 0$ case), more antennas should be utilized for transmission. For the received sensing SNR between -17 dB and -12 dB, fewer antennas should be assigned for transmission to achieve the maximum throughput. When the γ_{sp} falls into the range between -12 dB and -8 dB, the balanced antenna partitioning, i.e. $M_{\mathrm{s}} = M_{\mathrm{t}} = 4$, should be applied for the best transmission performance in the investigated case.

Under the FDSS scheme, when the PU is sensed as present, SUs are not allowed to transmit, so the transmission performance can be influenced by the sensing results seriously. Firstly, in the extremely low or high SNR scenario, the SU can obtain quite similar sensing performance under different antenna partitioning cases. Thus, the number of transmit antennas is the dominant factor in the achievable throughput in this situation. Secondly, for the medium SNR range (-17 dB $\leq \gamma_{\rm sp} \leq -9$ dB for $a = b = 0$ case), the optimal antenna partitioning combination is $(M_{\rm s}, M_{\rm t}) = (6, 2)$ for the first segment (i.e., -17 dB $\leq \gamma_{\rm sp} \leq -12$ dB) and $(4, 4)$ for the second segment. Generally, within this medium SNR range, the sensing performance dominates the achievable throughput. In detail, the combination $(M_{\rm s}, M_{\rm t}) = (6, 2)$ converges faster than $(M_{\rm s}, M_{\rm t}) = (4, 4)$ with the increasing $\gamma_{\rm sp}$ due to more sensing antennas assigned. After $\gamma_{\rm sp}$ is larger than -12 dB, $(M_{\rm s}, M_{\rm t}) = (6, 2)$ and $(4, 4)$ obtain almost same sensing performance so that the advantage of employing more transmit antennas is revealed. Therefore, for $a = b = 0$ case, $(M_{\rm s}, M_{\rm t}) = (6, 2)$ performs the best achievable throughput between -17 dB and -13 dB, but $(M_{\rm s}, M_{\rm t}) = (4, 4)$ shows the best transmission performance from -12 dB to -9 dB.

5.6 Summary

This chapter investigated the non-time-slotted FD spectrum sensing and sharing systems based on ED with multiple sensing antennas. In terms of the FDSS scheme, firstly, the generalized theoretical expressions of the probabilities of false alarm and missed detection were derived when considering the asynchronism between the primary and secondary networks. Secondly, in order to benefit both the PU and SUs, the total error rate of the system was studied and the optimal decision threshold pairs were obtained to minimize the total error rate. The SU-Tx may transmit or keep silent, so a decision threshold pair (r_0, r_1) was necessary for the two different states of the SU-Tx. The expressions of r_0 and r_1 were also obtained for a given sensing error rate of the system $P_{\rm m}$ and $P_{\rm fa}$. Finally, from our results, the spectrum sensing performance of the proposed FD technique outperformed the traditional HD approach based on the non-time-slotted model due to the longer sensing time and improved SIS capability. Furthermore, the obtained optimal decision threshold pairs minimized the total error rates, which considered the interests of the PU and SUs simultaneously. In the meanwhile, FD-SBSS scheme was also proposed and investigated. Firstly, the collision and spectrum waste probabilities were studied based on the obtained expressions of false alarm and detection rates. Secondly, the achievable throughput of the secondary network under FD-SBSS was investigated and the obtained

results revealed the improvement compared with the FDSS scheme. Specifically, antenna partitioning was explored in order to maximize the achievable throughput. Different antenna partitioning methods were proposed and analysed for FD-SBSS and FDSS schemes respectively.

Chapter 6

Conclusions and Future Work

This thesis analyzed and discussed spectrum sensing techniques in CR networks. Generally, these analyses are presented from three aspects, including the total error rates and sensing-throughput trade-off of eigenvalue-based spectrum sensing techniques, the optimal number of cooperative SUs when employing collaborative spectrum sensing under random secondary networks, and the sensing and transmission performance of FDSS and FD-SBSS schemes. Furthermore, the theoretical and simulation results have demonstrated the effectiveness of the proposed techniques and analysis in this thesis. The detailed conclusions of this thesis are presented in the following part and certain possible future research directions are also provided in this chapter.

6.1 Conclusions

This thesis focused on spectrum sensing techniques in order to advance the sensing and transmission performances of secondary networks. Initially, the eigenvalue-based spectrum sensing methods were investigated in terms of total error rates, including MED, MME, EME and the GLRT eigenvalue-based detections. The optimal decision thresholds were obtained for minimizing total error rates in order to consider the benefits of PUs and SUs simultaneously. For MME and EME detections, only cases with 2 receive antennas were studied because of the lack of generalized expressions of detection rates. The generalized cases of MED and the GLRT-based eigenvalue detection were investigated with arbitrary number of receive antennas. In terms of transmission performance of secondary networks, the sensing-throughput trade-off of the GLRT-based spectrum sensing techniques was discussed for the general case and the comparison with MED and ED was also presented in the thesis. The optimal sensing time was obtained for maximizing the achievable throughput when the target detection rate was achieved. Therefore, the transmission performance of SUs could be optimized and, at the same time, the interests of PUs could get enough protection from harmful interference caused by the collision between primary and secondary transmissions.

Secondly, cooperative spectrum sensing was investigated in order to achieve better sensing performance than the single-node spectrum sensing. Unlike the work in the literature on cooperative sensing, this thesis explored the sensing performance considering the randomness of secondary networks, which is more practical in realistic situations. Thus, a homogeneous PPP was applied in this investigation and the PDF of the distance between the i-th nearest SU and the PU was derived for CR networks. The number of optimal cooperating SUs was investigated based on OR and AND decision fusion rules, which could minimize the total error rate of the final decision. When the SUs follow a homogeneous PPP with a density ρ, there might exist some unreliable SUs with quite low received SNR so that their local sensing result could affect the cooperative sensing and mislead the final sensing decision. Besides, the achievable ergodic capacity and throughput of the SUs were also discussed when considering the effects of cooperative spectrum sensing under the random secondary network. Based on the obtained sensing and transmission performance, effective cooperating strategies on the number of collaborating SUs were proposed in order to optimize the transmission performance while guaranteeing the sensing performance.

Lastly, in order to realize the simultaneous spectrum sensing and secondary transmission, FD techniques were applied in spectrum sensing. This thesis investigated two different FD spectrum sensing schemes, including FDSS and FD-SBSS. Under the FDSS scenario, the theoretical expressions of false alarm and missed detection rates were derived based on ED with multiple sensing antennas. Furthermore, the optimal decision threshold pairs were investigated for minimizing the total error rate based on CDR and CFAR requirements and the simulation results were presented for the CDR case. Besides, in order to improve the transmission performance of the secondary network, the FD-SBSS scheme was proposed. The collision and spectrum waste probabilities under this scheme were studied. Compared with the FDSS scheme, the obtained results show the advantages of FD-SBSS scheme in terms of achievable throughput of the secondary network. Meanwhile, this thesis also explored the effect of antenna partitioning on the achievable throughput of SUs under both the FDSS and FD-SBSS schemes. Based on the simulation results, different antenna partitioning methods were proposed for FDSS and FD-SBSS schemes in order to maximize the achievable throughput.

6.2 Limitations and Future Work

This thesis has obtained some interesting results on spectrum sensing techniques in CR networks and contributed to the improvement of sensing and transmission performances of the secondary network.

However, it has to be admitted that there still exist certain limits in the work presented in this thesis because of some constraints. Thus, this section will give some possible directions for the future work in order to compensate for the limitations in this thesis to some extent.

6.2.1 Optimal Beamforming on FD-SBSS

The work on FD spectrum sensing and sharing can be further extended in terms of optimizations. One possible and interesting direction of the future work is the design of optimal beamforming vectors which can maximize the achievable throughout of the SUs with some constraints. The new expression of achievable throughput with beamforming vectors can be obtained based on the expression without beamforming vectors given in last chapter. It should be noted that there should exist a beamforming vector pair $(\mathbf{v}_0, \mathbf{v}_1)$, i.e. two separate beamforming vectors, to be optimized for the absence and presence of secondary communications respectively. This is similar to the design of decision threshold pairs. This optimization is considered with the selection of decision threshold pairs together. In detail, the objective function is the achievable throughput of the SU which includes the sensing error probability. Meanwhile, two constraints are also considered. In the first constraint, the collision probability should not be more than a target value in order to protect the interests of PUs. Besides, the average transmit power of the SU should not exceed the maximum value. One of the challenges in this optimization work is how to convert the current problem into a convex optimization issue. Since the expression of achievable throughput consists of certain expressions of probabilities which includes some Q-functions. It is well-known that the Q-function is a non-convex function. Furthermore, these Q-functions appear in the denominator and nominator of a fraction and their exponent might be 2 in the denominator which increases the difficulty.

6.2.2 Spectrum Sharing between Radar Systems and Cellular Networks

Unlike the spectrum sensing and sharing work mentioned in previous chapters, another possible research direction is the spectrum sharing between the cellular networks and radar systems. Recently, in US and Europe, the spectrum resources between 3.5 GHz and 3.6 GHz are prepared to release for sharing. The incumbents in this frequency band are radar and satellite systems [122]. This release gives opportunity to the coexistence between cellular communication systems and radar systems. Therefore, it is necessary to conduct academic research before this coexistence is employed in practice. Specifically, the coexistence between a single-UE cellular network and a collocated multiple-input-

multiple-output (MIMO) radar system has been studied in [123]. However, the secondary network with multiple UEs has not been considered in the literature. Meanwhile, in order to improve the transmission performance of the secondary network, FD technology can be also considered in this scenario.

In detail, the coexistence between the FD wireless communication network and MIMO radar system is considered in this scenario. The spectrum sharing between these two systems are considered and the interference to the radar receiver caused by this sharing has to be under the maximum interference value. Furthermore, the wireless and radar models in this work are set up as follows. In terms of cellular networks, we consider the wireless system with single base station and multiple UEs. Specifically, the base station has FD capability and every HD UE is equipped with a single antenna. It is assumed that there exist multiple UEs for both the secondary uplink and downlink communications. With regard to the radar systems involved in this spectrum sharing scheme, we consider a collocated MIMO radar which is equipped with uniform linear arrays. The target is assumed as a point source at the far field and the MIMO radar is assumed to transmit orthogonal waveforms.

Based on the system model described above, the optimal beamforming and transmit power for wireless networks can be investigated. Initially, the expression of the detection rate of the radar system should be derived in terms of false alarm rates. These two probabilities are the key metrics for evaluating the detection performance of the radar. The specific expressions depend on the detectors used for radar detections and the popular detectors are ED and GLRT, etc. In order to realize the spectrum sharing between FD cellular networks and the radar system without harmful interference to each other, the optimal beamforming and transmit power can be investigated jointly for the wireless system. Specifically, the objective is to obtain the optimal beamforming vector for the downlink communication and optimum transmit power for the uplink communication in order to maximize the probability of detection of the MIMO radar, while guaranteeing the quality of service of the FD communication system and fulfilling the transmit power requirement of the cellular network. Considering the difficulty of estimating the accurate channel state information in practice, this optimization issue can be studied based on different conditions, i.e., perfect and imperfect channel state information.

Appendix A

Stochastic Geometry

Rencetly, large wireless communication systems, such as cellular and sensor networks, have gained much attention from the researchers in the field of wireless communications [99]. As Shannon presented in his work [124], SNR or SINR have been a significant metric to evaluate the performance of a wireless communication system, which is closely related to detection performance, outage probability and throughput, etc. However, for contemporary communication systems, the dramatically increased amount of uncertainty in large wireless systems compared with point-to-point communication system, could influence SNR or SINR hugely. Therefore, the classical approaches of analyzing point-to-point communication systems are not appropriate when dealing with random networks. For instance, within a same cell, the users located at the edge of coverage area and near the transmitter may have dozens of dBs difference in terms of received SNR or SINR. This big gap is caused by many factors, including path loss, shadowing and multipath effects. Therefore, stochastic geometry is used for coping with the above difficulties, which helps to understand the random phenomena and analyze the statistically average performance over a random wireless network.

A.1 Point Processes

As a branch of applied probability, stochastic geometry is closely related to point processes [5, 111]. Point processes could be described as random collections of points in a measurable space. Academically, point processes are defined as a mapping from a probability space to the space of point measures on some space. The PPP is one type of the point processes. Before moving on to the introduction to PPP, it is good to know certain related knowledge on point processes.

Dirac measure:
The Dirac measure $\delta_x(A)$ refers to the measure on a set X and any set $A \in X$. Specifically, for a point $x \in X$, the Dirac measure is equal to 1 if $x \in A$; otherwise, this figure is equal to 0. In mathematics,

the Dirac measure can be expressed by

$$\delta_x(A) = \mathbf{1}_A(x) = \begin{cases} 0 & if \quad x \notin A \\ 1 & if \quad x \in A, \end{cases}$$

where $\mathbf{1}_A$ denotes the indicator function of A.

Point measure:
For a point process Φ on some space A, the point measure is a counting measure which counts the number of points falling in the space A. Thus each point measure $\Phi(A)$ can be denoted by the summation of Dirac measures on the space A [5, 99], which can be expressed as

$$\Phi(A) = \sum_i \delta_{x_i}(A). \tag{A.1}$$

Intensity measure:
The intensity measure is defined as the expectation of the number of points falling in some space A [5, 99], so the intensity measure of set A can be expressed as

$$\Lambda(A) = \mathbb{E}[\Phi(A)], \tag{A.2}$$

where $\mathbb{E}[\cdot]$ denotes the expectation operator.

Point processes on Euclidean space $\mathbb{R}^\nu$ can be classified into various dichotomous groups according to different characteristics, where $\nu > 1$ is the space dimension. These classifications [99] are detailed as follows [99]:

- *Stationary*: A point process Φ on the subset $A \in \mathbb{R}^\nu$ can be regarded as stationary, if the distribution of Φ does not change with translation. In other words, $\Phi + y$ has the same distribution as Φ for all $y \in \mathbb{R}^\nu$, where $\Phi + y$ is defined to be $\sum_i \delta_{x_i+y}$. More crudely, the stationarity of Φ on space A holds when the expected number of points falling in A is determined by the size of A and independent of the locations of the points.

- *Simple*: A point process is simple, when the multiplicity of a point in this process is no larger than 1. Intuitively, a point process is simple if there are no multiple points falling at the same location [99].

- *Isotropic*: If a point process is isotropic, its distribution is not influenced by rotation. Furthermore, a point process is called motion-invariant when it is stationary and isotropic.

- *Marked*: A marked point process consists of a point process and the labels assigned to points. It should be noted that the marks (or labels) mentioned here are typically irrelevant to this point process and i.i.d.

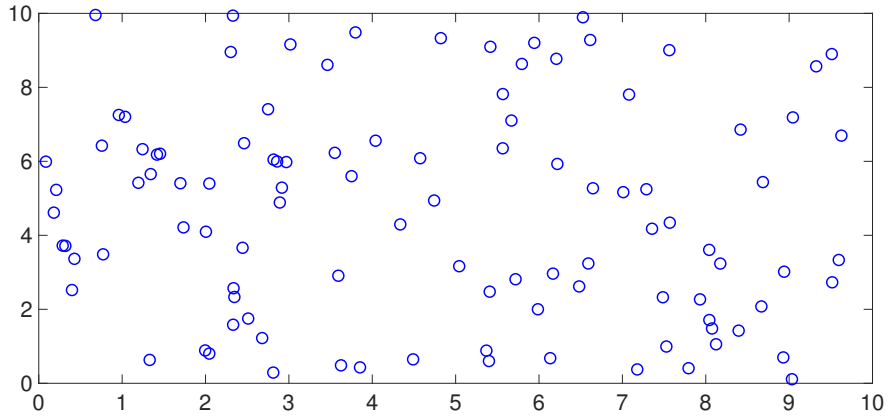

Figure A.1: *A homogeneous PPP with unit intensity of a 2-dimensional space.*

A.2 Poisson Point Process

A point process Φ on some space A can be a defined as a PPP, if the following requirements are satisfied.

- For all the disjoint subsets of the space A, i.e. $B_1, \cdots, B_n$, the point measures $\Phi(B_i)$ are independent random variables.

- For all subsets B of A, $\Phi(B)$ follows Poisson distribution.

It is worth mentioning that points in PPP of some space A are located independently in A. Homogeneous and non-homogenous PPPs have different characters and they are utilized for modeling and analyzing different wireless communication networks. A homogeneous PPP is shown in Fig. A.1 and certain key properties of homogeneous PPP [99] are summarized as follows:

- The density of the points in homogenous PPP is constant across the whole space, thus homogeneous PPP can be used to model the distributions of nodes which are located uniformly across the space of interest.

- Based on the classified characters of a point process in last subsection, a homogeneous PPP is stationary, isotropic and simple.

- For a homogeneous PPP with density ρ, the probability that there exist n nodes in a bounded region $A \in \mathbb{R}^{\nu}$ can be given by

$$P[n \quad nodesin \quad A] = e^{-\rho\Theta(A)} \frac{(\rho\Theta(A))^n}{n!}, \tag{A.3}$$

  where $\Theta(\cdot)$ denotes the Lebesgue measure operator for evaluating the volume of a Euclidean space of interest.

In wireless communications, in order to evaluate the detection or transmission performance of a system without the knowledge of terminals' locations or with random locations of users, homogeneous PPP is a popular modeling tool, e.g. [98, 125, 126]. Furthermore, the distributions of the distances between transmitters and receivers are of significance to the system performance analysis. Therefore, the Euclidean distance of the i-th nearest neighbor in a homogeneous PPP with intensity ρ in space $\mathbb{R}^{\nu}$ is studied and the corresponding PDF is given by

$$f_{r_i}(r) = e^{-\rho c_\nu r^\nu} \frac{\nu(\rho c_\nu r^\nu)^i}{r\Gamma(i)}, \tag{A.4}$$

where the coefficient c_ν is given by

$$c_\nu = \begin{cases} \frac{\pi^{\frac{\nu}{2}}}{(\frac{\nu}{2})!}, & foreven \quad \nu \\ \frac{\pi^{\frac{\nu-1}{2}} 2^\nu (\frac{\nu-1}{2})!}{\nu!}, & forodd \quad \nu. \end{cases}$$

This thesis focuses on the application of homogeneous PPP in CR networks and related work has been presented in Chapter 4, since homogeneous PPP is regarded as the most natural and simplest point process [99].

Appendix B
Proofs

Proof of Eq. (3.40). We aim to solve $P_{\text{fa}}(x) = \epsilon$ given that $\epsilon \in [0, 1]$ and

$$P_{\text{fa}}(x) = 1 - \frac{\Gamma(mn)(mc)^{-d}}{d\Gamma(mn-d)\Gamma(d)} \times \left[{}_2F_1\left(d, d-mn+1; d+1; \frac{x}{c}\right)(mx)^d \right.$$
$$\left. - {}_2F_1\left(d, d-mn+1; d+1; \frac{1}{mc}\right) \right], \tag{B.1}$$

where $\frac{1}{m} \leq x \leq 1$. The previous equation is equivalent to finding the value of x that satisfies

$${}_2F_1\left(d, d-mn+1; d+1; \frac{x}{c}\right)(mx)^d$$
$$= {}_2F_1\left(d, d-mn+1; d+1; \frac{1}{mc}\right) + \frac{d\Gamma(mn-d)\Gamma(d)}{\Gamma(mn)(mc)^{-d}}(1-\epsilon), \tag{B.2}$$

which can be rewritten as

$$G^{1,2}_{2,2}\left(\begin{matrix} 1-d, mn-d \\ 0, -d \end{matrix} \middle| -\frac{x}{c} \right)$$
$$= (mx)^{-d}{}_2F_1\left(d, d-mn+1; d+1; \frac{1}{mc}\right) + d!(mn)_{-d}(1-\epsilon)\left(\frac{c}{x}\right)^d, \tag{B.3}$$

which can be expressed as an incomplete beta function, and hence the value of x can be given by the inverse. □

Proof of Corollary 2. The CDF can be obtained by integrating (3.42), and after further manipulations the integral can be written as

$$F^1_{\text{GLRT}}(x) = \widetilde{\mathcal{A}}\widetilde{\mathcal{B}} \int_{\frac{1}{m-1}}^{\frac{x}{1-x}} \exp\left[-\frac{y^2}{8n(m-1)^2}\left(\frac{1}{1+m\gamma} - \frac{1}{nm\gamma}\right)^{-2} \right.$$
$$\left. - yn(m-1)\left(\frac{1}{nm\gamma} - \frac{1}{1+m\gamma}\right)\left(1 + \frac{m-1}{nm\gamma}\right) \right] \mathrm{d}y, \tag{B.4}$$

where $\widetilde{\mathcal{A}}$ and $\widetilde{\mathcal{B}}$ are given by

$$\widetilde{\mathcal{A}} = \sqrt{\frac{n}{2\pi}} \left(\frac{m-1}{1+m\gamma} \right) \left(1 - \frac{1+m\gamma}{nm\gamma} \right), \tag{B.5}$$

$$\widetilde{\mathcal{B}} = \exp\left(-\frac{n}{2} \left(1 + \frac{m-1}{nm\gamma} \right)^2 \right). \tag{B.6}$$

With the aid of [115, (3.322.1)], we arrive at the expression

$$\begin{aligned} F^1_{\mathrm{GLRT}}(x) &= \widetilde{\mathcal{A}}\widetilde{\mathcal{B}}\sqrt{\pi\beta}\exp\left(\beta\alpha^2\right) \\ &\times \left(\left[1 - \Phi\left(\alpha\sqrt{\beta} + \frac{1}{2\sqrt{\beta}(m-1)} \right) \right] - \left[1 - \Phi\left(\alpha\sqrt{\beta} + \frac{x}{2\sqrt{\beta}(1-x)} \right) \right] \right), \end{aligned} \tag{B.7}$$

where α and β are defined in (4.14) and (4.15) and then after further manipulations we arrive at the expression of the CDF given by (3.48). □

Proof of Equation (4.16). The equation (4.13) can be reorganized as follows:

$$\Phi\left(\tau_i\sqrt{\varphi_i} + \frac{r_i}{2\sqrt{\varphi_i}(1-r_i)} \right) = \Phi\left(\tau_i\sqrt{\varphi_i} + \frac{1}{2\sqrt{\varphi_i}(m-1)} \right) + 2(1 - P^{\mathrm{su}}_{\mathrm{d},i}). \tag{B.8}$$

Based on the Maclaurin series expansion of the inverse error function [127] which is given as

$$\Phi^{-1}(x) = \sum_{t=0}^{\infty} \frac{C_t}{2t+1} \left(\frac{\sqrt{\pi}}{2} x \right)^{2t+1}, \tag{B.9}$$

where $C_0 = 1$ and $C_t = \sum_{q=0}^{t-1} \frac{C_q C_{t-1-q}}{(q+1)(2q+1)}$, then we can have

$$\tau_i\sqrt{\varphi_i} + \frac{r_i}{2\sqrt{\varphi_i}(1-r_i)} = \sum_{t=0}^{\infty} \frac{C_t}{2t+1} \left(\frac{\sqrt{\pi}}{2} \left[\Phi\left(\tau_i\sqrt{\varphi_i} + \frac{1}{2\sqrt{\varphi_i}(m-1)} \right) + 2(1 - P^{\mathrm{su}}_{\mathrm{d},i}) \right] \right)^{2t+1}, \tag{B.10}$$

$$r_i = \left(\frac{\left[\sum_{t=0}^{\infty} \frac{C_t}{2t+1} \left(\frac{\sqrt{\pi}}{2} \left[\Phi\left(\tau_i\sqrt{\varphi_i} + \frac{1}{2\sqrt{\varphi_i}(m-1)} \right) + 2(1 - P^{\mathrm{su}}_{\mathrm{d},i}) \right] \right)^{2t+1} - \tau_i\sqrt{\varphi_i} \right]^{-1}}{2\sqrt{\varphi_i}} + 1 \right)^{-1} \tag{B.11}$$

After further reorganizations, the equation (4.16) can be obtained. □

Proof of Theorem 3. When the PU is far from the SUs within the coverage radius of the FC, the area of the shadowing region $S\ \mathrm{m}^2$ in the Fig. 4.1 can be approximated as

$$\begin{aligned} S &= 2\pi(D-R)\frac{2\theta}{2\pi}\big(d-(D-R)\big) \\ &= 2\theta(D-R)(d-D+R). \end{aligned} \tag{B.12}$$

Since in a homogeneous 2-dimensional PPP with density ρ, the probability of having i nodes in a region $\mathcal{A}$ with the area $S\ \mathrm{m}^2$ is given by

$$\mathbf{P}\{i \text{ nodes in } \mathcal{A}\} = e^{-\rho S}\frac{(\rho S)^i}{i!}. \tag{B.13}$$

The complementary CDF of d_i can be computed as the probability that there are fewer than i SUs within the shadowing area (as defined in Section 4.2 and Fig. 4.1), which is given by

$$\begin{aligned} P_i &= \mathbf{P}\{0,1,\cdots,i-1 \text{ nodes between } D\text{–}R \text{ and } d_i\text{–}(D\text{–}R)\} \\ &= \sum_{j=0}^{i-1} e^{-\rho S_j}\frac{(\rho S_j)^j}{j!}, \end{aligned} \tag{B.14}$$

By utilizing the relationship between the complementary CDF and the PDF, i.e.,

$$f_{d_i}(d) = -\frac{\mathrm{d}P_i}{\mathrm{d}d}, \tag{B.15}$$

The PDF of d_i can be derived as

$$\begin{aligned} f_{d_i}(d) &= 2\rho\theta(D-R)e^{-\rho 2\theta(D-R)(d-D+R)} \\ &\times\left[\sum_{j=0}^{i-1}\frac{\big(\rho 2\theta(D-R)(d-D+R)\big)^j}{j!} - \sum_{j=1}^{i-1}\frac{\big(\rho 2\theta(D-R)(d-D+R)\big)^{j-1}}{(j-1)!}\right], \end{aligned} \tag{B.16}$$

After further manipulations, the expression of (4.25) can be obtained. □

Proof of the Eqs. (5.8), (5.9), (5.10) *and* (5.11). In order to obtain the expressions of sensing error rates under different hypotheses, the distributions of the test statistic T_{ED} have to be derived under the hypotheses $\mathcal{H}_{10}, \mathcal{H}_{00}, \mathcal{H}_{11}, \mathcal{H}_{01}$. When the total sample size of the received signal N is relatively large, these distributions could be modelled as normal distribution by using CLT. Therefore, the objective for this derivation is to derive the expectation and variance of T_{ED}.

In non-time-slotted FD CR system, the PU may have two different states $\mathrm{s1}$ and $\mathrm{s2}$ within one periodic secondary sensing frame. Assuming the received sample sizes for the state $\mathrm{s1}$ and $\mathrm{s2}$ are A and B respectively. Then, the expectation and variance of T_{ED} can be given by

$$\begin{aligned}\mathbb{E}[T_{\mathrm{ED}}] &= \frac{A}{N}\mathbb{E}[|y_i(n)|^2_{\mathrm{s1}}] + \frac{B}{N}\mathbb{E}[|y_i(n)|^2_{\mathrm{s2}}] \\ &= \frac{A}{N}\sigma^2_{y,\mathrm{s1}} + \frac{B}{N}\sigma^2_{y,\mathrm{s2}}, \qquad \text{(B.17)} \\ \mathrm{Var}[T_{\mathrm{ED}}] &= \frac{A}{M_{\mathrm{s}}N^2}\mathrm{Var}[|y_i(n)|^2_{\mathrm{s1}}] + \frac{B}{M_{\mathrm{s}}N^2}\mathrm{Var}[|y_i(n)|^2_{\mathrm{s2}}] \\ &= \frac{A}{M_{\mathrm{s}}N^2}\sigma^4_{y,\mathrm{s1}} + \frac{B}{M_{\mathrm{s}}N^2}\sigma^4_{y,\mathrm{s2}}. \qquad \text{(B.18)}\end{aligned}$$

Under $\mathcal{H}_{10}$, from the equation (5.7), we can obtain

$$\sigma^2_{y,\mathrm{s1}} = (\gamma_{\mathrm{sp}} + \chi^2\gamma_{\mathrm{in}} + 1)\sigma^2_u, \quad \sigma^2_{y,\mathrm{s2}} = (\chi^2\gamma_{\mathrm{in}} + 1)\sigma^2_u. \qquad \text{(B.19)}$$

By substituting the equation (B.19) into (B.17) and (B.18), the expressions of $\mathbb{E}[T_{\mathrm{ED}}]$ and $\mathrm{Var}[T_{\mathrm{ED}}]$ under $\mathcal{H}_{10}$ can be obtained. Then, by using the CLT and $P_{\mathrm{fa},1}(x) = \Pr\{T_{\mathrm{ED}} > x|\mathcal{H}_{10}\}$, the equation (5.8) can be derived.

Meanwhile, the distributions under $\mathcal{H}_{00}, \mathcal{H}_{11}, \mathcal{H}_{01}$ can be obtained in the same way and equations (5.9), (5.10) and (5.11) can be obtained by taking similar steps. □

Appendix C
Publication List

C.1 Journal Publications

[1] **Y. He**, J. Xue, T. Ratnarajah, M. Sellathurai and F. Khan, "On the performance of cooperative spectrum sensing in random cognitive radio networks using stochastic geometry," *IEEE Systems Journal*, Vol. PP, no. 99, pp. 1-12, July 2016.

[2] **Y. He**, T. Ratnarajah, E. H.G. Yousif, J. Xue and M. Sellathurai, "Performance analysis of multi-antenna GLRT-based spectrum sensing for cognitive radio," *Signal Processing (Elsevier)*, Vol.120, pp. 580-593, March 2016.

C.2 Conference Publications

[1] **Y. He**, J. Xue, T. Ratnarajah and M. Sellathurai, "Full-duplex spectrum sensing for multi-antenna non-time- slotted cognitive radio networks," in *IEEE International Workshop on Signal Processing Advances in Wireless Communications (SPAWC)*, Edinburgh, July 2016.

[2] **Y. He**, J. Xue, T. Ratnarajah and M. Sellathurai, "Cooperative sensing technique for random secondary wireless networks," in *IEEE International Conference on Communications (ICC) Workshops*, London, June 2015.

[3] **Y. He**, T. Ratnarajah, E. H.G. Yousif, J. Xue and M. Sellathurai, "Optimization of multi-antenna GLRT-based spectrum sensing for cognitive radio," in *IEEE Annual International Symposium on Personal, Indoor and Mobile Radio Communications (PIMRC)*, Hong Kong, August 2015.

[4] **Y. He**, T. Ratnarajah, J. Xue, E. H.G. Yousif and M. Sellathurai, "Optimal decision threshold for eigenvalue- based spectrum sensing techniques," in *IEEE International Conference on Acoustics, Speech and Signal Processing (ICASSP)*, Florence, May 2014.

Appendix D
Publications

The Appendix C contains the published papers which are related to this thesis.

This article has been accepted for inclusion in a future issue of this journal. Content is final as presented, with the exception of pagination.

On the Performance of Cooperative Spectrum Sensing in Random Cognitive Radio Networks

Yibo He, *Student Member, IEEE*, Jiang Xue, *Member, IEEE*, Tharmalingam Ratnarajah, *Senior Member, IEEE*, Mathini Sellathurai, *Senior Member, IEEE*, and Faheem Khan, *Member, IEEE*

***Abstract*—This paper investigates the performance of cooperative spectrum sensing in cognitive radio networks using the stochastic geometry tools. In order to cope with the diversity of received signal-to-noise ratios at secondary users, a practical and efficient cooperative spectrum sensing model is proposed and investigated based on the generalized likelihood ratio test detector. In order to investigate the cooperative spectrum sensing system, the theoretical expressions of the probabilities of false alarm and detection of the local decision are derived. The optimal number of cooperating secondary users is then investigated to achieve the minimum total error rate of the final decision by assuming that the secondary users follow a homogeneous Poisson point process. Moreover, the theoretical expressions for the achievable ergodic capacity and throughput of the secondary network are derived. Furthermore, the technique of determining an appropriate number of cooperating secondary users is proposed in order to maximize the achievable ergodic capacity and throughput of the secondary network based on a target total error rate requirement. The analytical and simulation results validate the chosen optimal number of collaborating secondary users in terms of spectrum sensing, achievable ergodic capacity, and throughput of the secondary network.**

***Index Terms*—Cognitive radio (CR), ergodic capacity, Poisson point process (PPP), spectrum sensing, throughput.**

I. Introduction

In recent years, the explosive growth of wireless data traffic has led to spectrum scarcity due to ever-increasing demand for additional spectrum to provide new wireless services and applications. Cognitive radio (CR) has been put forward as a promising solution to end the spectrum scarcity, which exists mainly due to rigid spectrum allocation policies. CR allows the secondary (unlicensed) users (SUs) to use the available spectrum opportunities when primary (licensed) users (PUs) are inactive, based on the condition that secondary transmission must not cause harmful interference to PUs. It is, therefore, of utmost importance to develop highly reliable and efficient spectrum sensing techniques which are crucial to the implementation of CR system and other CR-based derivatives, such as licensed shared access [1].

Manuscript received October 23, 2015; revised March 07, 2016; accepted April 10, 2016. This work was supported by the Seventh Framework Programme for Research of the European Commission under Grant ADEL-619647. *(Corresponding author: Jiang Xue.)*

Y. He, J. Xue, T. Ratnarajah, and F. Khan are with the Institute for Digital Communications, School of Engineering, The University of Edinburgh, Edinburgh EH9 3JL, U.K. (e-mail: y.he@ed.ac.uk; j.xue@ed.ac.uk; t.ratnarajah@ed.ac.uk; faheem.khan@ed.ac.uk).

M. Sellathurai is with the School of Engineering and Physical Sciences, Heriot-Watt University, Edinburgh EH14 4AS, U.K. (e-mail: m.sellathurai@hw.ac.uk).

Digital Object Identifier 10.1109/JSYST.2016.2554464

A. Related Work

The objective of spectrum sensing is to determine whether the PU is present so that the SU can decide when to access the licensed frequency bands. Generally, spectrum sensing techniques utilize single node or cooperative spectrum sensing. Cooperative spectrum sensing technique can improve the performance of the spectrum sensing system [2] by making a final decision on the status of the PU in a centralized or distributed manner. Many different combining techniques, fusion strategies, and sensing techniques have been proposed to improve the accuracy and efficiency of cooperative spectrum sensing [3]–[9]. In [10], the sensing throughput tradeoff of the secondary network was studied based on energy detector (ED). The performance of cooperative spectrum sensing with ED was investigated in [11] based on the constant detection rate (CDR) and the constant false alarm rate (CFAR) requirements when the SUs were distributed randomly. Besides, the optimization of cooperative spectrum sensing with ED was studied in [12], but the locations of SUs were assumed to be identical and fixed.

Meanwhile, the stochastic geometry approach using a Poisson point process (PPP) has been used to analyze the performance of random wireless networks and CR networks [13]–[14]. In [15], the spectrum-sharing transmission capacity was investigated by applying stochastic geometry in overlay and underlay CR networks. Peng *et al.* [16] derived the ergodic capacity achieved by the single nearest and Nth-nearest remote radio head (RRH) association strategies in cloud radio access networks and investigated the impact of RRH density and number of antennas per RRH on the ergodic capacity gain.

Besides, in the existing works, multichannel CR network has been exploited, a semidistributed cooperative spectrum sensing protocol was proposed and the throughput maximization issue was investigated from the perspectives of the channel assignment, the spectrum sensing time, and the access parameters. The total transmit capacity over all the subchannels for the secondary network was studied in [18] under the transmit power and the interference power constraints. But we focus on the narrowband spectrum sensing in this paper, since the single-channel spectrum sensing performance with the homogeneous PPP still needs certain further exploration and the results in this paper are also valid for wideband spectrum sensing when the subchannel is sensed in a sequential manner.

B. Motivations

This paper investigates the cooperative spectrum sensing with the generalized likelihood ratio test (GLRT) eigenvalue-based

detector in interweave CR networks while assuming that the SUs follow a homogeneous PPP and this is motivated by multiple factors. First, it is more practical to assume that SUs follow a homogeneous PPP compared with the traditional assumption in the literatures. Most of the previous works assumed that the received signal-to-noise ratios (SNRs) at SUs were identical, but in practice the received SNRs could vary depending on the locations of SUs. Second, the cooperative spectrum sensing with PPP is a challenging topic and still needs further investigations. Specifically, a new strategy is required to cope with the diversity of the received SNRs in the PPP model, which has not been studied in the literatures. Third, the existing works are mainly based on ED when the stochastic geometry is employed, but one of the limitations of the ED-based methods is the sensitivity to the noise uncertainty. Therefore, the robust GLRT detector [19] is employed to evaluate the cooperative spectrum sensing and secondary transmission performances. Finally, a minimum total error rate considers the benefits of PUs and SUs simultaneously, but the previous works such as [20] and [21] mainly focused on the probability of false alarm due to the lack of generalized closed-form expression of the detection probability, which only considered the interests of SUs. A low probability of false alarm can make SUs have more chances to access the spectrum holes, however, the benefits of PUs may not be guaranteed. Therefore, the aforementioned issues motivate us to investigate the total error rate performance and the optimality of the cooperative spectrum sensing system with the GLRT detector by applying stochastic geometry, which considers the benefits of PU and SUs concurrently.

C. Main Contributions

The main contributions of this paper can be summarized as follows.

1) First, the sensing performance of each SU based on the GLRT detector is investigated as cooperative spectrum sensing requires sensing by each node. We derive the generalized closed-form expressions of probabilities of false alarm and detection of the GLRT detector for each SU, which is required to analyze the total error rate, achievable ergodic capacity, and throughput. Unlike the theoretical expressions on the sensing performance provided in [21] and [22], the expressions derived in this paper are with low computational complexity and valid for the general case with an arbitrary number of receive antennas.
2) Second, an efficient GLRT-based cooperative spectrum sensing technique is proposed by using stochastic geometry, which can utilize only a few, not always all, SUs to achieve the minimum total error rate. Meanwhile, the optimal number of the cooperating SUs is also studied, which enables the total error rate to achieve the minimum value. Therefore, the speed and accuracy of cooperative spectrum sensing is improved compared to the cooperation among all SUs, when sending local decisions in different time slots is chosen for decision combining.
3) Finally, in order to maximize the achievable ergodic capacity and throughput of the random secondary network, effective methods are proposed for different fusion rules to determine the appropriate number of cooperating SUs when the target total error rate is not exceeded.

D. Mathematical Notations

Throughout the paper, vectors are denoted by lower-case boldfaced characters and matrices are represented by upper-case boldfaced characters. The notation $|\cdot|$ denotes the magnitude operator. The $\boldsymbol{A}^{\dagger}$ denotes the conjugate transpose of matrix $\boldsymbol{A}$. $\hat{a}$ and $\overline{a}$ are the estimated parameter and average value, respectively. The notation $\otimes$ is the Kronecker product. The identity matrix of size N is $\boldsymbol{I}_N$, and $\mathbf{0}$ is the null vector (or matrix). The notation $\mathbb{E}[\cdot]$ is the statistical expectation operator. The complex normal distribution with mean $\boldsymbol{\mu}$ and covariance matrix $\boldsymbol{\Sigma}$ is $\mathcal{CN}(\boldsymbol{\mu}, \boldsymbol{\Sigma})$. The central Wishart distribution with parameters a, b, and $\boldsymbol{\Sigma}$ is $\mathcal{CW}_a(b, \boldsymbol{\Sigma})$, where $\boldsymbol{\Sigma}$ is an $a \times a$ positive definite covariance matrix. Other special functions (please refer to [23] for more information on special functions) used throughout the paper include

1) $(\cdot)_a$ is the Pochhammer symbol.
2) $\Gamma(\cdot)$ is the gamma function.
3) $\Phi(\cdot)$ is the error function and $\Phi(y) \triangleq \frac{2}{\sqrt{\pi}} \int_0^y e^{-t^2} \mathrm{d}t$.
4) $I^{-1}(z, a, b)$ is used to denote inverse regularised incomplete beta function $I_z^{-1}(a, b)$ for convenience.
5) ${}_2F_1(\cdot, \cdot; \cdot; \cdot)$ is the Gaussian hypergeometric function.
6) $G_{p,q}^{m,n}\left(\begin{matrix} a_1, \ldots, a_p \\ b_1, \ldots, b_q \end{matrix} \middle| z \right)$ is the Meijer *G*-function.

The remainder of this paper is organized as follows. Section II describes the system model of cooperative spectrum sensing based on the GLRT detector. Section III derives the closed-form expressions of the probabilities of detection and false alarm when utilizing the GLRT detector and investigates the optimal number of collaborating SUs. The achievable ergodic capacity and throughput of the secondary network are analyzed in Section IV. Section V presents the simulation results and discussions and Section VI concludes this paper.

II. System Model

We consider a centralized cooperative spectrum sensing system with decision fusion, shown in Fig. 1. The fusion center (FC) is used to collect the decisions made by the SUs to make a final decision. The SUs which are used to sense the status of PU are comprised of certain RRHs or user equipments. During the cooperative spectrum sensing process, each SU within the coverage radius of the FC detects the status of the PU independently and then sends the detection result to the FC. After that, the FC gives a final decision on the status of the PU through an appropriate voting rule. The PU is assumed to be equipped with single antenna and each SU has multiple antennas.

A practical assumption is that the SUs are uniformly distributed on a two-dimensional (2-D) plane $\mathbb{R}^2$ based on a homogenous PPP with density ρ. According to the Palm theory, the SUs located within the coverage radius of the FC follow the same PPP. The coverage radius of the FC is denoted by R and the distance between the PU and the secondary receiver located

This article has been accepted for inclusion in a future issue of this journal. Content is final as presented, with the exception of pagination.

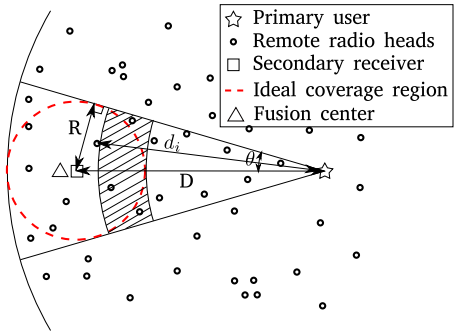

Fig. 1. System model.

at the origin of the coverage area of the FC is represented by D. Since only the SUs within the coverage radius of the corresponding FC can be collaborated together to detect the status of the PU, we only consider the SUs that are located within the area of interest in this paper. Assuming the transmitted signals between the PU and secondary network experience path loss and Rayleigh fading, the received signal power at the ith SU can be given as

$$P_i = \frac{P_{\mathrm{T}}}{d_i^{\varepsilon}}\omega_i \tag{1}$$

where ω_i denotes the Rayleigh fading gain and follows the gamma distribution when maximal ratio combining is used to achieve full diversity gain, i.e., $\omega_i \sim \Gamma(m,1)$, m is the number of receive antennas of each SU, P_{T} denotes the PU's signal power, d_i means the distance between the PU and the ith nearest SU from the PU, and ε is the path loss exponent factor. The shadowing area in Fig. 1 is defined as the region whose distance is equal or greater than $D-R$ but less than $d_i - D + R$. The probability density function (pdf) of ω_i can be written as

$$f_{\omega_i}(\omega) = \frac{\omega^{m-1}e^{-\omega}}{(m-1)!}. \tag{2}$$

The spectrum sensing between each SU and the PU is assumed to be a GLRT-based sensing system with m receive antennas. Let $\mathcal{H}_0$ (PU is absent) and $\mathcal{H}_1$ (PU is present) denote the null and the alternate hypotheses. During the sensing period, the matrix of received signal samples $\mathbf{Y} \in \mathbb{C}^{m\times n}$ at the SU is

$$\mathcal{H}_0 : \mathbf{Y} = \mathbf{V} \tag{3a}$$

$$\mathcal{H}_1 : \mathbf{Y} = \mathbf{h}\mathbf{s}^{\dagger} d^{-\frac{\varepsilon}{2}} + \mathbf{V} \tag{3b}$$

where n is the sample number, $\mathbf{V} \in \mathbb{C}^{m\times n}$ represents the samples from a circularly symmetric complex additive white Gaussian noise process, where $\mathbf{V} \sim \mathcal{CN}\left(\mathbf{0}, \sigma_v^2 \mathbf{I}_{\mathrm{m}} \otimes \mathbf{I}_n\right)$, $\mathbf{s} \sim \mathcal{CN}\left(\mathbf{0}, P_{\mathrm{T}}\mathbf{I}_n\right) \in \mathbb{C}^{n\times 1}$ is the transmit signal of the PU. Finally, $\mathbf{h} \in \mathbb{C}^{m\times 1}$ is the channel vector. Henceforth, the covariance matrix of $\mathbf{Y}$, $\mathbf{R}_{\mathrm{yy}} = \mathbb{E}[\mathbf{Y}\mathbf{Y}^{\dagger}]$, is given by

$$\mathcal{H}_0 : \quad \mathbf{R}_{\mathrm{yy}} = \sigma_v^2 \mathbf{I}_{\mathrm{m}} \tag{4a}$$

$$\mathcal{H}_1 : \quad \mathbf{R}_{\mathrm{yy}} = P_{\mathrm{T}} d^{-\varepsilon}\mathbf{h}\mathbf{h}^{\dagger} + \sigma_v^2 \mathbf{I}_{\mathrm{m}}. \tag{4b}$$

Within the sensing duration of n samples, the sample covariance matrix estimated from $\mathbf{Y}$ is $\widehat{\mathbf{R}}_{\mathrm{yy}} = \frac{1}{n}\mathbf{Y}\mathbf{Y}^{\dagger}$. Thus, $\mathbf{W} = n\widehat{\mathbf{R}}_{\mathrm{yy}} = \mathbf{Y}\mathbf{Y}^{\dagger} \in \mathbb{C}^{m\times m}$ is a complex Wishart matrix. Also, let $\hat{\lambda}_{\min} = \hat{\lambda}_{\mathrm{m}} < \ldots < \hat{\lambda}_1 = \hat{\lambda}_{\max}$ be the eigenvalues, in increasing order, estimated from $\widehat{\mathbf{R}}_{\mathrm{yy}}$. The decision statistic for the GLRT-based eigenvalue detector is given by $T_{\mathrm{GLRT}} = \frac{\hat{\lambda}_{\max}}{\sum_{l=1}^{m}\hat{\lambda}_l}$.

III. Sensing Performance Analysis Based On Stochastic Geometry

In this section, an efficient cooperative spectrum sensing technique is proposed while achieving the minimum total error rate of the final decision. First, collaborating all the possible SUs to implement cooperative spectrum sensing cannot always achieve the best performance due to the diversity of the SNRs received at SUs. An SU with very low received SNR can be classified as an unreliable node and may degrade the cooperative sensing performance. Second, combining all the local spectrum sensing decisions concurrently at the FC can lead to the high design complexity and the waste of bandwidth, such as sending local decisions on orthogonal frequency bands. Hence, sending different local decisions in different time slots is chosen in this paper, but this may affect the sensing speed. However, according to the IEEE 802.22 standard for wireless regional area networks [24], the SUs have to vacate the licensed frequency bands as soon as possible once the PU is active. Therefore, in order to address the two issues mentioned above, an efficient cooperative spectrum sensing technique using different time slots to receive local decisions is proposed to guarantee the accuracy and speed of the sensing process. Furthermore, the statistical optimal number of the cooperating SUs k_{opt} is studied, which can make the total error rate achieve the minimum value when the number of available SUs is large enough.

A. Distributions on the GLRT Detector

Both the probabilities of detection and false alarm of an individual SU are required to investigate the total error rate and transmission performance of secondary network in CR networks. Therefore, we derive the probability of detection $P_{d,i}^{\mathrm{su}}$ and probability of false alarm $P_{\mathrm{fa},i}^{\mathrm{su}}$ seen at the ith SU in this section. The sensing error probabilities seen at the FC will be discussed in the next section when considering decision reporting errors.

Theorem 1: The closed-form expression of the probability of false alarm seen at the ith SU using the GLRT detector with m receive antennas, i.e., $P_{\mathrm{fa},i}^{\mathrm{su}}$, is given by

$$P_{\mathrm{fa},i}^{\mathrm{su}}(r_i) = 1 - \frac{\Gamma(mn)(m\eta)^{-\xi}}{\xi\Gamma(mn-\xi)\Gamma(\xi)}\left(\mathbf{\Delta}(r_i) - \mathbf{\Delta}\left(\tfrac{1}{m}\right)\right) \tag{5}$$

where $\frac{1}{m} \le r_i \le 1$ denotes the decision threshold of ith SU and $\mathbf{\Delta}(\cdot)$ is defined by

$$\mathbf{\Delta}(y) = {}_2F_1\left(\xi, 1+\xi-mn;\ \xi+1; \frac{y}{\eta}\right)(my)^{\xi} \tag{6}$$

This article has been accepted for inclusion in a future issue of this journal. Content is final as presented, with the exception of pagination.

where η and ξ are given by

$$\eta = \frac{0.8132b^2}{a-1.7711b}, \quad \xi = \frac{(a-1.7711b)^2}{0.8132b^2} \tag{7}$$

and a, b are defined as

$$a = (\sqrt{m}+\sqrt{n})^2,\ b = (\sqrt{m}+\sqrt{n})\left(\sqrt{\frac{1}{m}}+\sqrt{\frac{1}{n}}\right)^{\frac{1}{3}}. \tag{8}$$

Proof: The proof is omitted because of the space limit. ■

Hence, for a complex Gaussian signal, the decision threshold r_i with respect to the individual probability of false alarm seen at the ith SU can be calculated by (9) at the bottom of the page. This expression is used to calculate the required decision threshold for a desired false alarm rate, which is necessary for the individual and cooperative spectrum sensing under the CFAR requirement.

Theorem 2: The detection probability $P_{\mathrm{d},i}^{\mathrm{su}}$ seen at the ith SU using the GLRT detector is derived as

$$P_{\mathrm{d},i}^{\mathrm{su}}(r_i) = 1 - \frac{1}{2}\left[\Phi\left(\tau_i\sqrt{\varphi_i} + \frac{r_i}{2\sqrt{\varphi_i}(1-r_i)}\right) - \Phi\left(\tau_i\sqrt{\varphi_i} + \frac{1}{2(m-1)\sqrt{\varphi_i}}\right)\right] \tag{10}$$

where τ_i and φ_i are given by

$$\tau_i = n(m-1)\left(\frac{1}{mn\gamma_i} - \frac{1}{1+m\gamma_i}\right)\left(1+\frac{m-1}{mn\gamma_i}\right) \tag{11}$$

$$\varphi_i = \frac{1}{2n(m-1)^2}\left(\frac{1}{1+m\gamma_i} - \frac{1}{mn\gamma_i}\right)^{-2} \tag{12}$$

and γ_i denotes the average received SNR at the ith SU. It is worth noting that γ_i varies considering the homogeneous PPP model in this paper and the corresponding closed-form expression is derived as (20) in Section III-C.

Proof: The proof is omitted because of the space limit. ■

Meanwhile, we derive the analytical expression for calculating the decision threshold in terms of the individual probability of detection seen at the ith SU, which is given by (13) at the bottom of the page, where the coefficient $C_t = 1$ for $t = 0$ and $C_t = \sum_{q=0}^{t-1} \frac{C_q C_{t-1-q}}{(q+1)(2q+1)}$ for otherwise.

B. Cooperative Sensing With Reporting Errors

In the cooperative spectrum sensing system, the final decision on the status of the PU can be made through different techniques, including decision fusion and data fusion. In this paper, we apply decision fusion to investigate the performance of the system. During a decision fusion process, each SU processes the data individually and makes a local decision that is represented by a single bit ($1/0$ represents the presence/absence of the PU) independently. Then, the final decision is made by fusing these individual decisions through a voting rule. Due to the imperfection of the reporting channel between the SUs and the FC, the reporting error may occur during the decision reporting frame of the spectrum sensing process [25]. Assuming the reporting channel bit error probability (BEP) under $\mathcal{H}_0$ and $\mathcal{H}_1$ are represented by $P_{\mathrm{b},i}^0$ and $P_{\mathrm{b},i}^1$ for the ith reporting channel, the probability of false alarm of the ith SU seen at the FC $P_{\mathrm{fa},i}$ with the presence of reporting errors is given by

$$\begin{aligned} P_{\mathrm{fa},i} &= \mathbf{P}\left(u_i^{\mathrm{fc}} = 1 \mid \mathcal{H}_0\right) \\ &= \mathbf{P}\left(u_i^{\mathrm{fc}} = 1 \mid u_i^{\mathrm{su}} = 1\right)\mathbf{P}\left(u_i^{\mathrm{su}} = 1 \mid \mathcal{H}_0\right) \\ &\quad + \mathbf{P}\left(u_i^{\mathrm{fc}} = 1 \mid u_i^{\mathrm{su}} = 0\right)\mathbf{P}\left(u_i^{\mathrm{su}} = 0 \mid \mathcal{H}_0\right) \\ &= (1-P_{\mathrm{b},i}^0)P_{\mathrm{fa},i}^{\mathrm{su}} + P_{\mathrm{b},i}^0(1-P_{\mathrm{fa},i}^{\mathrm{su}}) \end{aligned} \tag{14}$$

where u_i^{fc} and u_i^{su} denote the decision on the status of the PU made by the ith SU seen at the FC and SU, respectively. Similarly, the probability of detection of the ith SU seen at the FC with the presence of reporting errors is given by

$$\begin{aligned} P_{\mathrm{d},i} &= \mathbf{P}\left(u_i^{\mathrm{fc}} = 1 \mid \mathcal{H}_1\right) \\ &= \mathbf{P}\left(u_i^{\mathrm{fc}} = 1 \mid u_i^{\mathrm{su}} = 1\right)\mathbf{P}\left(u_i^{\mathrm{su}} = 1 \mid \mathcal{H}_1\right) \\ &\quad + \mathbf{P}\left(u_i^{\mathrm{fc}} = 1 \mid u_i^{\mathrm{su}} = 0\right)\mathbf{P}\left(u_i^{\mathrm{su}} = 0 \mid \mathcal{H}_1\right) \\ &= (1-P_{\mathrm{b},i}^1)P_{\mathrm{d},i}^{\mathrm{su}} + P_{\mathrm{b},i}^1(1-P_{\mathrm{d},i}^{\mathrm{su}}). \end{aligned} \tag{15}$$

Generally, the BEP depends on the modulation scheme and the SNR or signal-to-interference-plus-noise ratio (SINR) between the SU and the FC. In order to confine the interference to the PU caused by the missed detection, the FC has to be far away from the PU in practice. Therefore, $P_{\mathrm{b},i}^0$ and $P_{\mathrm{b},i}^1$ are quite close so that the approximation relation $P_{\mathrm{b},i}^0 = P_{\mathrm{b},i}^1$ can be obtained. Furthermore, the BEPs can be controlled within a very low and similar value for different SUs by applying error rate control techniques. Thus, the difference of BEPs between different SUs is quite small after employing appropriate error rate control techniques, so that it has little influence on the sensing error rate of the final decision in practice. Based on these conditions in practice, a simplified and reasonable assumption is the reporting processes of different SUs are independent and the BEPs are

$$r_i = \eta I^{-1}\left(\frac{\Gamma(mn)(m\eta)^{-\xi}}{\xi\Gamma(mn-\xi)\Gamma(\xi)}\left(\mathbf{\Delta}\left(\frac{1}{m}\right) + (1-P_{\mathrm{fa},i}^{\mathrm{su}})\frac{\xi\Gamma(mn-\xi)\Gamma(\xi)}{\Gamma(mn)(m\eta)^{-\xi}}\right),\ \xi, mn-\xi\right). \tag{9}$$

$$r_i = \left(\frac{1}{2}\left(\sum_{t=0}^{\infty}\frac{C_t\sqrt{\varphi_i}}{2t+1}\left[\frac{\sqrt{\pi}}{2}\Phi\left(\tau_i\sqrt{\varphi_i}+\frac{1}{2(m-1)\varphi_i}\right)+\sqrt{\pi}(1-P_{\mathrm{d},i}^{\mathrm{su}})\right]^{2t+1} - \tau_i\varphi_i\right)^{-1} + 1\right)^{-1} \tag{13}$$

identical for different SUs, which indicates that $P_{\mathrm{b},i}^0 = P_{\mathrm{b},i}^1 = P_{\mathrm{b}}$. This approximation would not affect the analyses on sensing and transmission performances in this paper, since the difference of BEPs between different SUs is quite small and has little influence on performances of the system after employing error rate control techniques.

Specifically, voting rules Logic-OR (OR) and Logic-AND (AND) are used in this paper in order to find out the optimal number of the collaborating SUs conveniently. Assuming there are k cooperating SUs, the properties of the OR and AND rules are as follows.

1) *OR rule:* When at least one local decision among the k local decisions indicates the PU is present, the final decision declares the PU is present. The probabilities of detection and false alarm of the final decision are given by

$$P_{\mathrm{d}} = 1 - \prod_{i=1}^{k}(1 - P_{\mathrm{d},i}), \quad P_{\mathrm{fa}} = 1 - \prod_{i=1}^{k}(1 - P_{\mathrm{fa},i}). \tag{16}$$

2) *AND rule:* Only when all local decisions indicate the PU is present, the final decision declares the PU is present. The corresponding probabilities of detection P_{d} and false alarm P_{fa} of the final decision are given by

$$P_{\mathrm{d}} = \prod_{i=1}^{k} P_{\mathrm{d},i}, \quad P_{\mathrm{fa}} = \prod_{i=1}^{k} P_{\mathrm{fa},i}. \tag{17}$$

The total error rate of the final decision is defined to be the summation of the false alarm and missed detection rates of the final decision, which is given by

$$P_{\mathrm{te}} = P_{\mathrm{fa}} + P_{\mathrm{m}} \tag{18}$$

where the probability of missed detection of the final decision P_{m} is defined as $P_{\mathrm{m}} = 1 - P_{\mathrm{d}}$.

C. Optimal Number of Cooperating SUs

The optimization of the cooperative spectrum sensing can be considered from three perspectives. First, it can be considered under the CDR requirement, which aims to minimize the probability of false alarm for a given probability of detection. This guarantees the benefits of PU preferentially. Second, the probability of detection can be minimized for a desired CFAR, which gives priority to the interests of the SUs. Third, this issue can be considered to minimize the total error rate for a given constant decision threshold (CDT), which considers the interests of PU and SUs concurrently. In this paper, the optimization of cooperative spectrum sensing is investigated only under the CDT requirement, however all the expressions and the techniques proposed in this paper can also be applied to the CDR and CFAR cases.

Under the CDT requirement, the decision threshold is fixed and identical for every individual spectrum sensing period. Therefore, the individual probability of false alarm $P_{\mathrm{fa},i}$ for each SU is constant. However, the individual probability of detection varies depending on γ_i. From (10), it can be found that a higher received SNR helps to achieve a higher individual probability of detection $P_{\mathrm{d},i}$. Therefore, the SUs with higher received SNRs should be chosen first to implement the cooperative spectrum sensing. In order to study the received SNR at the ith nearest SU, the Euclidean distance d_i between the PU and the ith nearest SU within the coverage radius of FC (shown as Fig. 1) needs to be investigated. The pdf of d_i is derived as the following theorem.

Theorem 3: In a PPP with density ρ on a 2-D plane, the pdf of the distance d_i between the ith nearest SU within the coverage radius of FC from the PU and the PU outside the region of interest is given by

$$f_{d_i}(d) = \frac{2\rho\theta(D-R)e^{-2\rho\theta(D-R)(d-D+R)}}{\Gamma(i)\big(2\rho\theta(D-R)(d-D+R)\big)^{1-i}} \tag{19}$$

where $\theta = \sin^{-1}\left(\frac{R}{D}\right)$ and $D \gg R$.

Proof: The proof is provided in the Appendix. ■

Hence, the average received SNR γ_i at the ith nearest SU can be derived as

$$\begin{aligned}\gamma_i &= \int_{D-R}^{\infty}\int_{0}^{\infty} \frac{P_{\mathrm{T}}\omega}{\sigma_v^2 d^{\varepsilon}} f_{\omega_i}(\omega) f_{di}(d) \quad \mathrm{d}\omega\mathrm{d}d \\ &= \frac{P_{\mathrm{T}} m e^{2\rho\theta(D-R)^2}}{\sigma_v^2\left(2\rho\theta(D-R)\right)^{-\varepsilon}} \sum_{j=0}^{i-1}\binom{i-1}{j}\frac{\Gamma\left(i-j-\varepsilon, 2\rho\theta(D-R)^2\right)}{\Gamma(i)\left(-2\rho\theta(D-R)^2\right)^{-j}}\end{aligned} \tag{20}$$

where $\Gamma(\cdot,\cdot)$ denotes the upper incomplete gamma function. Therefore, by using the above result, $P_{\mathrm{fa},i}$ and $P_{\mathrm{d},i}$ can be computed under the CDT requirement. Also, the total error rate P_{te} can be obtained under specific decision fusion rules.

According to the above expression of the received SNR measured at the ith nearest SU under the homogeneous PPP model, the received SNR decreases with the increasing i. With the increase of the number of the SUs involved in the cooperative sensing k, the local decision made by the SU with very low received SNR may be included in the final decision so that the sensing performance would be affected. Thus, there exists an optimal number of cooperating SUs k_{opt} that can minimize the total error rate of the final decision. Meanwhile, the decision threshold is predetermined under the CDT requirement. Therefore, the optimization issue can be formulated as follows:

$$k_{\mathrm{opt}} = \arg\min_{k} P_{\mathrm{te}}(k). \tag{21}$$

Since the total number of available SUs follows the Poisson distribution, the optimal solution k_{opt} is difficult to obtain. Therefore, the exhaustive search approach is applied in our work to find the solution to the above optimization issue.

There exist many benefits when cooperating k_{opt} SUs to perform spectrum sensing rather than collaborating all the available SUs all the time. Specifically, first, only cooperating a few, not always all, the SUs to implement spectrum sensing, the sensing performance (i.e., the total error rate of the final decision in this paper) can be improved which can be seen from Fig. 4. Second, comparing with the traditional approach, less cooperating SUs brings less energy consumption since the unemployed SUs are silent during the sensing and reporting durations. Finally, it is obvious that less cooperating SUs can reduce the reporting time in the time division mode so that the spectrum sensing process can be accelerated. Therefore, for a fixed periodic spectrum

This article has been accepted for inclusion in a future issue of this journal. Content is final as presented, with the exception of pagination.

sensing frame, the SUs can have more time for data transmission, which helps to enhance the achievable ergodic capacity or throughput of the secondary network.

Under the CDT requirement, when an additional SU is added into the cooperative spectrum sensing, the additional SU has the worst individual probability of detection, i.e., $P_{d,k}$, among the cooperating SUs. However, the individual probability of false alarm of the additional SU $P_{\mathrm{fa},k}$ is identical with the other cooperating SUs. Meanwhile, the additional SU does not affect the performance of the other SUs.

1) OR Rule: The total error rate of the final decision P_{te} under the OR rule can be given by

$$P_{\mathrm{te}} = 1 - \prod_{i=1}^{k}(1 - P_{\mathrm{fa},i}) + \prod_{i=1}^{k}(1 - P_{\mathrm{d},i}). \tag{22}$$

Because of the properties of $P_{\mathrm{fa},i}$ and $P_{m,i}$ mentioned above, it can be seen from (16) that the probability of false alarm of the final decision P_{fa} increases with the increase of the cooperating SUs' number k, but the probability of missed detection of the final decision P_{m} falls down. Due to the monotonicity of P_{m} and P_{fa}, it can be seen from (18) that collaborating all the SUs in the secondary network is not always the best option. The performance of the total error rate is determined by the absolute values of the slope of P_{fa} and P_{m} with the increase of k. Therefore, under two cases, collaborating all the available SUs may not achieve the minimum total error rate. First, when the absolute values of the slope of P_{fa} and P_{m} are similar, the total error rate of the final decision will reduce initially and rise later with the increase of k. Second, when the absolute value of the slope of P_{fa} is larger than the value of P_{m}, the total error rate increases with the increasing k. By utilizing (5), (10), (14), (15), and (22), the total error rate can be calculated and the optimal number of the cooperating SUs k_{opt} can be obtained.

2) AND Rule: Under the AND rule, the total error rate is given by

$$P_{\mathrm{te}} = 1 - \prod_{i=1}^{k} P_{\mathrm{d},i} + \prod_{i=1}^{k} P_{\mathrm{fa},i}. \tag{23}$$

Compared with the OR rule, it can be seen from (17) that P_{fa} is a decreasing function and P_{m} is an increasing function with regard to the number of the cooperating SUs k under the AND rule. From (18), the trend of the total error rate of the final decision is also decided by the absolute values of the slope of P_{fa} and P_{m}. Hence, collaborating all the SUs in the network may not guarantee that the total error rate achieves the minimum value. By utilizing (5), (10), (14), (15), and (23), the total error rate when using AND rule under CDT requirement can be computed and the optimal number of the cooperating SUs can be obtained when the number of available SUs is large.

Remark 1: Nowadays, there exists many wideband signals in practical applications, e.g., the orthogonal-frequency-division-multiplexing encoding signals, multitone transmit signals, and signals over consecutive block-fading channels. The spectrum sensing techniques for these wideband signals have been proposed and studied in literatures, such as using the variational message passing algorithm or wavelet transform to estimate the power spectral density of wideband signals. However, the results shown in this paper are still valid for wideband spectrum sensing, when the subchannel is sensed in a sequential manner. One potential solution is the radio frequency front-end is equipped with a tunable narrowband bandpass filter [26]. So one narrow frequency band can be searched at a time and existing narrowband spectrum sensing techniques can be applied. This is a way to extend our current work to a practical system with wideband primary signals.

IV. Achievable Ergodic Capacity and Throughput

In this section, the achievable ergodic capacity and throughput of the CR network are investigated in order to capture the performance of the sensing-based secondary links. As shown in Fig. 1, the RRHs are the secondary transmitters (SU-Txs) and the secondary receiver (SU-Rx) is located at the origin of the secondary network region. As agreed in Section II, each SU-Tx is equipped with multiple antennas and the SU-Rx is with single antenna. The path loss and Rayleigh fading between the SU-Tx and SU-Rx are considered in this paper. When the PU is absent, the received SNR at the SU-Rx sourced from each SU-Tx is given as

$$\gamma^{s0} = \frac{P_{\mathrm{ST}}}{L^{\varepsilon}\sigma^2}\alpha \tag{24}$$

where P_{ST} denotes the transmitted signal power from the SU-Tx, σ^2 is the additive noise power at the SU-Rx, L is the distance between each SU-Tx and SU-Rx, ε is the path loss factor and α denotes the Rayleigh fading channel gain in each secondary link. When the maximal ratio transmission is applied, the pdf of α is given as

$$f_{\alpha}(\alpha) = \frac{\alpha^{m-1}e^{-\alpha}}{(m-1)!} \tag{25}$$

and the pdf of L is given by

$$f_{L}(L) = \frac{2L}{R^2}. \tag{26}$$

Meanwhile, when the PU is present, the interference from the PU's signal is considered and the received SINR is given by

$$\gamma^{s1} = \frac{P_{\mathrm{ST}}L^{-\varepsilon}\alpha}{\sigma^2 + P_{\mathrm{T}}D^{-\varepsilon}\beta} \tag{27}$$

where β denotes the Rayleigh fading gain between the PU and the SU-Rx and β follows the exponential distribution with mean 1, i.e.,

$$f_{\beta}(\beta) = \exp(-\beta). \tag{28}$$

For a CR network, one periodic spectrum sensing frame T_{f} consists of three parts, including the sensing slot T_{s}, decision reporting slot T_{r}, and data transmission slot T_{t}. In the interweave method, the data transmission of the secondary links can be carried out under two situations, one is there is no false alarm when the PU is absent and the other is missed detection occurs when the PU is present. Therefore, the achievable ergodic capacity and throughput of the secondary network are also comprised of these two parts.

This article has been accepted for inclusion in a future issue of this journal. Content is final as presented, with the exception of pagination.

A. Achievable Ergodic Capacity

Based on the structure of the CR system mentioned above, the achievable capacity of each secondary link in the CR system can be given by

$$C_{\rm ac} = C_{\rm ac0} + C_{\rm ac1} \tag{29}$$

where $C_{\rm ac0}$ denotes the achievable capacity with the absence of the PU and $C_{\rm ac1}$ denotes the achievable capacity with the presence of the PU. Specifically, $C_{\rm ac0}$ and $C_{\rm ac1}$ can be obtained as follows:

$$C_{\rm ac0} = \left(\frac{T_{\rm f} - T_{\rm s} - kT_{\rm r}}{T_{\rm f}}\right)\log_2(1+\gamma^{\rm s0})(1-P_{\rm fa})P(\mathcal{H}_0) \tag{30}$$

$$C_{\rm ac1} = \left(\frac{T_{\rm f} - T_{\rm s} - kT_{\rm r}}{T_{\rm f}}\right)\log_2(1+\gamma^{\rm s1})(1-P_{\rm d})P(\mathcal{H}_1) \tag{31}$$

where k is the number of the SUs involved in the cooperative sensing, $P(\mathcal{H}_0)$ and $P(\mathcal{H}_1)$ represent the probabilities when the PU is absent and present, respectively.

1) Achievable Ergodic Capacity Under $\mathcal{H}_0$:

Proposition 1: The achievable ergodic capacity of each secondary link when the PU is absent can be derived as

$$\overline{C_{\rm ac0}} = \frac{2G_{4,3}^{2,3}\left(\frac{P_{\rm ST}R^{-\varepsilon}}{\sigma^2}\middle|\begin{matrix}1-m,1,1,\frac{2}{\varepsilon}+1\\ \frac{2}{\varepsilon},1,0\end{matrix}\right)}{\varepsilon(m-1)!\ln(2)} \times\left(\frac{T_{\rm f}-T_{\rm s}-kT_{\rm r}}{T_{\rm f}}\right)(1-P_{\rm fa})P(\mathcal{H}_0). \tag{32}$$

Proof: In order to derive the expression of $\overline{C_{\rm ac0}}$, we first obtain the statistical average of $\log_2(1+\gamma^{\rm s0})$. Let $C_{\rm ec0} = \log_2(1+\gamma^{\rm s0})$ and the statistical average $\overline{C_{\rm ec0}}$ can be calculated by

$$\begin{aligned}\overline{C_{\rm ec0}} &= \int_0^R\int_0^\infty \log_2\left(1+\frac{P_{\rm ST}}{L^\varepsilon\sigma^2}\alpha\right)f_\alpha(\alpha)f_L(L){\rm d}\alpha{\rm d}L\\ &= \int_0^R\int_0^\infty \frac{\ln\left(1+\frac{P_{\rm ST}}{L^\varepsilon\sigma^2}\alpha\right)}{\ln(2)}\frac{\alpha^{m-1}e^{-\alpha}}{(m-1)!}\frac{2L}{R^2}{\rm d}\alpha{\rm d}L.\end{aligned} \tag{33}$$

By utilizing the equality relationship

$$\ln(1+ax) = G_{2,2}^{1,2}\left(ax\middle|\begin{matrix}1,1\\1,0\end{matrix}\right),$$

the calculation of $\overline{C_{\rm ec0}}$ can be rewritten as

$$\begin{aligned}\overline{C_{\rm ec0}} &= \int_0^R\int_0^\infty G_{2,2}^{1,2}\left(\frac{P_{\rm ST}\alpha}{\sigma^2L^\varepsilon}\middle|\begin{matrix}1,1\\1,0\end{matrix}\right)\frac{\alpha^{m-1}}{e^\alpha}{\rm d}\alpha\frac{2L/\ln(2)}{R^2(m-1)!}{\rm d}L\\ &= \int_0^R G_{3,2}^{1,3}\left(\frac{P_{\rm ST}}{\sigma^2L^\varepsilon}\middle|\begin{matrix}1-m,1,1\\1,0\end{matrix}\right)\frac{2L/\ln(2)}{(m-1)!R^2}{\rm d}L.\end{aligned} \tag{34}$$

Let $z = \left(\frac{R}{L}\right)^\varepsilon$, the equation above can be reorganized. After further manipulations with the aid of [23, (7.811.3)], the expression of $\overline{C_{\rm ec0}}$ can be derived and the expression (32) can be achieved. ■

2) Achievable Ergodic Capacity Under $\mathcal{H}_1$: The achievable ergodic capacity of each secondary link when the PU is present can be derived as

$$\begin{aligned}\overline{C_{\rm ac1}} &= (1-P_{\rm d})P(\mathcal{H}_1)\int_0^\infty\int_0^R\int_0^\infty \log_2\left(1+\frac{P_{\rm ST}L^{-\varepsilon}\alpha}{\sigma^2+P_{\rm T}D^{-\varepsilon}\beta}\right)\\ &\quad\times f_\alpha(\alpha)f_L(L)f_\beta(\beta){\rm d}\alpha{\rm d}L{\rm d}\beta\\ &= \int_0^\infty \frac{2G_{4,3}^{2,3}\left(\frac{P_{\rm ST}R^{-\varepsilon}}{\sigma^2+P_{\rm T}D^{-\varepsilon}\beta}\middle|\begin{matrix}1-m,1,1,\frac{2}{\varepsilon}+1\\ \frac{2}{\varepsilon},1,0\end{matrix}\right)}{\varepsilon(m-1)!\ln(2)}e^{-\beta}{\rm d}\beta\\ &\quad\times\left(\frac{T_{\rm f}-T_{\rm s}-kT_{\rm r}}{T_{\rm f}}\right)(1-P_{\rm d})P(\mathcal{H}_1).\end{aligned} \tag{35}$$

By utilizing the expressions (32) and (35), the achievable ergodic capacity of each secondary link $\overline{C_{\rm ac}}$ can be obtained by

$$\overline{C_{\rm ac}} = \overline{C_{\rm ac0}} + \overline{C_{\rm ac1}}. \tag{36}$$

Therefore, considering all the secondary links, the achievable ergodic capacity of the secondary network[1] based on the homogeneous PPP is given by

$$\begin{aligned}\overline{C_c} &= \sum_{N=1}^\infty N\overline{C_{\rm ac}}\mathbf{P}\{N \quad \text{SU-Txs within secondary network}\}\\ &= \sum_{N=1}^\infty \overline{C_{\rm ac}}e^{-4\rho\theta DR}\frac{(4\rho\theta DR)^N}{(N-1)!}.\end{aligned} \tag{37}$$

The value of $\overline{C_c}$ converges with the increasing N, since the probability that there exists N secondary links approaches 0 with the increase of N.

B. Achievable Throughput

Similarly, the achievable throughput $C_{\rm at}$ of each secondary link can be defined as

$$C_{\rm at} = C_{\rm at0} + C_{\rm at1} \tag{38}$$

where $C_{\rm at0}$ and $C_{\rm at1}$ denote the achievable throughput of each secondary link when the PU is absent and present, respectively. In detail, $C_{\rm at0}$ and $C_{\rm at1}$ can be calculated as

$$C_{\rm at0} = \left(\frac{T_{\rm f}-T_{\rm s}-kT_{\rm r}}{T_{\rm f}}\right)\log_2(1+T)P_{\rm cov0}(1-P_{\rm fa})P(\mathcal{H}_0) \tag{39}$$

$$C_{\rm at1} = \left(\frac{T_{\rm f}-T_{\rm s}-kT_{\rm r}}{T_{\rm f}}\right)\log_2(1+T)P_{\rm cov1}(1-P_{\rm d})P(\mathcal{H}_1) \tag{40}$$

where the coverage probabilities $P_{\rm cov0}$ and $P_{\rm cov1}$ are defined as the probability that the received SNR or SINR at the SU-Rx is larger than the preset threshold T when the PU is absent and present, respectively.

[1]In this paper, the achievable ergodic capacity of the secondary network means the summation of the achievable ergodic capacity of all the possible secondary links. Similarly, the achievable throughput of the secondary network is defined in the same way.

This article has been accepted for inclusion in a future issue of this journal. Content is final as presented, with the exception of pagination.

1) Achievable Throughput Under $\mathcal{H}_0$:

Proposition 2: The coverage probability $P_{\rm cov0}$ achieved by each secondary link when the PU is absent, i.e., under the hypothesis $\mathcal{H}_0$, can be derived as

$$P_{\rm cov0} = \sum_{t=0}^{m-1} \frac{2T^{-\frac{2}{\varepsilon}} \left(\frac{P_{\rm ST}}{\sigma^2}\right)^{\frac{2}{\varepsilon}}}{\varepsilon R^2 t!} \gamma\left(t+\frac{2}{\varepsilon}, \frac{T\sigma^2}{P_{\rm ST}} R^{\varepsilon}\right) \tag{41}$$

where $\gamma(\cdot,\cdot)$ denotes the lower incomplete gamma function.

Proof: According to the definition of the coverage probability, the coverage probability under the hypothesis $\mathcal{H}_0$ can be written as

$$\begin{aligned} P_{\rm cov0} &= \Pr[\gamma^{\rm s0} \geq T] \\ &= \mathbb{E}\left[\Pr\left[\alpha \geq T\frac{L^{\varepsilon}\sigma^2}{P_{\rm ST}}\right] \middle| L\right] \\ &= \mathbb{E}\left[\frac{\Gamma\left(m, \frac{T\sigma^2}{P_{\rm ST}} L^{\varepsilon}\right)}{(m-1)!} \middle| L\right] \\ &= \int_0^R \sum_{t=0}^{m-1} \exp\left(-\frac{T\sigma^2}{P_{\rm ST}} L^{\varepsilon}\right) L^{\varepsilon t} \frac{T^t \sigma^{2t}}{{P_{\rm ST}}^t t!} \frac{2L}{R^2} {\rm d}L \end{aligned} \tag{42}$$

by utilizing the definition of the lower incomplete gamma function and after further manipulations, the closed-form expression of the coverage probability under the hypothesis $\mathcal{H}_0$ can be obtained as (41). ■

Therefore, the closed-form expression of the achievable throughput for each secondary link under the hypothesis $\mathcal{H}_0$ can be obtained by utilizing (39) and (41).

2) Achievable Throughput Under $\mathcal{H}_1$:

Proposition 3: When the PU is present, the interference to the secondary network sourced from the PU is considered. The coverage probability of each secondary link under the hypothesis $\mathcal{H}_1$ is derived as

$$P_{\rm cov1} = \sum_{t=0}^{m-1} \sum_{w=0}^{\infty} \frac{2(-1)^w R^{\varepsilon(t+w)} e^{\frac{\sigma^2 D^{\varepsilon}}{P_{\rm T}}} \Gamma\left(t+w+1, \frac{\sigma^2 D^{\varepsilon}}{P_{\rm T}}\right)}{\varepsilon t! w! \left(t+w+\frac{2}{\varepsilon}\right) \left(P_{\rm T} D^{-\varepsilon} T / P_{\rm ST}\right)^{-t-w}}. \tag{43}$$

Proof: Based on the definition of the coverage probability, the coverage probability under the hypothesis $\mathcal{H}_1$ can be calculated as

$$\begin{aligned} P_{\rm cov1} &= \Pr[\gamma^{\rm s1} \geq T] \\ &= \mathbb{E}\left[\Pr\left[\alpha \geq \frac{\sigma^2 + P_{\rm T} D^{-\varepsilon}\beta}{P_{\rm ST} L^{-\varepsilon}} T\right] \middle| \beta, L\right] \\ &= \mathbb{E}\left[\frac{\Gamma\left(m, \frac{T(\sigma^2 + P_{\rm T} D^{-\varepsilon}\beta)}{P_{\rm ST}} L^{\varepsilon}\right)}{\Gamma(m)} \middle| \beta, L\right] \\ &= \int_0^{\infty} \sum_{t=0}^{m-1} \frac{2\gamma\left(t+\frac{2}{\varepsilon}, \frac{TR^{\varepsilon}}{P_{\rm ST}}(\sigma^2 + P_{\rm T} D^{-\varepsilon}\beta)\right)}{\varepsilon t! R^2 e^{\beta} \left(\frac{P_{\rm ST}/T}{\sigma^2 + P_{\rm T} D^{-\varepsilon}\beta}\right)^{-\frac{2}{\varepsilon}}} {\rm d}\beta. \end{aligned} \tag{44}$$

By defining $z = \frac{T}{P_{\rm ST}}(\sigma^2 + P_{\rm T} D^{-\varepsilon}\beta)$ and utilizing the power series expansion of the lower incomplete gamma function, the integral above can be rewritten as

$$P_{\rm cov1} = \int_{\frac{T\sigma^2}{P_{\rm ST}}}^{\infty} \sum_{t=0}^{m-1} \sum_{w=0}^{\infty} \frac{2D^{\varepsilon} P_{\rm ST} R^{\varepsilon(t+w+\frac{2}{\varepsilon})} e^{\frac{T\sigma^2 - z P_{\rm ST}}{P_{\rm T} D^{-\varepsilon} T}}}{(-1)^{-w} P_{\rm T} T \varepsilon t! w! R^2 (t+w+\frac{2}{\varepsilon})} z^{t+w} {\rm d}z.$$

The above integral can be calculated with the aid of the definition of the upper incomplete gamma function and then the expression of (43) can be arrived. ■

By using (40) and the expression (43), the achievable throughput of each secondary link can be obtained under the presence of the PU.

After the expressions of the coverage probability under the hypotheses $\mathcal{H}_0$ and $\mathcal{H}_1$ are derived, the closed-form expressions of the achievable throughput under the absence and presence of the PU can be obtained by utilizing (39) and (40). Therefore, the achievable throughput $C_{\rm at}$ of each secondary link can be obtained by using (38).

Furthermore, considering all the available secondary links, the achievable throughput of the secondary network based on the homogeneous PPP is given by

$$\begin{aligned} C_{\rm th} &= \sum_{N=1}^{\infty} N C_{\rm at} \mathbf{P}\{N \text{ SU-Txs within secondary network}\} \\ &= \sum_{N=1}^{\infty} C_{\rm at} e^{-4\rho\theta D R} \frac{(4\rho\theta D R)^N}{(N-1)!}. \end{aligned} \tag{45}$$

It is worth mentioning that the value of $C_{\rm th}$ converges with the increase of N, since the probability of having N secondary links approaches 0 when N is large enough.

V. Simulation Results And Discussions

In this section, simulation results are provided to validate the derived expressions and the analyses throughout this paper. In the simulation results, it is assumed that the coverage radius of the FC is $R = 5$ km, the distance between the FC and PU is $D = 50$ km. The transmit power of PU is 5 W, the additive noise power is -90 dBm. The path loss exponent factor is $\varepsilon = 3.1$. When employing binary phase-shift keying modulation scheme and error rate control methods, the BEP during the decision reporting process is assumed as $P_{\rm b} = 10^{-2}$. The sampling frequency of the signal $f_{\rm s} = 6$ MHz, the data rate of the reporting channel $R_{\rm b} = 100$ Kb/s so that $T_{\rm r} = \frac{1}{R_{\rm b}}$. One periodic frame of the SU is $T_{\rm f} = 100$ ms and the density in the considered PPP is $\rho = 10^{-7}$ nodes/m^2.

Fig. 2 verifies the generalized expressions of the individual probabilities of false alarm and detection seen at the ith SU. Assuming each SU is equipped with six receive antennas, i.e., $m = 6$, the analytical and Monte-Carlo results of $P_{{\rm fa},i}$ and $P_{{\rm d},i}$ are plotted for various cases of the received signal sample size $n = \{500, 1000\}$. Besides, $P_{{\rm d},i}$ is plotted under the received SNR $= -15$ dB. It can be observed that the analytical results match the Monte-Carlo simulations even under very low received SNR. Fig. 3 validates the expression of the pdf of the distance between the ith nearest SU and the PU derived as (19) in this paper. This

This article has been accepted for inclusion in a future issue of this journal. Content is final as presented, with the exception of pagination.

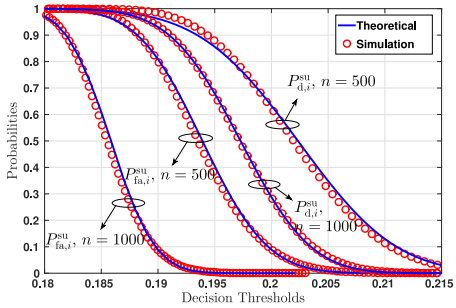

Fig. 2. Individual probabilities of false alarm and detection seen at the ith SU versus decision thresholds for various sample sizes n, the number of receive antennas for each SU is $m = 6$ and the received SNR $= -15$ dB.

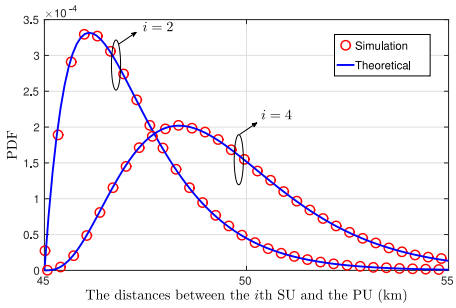

Fig. 3. Pdf of the distances between the ith SU within the area of interest and the PU.

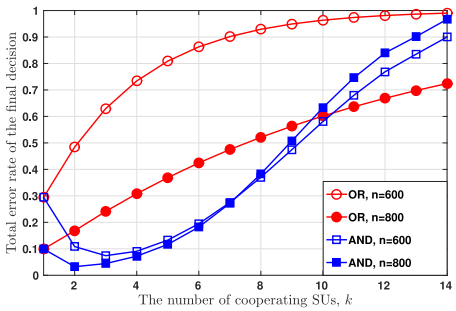

Fig. 4. Total error rate of the final decision versus the number of cooperating SUs k for various sample sizes n by using OR and AND fusion rules under the CDT requirement.

figure represents the pdf of the Euclidean distance of the second and fourth nearest SU from the PU. It can be seen that the analytical results match with the Monte-Carlo results very well, which proves that the closed-form expression of the distance between the PU and its ith nearest neighbour is located within the area of interest.

Fig. 4 depicts the total error rate of the final decision versus the number of collaborating SUs under the CDT requirement by using OR and AND fusion rules, respectively. Due to the verifications in Figs. 2 and 3, only the analytical results are shown in

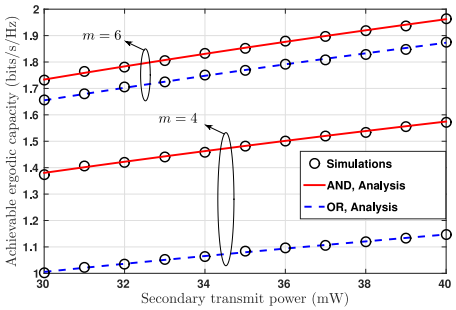

Fig. 5. Achievable ergodic capacity versus the secondary transmit power under different fusion rules, the antenna number at each SU-Tx is $m = 4, 6$ and the sample size is $n = 600$.

this figure. In this figure, the preset decision threshold is 0.28, each SU is assumed with four receive antennas ($m = 4$), and the sample size of received signal is $n = \{600, 800\}$. The total error rate of the final decision can be calculated as described in Section III. Since the number of available SUs in PPP is random, it is impossible to show all the possible cases of different number of SUs. However, the probability of above certain number of SUs within the coverage radius of FC can be calculated by using (55). For the PPP with the determined density ρ considered in this paper, the probability of over 14 SUs located within the area of interest is under 0.05. Thus, Fig. 4 only shows the cases of the number of available SUs up to 14, which is enough for analysis. It can be seen that the total error rate decreases first and then increases with the increase in the number of cooperating SUs, under the AND rule. The optimal numbers of cooperating SUs are $k_{\mathrm{opt}} = \{3, 2\}$ which makes the total error rates achieve the minimum values $\{0.07, 0.03\}$ for the cases of $n = \{600, 800\}$, respectively. Under the OR rule, the total error rate increases with the increasing k. Hence, single node spectrum sensing based on the nearest SU can achieve the best sensing performance. Therefore, it can be deduced that cooperating all the available SUs is not always necessary to achieve the best sensing performance. When the SUs follow a homogeneous PPP and the number of available SUs is large, cooperating k_{opt} SUs (not always all the SUs) not only improves the accuracy of spectrum sensing, but also accelerates the cooperative spectrum sensing.

Fig. 5 shows the achievable ergodic capacity of each secondary link versus the transmit power of the SU-Tx from 30 to 40 mW under the CDT requirement when achieving the minimum total error rate. The minimum total error rate can be obtained by utilizing the method proposed in Section III. In this figure, various cases are presented under different numbers of SU-Tx antennas (i.e., $m = 4$, $m = 6$) and different decision fusion rules. Besides, the sample number of the PU's signal is $n = 600$. Under the CDT requirement, a preset decision threshold is required. The definition area of the decision threshold is $[1/m, 1]$, which means the definition area of the decision thresholds can vary depending on the number of antennas at each SU-Tx. Therefore, the predefined decision thresholds are assumed

This article has been accepted for inclusion in a future issue of this journal. Content is final as presented, with the exception of pagination.

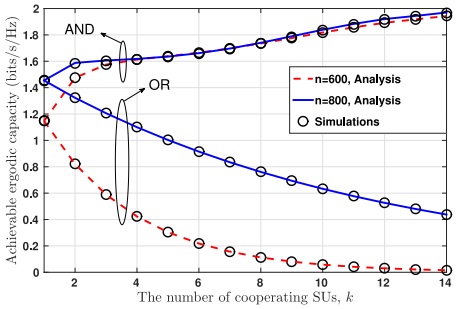

Fig. 6. Achievable ergodic capacity versus the number of cooperating SUs under different fusion rules, each SU-Tx is with four antennas and the sample size is $n = 600, 800$.

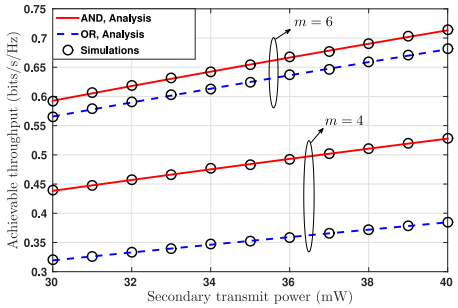

Fig. 7. Achievable throughput versus the secondary transmit power under different fusion rules, the antenna number at each SU-Tx is $m = 4, 6$ and the sample size is $n = 600$.

to be 0.28 and 0.24 for the cases of $m = 4$ and $m = 6$, respectively. Furthermore, it can be seen that the achievable ergodic capacity of the secondary network rises monotonously with the increasing transmit power of the SU-Tx. When comparing the achievable ergodic capacity in terms of decision fusion rules, the AND rule outperforms the OR rule for the same number of SU-Tx antennas. Besides, it can be seen that the gap of the achievable ergodic capacity between the AND and OR fusion rules reduces with the increasing m.

Fig. 6 represents the achievable ergodic capacity of each secondary link versus the number of the cooperating SUs under the CDT requirement when the SUs follow a PPP with density ρ. In this figure, each SU-Tx is equipped with four antennas and the sample number of the PU's signal is $n = 600, 800$. The predefined decision threshold is 0.28 and the transmit power of the SU-Tx is $P_{\mathrm{ST}} = 40$ mW. The other parameter setting is same with the previous part. First, the achievable ergodic capacity by using the AND decision fusion rule is higher than the results by using the OR rule when each SU-Tx is with the same number of antennas. Second, it can also be seen that a larger sample number of the PU's signal can help to improve the achievable ergodic capacity of the secondary network. Furthermore, when the AND fusion rule is applied, the achievable ergodic capacity increases with the increasing k. However, under the OR fusion rule, the achievable ergodic capacity decreases with the increasing k. Under the CDT requirement, for the AND decision fusion rule, both P_{fa} and P_{d} are decreasing functions with regard to k. However, when the OR fusion rule is applied, P_{fa} and P_{d} both increase with the increasing k. Thus, for the given primary and secondary transmit powers, it can be found from (29), (30), and (31) that the achievable ergodic capacity of the secondary network increases under the AND rule and decreases under the OR rule with the increase of k. Therefore, considering the total error rate of the final decision performance shown in Fig. 4 and the achievable ergodic capacity described in Fig. 6 together, the method of choosing the optimum number of cooperating SUs should be as follows.

In order to achieve a high achievable ergodic capacity and an acceptable total error rate concurrently, the eligible numbers of the cooperating SUs can be determined first for a target total error rate and then the optimum number of cooperating

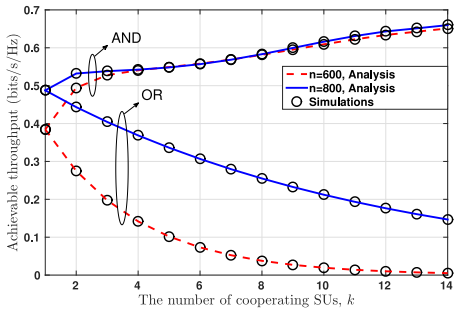

Fig. 8. Achievable throughput versus the number of cooperating SUs under different fusion rules, each SU-Tx is with four antennas and the sample size is $n = 600, 800$.

SUs which maximizes the achievable ergodic capacity can be selected among the eligible numbers obtained. Specifically, the achievable ergodic capacity is an increasing function with regard to k for the AND rule, but it is a decreasing function for the OR rule. Hence, the largest number of the cooperating SUs which satisfies the desired total error rate requirement should be chosen to maximize the achievable ergodic capacity for the AND rule. On the contrary, the smallest number of the collaborating SUs that makes the total error rate under or equal to the targeted value is selected for the OR rule.

Fig. 7 shows the achievable throughput performance of each secondary link with the increase of the secondary transmit power from 30 to 40 mW when the minimum total error rate is achieved. Multiple cases are represented for different numbers of antennas at each SU-Tx (i.e., $m = 4, m = 6$) and decision fusion rules. It can be seen that the achievable throughput increases with the increase of the secondary transmit power and the number of the antennas at each SU-Tx under both of the fusion rules. Besides, the AND fusion rule can achieve a better achievable throughput than the OR rule.

Fig. 8 presents the achievable throughput of each secondary link with the increase of the number of the cooperating SUs under the CDT requirement. The transmit power of the SU-

$$f_{d_i}(d) = 2\rho\theta(D-R)e^{-\rho 2\theta(D-R)(d-D+R)} \times \left[\sum_{j=0}^{i-1} \frac{\big(\rho 2\theta(D-R)(d-D+R)\big)^j}{j!} - \sum_{j=1}^{i-1} \frac{\big(\rho 2\theta(D-R)(d-D+R)\big)^{j-1}}{(j-1)!}\right] \tag{49}$$

Tx is 40 mW and the preset decision threshold is 0.28. First, for a given sample size, the AND rule can achieve a higher achievable throughput of the secondary network than the OR rule under the CDT requirement. Second, a larger sample size helps to obtain a higher achievable throughput of the secondary network. Finally, the achievable throughput of the secondary network increases with the number of cooperating SUs under the AND rule, however, it decreases with the increasing k under the OR rule. Therefore, considering the total error rate performance and the achievable throughput of the secondary network concurrently, different strategies should be used to determine the optimal number of cooperating SUs for different decision fusion rules. Specifically, under the AND rule, the chosen number of cooperating SUs should be as large as possible while not exceeding the target total error rate. On the contrary, under the OR rule, the chosen number of cooperating SUs should be as small as possible based on the target total error rate requirement.

VI. Conclusion

This paper investigated the efficient cooperative spectrum sensing in CR networks by using the GLRT detector when SUs follow a homogeneous PPP. The analytical expressions of the individual probabilities of false alarm and detection were derived for the general case of the GLRT detector in order to analyze the total error rate performance of the cooperative sensing system. The total error rate of the final decision was then investigated when cooperating different numbers of SUs under OR and AND fusion rules, respectively. The analytical results indicated that cooperating all the SUs could not always achieve the best spectrum sensing performance and the obtained optimal numbers of cooperating SUs in this paper minimized the total error rates of the final decisions. It is worth noting that the SUs with higher received SNRs are preferred to implement cooperative spectrum sensing. We also studied the impact of the number of cooperating SUs to conduct spectrum sensing on the achievable ergodic capacity and throughput of the secondary network. Accordingly, different strategies were proposed to determine the optimum number of cooperating SUs in order to achieve the best transmission performances for different fusion rules while not exceeding the target total error rate.

Appendix

A. Proof of Theorem 3

When the PU is far from the SUs within the coverage radius of FC, the area of the shadowing region S m^2 in Fig. 1 can be approximated as

$$S = 2\pi(D-R)\frac{2\theta}{2\pi}\big(d-(D-R)\big) = 2\theta(D-R)(d-D+R). \tag{46}$$

Since in a homogeneous 2-D PPP with density ρ, the probability of having i nodes in a region $\mathcal{A}$ with the area S m^2 is given by

$$\mathbf{P}\{i \quad \text{nodes in} \quad \mathcal{A}\} = e^{-\rho S}\frac{(\rho S)^i}{i!}. \tag{47}$$

The complementary CDF of d_i can be computed as the probability that there are less than i SUs within the shadowing area (as defined in Section II and Fig. 1), which is given by

$$P_i = \mathbf{P}\{0, 1, \cdots, i-1 \text{ nodes between } D-R \text{ and } d_i - (D-R)\} = \sum_{j=0}^{i-1} e^{-\rho S_j}\frac{(\rho S_j)^j}{j!}. \tag{48}$$

By utilizing the relationship between the complementary CDF and the pdf $\big(\text{i.e., } f_{d_i}(d) = -\frac{\mathrm{d}P_i}{\mathrm{d}d}\big)$, the pdf of $\mathrm{d_i}$ can be derived as (49) at the top of the page. After further manipulations, the expression of (19) can be obtained.

References

[1] CEPT-ECC, "ECC report 205: Licensed shared access (LSA)," Feb. 2014.

[2] S. M. Mishra, A. Sahai, and R. W. Broderson, "Cooperative sensing among cognitive radio," in *Proc. IEEE Int. Conf. Commun.*, Jun. 2006, pp. 1658–1663.

[3] J. Unnikrishnan and V. V. Veeravalli, "Cooperative sensing for primary detection in cognitive radio," *IEEE J. Select. Topics Signal Process.*, vol. 2, no. 1, pp. 18–27, Feb. 2006.

[4] S. Xie, Y. Liu, Y. Zhang, and R. Yu, "A parallel cooperative spectrum sensing in cognitive radio networks," *IEEE Trans. Veh. Technol.*, vol. 59, no. 8, pp. 4079–4092, Oct. 2006.

[5] A. Kortun, T. Ratnarajah, M. Sellathurai, C. Zhong, and C. B. Papadias, "On the performance of eigenvalue-based cooperative spectrum sensing for cognitive radio," *IEEE J. Sel. Topics Signal Process.*, vol. 5, no. 1, pp. 49–55, Feb. 2006.

[6] H. Mu and J. K. Tugnait, "Joint soft-decision cooperative spectrum sensing and power control in multiband cognitive radios," *IEEE Trans. Signal Process.*, vol. 60, no. 10, pp. 5334–5346, Oct. 2006.

[7] A. Mariani, A. Giorgetti, and M. Chiani, "Test of independence for cooperative spectrum sensing with uncalibrated receivers," in *Proc. IEEE Global Commun. Conf.*, Dec. 2006, pp. 1374–1379.

[8] D. Hamza, S. Assa, and G. Aniba, "Equal gain combining for cooperative spectrum sensing in cognitive radio networks," *IEEE Trans. Wireless Commun.*, vol. 13, no. 8, pp. 4334–4345, Aug. 2006.

[9] T. Q. Duong, T. T. Le, and H. J. Zepernick, "Performance of cognitive radio networks with maximal ratio combining over correlated Rayleigh fading," in *Proc. IEEE Int. Conf. Commun. Electron.*, Aug. 2006, pp. 65–69.

[10] Y. C. Liang, Y. Zeng, E. C. Peh, and A. T. Hoang, "Sensing-throughput tradeoff for cognitive radio networks," *IEEE Trans. Wireless Commun.*, vol. 7, no. 4, pp. 1326–1337, Apr. 2006.

[11] E. Peh and Y. C. Liang, "Optimization for cooperative sensing in cognitive radio networks," in *Proc. IEEE Wireless Commun. Netw. Conf.*, Mar. 2006, pp. 27–32.

[12] W. Zhang, R. K. Mallik, and K. B. Letaief, "Optimization of cooperative spectrum sensing with energy detection in cognitive radio networks," *IEEE Trans. Wireless Commun.*, vol. 8, no. 12, pp. 5761–5766, Dec. 2006.

[13] M. Haenggi, "On distances in uniformly random networks," *IEEE Trans. Inf. Theory*, vol. 51, no. 10, pp. 3584–3586, Oct. 2006.

[14] S. A. R. Zaidi, M. Ghogho, D. C. Mclernon, and A. Swami, "Achievable spatial throughput in multi-antenna cognitive underlay networks with multi-hop relaying," *IEEE J. Sel. Areas Commun.*, vol. 31, no. 8, pp. 1543–1558, Aug. 2006.

[15] J. Lee, J. G. Andrews, and D. Hong, "Spectrum-sharing transmission capacity," *IEEE Trans. Wireless Commun.*, vol. 10, no. 9, pp. 3053–3063, Sep. 2006.
[16] M. Peng, S. Yan, and H. V. Poor, "Ergodic capacity analysis of remote radio head associations in cloud radio access networks," *IEEE Wireless Commun. Lett.*, vol. 3, no. 4, pp. 365–368, Aug. 2006.
[17] L. T. Tan and L. B. Le, "Joint cooperative spectrum sensing and MAC protocol design for multi-channel cognitive radio networks," *EURASIP J. Wireless Commun. Netw.*, vol. 2014, no. 1, pp. 101–121, Dec. 2014.
[18] R. Zhang and Y. C. Liang, "Exploiting multi-antennas for opportunistic spectrum sharing in cognitive radio networks," *IEEE J. Sel. Topics Signal Process.*, vol. 2, no. 1, pp. 88–102, Feb. 2006.
[19] R. Zhang, T. J. Lim, Y. C. Liang, and Y. Zeng, "Multi-antenna based spectrum sensing for cognitive radios: A GLRT approach," *IEEE Trans. Commun.*, vol. 58, no. 1, pp. 84–88, Jan. 2006.
[20] L. Wei and O. Tirkkonen, "Analysis of scaled largest eigenvalue based detection for spectrum sensing," in *Proc. IEEE Int. Conf. Commun.*, Jun. 2006, pp. 1–5.
[21] A. Kortun, M. Sellathurai, T. Ratnarajah, and C. Zhong, "Distribution of the ratio of the largest eigenvalue to the trace of complex Wishart matrices," *IEEE Trans. Signal Process.*, vol. 60, no. 10, pp. 5527–5532, Oct. 2006.
[22] Y. He, T. Ratnarajah, J. Xue, E. H. G. Yousif, and M. Sellathurai, "Optimal decision threshold for eigenvalue-based spectrum sensing techniques," in *Proc. IEEE Int. Conf. Acoust. Speech Signal Process.*, May 2014, pp. 7734–7738.
[23] I. S. Gradshteyn and I. M. Ryzhik, *Table of Integrals, Series, and Products*. 7th ed., A. Jeffrey and D. Zwillinger, Eds., New York, NY, USA: Academic, 2007.
[24] C. R. Stevenson, C. Cordeiro, E. Sofer, and G. Chouinard, "IEEE P802.22 wireless RANs functional requirements for the 802.22 WRAN standard doc.:IEEE 802.22-05/0007r46," WK3C Wireless LLC, pp. 101–121, Sep. 2006.
[25] S. Chaudhari, J. Lunden, V. Koivunen, and H. V. Poor, "Cooperative sensing with imperfect reporting channels: Hard decisions or soft decisions?" *IEEE Trans. Signal Process.*, vol. 60, no. 1, pp. 18–28, Jan. 2006.
[26] A. Sahai and D. Cabric, "A tutorial on spectrum sensing: Fundamental limits and practical challenges," presented at the IEEE Symp. New Frontiers Dynamic Spectrum Access Networks, Baltimore, MD, USA, Nov. 2006.

Yibo He (S'15) received the B.Eng. degree in electronic information engineering from Zhengzhou University, Zhengzhou, China, in 2011, the M.S. degree in signal processing and communications from the University of Edinburgh, Edinburgh, UK, in 2012. Since 2013, he has been working toward the Ph.D. degree at the Institute for Digital Communications, the University of Edinburgh.

His main research interests include cognitive radio networks, stochastic geometry, and full-duplex communications.

Jiang Xue (S'10–M'12) received the B.S. degree in information and computing science from the Xi'an Jiaotong University, Xi'an, China, in 2005, the M.S. degrees in applied mathematics from Lanzhou University, Lanzhou, China and Uppsala University, Uppsala, Sweden, in 2008 and 2009, respectively, and the Ph.D. degree in electrical and electronic engineering from the Institute of Electronics, Communications and Information Technology, Queen's University of Belfast, Belfast, U.K., in 2012.

He is currently a Research Fellow with the University of Edinburgh, Edinburgh, U.K. His main research interests include performance analysis of general multiple antenna systems, stochastic geometry, cooperative communications, and cognitive radio.

Tharmalingam Ratnarajah (A'96–M'05–SM'05) is currently a Professor of digital communications and signal processing in the Institute for Digital Communications, University of Edinburgh, Edinburgh, U.K. His research interests include signal processing and information theoretic aspects of 5G wireless networks, full-duplex radio, mmWave communications, random matrices theory, interference alignment, statistical and array signal processing, and quantum information theory. He has published more than 280 publications in these areas and holds four U.S. patents. He is currently the Coordinator of the FP7 projects Advanced Dynamic spectrum 5G mobile networks Employing Licensed shared access (ADEL) (3.7M€) in the area of licensed shared access for 5G wireless networks. Previously, he was the Coordinator of the FP7 project High capacity network Architecture with Remote radio heads and Parasitic antenna arrays (HARP) (3.2M€) in the area of highly distributed multiple-input, multiple-output and FP7 Future and Emerging Technologies projects enHanced Interference Alignment Techniques for Unprecedented Spectral Efficiency (HIATUS) (2.7M€) in the area of interference alignment, and Cognitive Radio Oriented Wireless Networks (CROWN) (2.3M€) in the area of cognitive radio networks.

Dr. Ratnarajah is a Fellow of Higher Education Academy, U.K., and an Associate Editor of the IEEE TRANSACTIONS ON SIGNAL PROCESSING.

Mathini Sellathurai (S'95-M'02-SM'06) received her Ph.D. degree in Electrical Engineering, from McMaster University, Canada, in 2001. She is currently a Reader with the Heriot-Watt University, Edinburgh, U.K., and leading research in signal processing for intelligent systems and wireless communications. Her research interests include adaptive, cognitive, and statistical signal processing techniques in a range of applications including radar and RF networks, network coding, cognitive radio, multiple-input, multiple-output (MIMO) signal processing, satellite communications, and electronically steerable passive array radiator antenna communications. For the past 15 years, she has been active in the area of signal processing research and has a strong international track record in MIMO signal processing with applications in radar and wireless communications research. She has 5 years of industrial research experience. She held positions with Bell-Laboratories, New Jersey, USA, as a Visiting Researcher (2000); and with the Canadian (Government) Communications Research Centre, Ottawa Canada as a Senior Research Scientist (2001–2004). Since 2004 August, she has been with academia. She also holds an honorary Adjunct/Associate Professorship at McMaster University, Ontario, ON, Canada, and an Associate Editorship for the IEEE TRANSACTIONS ON SIGNAL PROCESSING between 2009 and 2013 and currently serving as a Member of IEEE SPCOM Technical Committee. She has published more than 150 peer reviewed papers in leading international journals and IEEE conferences; given invited talks and written several book chapters as well as a research monograph titled "Space-Time Layered Processing" as a lead author.

Dr. Sellathurai received the IEEE Communication Society Fred W. Ellersick Best Paper Award in 2005, Industry Canada Public Service Awards for contributions in science and technology in 2005, and awards for contributions to technology Transfer to industries in 2004. She received the Natural Sciences and Engineering Research Council of Canadas Doctoral Award for her Ph.D. dissertation.

Faheem A. Khan (M'02) received the Ph.D. degree in electrical and electronic engineering from Queen's University Belfast, Belfast, U.K., in 2012.

He is currently a Research Associate in wireless communications and signal processing with the Institute for Digital Communications, The University of Edinburgh, Edinburgh, U.K., under the EU funded FP7 project ADEL. He also participated in the past EU FP7 projects, CROWN, HIATUS, and HARP. His research interests include cognitive radio networks, 5G wireless networks, millimeter wave communications, and cooperative communications.

Signal Processing 120 (2016) 580–593

Contents lists available at ScienceDirect

Signal Processing

journal homepage: www.elsevier.com/locate/sigpro

Performance analysis of multi-antenna GLRT-based spectrum sensing for cognitive radio

Yibo He [a], T. Ratnarajah [a], Ebtihal H.G. Yousif [a], Jiang Xue [a,*], Mathini Sellathurai [b]

[a] Institute for Digital Communications, The University of Edinburgh, King's Buildings, Edinburgh EH9 3JL, United Kingdom
[b] School of Engineering & Physical Sciences, Heriot-Watt University, Edinburgh EH14 4AS, United Kingdom

ARTICLE INFO

Article history:
Received 20 May 2015
Received in revised form
7 September 2015
Accepted 17 October 2015
Available online 24 October 2015

Keywords:
Complex Wishart matrices
Generalized likelihood ratio test
Spectrum sensing
Optimization
Sensing-throughput trade-off

ABSTRACT

This paper addresses the generalized likelihood ratio test (GLRT) eigenvalue based detector with an arbitrary number of receive antennas. We investigate the optimum decision threshold, the minimum sensing time and the achievable sensing throughput trade-off of the secondary network. First, we derive the generalized asymptotic distributions of the test statistic. Second, we investigate the optimal decision threshold that can minimize the total error rate with constraints. Third, we provide the algorithm to find out the shortest sensing time that enables the minimum total error rate to achieve the target value. Finally, we formulate the achievable sensing throughput trade-off for the secondary network and investigate the optimal sensing time which can maximize the achievable throughput for the GLRT detector with multiple antennas under the absence and presence of the noise uncertainty. The accuracy of the derived theoretical models is supported by simulations. The results have shown that the optimized decision threshold and the minimum sensing time can satisfy the target value of the minimum total error rate speedily while both the interests of primary and secondary users are guaranteed simultaneously. In addition, the chosen optimal sensing time maximizes the throughput with and without noise uncertainty.

1. Introduction

The issue of spectrum scarcity has become a major problem that threatens the future of wireless communication systems. In fact, most of the RF spectrum is already licensed for the existing services. However, licensed bands are underutilized most of the time. On the other hand, there is a massively overgrowing demand for wireless communication services, which motivates further research on dynamic spectrum reuse [1]. One promising technology is the cognitive radio (CR) [2,3], which allows unlicensed/secondary users (SUs) to take advantage of spectrum holes. However, during the exploitation of spectrum holes, licensed/primary users (PUs) should be protected from any harmful interference caused by SUs. Therefore, reliable spectrum sensing techniques are essential and crucial to the implementation of cognitive radio systems or other CR-based derivatives, e.g., licensed shared access (LSA) [4]. Considering the reliability, an efficient detection scheme should be robust under very low SNR. For example, the IEEE 802.22 standard for Wireless Regional Area Networks (WRANs) requires both the probability of false alarm and the probability of missed detection to have a maximum value of 0.1 [5].

1.1. Existing work and motivations

Among many spectrum sensing techniques, eigenvalue-based spectrum sensing does not require much prior

* Corresponding author.
E-mail addresses: y.he@ed.ac.uk (Y. He), t.ratnarajah@ed.ac.uk (T. Ratnarajah), e.yousif@ed.ac.uk (E.H.G. Yousif), j.xue@ed.ac.uk (J. Xue), m.sellathurai@hw.ac.uk (M. Sellathurai).

http://dx.doi.org/10.1016/j.sigpro.2015.10.018
0165-1684/

knowledge about the primary signal and can detect spectrum holes with high accuracy. Various eigenvalue-based detection techniques have been considered in the literatures, including maximum eigenvalue detection (MED) [6], maximum minimum eigenvalue (MME) detection [7], energy with minimum eigenvalue (EME) detection [8] and the generalized likelihood ratio test (GLRT) eigenvalue detector [9,10]. In order to analyse the sensing performance, the optimality and the sensing throughput tradeoff, the closed form expressions for probabilities of false alarm and detection are required. However, previous studies, e.g., [6–10], have mainly focused on the probability of false alarm. This is attributed to the difficulty and complexity of obtaining the expressions for the probability of detection for eigenvalue-based detectors.

This paper mainly addresses the GLRT detector. In reviewing the literature, it is found that the exact probability density function (PDF) of the test statistic assuming the alternate hypothesis, i.e., the presence of PUs, was derived in [9] for the GLRT detector. However, this result in [9] is only valid for the special case of 2 receive antennas. Also, the exact expression of probability of false alarm provided in [9] is very complex. Therefore, the aforementioned issues form our major motivation to investigate the generalized asymptotic behaviour of the GLRT eigenvalue-based detector assuming an arbitrary number of receive antennas. Besides, the optimization of the GLRT detector is investigated in terms of optimal decision threshold and minimum sensing time. The purpose of this optimality investigation is to accelerate the spectrum sensing process while maintaining a superior sensing performance. Furthermore, based on the tradeoff relationship between the probabilities of false alarm and detection, the achievable sensing-throughput tradeoff is formulated for the secondary network. The sensing-throughput tradeoff for the ED was addressed in [11], but only special cases of eigenvalue-based detection, with only 2 receive antennas, were studied in [12]. Hence, in this paper, focusing on the general case for the GLRT eigenvalue detector, we study the optimal sensing time for the sensing throughput tradeoff and compare the results from our detector model with the MED and the conventional ED.

1.2. Contributions

The main contributions of this paper are summarized as follows:

- This paper derives the generalized asymptotic closed form expressions of the PDF and cumulative distribution function (CDF) of the test statistic for the general case of the GLRT detector (with arbitrary number of receive antennas). In addition, the expressions of the decision threshold with regard to the probabilities of false alarm and detection are also derived respectively. Furthermore, taking noise uncertainty into consideration, the expressions of the probabilities of false alarm and detection are also presented.
- In terms of the optimization of the considered detector, we first investigate the optimal decision threshold to minimize the total error rate with constraints. This can enable the probability of false alarm and probability of missed detection to achieve desired values concurrently. A main purpose of spectrum sensing is finding out a sensing threshold to achieve a high probability of detection and a low probability of false alarm. On the one hand, a high probability of detection serves the interests of PUs, which makes PUs well protected. On the other hand, a low probability of false alarm benefits SUs only, which enables SUs getting more chances to access the idle licensed frequency bands. Therefore, it is necessary to minimize the total error rate so that both the probability of false alarm and the probability of missed detection can achieve acceptable values simultaneously. It should be noted that the results of optimal decision thresholds in this paper generalize the results of our previous work in [13]. The analysis in [13] is only valid for the GLRT detector with 2 receive antennas. Optimization of the energy detector (ED) was studied in [14], but it is worth mentioning that the ED is sensitive to noise uncertainty. Second, for a given transmit signal, a longer sensing time can provide a larger sample size, which can improve the performance of the detector [15]. However, a long sensing time affects the speed of spectrum sensing. Thus, we also propose a method to determine the minimum sensing time which can satisfy the desired total error rate requirement.
- In addition, the optimal sensing time is determined to maximize the achievable throughput of the secondary network when the PU's benefits are guaranteed simultaneously. For a fixed periodic spectrum sensing duration, a longer sensing time can improve the sensing performance but it will reduce the data transmission time which is closely related to the achievable throughput of the secondary network. Two scenarios are considered in this paper for the achievable throughput, including the absence and presence of the noise uncertainty, and the cases of the ED are also presented for comparison.

The remainder of this paper is organized as follows. Section 2 describes the considered system model. Section 3 derives the asymptotic closed-form expressions of the probabilities of false alarm and detection for the GLRT detector with multiple antennas. Section 4 investigates the optimization of the GLRT detector in terms of the optimal decision threshold and the minimum sensing time. Section 5 investigates the achievable sensing throughput tradeoff for the secondary network under the presence and absence of noise uncertainty and compares the results with the conventional ED model. Section 6 presents simulation results and finally Section 7 concludes this paper.

2. System model

2.1. Mathematical notations

Throughout the paper, vectors are denoted by lower-case boldfaced characters and matrices are represented by upper-case boldfaced characters. The notations $\lceil \cdot \rceil$, $|\cdot|$

and $\|\cdot\|$ denote the ceiling function, the magnitude operator and the Frobenius norm operator respectively. The $\boldsymbol{A}^{\dagger}$ denote the conjugate transpose of matrix $\boldsymbol{A}$. $\hat{a}$ and $\overline{a}$ are the estimated parameter and average value, respectively. The notation $\otimes$ is the Kronecker product. The identity matrix of size N is $\boldsymbol{I}_N$, and $\mathbf{0}$ is the null vector (or matrix). The notation $\mathbb{E}[\cdot]$ is the statistical expectation operator. The complex normal distribution with mean $\boldsymbol{\mu}$ and covariance matrix $\boldsymbol{\Sigma}$ is $\mathcal{CN}(\boldsymbol{\mu},\boldsymbol{\Sigma})$. The central Wishart distribution with parameters a, b and $\boldsymbol{\Sigma}$ is $\mathcal{CW}_a(b,\boldsymbol{\Sigma})$ where $\boldsymbol{\Sigma}$ is an $a\times a$ positive definite covariance matrix. Other special functions used throughout the paper include $(\cdot)_a$ is the Pochhammer symbol. $\Gamma(\cdot)$ is the gamma function. $\Phi(\cdot)$ is the error function. $Q(\cdot)$ is the Gaussian Q-function and $Q(\cdot)^{-1}$ is its inverse. $I_z^{-1}(a,b)$ is inverse regularized incomplete Beta function. However, for convenience we will use the notation $I^{-1}(z,a,b)$. ${}_2F_1(\cdot,\cdot;\cdot;\cdot)$ is the Gaussian hypergeometric function. $G_{p,q}^{m,n}\left(\begin{matrix}a_1,\ldots,a_p\\ b_1,\ldots,b_q\end{matrix}\middle| z\right)$ is the Meijer G-function.

2.2. System setup

Let us consider a spectrum sensing scenario which consists of m receive antennas. The PU is assumed to be equipped with a single antenna, and the transmitted signal is assumed to have a length of n samples, where $n>m$. Let $\mathcal{H}_0$ (PU is absent) and $\mathcal{H}_1$ (PU is present) denote the null and the alternate hypotheses respectively. During the sensing period, the matrix of received signal samples, $\mathbf{Y}\in\mathbb{C}^{m\times n}$, by the secondary user is

$$\mathcal{H}_0:\mathbf{Y}=\mathbf{V}, \tag{1}$$

$$\mathcal{H}_1:\mathbf{Y}=\mathbf{h}\mathbf{x}^{\dagger}+\mathbf{V}, \tag{2}$$

where $\mathbf{V}\in\mathbb{C}^{m\times n}$ represents the samples from a circular symmetric complex additive white Gaussian noise (AWGN), where $\mathbf{V}\sim\mathcal{CN}(\mathbf{0},\sigma_v^2\mathbf{I}_m\otimes\mathbf{I}_n)$, $\mathbf{x}\in\mathbb{C}^{n\times 1}$ consists of the transmitted signal samples which are assumed to be circularly symmetric complex Gaussian variables, where $\mathbf{x}\sim\mathcal{CN}(\mathbf{0},\sigma_x^2\mathbf{I}_n)$. Finally, $\mathbf{h}\in\mathbb{C}^{m\times 1}$ is the channel vector. Henceforth, the covariance matrix of $\mathbf{Y}$, $\mathbf{R}_{yy}\triangleq\mathbb{E}[\mathbf{Y}\mathbf{Y}^{\dagger}]$, is given by

$$\mathcal{H}_0:\mathbf{R}_{yy}=\sigma_v^2\mathbf{I}_m, \tag{3}$$

$$\mathcal{H}_1:\mathbf{R}_{yy}=\sigma_x^2\mathbf{h}\mathbf{h}^{\dagger}+\sigma_v^2\mathbf{I}_m. \tag{4}$$

Within the sensing duration of n samples, the sample covariance matrix estimated from $\mathbf{Y}$ is

$$\widehat{\mathbf{R}}_{yy}=\frac{1}{n}\mathbf{Y}\mathbf{Y}^{\dagger}. \tag{5}$$

Let $\mathbf{W}\in\mathbb{C}^{m\times m}$ be the complex Wishart matrix that is given by $\mathbf{W}=n\widehat{\mathbf{R}}_{yy}=\mathbf{Y}\mathbf{Y}^{\dagger}$. Also, let $\hat{\lambda}_m<\cdots<\hat{\lambda}_1$ be the eigenvalues, in ascending order, estimated from $\widehat{\mathbf{R}}_{yy}$, i.e., the maximum eigenvalue is $\hat{\lambda}_{\max}=\hat{\lambda}_1$ and the minimum eigenvalue is $\hat{\lambda}_{\min}=\hat{\lambda}_m$. The decision statistic for the GLRT-based eigenvalue detector is given by

$$T_{\mathrm{GLRT}}=\frac{\hat{\lambda}_{\max}}{\sum_{i=1}^{m}\hat{\lambda}_i}. \tag{6}$$

For a predetermined decision threshold r, the probability of false alarm P_{fa} and the probability of detection P_{d} are defined as

$$P_{\mathrm{fa}}(r)=\mathrm{Prob}[T_{\mathrm{GLRT}}>r|\mathcal{H}_0]=\int_r^{\infty}f_0(t)\,\mathrm{d}t, \tag{7}$$

$$P_{\mathrm{d}}(r)=\mathrm{Prob}[T_{\mathrm{GLRT}}>r|\mathcal{H}_1]=\int_r^{\infty}f_1(t)\,\mathrm{d}t, \tag{8}$$

where $f_0(t)$ and $f_1(t)$ denote the PDFs of the test statistic T_{GLRT} under the hypotheses $\mathcal{H}_0$ and $\mathcal{H}_1$ respectively. For a given sampling frequency f_s, let τ denote the sensing time such that the received number of samples by each receive antenna is $n=\tau f_s$.

Many detectors assume that the exact noise power is known precisely. However, in practice, the precise value of the noise power is difficult to be obtained because of many involved factors. Noise uncertainty is mainly caused by fluctuations of noise power due to nonlinearity of receiver components and the time-varying thermal noise in these components, as well as the transmissions of other users [16,17]. Thus, the performance of detection methods, that require the exact noise power, can be significantly affected by noise uncertainty, e.g., the energy detector (ED) [18]. Let the estimated noise power be $\hat{\delta}_v^2=\mu\sigma_v^2$ where μ is the noise uncertainty factor and the upper bound (in dB) of the noise uncertainty is defined as [19,17]

$$B=\sup\{10\log_{10}\mu\}. \tag{9}$$

Assuming that noise uncertainty (in dB) is uniformly distributed within the interval $[-B,B]$, then the variation in noise power ranges between $10^{-B/10}$ and $10^{B/10}$.

3. Statistical distributions of the test statistic

Considering the GLRT eigenvalue detector, in this section we investigate the generalized asymptotic statistical distributions of the decision statistic T_{GLRT}, assuming an arbitrary number of receive antennas. For both hypotheses of $\mathcal{H}_0$ and $\mathcal{H}_1$, the PDF and the CDF of T_{GLRT} are necessary to quantify the performance of the detector and to investigate other performance measures such as the achievable throughput. This is also necessary to obtain optimized versions of the detector such as investigation of the optimal sensing threshold that minimizes the total error rate and the analysis of the minimum sensing time which can make spectrum sensing efficient. Hence, in this part we derive the generalized asymptotic PDF and CDF of T_{GLRT} when $n\gg m$.

3.1. Statistical distributions under the hypothesis $\mathcal{H}_0$

Considering the null hypothesis $\mathcal{H}_0$, an asymptotic expression for the PDF of the test statistic T_{GLRT} is presented in the following theorem.

Theorem 1. *Given the complex central uncorrelated Wishart matrix* $\mathbf{W}\sim\mathcal{CW}_m(n,\sigma_v^2\mathbf{I}_m)$, *where* $m\ll n$, *then the PDF of* $T_{\mathrm{GLRT}}=\frac{\hat\lambda_{\max}}{\sum_{i=1}^m\hat\lambda_i}$ *under the hypothesis* $\mathcal{H}_0$ *is given by*

$$f^0_{\mathrm{GLRT}}(x)=\frac{\Gamma(mn)c^{1-mn}}{\Gamma(mn-d)\Gamma(d)}x^{d-1}(c-x)^{mn-d-1},\quad \frac{1}{m}\le x\le 1, \tag{10}$$

where c *and* d *are given by*

$$c=\frac{0.8132b^2}{a-1.7711b},\quad d=\frac{(a-1.7711b)^2}{0.8132b^2}, \tag{11}$$

where a *and* b *are defined as*

$$a=(\sqrt{m}+\sqrt{n})^2,\quad b=(\sqrt{m}+\sqrt{n})\left(\sqrt{\frac{1}{m}}+\sqrt{\frac{1}{n}}\right)^{1/3}. \tag{12}$$

Proof. The test statistic T_{GLRT} can be rewritten as

$$T_{\mathrm{GLRT}}=\frac{1}{m}\frac{m\hat\lambda_{\max}}{\sum_{i=1}^m\hat\lambda_i}=x. \tag{13}$$

Let $z=\frac{m\hat\lambda_{\max}}{\sum_{i=1}^m\hat\lambda_i}$ and $f_z(z)$ denote the PDF of z, therefore $x=g(z)\triangleq\frac{z}{m}$ and the PDF of T_{GLRT} can be calculated by

$$f^0_{\mathrm{GLRT}}(x)=\left.\frac{f_z(z)}{\left|\frac{\mathrm{d}}{\mathrm{d}z}(g(z))\right|}\right|_{z=mx}, \tag{14}$$

where the expression of $f_z(z)$ is referred in [20]. After further calculations, the expression of (10) can be obtained. It is worth mentioning that the parameters a,b,c and d are related to the Tracy–Widom distribution of order 2. Specifically, it is known from [21] that $\frac{\hat\lambda_{\max}-a}{b}$ converges to the Tracy–Widom distribution of order 2 under $\mathcal{H}_0$, when $m\ll n$ and n is large enough. Therefore, the expectation and variance of $\hat\lambda_{\max}$ is given as

$$\mathbb{E}[\hat\lambda_{\max}]=a-1.7711b,\quad \mathrm{Var}[\hat\lambda_{\max}]=0.8132b^2, \tag{15}$$

where -1.7711 and 0.8132 are the statistical expectation and variance of the Tracy–Widom distribution of order 2. Meanwhile, $\hat\lambda_{\max}$ can be approximated well by the Gamma distribution with scale and shape parameters c, d so that

$$\mathbb{E}[\hat\lambda_{\max}]=cd,\quad \mathrm{Var}[\hat\lambda_{\max}]=c^2d. \tag{16}$$

By using Eqs. (15) and (16), the expressions of parameters c and d can be obtained.□

By integrating the PDF of the test statistic derived as (10) and conducting further manipulations, the asymptotic expression of the CDF of the test statistic T_{GLRT} under the hypothesis $\mathcal{H}_0$ is given by the following corollary.

Corollary 1. *Given the complex central uncorrelated Wishart matrix* $\mathbf{W}\sim\mathcal{CW}_m(n,\sigma_v^2\mathbf{I}_m)$, *where* $m\ll n$, *then the CDF of the test statistic* T_{GLRT} *under the hypothesis* $\mathcal{H}_0$ *is given by*

$$F^0_{\mathrm{GLRT}}(x)=\frac{\Gamma(mn)(mc)^{-d}}{d\Gamma(mn-d)\Gamma(d)}\left(\Delta(x)-\Delta\left(\frac{1}{m}\right)\right),\quad \frac{1}{m}\le x\le 1, \tag{17}$$

where $\Delta(\cdot)$ *is defined by*

$$\Delta(y)={}_2F_1\left(d,1+d-mn;d+1;\frac{y}{c}\right)(my)^d. \tag{18}$$

Using the result from the previous corollary and the definition in (7), the probability of false alarm P_{fa} is obtained as

$$P_{\mathrm{fa}}(x)=1-F^0_{\mathrm{GLRT}}(x),\quad \frac{1}{m}\le x\le 1. \tag{19}$$

The CDF given by (17) is verified in Fig. 1. The theoretical and empirical CDF curves in Fig. 1 are plotted for various cases of the number of received samples n, and it can be observed that the asymptotic and empirical results are identical.

Hence, for a complex Gaussian signal, the decision threshold r with respect to the probability of false alarm can be calculated from

$$r=cI^{-1}\left(\frac{\Gamma(mn)(mc)^{-d}}{d\Gamma(mn-d)\Gamma(d)}\left(\Delta\left(\frac{1}{m}\right)+(1-P_{\mathrm{fa}})\frac{d\Gamma(mn-d)\Gamma(d)}{\Gamma(mn)(mc)^{-d}}\right),d,mn-d\right), \tag{20}$$

where $I^{-1}(.,.,.)$ represents the inverse regularized incomplete Beta function [22]. See the provided Appendix for full proof.

When taking noise uncertainty into consideration, the expression of the average probability of false alarm $\overline{P}_{\mathrm{fa}}$ is still the same as the expression of the probability of false alarm without considering noise uncertainty, therefore

$$\overline{P}_{\mathrm{fa}}(x)=P_{\mathrm{fa}}(x). \tag{21}$$

3.2. Statistical distributions under the hypothesis $\mathcal{H}_1$

In this part, the asymptotic expressions of the distributions of the ratio T_{GLRT} are derived assuming the alternate hypothesis $\mathcal{H}_1$. In this case, we have $\mathbf{W}\sim\mathcal{CW}_m(n,\mathbf{\Sigma}_m)$. The PDF of the test statistic T_{GLRT} under the hypothesis $\mathcal{H}_1$ is given in the following theorem.

Theorem 2. *Given the complex central correlated Wishart matrix* $\mathbf{W}\sim\mathcal{CW}_m(n,\Sigma_m)$, *the PDF of the test statistic* T_{GLRT} *for GLRT detector under the hypothesis* $\mathcal{H}_1$ *is derived as*

$$\begin{aligned}f^1_{\mathrm{GLRT}}(x)=&\frac{(m-1)\left(1-\frac{1+m\gamma}{mn\gamma}\right)}{\sqrt{\frac{2\pi}{n}}(1+m\gamma)(1-x)^2}\\&\times\exp\left(-\frac{n}{2}\left[\frac{x(m-1)}{1-x}\left(\frac{1}{1+m\gamma}-\frac{1}{mn\gamma}\right)\right.\right.\\&\left.\left.-\left(1+\frac{m-1}{mn\gamma}\right)\right]^2\right),\end{aligned} \tag{22}$$

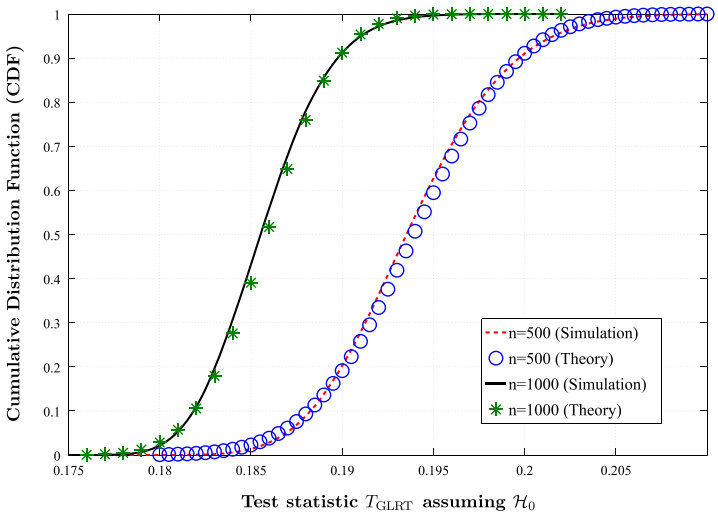

Fig. 1. The CDF of the GLRT detector under the hypothesis $\mathcal{H}_0$ with $m=6$.

where γ is the average received SNR of the PU's signals at the secondary user, which is given by

$$\gamma \triangleq \frac{\sigma_x^2 \|\mathbf{h}\|^2}{m\sigma_v^2}. \tag{23}$$

Proof. The largest eigenvalue $\hat{\lambda}_{\max}$ of the sample covariance matrix follows a Gaussian distribution [23] under the hypothesis $\mathcal{H}_1$, which is given as follows:

$$\hat{\lambda}_{\max} \sim \mathcal{N}\left(\lambda_{\max} + \frac{(m-1)\lambda_{\max}\sigma_v^2}{n(\lambda_{\max}-\sigma_v^2)}, \frac{\lambda_{\max}^2}{n}\right), \tag{24}$$

where $\lambda_{\max}$ is the actual maximum eigenvalue of the actual covariance matrix $\mathbf{R}_{yy}$ under the hypothesis $\mathcal{H}_1$. Since the determinant of the actual covariance matrix $\det(\mathbf{R}_{yy}) = (\sigma_v^2)^{m-1}(\sigma_x^2\|\mathbf{h}\|^2+\sigma_v^2)$ and $\lambda_{\max} = \lambda_1 > \lambda_2 = \lambda_3 = \cdots = \lambda_m$, it can be deduced that $\lambda_{\max} = \sigma_x^2\|\mathbf{h}\|^2 + \sigma_v^2$.

The summation of the eigenvalues of the sample covariance matrix $\hat{\mathbf{R}}_{yy}$ excluding the maximum eigenvalue can be approximated as [24]

$$\sum_{i=2}^{m} \hat{\lambda}_i \approx (m-1)\left(\sigma_v^2 - \frac{\sigma_v^2\lambda_{\max}}{(\lambda_{\max}-\sigma_v^2)n}\right) = \psi. \tag{25}$$

The test statistic of the GLRT detector can be rewritten as

$$T_{\mathrm{GLRT}} = \frac{\hat{\lambda}_{\max}}{\sum_{i=1}^{m}\hat{\lambda}_i} = \frac{\hat{\lambda}_{\max}}{\hat{\lambda}_{\max}+\sum_{i=2}^{m}\hat{\lambda}_i} = x. \tag{26}$$

Thus, it can be obtained that $\hat{\lambda}_{\max} = \frac{x\psi}{1-x}$. Let $\hat{\lambda}_{\max} = z$ and $f_{\hat{\lambda}_{\max}}(z)$ denote the PDF of $\hat{\lambda}_{\max}$, then the generalized PDF of the test statistic T_{GLRT} under $\mathcal{H}_1$ can be derived through

$$f_{\mathrm{GLRT}}^1(x) = \left.\frac{f_{\hat{\lambda}_{\max}}(z)}{\left|\frac{\mathrm{d}}{\mathrm{d}z}\left(\frac{z}{z+\psi}\right)\right|}\right|_{z=x\psi/(1-x)}, \tag{27}$$

after further manipulations, the expression of the PDF of T_{GLRT} can be derived as (22).□

Hence, by making use of the result from the previous theorem, the asymptotic expression of the CDF of the test statistic T_{GLRT} is given in the following corollary.

Corollary 2. *Given the complex central correlated Wishart matrix $\mathbf{W} \sim \mathcal{CW}_m(n, \Sigma_m)$, the CDF of the test statistic T_{GLRT} for the GLRT detector under the hypothesis $\mathcal{H}_1$ is expressed as*

$$F_{\mathrm{GLRT}}^1(x) = \frac{1}{2}\left[\Phi\left(\alpha\sqrt{\beta}+\frac{x}{2\sqrt{\beta}(1-x)}\right) - \Phi\left(\alpha\sqrt{\beta}+\frac{1}{2(m-1)\sqrt{\beta}}\right)\right], \tag{28}$$

where $\Phi(y) \triangleq \frac{2}{\sqrt{\pi}}\int_0^y e^{-t^2}\,\mathrm{d}t$ denotes the error function, α and β are given by

$$\alpha = n(m-1)\left(\frac{1}{mn\gamma} - \frac{1}{1+m\gamma}\right)\left(1+\frac{m-1}{mn\gamma}\right), \tag{29}$$

$$\beta = \frac{1}{2n(m-1)^2}\left(\frac{1}{1+m\gamma} - \frac{1}{mn\gamma}\right)^{-2}. \tag{30}$$

Proof. The CDF can be obtained by integrating (22), and after further manipulations the integral can be written as

$$F_{\mathrm{GLRT}}^1(x) = \tilde{\mathcal{A}}\tilde{\mathcal{B}}\int_{1/(m-1)}^{x/(1-x)} \exp\left[-\frac{y^2}{8n(m-1)^2}\left(\frac{1}{1+m\gamma}-\frac{1}{mn\gamma}\right)^{-2} - yn(m-1)\left(\frac{1}{mn\gamma}-\frac{1}{1+m\gamma}\right)\left(1+\frac{m-1}{mn\gamma}\right)\right]\mathrm{d}y, \tag{31}$$

where $\tilde{\mathcal{A}}$ and $\tilde{\mathcal{B}}$ are given by

$$\tilde{\mathcal{A}} = \sqrt{\frac{n}{2\pi}}\left(\frac{m-1}{1+m\gamma}\right)\left(1-\frac{1+m\gamma}{mn\gamma}\right), \quad \tilde{\mathcal{B}} = \exp\left(-\frac{n}{2}\left(1+\frac{m-1}{mn\gamma}\right)^2\right). \tag{32}$$

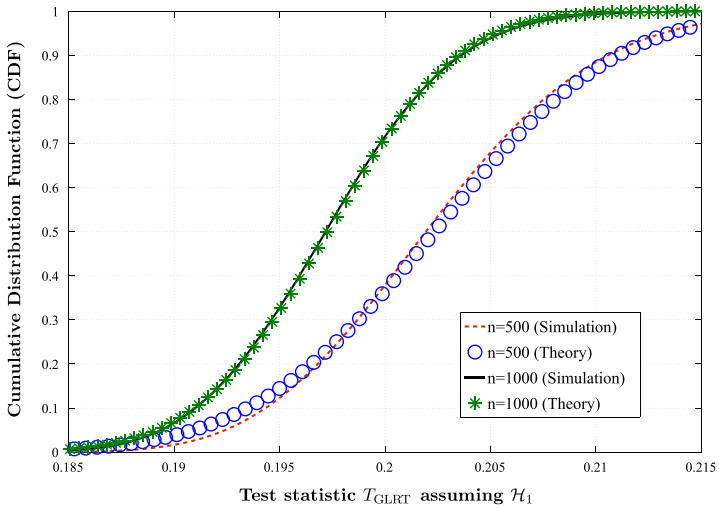

Fig. 2. The CDF of the GLRT detector under the hypothesis $\mathcal{H}_1$ with $m=6$ and $\gamma=-15$ dB.

With the aid of [25, (3.322.1)], we arrive at the expression

$$F^1_{\mathrm{GLRT}}(x)=\breve{\mathcal{A}}\breve{\mathcal{B}}\sqrt{\pi\beta}\exp(\beta\alpha^2)\times\left(\left[1-\Phi\left(\alpha\sqrt{\beta}+\frac{1}{2\sqrt{\beta}(m-1)}\right)\right]-\left[1-\Phi\left(\alpha\sqrt{\beta}+\frac{x}{2\sqrt{\beta}(1-x)}\right)\right]\right),\tag{33}$$

where α and β are defined in (29) and (30) and then after further manipulations we arrive at the expression of the CDF given by (28).□

Hence, the probability of detection can be expressed as

$$P_{\mathrm{d}}(x)=1-F^1_{\mathrm{GLRT}}(x),\quad \frac{1}{m}\le x\le 1.\tag{34}$$

Fig. 2 illustrates the CDF curves obtained from the derived CDF expression for the case of $\mathcal{H}_1$ versus Monte Carlo simulations for various received sample sizes $n=\{500,1000\}$. It can be found that the theoretical results match the simulation results, which demonstrates our analytical expression is consistent with the empirical data.

Besides, we also derive the expression for calculating the decision threshold in terms of the probability of detection, which is given by

$$r=\left(\frac{1}{2}\left(\sum_{k=0}^{\infty}\frac{C_k\sqrt{\beta}}{2k+1}\left[\frac{\sqrt{\pi}}{2}\Phi\left(\alpha\sqrt{\beta}+\frac{1}{2(m-1)\beta}\right)+\sqrt{\pi}(1-P_{\mathrm{d}})\right]^{2k+1}-\alpha\beta\right)^{-1}+1\right)^{-1},\tag{35}$$

where the coefficient

$$C_k=\begin{cases}1, & k=0,\\ \sum_{i=0}^{k-1}\frac{C_iC_{k-1-i}}{(i+1)(2i+1)}, & \text{otherwise.}\end{cases}$$

Furthermore, taking noise uncertainty into account, the expected probability of detection $\overline{P}_{\mathrm{d}}$ can be obtained by

$$\overline{P}_{\mathrm{d}}(x)=\int_{10^{-B/10}}^{10^{B/10}}\left(1-\frac{1}{2}\left[\Phi\left(\breve{\alpha}\sqrt{\breve{\beta}}+\frac{x}{2\sqrt{\breve{\beta}}(1-x)}\right)-\Phi\left(\breve{\alpha}\sqrt{\breve{\beta}}+\frac{1}{2(m-1)\sqrt{\breve{\beta}}}\right)\right]\right)\frac{5}{Bt\ln(10)}\,\mathrm{d}t,\tag{36}$$

where $\breve{\alpha}$ and $\breve{\beta}$ are given by

$$\breve{\alpha}=n(m-1)\left(\frac{1}{mnt\gamma}-\frac{1}{1+mt\gamma}\right)\left(1+\frac{m-1}{mnt\gamma}\right),\tag{37}$$

$$\breve{\beta}=\frac{1}{2n(m-1)^2\left(\frac{1}{1+mt\gamma}-\frac{1}{mnt\gamma}\right)^2}.\tag{38}$$

3.3. Performance using the MED

The test statistic of the maximum eigenvalue detection is defined as the largest eigenvalue of the sample covariance matrix $\widehat{\mathbf{R}}_{yy}$, i.e.,

$$T_{\mathrm{MED}}=\hat{\lambda}_{\max}.\tag{39}$$

The maximum eigenvalue of $n\widehat{\mathbf{R}}_{yy}$ under the hypothesis $\mathcal{H}_0$ was approximated tightly by using Gamma distribution in [20], hence the probability of false for MED under the absence of noise uncertainty can be easily obtained as

$$P_{\mathrm{fa}}(x)=1-\frac{\gamma\left(d,\frac{nx}{c\sigma_v^2}\right)}{\Gamma(d)},\tag{40}$$

where $\gamma(\cdot,\cdot)$ denotes the lower incomplete Gamma function and c, d are defined in (11). Meanwhile, the largest eigenvalue $\hat{\lambda}_{\max}$ of the sample covariance matrix $\widehat{\mathbf{R}}_{yy}$ follows a Gaussian distribution [23] under the hypothesis $\mathcal{H}_1$,

therefore the probability of detection for MED under the absence of noise uncertainty can be given by

$$P_{\mathrm{d}}(x)=Q\left(\frac{\frac{x}{\sigma_v^2}-m\gamma-1-\frac{(m-1)(m\gamma+1)}{mn\gamma}}{m\gamma+1}\sqrt{n}\right). \tag{41}$$

Based on the above expressions, the expected probabilities of false alarm $\overline{P}_{\mathrm{fa}}$ and detection $\overline{P}_{\mathrm{d}}$ for MED under the presence of noise uncertainty are derived as

$$\overline{P}_{\mathrm{fa}}(x)=\int_{10^{-B/10}}^{10^{B/10}}\left(1-\frac{\gamma\left(d,\frac{nxt}{c\sigma_v^2}\right)}{\Gamma(d)}\right)\frac{5}{Bt\ln(10)}\,\mathrm{d}t, \tag{42}$$

$$\overline{P}_{\mathrm{d}}(x)=\int_{10^{-B/10}}^{10^{B/10}}Q\left(\frac{\frac{xt}{\sigma_v^2}-m\gamma t-1-\frac{(m-1)(m\gamma t+1)}{mn\gamma t}}{m\gamma t+1}\sqrt{n}\right)\frac{5}{Bt\ln(10)}\,\mathrm{d}t. \tag{43}$$

3.4. Performance using the ED

The statistical distributions of the test statistic of the energy detector were derived in [26] and assuming noise uncertainty in [12]. Considering the system model employed in this paper, the decision statistic T_{ED} is the average power at the end of the sensing period which is given by

$$T_{\mathrm{ED}}=\frac{1}{n}\sum_{i=1}^{m}w_i\sum_{j=1}^{n}|y_i(j)|^2, \tag{44}$$

where w_i is the weighting factor and the equal gain combining scheme is employed for ED such that $w_i=\frac{1}{m}$. Detection of PUs is performed by comparing the average received power with the noise power when the noise power is assumed to be pre-known. Without noise uncertainty, the probability of false alarm P_{fa} and the probability of detection P_{d} for the ED are given by

$$P_{\mathrm{fa}}(x)=Q\left((x-1)\sqrt{mn}\right), \tag{45}$$

$$P_{\mathrm{d}}(x)=Q\left((x-1-\gamma)\left(\frac{m\gamma^2+2\gamma+1}{mn}\right)^{-1/2}\right). \tag{46}$$

Based on the equations of P_{fa} and P_{d} for ED above, we can obtain the expressions to calculate the decision thresholds in terms of the probabilities of false alarm and detection respectively, which are given as follows:

$$r=\frac{Q^{-1}(P_{\mathrm{fa}})}{\sqrt{mn}}+1, \tag{47}$$

$$r=\sqrt{\frac{m\gamma^2+2\gamma+1}{mn}}Q^{-1}(P_{\mathrm{d}})+1+\gamma, \tag{48}$$

where $Q^{-1}(\cdot)$ stands for the inverse Q-function. For the case in which the noise uncertainty is assumed, the expected probabilities of false alarm $\overline{P}_{\mathrm{fa}}$ and detection $\overline{P}_{\mathrm{d}}$ for ED are obtained as [12].

$$\overline{P}_{\mathrm{fa}}(x)=\int_{10^{-B/10}}^{10^{B/10}}Q\left((xt-1)\sqrt{mn}\right)\frac{5}{Bt\ln(10)}\,\mathrm{d}t, \tag{49}$$

$$\overline{P}_{\mathrm{d}}(x)=\int_{10^{-B/10}}^{10^{B/10}}Q\left(\frac{xt-1-\gamma t}{\sqrt{\frac{m\gamma^2t^2+2\gamma t+1}{mn}}}\right)\frac{5}{Bt\ln(10)}\,\mathrm{d}t. \tag{50}$$

4. Optimization of spectrum sensing based on the GLRT detector

In this section, we consider optimization of the GLRT eigenvalue detector based on two criteria. In the previous work, only the constant false alarm rate scenario was considered, which only considered the interests of SUs, so that the benefits of PUs were neglected. In this paper, we investigate the optimal decision threshold that can make the total error rate achieve the minimum value with constraints of target probabilities of false alarm and missed detection. Therefore, the benefits of PUs and SUs can be guaranteed simultaneously. Moreover, the minimum sensing time is analysed, which enables the minimum total error rate to achieve the desired value speedily. According to the IEEE 802.22 standard for WRANs, the SUs have to vacate the licensed frequency bands as soon as possible once the PUs are active in order to avoid the harmful interference to PUs. Therefore, it is of significance to the CR system to complete the spectrum sensing process within the shortest sensing time while guaranteeing the target total error rate.

4.1. Optimal decision threshold analysis

In this part, the optimal decision threshold is investigated. The optimal decision threshold can minimize the total error rate P_{te} with the constraints of target P_{fa} and P_{m}. Let us assume that the number of the receive antennas m, the width of the sensing windows n, and the average received SNR of the PU's signals measured at the secondary user γ are known. Hence, the optimal decision threshold r_{opt} can be determined. The total error rate is defined as the summation of the probabilities of false alarm and missed detection, i.e.,

$$P_{\mathrm{te}}(r)=P_{\mathrm{fa}}(r)+P_{\mathrm{m}}(r), \tag{51}$$

where

$$P_{\mathrm{m}}(r)=1-P_{\mathrm{d}}(r). \tag{52}$$

It can be seen that the total error rate $P_{\mathrm{te}}(r)$ decreases first and then increases monotonically and this implies that there exists one and only one value of r which minimizes $P_{\mathrm{te}}(r)$ under the constraints of target probabilities of false alarm and missed detection. Therefore, the optimal decision threshold r_{opt} with constraints is given by

$$r_{\mathrm{opt}}=\arg\min_{x}P_{\mathrm{te}}(x), \tag{53}$$

$$\text{s.t. } P_{\mathrm{fa}}(x)\le\xi_{\mathrm{fa}}, \tag{54}$$

$$P_{\mathrm{m}}(x)\le\xi_{\mathrm{m}}, \tag{55}$$

where ξ_{fa} and ξ_{m} are the desired values of P_{fa} and P_{m} respectively. An appropriate decision threshold r can achieve the desired value of probability of false alarm P_{fa},

but the corresponding probability of missed detection P_m may not meet an acceptable value concurrently. Therefore, in practical applications, it is essential to find an optimal decision threshold r_{opt} that minimizes the total error rate with constraints. This can lead to the minimum total error rate and also make both P_{fa} and P_m meet the acceptable values simultaneously.

The total error rate function is a quasi-convex function, so only one global minimum exists and no local minimum exists. Therefore, the optimal decision threshold r_{opt} can be obtained numerically by utilizing the Karush–Kuhn–Tucker (KKT) conditions and the point satisfying the KKT condition must be the globally optimal solution, then the optimization of the decision threshold can be reformulated as follows:

$$(1+\eta_2)f^1_{GLRT}(x)-(1+\eta_1)f^0_{GLRT}(x)=0, \tag{56}$$

$$P_{fa}(x)\le\xi_{fa}, \tag{57}$$

$$P_m(x)\le\xi_m, \tag{58}$$

$$\eta_1(P_{fa}(x)-\xi_{fa})=0, \tag{59}$$

$$\eta_2(P_m(x)-\xi_m)=0, \tag{60}$$

$$\eta_1,\eta_2\ge 0, \tag{61}$$

where η_1 and η_2 are the KKT multipliers. The objective function $P_{te}(x)$ and the constraints $P_{fa}(x)-\xi_{fa}$, $P_m(x)-\xi_m$ are all twice differentiable. Thus, the global optimality of the solution from the KKT conditions can be checked through the Second-order Sufficient Optimality Conditions (SSOC).

The asymptotic analysis above is valid for the GLRT detector with arbitrary number of receive antennas. For the special case of 2 receive antennas, the exact analysis for the optimal decision threshold can also be obtained. In order to obtain the exact total error rate and the exact optimal decision threshold for the GLRT detector with 2 receive antennas, the exact expressions of the probabilities of false alarm and missed detection are required. Starting with the null hypothesis, and since in this case $\boldsymbol{W}\sim\mathcal{CW}_2(n,\sigma_v^2\boldsymbol{I_2})$, the PDF of the test statistic T_{GLRT} is

$$f^0_{GLRT,2}(x)=\frac{\Gamma(2n)(2x-1)^2}{\Gamma(n)\Gamma(n-1)(x(1-x))^{2-n}}, \tag{62}$$

and then the probability of false alarm is obtained as

$$P^2_{fa}(x)=1-\frac{\Gamma(2n)\left(\boldsymbol{\Delta}_1(n,x)-\boldsymbol{\Delta}_1\left(n,\frac{1}{2}\right)\right)}{\Gamma(n)\Gamma(n-1)},\quad \frac{1}{2}\le x\le 1, \tag{63}$$

where $\Delta_1(\cdot,\cdot)$ is defined as

$$\Delta_1(n,y)=\sum_{k=0}^{n-2}\binom{n-2}{k}(-1)^{n-2-k}\times\left\{\frac{y^{2n-k-3}}{2n-k-3}-\frac{4y^{2n-k-2}}{2n-k-2}+\frac{4y^{2n-k-1}}{2n-k-1}\right\}. \tag{64}$$

Under the hypothesis $\mathcal{H}_1$, we have $\boldsymbol{W}\sim\mathcal{CW}_2(n,\boldsymbol{\Sigma_2})$, and therefore the PDF of T_{GLRT} is given by

$$f^1_{GLRT,2}(x)=C_g\frac{(x\delta_2+(1-x)\delta_1)^{1-2n}-(x\delta_1+(1-x)\delta_2)^{1-2n}}{(2x-1)^{-1}(x(1-x))^{2-n}}, \tag{65}$$

where $\delta_1>\delta_2$ are the non-zero ordered eigenvalues of $\boldsymbol{\Sigma_2}$, $C_g=\frac{\Gamma(2n-1)(\delta_1\delta_2)^n}{\Gamma(n)\Gamma(n-1)(\delta_1-\delta_2)}$, and $\frac{1}{2}\le x\le 1$. By applying the binomial expansion and some further mathematical manipulations, we derive the probability of missed detection given by

$$\begin{aligned}P^2_m(x)=C_g\sum_{k=0}^{n-2}\binom{n-2}{k}(-1)^k&\times\Bigg[2\left(\Delta_2(\delta_1,2n-1,k+n,\delta_1-\delta_2,x)-\Delta_2\left(\delta_1,2n-1,k+n,\delta_1-\delta_2,\frac{1}{2}\right)\right)\\&-2\left(\Delta_2(\delta_2,2n-1,k+n,\delta_2-\delta_1,x)-\Delta_2\left(\delta_2,2n-1,k+n,\delta_2-\delta_1,\frac{1}{2}\right)\right)\\&-\left(\Delta_2(\delta_1,2n-1,n+k-1,\delta_1-\delta_2,x)-\Delta_2\left(\delta_1,2n-1,n+k-1,\delta_1-\delta_2,\frac{1}{2}\right)\right)\\&+\left(\Delta_2(\delta_2,2n-1,n+k-1,\delta_2-\delta_1,x)-\Delta_2\left(\delta_2,2n-1,n+k-1,\delta_2-\delta_1,\frac{1}{2}\right)\right)\Bigg],\end{aligned} \tag{66}$$

where $\Delta_2(a,b,c,d,t)=\frac{a-bt^c}{c}{}_2F_1\left(b,c;1+c;\frac{d}{a}t\right)$. Henceforth, the exact total error rate and the exact optimal decision threshold for the GLRT detector with 2 receiving antennas can be obtained numerically by using Eqs. (62), (63), (65) and (66).

4.2. Minimum sensing time analysis

In this subsection, the minimum sensing time duration is investigated. Generally, a longer sensing time provides a larger number of received samples, which is helpful to achieve a better sensing performance to some extent. However, in real time, very long sensing periods may affect the speed of the spectrum sensing process. In order to address this issue, we propose a method to get the minimum sensing time which can make the total error rate achieve the desired value. Assuming that the average received SNR γ and the optimal decision threshold r_{opt} are known, the minimum sensing time τ_{min} can be determined, which can satisfy the desired total error rate, i.e., $P_{te}\le\xi$.

For a given transmit signal, the sampling frequency is known, thus the minimum sample numbers should be determined first in order to obtain the minimum sensing time. Let us define the objective function as a function of the number of samples n as

$$F(n,r_{opt})=P_{te}(n,r_{opt})-\xi, \tag{67}$$

where r_{opt} is as defined in the last subsection. The desired minimum number of samples n_{min} should satisfy the

conditions

$$F(n_{\min}, r_{\text{opt}}) \le 0, \tag{68}$$

$$F(n_{\min}-1, r_{\text{opt}}) > 0, \tag{69}$$

where $n_{\min}$ is the minimum sample size that enables $P_{\text{te}}(n, r_{\text{opt}}) \le \xi$. Hence, we get

$$n_{\min} = \lceil n^* \rceil, \tag{70}$$

where n^* is the first zero-crossing point of the curve $F(n, r_{\text{opt}})$ with respect to n. By utilizing the relation between the sample size n and the sensing time, the desired sensing time can be obtained as $\tau_{\min} = n_{\min}/f_s$. Therefore, the minimum sensing time $\tau_{\min}$ can be used for a spectrum sensing process so that the speed of spectrum sensing can be improved and the target total error rate can be also guaranteed at the same time.

5. The sensing-throughput trade-off analysis

The achievable throughput of the secondary network for the GLRT detector is analysed in this section. We focus on the optimal sensing time which enables the achievable throughput of the secondary network to achieve the maximum value while the PUs are protected sufficiently. Two scenarios are considered in this investigation, including the absence and the presence of noise uncertainty. For a cognitive radio network, one periodic spectrum sensing frame T consists of two parts which are the sensing period τ and the data transmission slot $(T-\tau)$. The secondary users can access the unlicensed frequency bands and transmit data in two cases. In detail, one case occurs when the primary user is inactive and the secondary user detect its absence correctly. The other case occurs when the primary user is active but the secondary user fails to detect its presence. As demonstrated and formulated in [11], the achievable throughput under the hypothesis $\mathcal{H}_0$ is larger than the one under $\mathcal{H}_0$, therefore the optimization issue of the achievable throughput of the secondary network can be formulated and simplified as

$$\max_{\tau} R(r,\tau) = \frac{T-\tau}{T}\log_2(1+SNR_s)(1-P_{\text{fa}}(r,\tau))P(\mathcal{H}_0) \tag{71}$$

$$\text{s.t. } P_{\text{d}}(r,\tau) \ge P_{\text{d}}^*, \tag{72}$$

where r is the decision threshold, SNR_s denotes the SNR of the secondary link and $P(\mathcal{H}_0)$ is the probability that the PU is absent. Normally, the probability of the absence of PU is greater than the probability of the presence based on the facts that spectrum resource is highly underutilized at some locations and time slots. P_{d}^* is the desired probability of detection which can make the primary users have sufficient protection. It is worth mentioning that the expressions of $P_{\text{fa}}(r,\tau)$ and $P_{\text{d}}(r,\tau)$ can be obtained easily by replacing n and x of $P_{\text{fa}}(x)$ and $P_{\text{d}}(x)$ by τf_s and r, respectively.

In order to optimize the sensing time for the achievable throughput, the optimum decision threshold should be determined first. It can be proven that the optimal decision threshold solution to (71) and (72) is achieved when the equality constraint in (72) is satisfied, which means that the chosen decision threshold r_{d} should satisfy $P_{\text{d}}(r_{\text{d}},\tau) = P_{\text{d}}^*$. Since, for a given sensing time τ, both $P_{\text{d}}(r,\tau)$ and $P_{\text{fa}}(r,\tau)$ are monotonically decreasing functions. If the arbitrary decision threshold r_{a} satisfies $P_{\text{d}}(r_{\text{a}},\tau) > P_{\text{d}}^*$, then $r_{\text{a}} < r_{\text{d}}$ and $P_{\text{fa}}(r_{\text{a}},\tau) > P_{\text{fa}}(r_{\text{d}},\tau)$. From Eq. (71), it can be obtained that $R(r_{\text{a}},\tau) < R(r_{\text{d}},\tau)$. Thus, the optimal solution to the formulation in (71) and (72) should be achieved with the equality constraint in (72).

When the noise uncertainty is not considered, the achievable throughput of the secondary network can be calculated as follows. First, the optimum decision threshold r_{d} can be obtained by computing the equality constraint in (72) for a target probability of detection P_{d}^*. Second, the corresponding value of $P_{\text{fa}}(r,\tau)$ can be determined by substituting the value of r_{d} obtained in first step. Finally, the achievable throughput of the secondary network can be calculated by substituting the value of $P_{\text{fa}}(r,\tau)$ obtained in second step into (71).

Similarly, considering noise uncertainty, the achievable throughput of the secondary network can be calculated by using $\overline{P}_{\text{fa}}(r,\tau)$ and $\overline{P}_{\text{d}}(r,\tau)$ instead of $P_{\text{fa}}(r,\tau)$ and $P_{\text{d}}(r,\tau)$ during the above calculation steps, respectively. Meanwhile, the expressions of $\overline{P}_{\text{fa}}(r,\tau)$ and $\overline{P}_{\text{d}}(r,\tau)$ can be obtained easily through replacing n and x of $\overline{P}_{\text{fa}}(x)$ and $\overline{P}_{\text{d}}(x)$ by τf_s and r, respectively.

6. Simulation results

In this section, simulation results are provided to validate the obtained results throughout this paper for the performance and the optimization of the GLRT eigenvalue detector. The results demonstrate the performance of the GLRT eigenvalue-based detector and the impact of other related parameters. The more insights will be provided into the optimal decision threshold, the minimum sensing time and the achievable sensing throughput trade-off analysis.

6.1. Optimal decision threshold for the GLRT detector

The total error rate P_{te} and the optimal decision threshold r_{opt} for the GLRT detector with multiple antennas are presented in this subsection. We are interested in the value of the optimal decision threshold and the performance of total error rate in different cases of low SNR. Fig. 3 shows the performance of the total error rate for the GLRT detector with 6 receive antennas and sample size of 500 samples, i.e., $m=6$, $n=500$, under different values of the received SNR, γ, from -12.5 dB to -7.5 dB. From Fig. 3, it can be observed that the minimum values of the total error rate are very low when the received SNR is $\gamma \ge -12.5$ dB. This indicates that the probability of false alarm and missed detection are also very low. The values of the optimal decision thresholds which minimize the total error rate with constraints can be obtained numerically. Specifically, the corresponding optimal decision thresholds r_{opt} are $\{0.2034, 0.2127, 0.2259\}$ for the different SNR values that are given by $\gamma = \{-12.5, -10, -7.5\}$ dB, respectively. The corresponding values

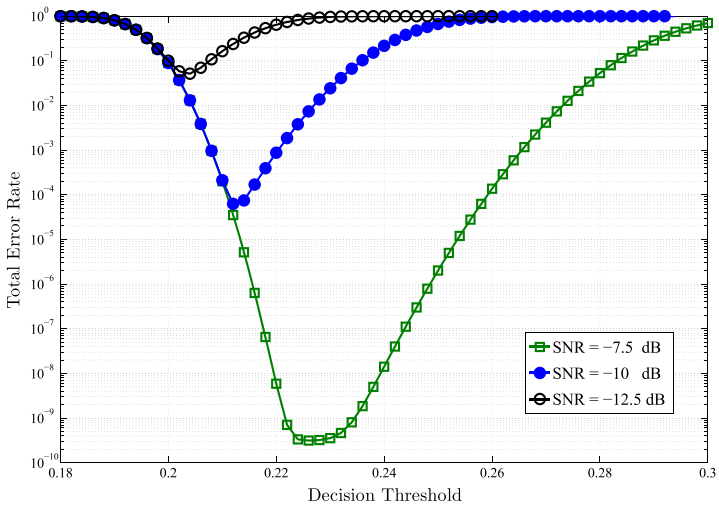

Fig. 3. The total error rate of the GLRT detector with multiple antennas under different received SNRs with $m=6$ and $n=500$.

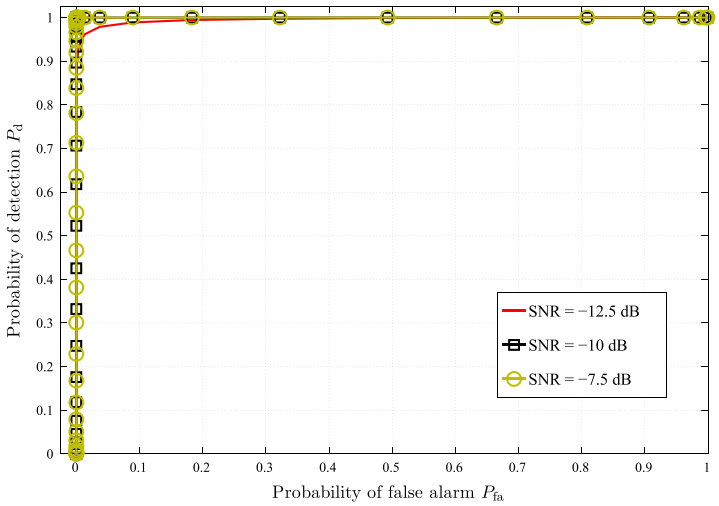

Fig. 4. The ROC curves of the GLRT detector with multiple antennas under different received SNRs with $m=6$ and $n=500$.

employed for the constraints of target probabilities of false alarm and missed detection ξ_{fa} and ξ_m are given by $\xi_{fa}=\xi_m=0.1$. All these obtained optimal decision thresholds minimize the total error rate. Meanwhile, the SUs can achieve a high probability of accessing an unlicensed band and the PUs are protected from the consequences of missed detections concurrently. In order to observe the performance in terms of the probability of false alarm P_{fa} and the probability of detection P_d, the receiver operating characteristic (ROC) curves are depicted in Fig. 4.

6.2. Minimum sensing time for the GLRT detector

The minimum sensing time τ_{min} and the total error rate P_{te} for the GLRT detector with multiple antennas are presented in this subsection. We are interested in the values of the minimum sensing time and the minimum total error rates in the low SNR regime. Fig. 5 shows the minimum total error rates with regard to different values of the sensing time for the GLRT detector with multiple antennas $m=\{4,6\}$ under low SNR values of $\gamma=\{-15,-12.5\}$ dB. It is found that the performance of

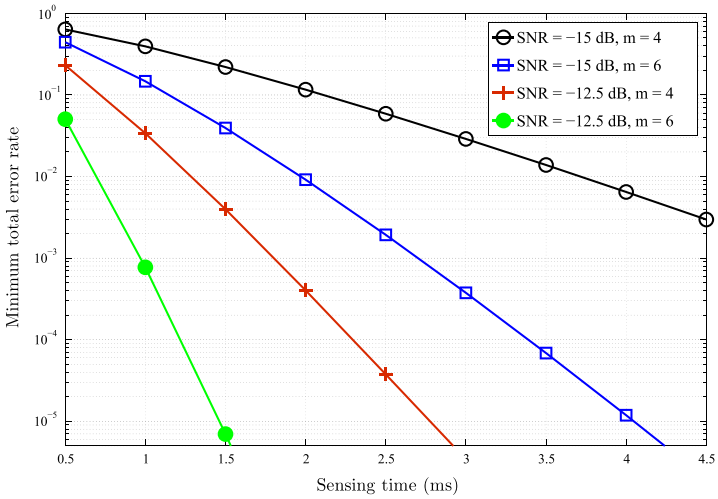

Fig. 5. The minimum total error rate versus sensing time of the GLRT detector with multiple antennas ($m=4$, $m=6$) under different values of the received SNR ($\gamma=-15$ dB, $\gamma=-12.5$ dB).

the minimum total error rate tends to be better by increasing the number of receive antennas and the sensing time. When the desired minimum total error rate is set at 0.01, for $\gamma=-15$ dB, it is found that the corresponding minimum sensing time should be 4.0 ms and 2.0 ms for $m=4$ and $m=6$, respectively, and for $\gamma=-12.5$ dB, the corresponding minimum sensing time can be obtained at 1.5 ms and 1.0 ms for $m=4$ and $m=6$, respectively. All these results for the obtained values of the minimum sensing time enable the minimum total error rates to achieve the target of minimum total error rate speedily and efficiently.

6.3. Achievable throughput of the secondary network

In this part, the results for the achievable throughput of the secondary network and the optimal sensing time which can maximize the throughput are considered and discussed. We assume that the SNR of the PU's signals measured at the secondary receiver is $\gamma=-15$ dB. The SNR of the secondary link between the secondary transmitter and receiver is set to be $SNR_s=20$ dB and the sampling frequency used for simulations is 1 MHz. Meanwhile, the probability of the absence of the PU is assumed as $P(\mathcal{H}_0)=0.8$, and the duration of single spectrum sensing frame is $T=100$ ms. Besides, the predefined target probability of detection is $P_d^*=0.9$. Also, the comparison of the achievable throughput of the secondary network with and without noise uncertainty is also presented in the subsection.

First, Fig. 6 shows the theoretical and Monte Carlo simulation results of the achievable throughput of the secondary network for the GLRT detector with 6 receive antennas, i.e., ($m=6$). In this figure, it can be seen that the theoretical results are matching the simulation results well. In addition, these results reveal that the optimal sensing times obtained from the theoretical and simulation curves are both 1.5 ms, which indicates that our proposed expressions in the previous section for calculating the achievable throughput of the GLRT detector with multiple antennas are correct. Thus, we will only show the theoretical results in the following figures.

Second, a comparison is provided in Figs. 7 and 8 for the achievable throughput of the secondary network using the GLRT detector, MED and ED. Simulations assume that the received SNR sourced from the PU's signal is $\gamma=-15$ dB. In these two figures, the achievable throughput using the three different detector models are illustrated for different numbers of receive antennas. Fig. 7 does not consider the noise uncertainty, while Fig. 8 does. Also, the values of the optimal sensing time which maximize the achievable throughput of the secondary network can be obtained. Specifically, from Fig. 7, when the noise uncertainty is absent, the optimal sensing time for the GLRT detector with 6 and 8 receive antennas are 1.50 ms and 1.00 ms, respectively. The optimal sensing time for the MED with 6 and 8 receive antennas are 1.25 ms and 1.00 ms respectively. Also, the optimal values of the sensing time for the ED with 6 and 8 receive antennas are 2.50 ms and 2.00 ms, respectively. From Fig. 8, it can be seen that when the noise uncertainty is present, the performance of the GLRT detector is not affected so that the optimal sensing times are unchanging. However, the performances of the MED and ED are affected. Specifically, for MED, the corresponding optimal sensing times are changed to be 6.00 ms and 5.50 ms for the cases with 6 and 8 receive antennas respectively. For ED, the corresponding optimal sensing times for 6 and 8 receive antennas both change to be 1.00 ms. Besides, it can be seen that the GLRT detector outperforms the MED and ED in terms of the achievable throughput of the secondary network under the presence of noise uncertainty. For all the investigated

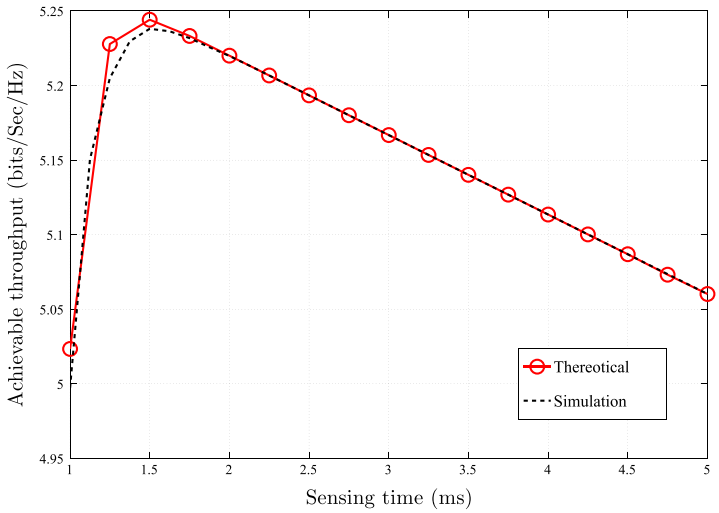

Fig. 6. The achievable throughput of the secondary network for the GLRT detector with $m=6, f_s=1$ MHz and $\gamma=-15$ dB.

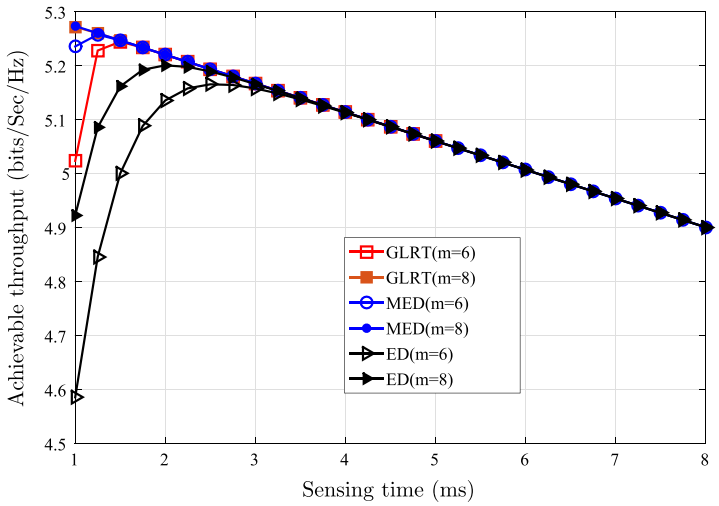

Fig. 7. The achievable throughput of the secondary network for the GLRT detector, MED and ED under the absence of the noise uncertainty with $f_s=1$ MHz and $\gamma=-15$ dB.

detection methods, it is obvious that the optimal sensing time will be shorter if the detector has more receive antennas.

7. Conclusion

This paper investigated the general case of the GLRT eigenvalue detector with an arbitrary number of receive antennas. Initially, we derived the asymptotic expressions of the probabilities of false alarm and detection when the sample size from each primary user was large enough compared with the number of receive antennas. Unlike the asymptotic expression of the probability of false alarm given in the previous work which was difficult to obtain the derivative, the expressions of probabilities of false alarm and detection derived in this paper were mathematically traceable and the noise uncertainty was also considered. Furthermore, the optimal decision threshold was studied for the GLRT detector and the results showed

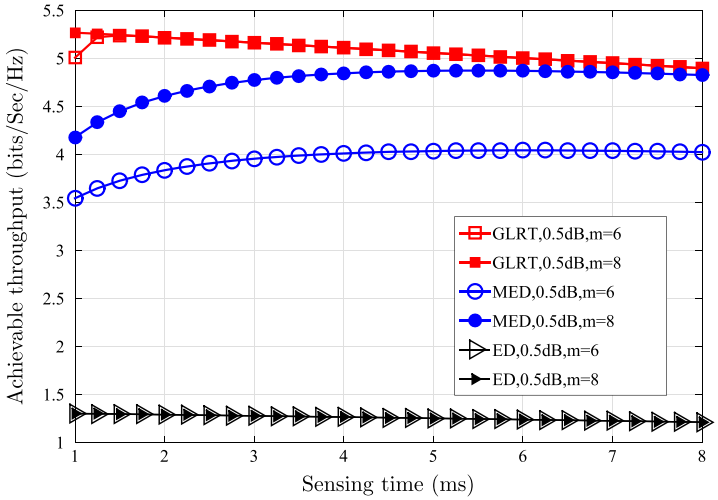

Fig. 8. The achievable throughput of the secondary network for the GLRT detector, MED and ED under the presence of the noise uncertainty with $f_s = 1$ MHz, $\gamma = -15$ dB and noise uncertainty is 0.5 dB.

that the proposed optimization model for the decision threshold could minimize the total error rate under different received SNR regimes. Moreover, the paper provided a fast spectrum sensing method which only required a shortest sensing time to satisfy the target of the minimum total error rate. Thus, the sensing time could be reduced while maintaining a desired total error rate and the chosen optimal decision thresholds were also applied during this process. Finally, by analysing the achievable sensing throughput trade-off for the secondary network, the optimal sensing time which maximized the achievable throughput was found. It is worth to notice that both cases of the absence and the presence of the noise uncertainty were considered and a comparison was also provided among the investigated detector, the MED and the conventional ED. The results revealed that the investigated GLRT eigenvalue detector outperformed the MED and ED under the presence of noise uncertainty.

Acknowledgement

This work is supported by the Seventh Framework Programme for Research of the European Commission under Grant number ADEL-619647.

Appendix A. Proof of Eq. (20)

We aim to solve $P_{\mathrm{fa}}(x) = \epsilon$ given that $\epsilon \in [0, 1]$ and

$$P_{\mathrm{fa}}(x) = 1 - \frac{\Gamma(mn)(mc)^{-d}}{d\Gamma(mn-d)\Gamma(d)} \times \left[{}_2F_1\left(d, d-mn+1; d+1; \frac{x}{c}\right)(mx)^d - {}_2F_1\left(d, d-mn+1; d+1; \frac{1}{mc}\right)\right], \tag{73}$$

where $\frac{1}{m} \le x \le 1$. The previous equation is equivalent to finding the value of x that satisfies

$${}_2F_1\left(d, d-mn+1; d+1; \frac{x}{c}\right)(mx)^d = {}_2F_1\left(d, d-mn+1; d+1; \frac{1}{mc}\right) + \frac{d\Gamma(mn-d)\Gamma(d)}{\Gamma(mn)(mc)^{-d}}(1-\epsilon), \tag{74}$$

which can be rewritten as

$$G_{2,2}^{1,2}\left(\begin{matrix} 1-d, mn-d \\ 0, -d \end{matrix}\middle| -\frac{x}{c}\right) = (mx)^{-d}\,{}_2F_1\left(d, d-mn+1; d+1; \frac{1}{mc}\right) + d!(mn)_{-d}(1-\epsilon)\left(\frac{c}{x}\right)^d, \tag{75}$$

which can be expressed as an incomplete beta function, and hence the value of x can be given by the inverse.

References

[1] F.C. Commission, Spectrum policy task force, ET Docket no. 02-135, November 2002.
[2] S. Haykin, Cognitive radio: brain-empowered wireless communications, IEEE J. Sel. Areas Commun. 23 (February (2)) (2005) 201–220.
[3] J. Mitola, G.Q. Maguire, Cognitive radio: making software radios more personal, IEEE Pers. Commun. 6 (August (4)) (1999) 13–18.
[4] CEPT-ECC, ECC report 205: licensed shared access (LSA), February 2014.
[5] C.R. Stevenson, C. Cordeiro, E. Sofer, G. Chouinard, IEEE P802.22 wireless RANs functional requirements for the 802.22 WRAN-standard doc.:IEEE 802.22-05/0007r46, WK3C Wireless LLC 1–49, September 2005.
[6] T. Ratnarajah, C. Zhong, A. Kortun, M. Sellathurai, C.B. Papadias, Complex random matrices and multiple-antenna spectrum sensing, in: IEEE International Conference on Acoustics, Speech and Signal Processing (ICASSP), May 2011.

[7] A. Kortun, T. Ratnarajah, M. Sellathurai, C. Zhong, C.B. Papadias, On the performance of eigenvalue-based cooperative spectrum sensing for cognitive radio, IEEE J. Sel. Top. Signal Process. 5 (February (1)) (2011) 49–55.
[8] Y. Zeng, Y.C. Liang, Eigenvalue-based spectrum sensing algorithms for cognitive radio, IEEE Trans. Commun. 57 (June (6)) (2009) 1784–1793.
[9] A. Kortun, M. Sellathurai, T. Ratnarajah, C. Zhong, Distribution of the ratio of the largest eigenvalue to the trace of complex Wishart matrices, IEEE Trans. Signal Process. 60 (October (10)) (2012) 5527–5532.
[10] L. Wei, O. Tirkkonen, P. Dharmawansa, M. McKay, On the exact distribution of the scaled largest eigenvalue, in: IEEE International Conference on Communications (ICC), June 2012.
[11] Y.C. Liang, Y. Zeng, E.C. Peh, A.T. Hoang, Sensing-throughput tradeoff for cognitive radio networks, IEEE Trans. Wirel. Commun. 7 (April (4)) (2008) 1326–1337.
[12] A. Kortun, T. Ratnarajah, M. Sellathurai, Y.C. Liang, Y. Zeng, On the eigenvalue-based spectrum sensing and secondary user throughput, IEEE Trans. Veh. Technol. 63 (March (3)) (2014) 1480–1486.
[13] Y. He, T. Ratnarajah, J. Xue, E.H.G. Yousif, M. Sellathurai, Optimal decision threshold for eigenvalue-based spectrum sensing techniques, in: IEEE International Conference on Acoustics, Speech and Signal Processing (ICASSP), May 2014.
[14] W. Zhang, R.K. Mallik, K.B. Letaief, Optimization of cooperative spectrum sensing with energy detection in cognitive radio networks, IEEE Trans. Wirel. Commun. (December (12)) (2009) 5761–5766.
[15] P. Wang, J. Fang, N. Han, H. Li, Multiantenna-assisted spectrum sensing for cognitive radio, IEEE Trans. Veh. Technol. 59 (May (4)) (2010) 1791–1800.
[16] A. Sonnenschein, P.M. Fishman, Radiometric detection of spread-spectrum signals in noise of uncertain power, IEEE Trans. Aerosp. Electron. Syst. 28 (July (3)) (1992) 654–660.
[17] Y. Zeng, Y.C. Liang, A.T. Hoang, R. Zhang, A review on spectrum sensing for cognitive radio: challenges and solutions, EURASIP J. Adv. Signal Process. 2010 (January) (2010) 1–15.
[18] W. Jouini, Energy detection limits under log-normal approximated noise uncertainty, IEEE Signal Process. Lett. 18 (July (7)) (2011) 423–426.
[19] Y. Zeng, Y.C. Liang, A.T. Hoang, E.C.Y. Peh, Reliability of spectrum sensing under noise and interference uncertainty, in: IEEE International Conference on Communications (ICC) Workshops, June 2009.
[20] L. Wei, O. Tirkkonen, Analysis of scaled largest eigenvalue based detection for spectrum sensing, in: IEEE International Conference on Communications (ICC), June 2011.
[21] K. Johansson, Shape fluctuations and random matrices, Commun. Math. Phys. 209 (February (2)) (2000) 437–476.
[22] K.L. Majumder, G.P. Bhattacharjee, Algorithm as 64: inverse of the incomplete beta function ratio, Appl. Stat. (1973) 411–414.
[23] F. Haddadi, M.M. Mohammadi, M.M. Nayebi, M.R. Aref, Statistical performance analysis of MDL source enumeration in array processing, IEEE Trans. Signal Process. 58 (January (1)) (2010) 452–457.
[24] K.M. Wong, Q. Zhang, J.P. Reilly, P.C. Yip, On information theoretic criteria for determining the number of signals in high resolution array, IEEE Trans. Acoust. Speech Signal Process. 38 (November (11)) (1990) 1959–1971.
[25] I.S. Gradshteyn, I.M. Ryzhik, Table of Integrals, Series, and Products, seventh edition, . Academic Press, New York, USA, 2007.
[26] D.C. Oh, Y.H. Lee, Energy detection based spectrum sensing for sensing error minimization in cognitive radio networks, Int. J. Commun. Netw. Inf. Secur. 1 (April (1)) (2009) 1–5.

Full-Duplex Spectrum Sensing for Multi-Antenna Non-Time-Slotted Cognitive Radio Networks

Yibo He †, Jiang Xue †, Tharmalingam Ratnarajah † and Mathini Sellathurai §
† IDCOM, The University of Edinburgh, King's Buildings, Edinburgh, EH9 3JL, U.K.
§ School of Engineering & Physical Sciences, Heriot-Watt University, U.K.

***Abstract*—In order to improve the spectral efficiency of a cognitive radio (CR) network and consider the asynchronism between the primary and secondary networks, this paper investigates a full-duplex (FD) non-time-slotted CR system based on the multi-antenna energy detection. The secondary transmitter with the FD technique can perform spectrum sensing and data transmission simultaneously. Firstly, the closed-form expressions of the probabilities of false alarm and missed detection are derived based on the proposed system with multiple sensing antennas. Secondly, the total error rate performance of the system is investigated in order to consider the benefits of the primary and secondary users concurrently. Meanwhile, the optimal decision threshold pair is investigated to minimize the total error rate of the system. Furthermore, the derived expressions in this paper are verified by simulation results and the obtained optimal decision threshold pairs achieve the minimum total error rates.**

***Index Terms*—Full-duplex, non-time-slotted, optimization, spectrum sensing, total error rate.**

I. Introduction

Cognitive radio (CR) has been proposed as one of the promising solutions to spectrum scarcity [1]. In CR networks, the secondary (unlicensed) users (SUs) can access the vacant licensed frequency bands which are allocated to the primary (licensed) users (PUs). During the implementation of the CR system, the PU should be protected from the harmful interference brought by the SUs in order to guarantee the quality of service (QoS) of PUs. Therefore, a reliable spectrum sensing is curial and necessary to CR networks, which aims to detect the state of PUs.

Full-duplex (FD) systems can conduct transmission and reception simultaneously at the same frequency bands, but self-interference will be introduced by the FD antennas. However, due to the recent advances on self-interference reduction techniques [2]–[4], the FD technique has been put forward to apply in CR networks to improve the sensing performance and spectral efficiency of the secondary network. In FD CR networks, the SU possesses FD capability and the antennas of the SU is partitioned into two parts, including the sensing and transmission antennas. Compared with the half-duplex (HD) CR network within the same length of periodic spectrum sensing frame, FD CR systems can implement sensing and transmission during the whole frame so that more samples can be accumulated for spectrum sensing and longer data transmission time can be obtained for the secondary network.

This work is supported by the Seventh Framework Programme for Research of the European Commission under grant number ADEL-619647.

In practical CR systems, the realization of the synchronization between the PUs and SUs is difficult since the types of the primary and secondary networks are different normally. However, in the previous works on CR networks, the system is usually assumed to be time-slotted which means that the PUs can only change their state (i.e., active or inactive) at the beginning of each time-slotted secondary frame. On the contrary, the PUs and SUs are asynchronous in the non-time-slotted network. Therefore, the non-time-slotted CR network is more practical and realistic. However, because of the complexity of the non-time-slotted model, enormous existing works on both HD and FD CR networks, e.g., [5]–[8], have mainly focused on the time-slotted system where the PUs and SUs are assumed to be perfectly synchronized.

Motivated by the benefits of the FD technique and the practical significance of the non-time-slotted system, we investigate the FD spectrum sensing performance for multi-antenna non-time-slotted CR networks in this paper. Most of the existing FD works for CR networks, e.g., [8]–[10], assumed that there was only a single antenna for sensing and another single antenna for transmission at the SU. Therefore multi-antenna energy detector (ED) is considered in this paper. A low probability of false alarm creates more chances to access the spectrum holes for SUs, which benefits the SUs. Meanwhile, a low missed detection rate helps to protect the PUs from the harmful interference caused by the SUs, which considers the interests of PUs. Thus, the total error rate is investigated in order to consider the benefits of PUs and SUs concurrently. In detail, firstly, the generalized closed-form expressions of the probabilities of false alarm and missed detection of the multi-antenna ED are derived based on the non-time-slotted FD system. Secondly, the total error rate is investigated in order to consider the interests of PUs and SUs simultaneously. Furthermore, the optimal decision threshold pair is obtained, which can minimize the total error rate.

The remainder of this paper is organized as follows. Section II describes the system model. In Section III, the closed-form expressions of the probabilities of false alarm and missed detection are derived. Meanwhile, optimal decision threshold pairs are investigated to minimize the total error rate. Section IV provides the simulation results. Finally, Section V concludes this paper.

II. System Model

We consider the FD non-time-slotted CR network based on the multi-antenna ED, which is shown as Fig. 1. The PU is

978-1-5090-1749-2/16/$31.00

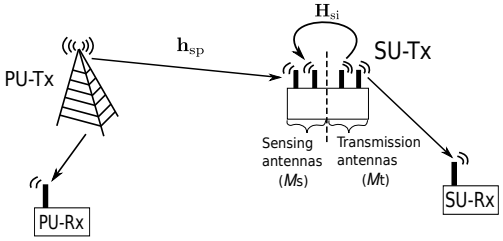

Fig. 1. The system model of FD spectrum sensing

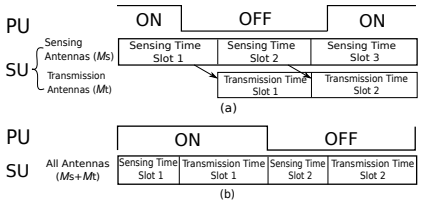

Fig. 2. (a) The FD non-time-slotted spectrum sensing system. (b) The HD time-slotted spectrum sensing system. (ON: The PU is active, OFF: The PU is inactive.)

assumed to be equipped with single antenna and the secondary transmitter (SU-Tx) has multiple antennas. The antennas of SU-Tx comprise of two parts, including the sensing and transmission antennas. Different from the most of the existing FD spectrum sensing works, it is worth mentioning that each part of the antennas at the SU-Tx is assumed to be multiple so that the model in this paper is more generalized. In detail, the sensing antennas perform spectrum sensing and the transmission antennas conduct the data transmission of the secondary network simultaneously, when the licensed frequency band is sensed as idle.

Besides, the considered non-time-slotted system is presented in Fig. 2(a), where the PU's state may change at any time within the periodic spectrum sensing frame so that the PU can access and leave the licensed frequency bands randomly. For comparison, the traditional HD time-slotted spectrum sensing system is also illustrated as Fig. 2(b). The activity of the PU is characterized as an alternating ON/OFF process. In practical applications, the state of the PU would not change frequently within one spectrum sensing frame, since each activity period of the PU is longer than each sensing/transmission period of the SU. Hence, without loss of generalization, we assume the PU may change its status up to once within one periodic spectrum sensing frame.

Specifically, in this non-time-slotted FD spectrum sensing system, the state of the PU is defined as the state at the end of each periodic frame of the SU's activity. Therefore, there exists 4 different hypotheses in terms of the activities of the PU and the SU, which can be summarized as follows:

- $\mathcal{H}_{10}$: The SU is active (1), the PU is active for a samples and then turns to inactive (0) within the secondary periodic frame,
- $\mathcal{H}_{00}$: The SU is inactive (0), the PU is active for a samples and then turns to inactive (0) within the secondary periodic frame,
- $\mathcal{H}_{11}$: The SU is active (1), the PU is inactive for b samples and then turns to active (1) within the secondary periodic frame,
- $\mathcal{H}_{01}$: The SU is inactive (0), the PU is inactive for b samples and then turns to active (1) within the secondary periodic frame,

where $0 \leq a, b < N$ and a, b vary depending on the realistic situations, thus different cases are shown in simulation results for various a, b.

The ED is employed at the sensing antennas of the SU-Tx in this paper, since the ED does not require the knowledge of the PU's signal and is easy to realize in hardware. Assuming the numbers of sensing and transmission antennas at the SU-Tx are denoted by $M_{\rm s}$ and $M_{\rm t}$ respectively and N is the total number of the samples of the received signals for each whole sensing period, the test statistic of the ED is given by [11]

$$T_{\rm ED} = \frac{1}{M_{\rm s} N} \sum_{i=1}^{M_{\rm s}} \sum_{n=1}^{N} |y_i(n)|^2 , \tag{1}$$

where $y_i(n)$ denotes the received signal of the nth sample observed at the ith sensing antenna of the SU. Also, the saturated traffic scenario is assumed, which means that the SUs always have data to transmit.

III. Performance Analysis of The FD Non-time-Slotted Spectrum Sensing

In this section, the performance of the multi-antenna ED based non-time-slotted spectrum sensing using the FD technique is investigated. In order to consider the interests of the PU and SUs simultaneously, the total error rate of the spectrum sensing is studied and the optimal decision threshold pair is obtained. The total error rate $P_{\rm te}$ is closely related to the probabilities of false alarm $P_{\rm fa}$ and missed detection $P_{\rm m}$. Therefore, the closed-form expressions of $P_{\rm fa}$ and $P_{\rm m}$ are required for the analyses of $P_{\rm te}$ and decision thresholds.

A. Probabilities of False Alarm and Missed Detection

As introduced in the previous section, the spectrum sensing of the SU-Tx can be implemented with the FD technique under two cases: (1) The transmission antennas of the SU-Tx are transmitting data; (2) The transmission antennas are silent. When the transmission antennas of the SU-Tx are active, the self-interference will be introduced to the spectrum sensing process at the sensing antennas. The self-interference can be reduced partly through existing self-interference reduction techniques [2]–[4], so the spectrum sensing can still be conducted with the residual self-interference. The capability of the self-interference reduction technique can be measured by the self-interference suppression (SIS) factor χ which is defined as

$$\chi^2 = \frac{\text{Power of the residual self-interference}}{\text{SU's transmit power}}. \tag{2}$$

$$\mathbf{y}(n)=\begin{cases}\chi\mathbf{H}_{\rm si}\mathbf{v}s_{\rm s}(n)+\mathbf{u}(n), & \text{PU is inactive (0) and SU is active(1),}\\ \mathbf{u}(n), & \text{PU is inactive (0) and SU is inactive (0),}\\ \mathbf{h}_{\rm sp}s_{\rm p}(n)+\chi\mathbf{H}_{\rm si}\mathbf{v}s_{\rm s}(n)+\mathbf{u}(n), & \text{PU is active (1) and SU is active (1),}\\ \mathbf{h}_{\rm sp}s_{\rm p}(n)+\mathbf{u}(n), & \text{PU is active (1) and SU is inactive (0),}\end{cases} \tag{3}$$

Considering the states of the PU and the SU jointly, the received signal observed at the sensing antennas of the SU-Tx is given by equation (3) at the top of this page, where $\mathbf{h}_{\rm sp}$ denotes the Rayleigh fading channel between the PU and the sensing antennas of SU-Tx, $\mathbf{H}_{\rm si} \in \mathbb{C}^{M_{\rm s}\times M_{\rm t}}$ is the self-interference channel between the transmission and sensing antennas at the SU-Tx, $\mathbf{v}$ is assumed to be the $M_{\rm t}\times 1$ beamforming vector of the SU-Tx, $s_{\rm p}(n)\sim\mathcal{CN}(0,\sigma_{\rm p}^2)$ represents the PU's circularly symmetric complex Gaussian signal, $s_{\rm s}(n)\sim\mathcal{CN}(0,\sigma_{\rm s}^2)$ denotes the transmit signal of the SU-Tx and $\mathbf{u}(n)\sim\mathcal{CN}(0,\sigma_{\rm u}^2\mathbf{I}_{M_{\rm s}})$ represents the sample of a complex additive white Gaussian noise.

In order to evaluate the sensing performance of the system, two sets of sensing error probabilities have to be investigated in FD non-time-slotted CR networks, i.e., (1) the probability of false alarm with the active SU $P_{\rm fa,1}$ and with the inactive SU $P_{\rm fa,0}$; (2) the probability of missed detection with the active SU $P_{\rm m,1}$ and with the inactive SU $P_{\rm m,0}$. Assuming that the received signal samples at the sensing antennas of the SU-Tx are identical and independent distributed (i.i.d.) and the total sample number for the entire secondary frame N is relatively large, the statistical distributions of the test statistic for the ED $T_{\rm ED}$ can be obtained by applying the central limit theorem (CLT). Thus the related sensing error probabilities for the hypotheses mentioned above can be derived as follows.

Firstly, when the SU-Tx is active (under $\mathcal{H}_{10}$), the probability of false alarm $P_{\rm fa,1}$ is derived as

$$P_{\rm fa,1}(r_1)=\mathcal{Q}\left(\frac{M_{\rm s}^{\frac{1}{2}}\left(\frac{Nr_1}{\sigma_u^2}-a\gamma_{\rm sp}-N\chi^2\gamma_{\rm in}-N\right)}{\sqrt{a(\gamma_{\rm sp}+\chi^2\gamma_{\rm in}+1)^2+(N-a)(\chi^2\gamma_{\rm in}+1)^2}}\right), \tag{4}$$

where $\gamma_{\rm sp}=\frac{\sigma_{\rm p}^2\|\mathbf{h}_{\rm sp}\|^2}{M_{\rm s}\sigma_u^2}$ is the received signal-to-noise ratio (SNR), $\gamma_{\rm in}=\frac{\sigma_{\rm s}^2\|\mathbf{H}_{\rm si}\mathbf{v}\|^2}{M_{\rm s}\sigma_u^2}$ denotes the self-interference-to-noise ratio (INR) measured at the sensing antennas, $\|\cdot\|^2$ is the Frobenius norm operator and $\mathcal{Q}(\cdot)$ denotes the complementary cumulative distribution function of the normal distribution. It is worth noting that different decision thresholds r_0, r_1 are required for the spectrum sensing because of the self-interference. Specifically, r_0 is the decision threshold under the absence of SU's transmission $(\mathcal{H}_{00},\mathcal{H}_{01})$. r_1 denotes the decision threshold when the SU-Tx is transmitting $(\mathcal{H}_{10},\mathcal{H}_{11})$.

Secondly, when the SU-Tx is inactive (under $\mathcal{H}_{00}$), the probability of false alarm $P_{\rm fa,0}$ is given by

$$P_{\rm fa,0}(r_0)=\mathcal{Q}\left(\frac{M_{\rm s}^{\frac{1}{2}}\left(\frac{Nr_0}{\sigma_u^2}-a\gamma_{\rm sp}-N\right)}{\sqrt{a\gamma_{sp}^2+2a\gamma_{\rm sp}+N}}\right). \tag{5}$$

Thirdly, based on the statistical distributions of $T_{\rm ED}$ under the hypothesis $\mathcal{H}_{11}$, the probability of missed detection under the presence of the secondary transmission $P_{\rm m,1}$ is derived as

$$P_{\rm m,1}(r_1)=1-\mathcal{Q}\left(\frac{M_{\rm s}^{\frac{1}{2}}\left(\frac{Nr_1}{\sigma_u^2}-(N-b)\gamma_{\rm sp}-N\chi^2\gamma_{\rm in}-N\right)}{\sqrt{(N-b)(\gamma_{sp}+\chi^2\gamma_{\rm in}+1)^2+b(\chi^2\gamma_{\rm in}+1)^2}}\right). \tag{6}$$

Finally, the probability of missed detection when the SU is inactive, $P_{\rm m,0}$, is given by

$$P_{\rm m,0}(r_0)=1-\mathcal{Q}\left(\frac{M_{\rm s}^{\frac{1}{2}}\left(\frac{Nr_0}{\sigma_u^2}-(N-b)\gamma_{\rm sp}-N\right)}{\sqrt{(N-b)\gamma_{sp}^2+2(N-b)\gamma_{\rm sp}+N}}\right). \tag{7}$$

The closed-form expression of sensing errors mentioned above are derived for the multi-sensing-antenna ED based FD non-time-slotted system. Furthermore, it is worth to notice that these expressions can be simplified to be the probabilities of false alarm and missed detection for the time-slotted CR network, when $a=b=0$. This reveals that the time-slotted spectrum sensing system is a special case of the non-time-slotted system and the model studied in this paper is more generalized and practical. The detailed proof for the above expressions is provided in the appendix.

In order to analyse the total error rate and the optimal decision threshold of the spectrum sensing system, both the probabilities of false alarm $P_{\rm fa}$ and missed detection $P_{\rm m}$ of the whole system are necessary. Therefore, the expressions of $P_{\rm fa}$ and $P_{\rm m}$ should be investigated based on equations (4), (5), (6) and (7). The transitions between the states of PU and SU can be modelled as the discrete-time Markov chains which is shown in Fig. 3 in the next page. Note that the states of PU stand for *the actual statuses of the PU observed at the end of a secondary sensing frame*. Assuming P_{q_1,q_2} is the probability that the FD CR system remains at the state (q_1,q_2), where $q_1,q_2=\{0,1\}$ represent the states of the SU-Tx and the PU respectively, the relationship among various sensing error probabilities can be achieved by using the steady-state of the Markov chains as follows,

$$\begin{cases}P_{0,1}P_{\rm m,0}=P_{1,1}(1-P_{\rm m,1}),\\ P_{0,0}(1-P_{\rm fa,0})=P_{1,0}P_{\rm fa,1},\\ P_{0,0}+P_{1,0}=1,\\ P_{0,1}+P_{1,1}=1,\\ P_{\rm m}=P_{1,1},\\ P_{\rm fa}=P_{0,0}.\end{cases} \tag{8}$$

By solving the above system of equations, the probability of false alarm of the whole system $P_{\rm fa}$ is given by

$$P_{\rm fa}(r_0,r_1)=\frac{P_{\rm fa,1}(r_1)}{1-P_{\rm fa,0}(r_0)+P_{\rm fa,1}(r_1)}, \tag{9}$$

$$\alpha_1 = \sqrt{\frac{\left[(N-b)\gamma_{\rm sp}^2 + 2(N-b)\gamma_{\rm sp}(\chi^2\gamma_{\rm in}+1) + N(\chi^2\gamma_{\rm in}+1)^2\right]}{M_{\rm s}}}, \quad \alpha_0 = \sqrt{\frac{(N-b)\gamma_{\rm sp}^2 + 2(N-b)\gamma_{\rm sp} + N}{M_{\rm s}}}. \tag{12}$$

$$\beta_1 = \sqrt{\frac{a\gamma_{\rm sp}^2 + 2a\gamma_{\rm sp}(\chi^2\gamma_{\rm in}+1) + N(\chi^2\gamma_{\rm in}+1)^2}{M_{\rm s}}}, \quad \beta_0 = \sqrt{\frac{a\gamma_{\rm sp}^2 + 2a\gamma_{\rm sp} + N}{M_{\rm s}}}. \tag{14}$$

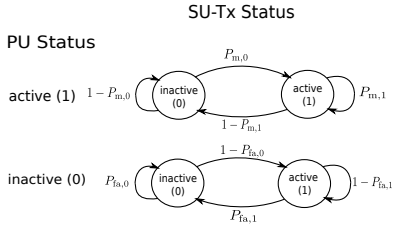

Fig. 3. The Markov chains of the activities of the PU and SU-Tx

and the probability of missed detection of the whole system is given by

$$P_{\rm m}(r_0, r_1) = \frac{P_{\rm m,0}(r_0)}{1 + P_{\rm m,0}(r_0) - P_{\rm m,1}(r_1)}. \tag{10}$$

B. Total Error Rate Analysis

In this subsection, the total error rate is investigated in order to consider the benefits of the PU and the SUs simultaneously. Since there exists two decision thresholds, i.e. r_0 and r_1, in the FD non-time-slotted spectrum sensing system, it is not easy to find the proper combination of r_0 and r_1. An exercisable and simple way is to obtain the appropriate combination of decision thresholds (r_0, r_1) based on the given $P_{\rm fa}$ or $P_{\rm m}$ and this will not affect the validity of the theoretical analyses.

Firstly, let us start with the scenario with a given probability of missed detection of the whole system $P_{\rm m}$. In practical applications, the probabilities of missed detection when the SU-Tx is silent $P_{\rm m,0}$ and active $P_{\rm m,1}$ should be guaranteed to be a similar value, so that there would be no gaps of the missed detection performance between the cases of active and inactive SU-Tx. According to this practical requirement, the probability of missed detection when the SU is transmitting is equal to the probability when the SU is silent, i.e., $P_{\rm m,1} = P_{\rm m,0}$. Then, from equation (10), it can be seen that $P_{\rm m,1} = P_{\rm m,0} = P_{\rm m}$.

Based on the above assumptions and analyses, the desired decision threshold r_1 for a given $P_{\rm m}$ (when the SU-Tx is active) can be derived as

$$r_1(P_{\rm m}) = \frac{\sigma_u^2}{N}\left(\mathcal{Q}^{-1}(1-P_{\rm m})\alpha_1 + (N-b)\gamma_{\rm sp} + N\chi^2\gamma_{\rm in} + N\right), \tag{11}$$

where α_1 is given by equation (12) at the top of this page. Thus, the corresponding false alarm rate $P_{\rm fa,1}$ when the SU is transmitting with respect to the given $P_{\rm m}$ can be obtained through (4) and (11) and is given by

$$P_{\rm fa,1}(P_{\rm m}) = \mathcal{Q}\left(\frac{\mathcal{Q}^{-1}(1-P_{\rm m})\alpha_1 + (N-b-a)\gamma_{\rm sp}}{\beta_1}\right), \tag{13}$$

where β_1 is given by equation (14) at the top of this page.

Meanwhile, when the SU-Tx is silent, the desired decision threshold r_0 for a given $P_{\rm m}$ can be obtained as

$$r_0(P_{\rm m}) = \frac{\sigma_u^2}{N}\left(\mathcal{Q}^{-1}(1-P_{\rm m})\alpha_0 + (N-b)\gamma_{\rm sp} + N\right), \tag{15}$$

where α_0 is shown by equation (12) at the top of this page. Thus, the corresponding probability of false alarm $P_{\rm fa,0}$ can be derived through (5) and (15) and is given by

$$P_{\rm fa,0}(P_{\rm m}) = \mathcal{Q}\left(\frac{\mathcal{Q}^{-1}(1-P_{\rm m})\alpha_0 + (N-b-a)\gamma_{\rm sp}}{\beta_0}\right), \tag{16}$$

where β_0 is given by equation (14) at the top of this page.

Herein, for a given probability of missed detection of the whole system $P_{\rm m}$, the desired decision threshold pair (r_0, r_1) can be obtained by equation (11) and (15) based on the above derivations.

Secondly, the scenario with a given probability of false alarm of the whole system $P_{\rm fa}$ is considered. Similarly, a practical assumption is $P_{\rm fa,0} = P_{\rm fa,1}$, so it can be seen from equation (9) that $P_{\rm fa} = P_{\rm fa,0} = P_{\rm fa,1}$. Therefore, when the SU-Tx is active, the desired decision threshold r_1 for a given $P_{\rm fa}$ is given by

$$r_1(P_{\rm fa}) = \frac{\sigma_u^2}{N}\left(\mathcal{Q}^{-1}(P_{\rm fa})\beta_1 + a\gamma_{\rm sp} + N\chi^2\gamma_{\rm in} + N\right). \tag{17}$$

By using equation (6) and (17), the corresponding probability of missed detection $P_{\rm m,1}$ can be represented with regard to the desired $P_{\rm fa}$ and is given by

$$P_{\rm m,1}(P_{\rm fa}) = 1 - \mathcal{Q}\left(\frac{\mathcal{Q}^{-1}(P_{\rm fa})\beta_1 + (a+b-N)\gamma_{\rm sp}}{\alpha_1}\right). \tag{18}$$

When the SU-Tx is silent, the desired decision threshold r_0 for a given $P_{\rm fa}$ is derived as

$$r_0(P_{\rm fa}) = \frac{\sigma_u^2}{N}\left(\mathcal{Q}^{-1}(P_{\rm fa})\beta_0 + a\gamma_{\rm sp} + N\right). \tag{19}$$

Then, the closed-form expression of the corresponding probability of missed detection $P_{\rm m,0}$ with regard to $P_{\rm fa}$ can be derived with the aid of equation (7) and (19), which is shown as

$$P_{\rm m,0}(P_{\rm fa}) = 1 - \mathcal{Q}\left(\frac{\mathcal{Q}^{-1}(P_{\rm fa})\beta_0 + (a+b-N)\gamma_{\rm sp}}{\alpha_0}\right). \tag{20}$$

Therefore, in a multi-antenna ED based FD spectrum sensing system, the desired decision threshold pair (r_0, r_1) based on a given probability of false alarm of the whole system $P_{\rm fa}$ can be obtained through equations (17) and (19).

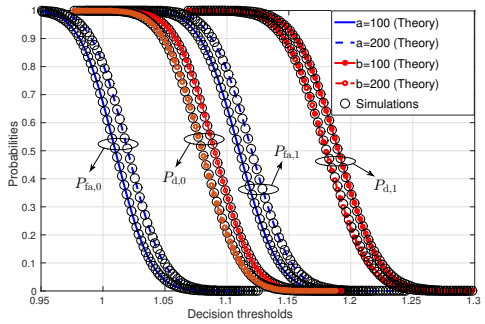

Fig. 4. The sensing performances under the hypotheses $\mathcal{H}_{11}, \mathcal{H}_{10}, \mathcal{H}_{01}$ and $\mathcal{H}_{00}$.

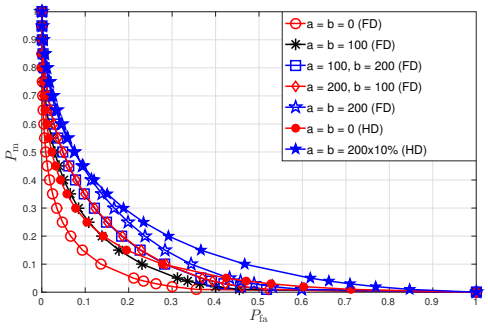

Fig. 5. The ROC curves of the FD spectrum sensing system and the comparison with the HD system.

In order to consider the benefits of both the PU and SUs, the total error rate of the whole system P_{te} is defined as

$$P_{\mathrm{te}}(r_0, r_1) = P_{\mathrm{fa}}(r_0, r_1)P(\mathcal{H}_0) + P_{\mathrm{m}}(r_0, r_1)P(\mathcal{H}_1), \quad (21)$$

where $P(\mathcal{H}_0)$ denotes the probability that the PU is actually idle and $P(\mathcal{H}_1)$ represents the probability that the PU is actually busy. One significant step and objective during the FD spectrum sensing process is determining the decision threshold pair. The optimal decision threshold pair can minimize the total error rate of the system and is formulated as

$$(r_0, r_1)_{\mathrm{opt}} = \arg\min_{r_0, r_1} P_{\mathrm{fa}}(r_0, r_1) + P_{\mathrm{m}}(r_0, r_1). \quad (22)$$

This optimal decision threshold pair can be obtained by using the derived equations in this section. It should be noted that this optimization issue can be investigated under the two different scenarios mentioned above, including the cases of a given P_{m} and P_{fa}.

IV. Simulation Results and Discussions

In this section, the simulation and theoretical results are provided to validate the derived expressions and analyses throughout this paper. The comparison with the traditional HD sensing system is also provided based on the non-time-slotted model. In the simulation results, the SU-Tx has 4 antennas, including the sensing antennas $M_{\mathrm{s}} = 2$ and the transmission antennas $M_{\mathrm{t}} = 2$. The total sample number for one periodic secondary frame is $N = 1000$. Various values of a and b are assumed because of the non-time-slotted model. The SIS factor χ can vary from 0.1 to 0.3. The received SNR at the sensing antennas of the SU-Tx is $\gamma_{\mathrm{sp}} = -10\mathrm{dB}$ and the recieved INR is $\gamma_{\mathrm{in}} = 10\mathrm{dB}$.

Fig. 4 verifies the derived expressions of sensing error rates under different hypotheses $\mathcal{H}_{10}, \mathcal{H}_{11}, \mathcal{H}_{01}, \mathcal{H}_{00}$. Specifically, this figure represents the probabilities of false alarm and missed detection when the SU-Tx is active and inactive under the condition $\chi = 0.1$. Note that $P_{\mathrm{d},1} = 1 - P_{\mathrm{m},1}, P_{\mathrm{d},0} = 1 - P_{\mathrm{m},0}$ are plotted instead of $P_{\mathrm{m},1}, P_{\mathrm{m},0}$ for the convenience of plotting. The Monte-Carlo simulation results match the theoretical results very well. Besides, comparing the results under different a and b, it can be seen that the sensing performance will degrade with the increase of a and b for every hypothesis mentioned above. Since large values of a and b imply that the PU changes its state late within one periodic secondary frame, a large number of samples that affect the sensing performance would be received.

The receiver operating characteristic (ROC) curves are depicted in Fig. 5 to show the sensing performance of the FD CR system under different conditions when $\chi = 0.3$. From this figure, it can be deduced that the sensing performance of the whole system will degrade with the increase of the summation of a and b, i.e., $a + b$. Besides, when $a + b$ is constant, the sensing performance of the FD non-time-slotted CR system is similar no matter what the specific values of a and b are. For instance, this system has a similar sensing performance when $a = 100, b = 200$ and $a = 200, b = 100$. In addition, it can be seen from the comparison with the HD spectrum sensing approach that the FD can achieve a better sensing performance based on the multi-sensing-antenna ED in the non-time-slotted CR network, since more received signal samples can be accumulated by employing FD technique. In order to ensure a fair comparison, the parameter settings for the HD sensing system in this figure are as follows. The number of the antennas at the SU-Tx for the HD system is $M = M_{\mathrm{s}} + M_{\mathrm{t}} = 4$ and the ratio between the sensing time τ and one periodic secondary frame duration T is $\kappa = \frac{\tau}{T} = 10\%$, since a large κ would degrade the throughput of the secondary network severely in the HD system. Specifically, a reasonable comparison is between the sensing performances of $a = b = q$ for the FD system and $a = b = q \times \kappa$ for the HD system.

Finally, the total error rate of the system is presented in Fig. 6 versus the different decision threshold pairs under different system conditions. The scenario of a given probability of missed detection is considered and $\chi = 0.3$. The probabilities that PU is absent and present actually are assumed as $P(\mathcal{H}_0) = 0.8$, $P(\mathcal{H}_1) = 0.2$, since the PU would not occupy the licensed frequency bands at a high probability in practical applications. The total error rate of the system increases with the increasing $a + b$, since more signal samples with negative effects are received for spectrum sensing. Meanwhile, it can be

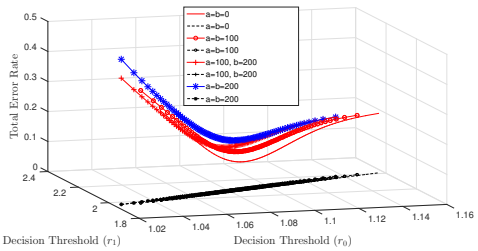

Fig. 6. The total error rate of the system $P_{\rm te}$ V.S. the decision threshold pair (r_0, r_1) (The dashed black lines on x-y plane are the projections of the original total error rate curves).

also seen from this figure that the total error rate of the system is a quasi-convex function with regard to the decision threshold pairs. This implies that there exists one and only one optimal decision threshold pair to minimize the total error rate. Therefore, the optimal decision threshold pair can be obtained by using the derived equations in the last section. Specifically, the optimal decision threshold pairs $(r_0, r_1)_{\rm opt}$ are $(1.086, 1.974)$, $(1.084, 1.980)$, $(1.080, 1.980)$ and $(1.085, 1.990)$ for the cases of $(a = b = 0), (a = b = 100), (a = 100, b = 200)$ and $(a = b = 200)$, respectively. Meanwhile, the corresponding minimum total error rates are $0.09, 0.12, 0.14$ and 0.16.

V. Conclusions

This paper investigated the non-time-slotted FD spectrum sensing system based on the ED with multiple sensing antennas. Firstly, the generalized theoretical expressions of the probabilities of false alarm and missed detection were derived when considering the asynchronism between the primary and secondary networks. Secondly, in order to benefit both the PU and SUs, the total error rate of the system was studied and the optimal decision threshold pairs were obtained to minimize the total error rate. The SU-Tx may transmit or keep silent, so a decision threshold pair (r_0, r_1) was necessary for the two different states of the SU-Tx. The expressions of r_0 and r_1 were also obtained for a given sensing error rate of the system $P_{\rm m}$ and $P_{\rm fa}$. Finally, from our results, the spectrum sensing performance of the proposed FD technique outperformed the traditional HD approach based on the non-time-slotted model due to the longer sensing time and improved SIS capability. Furthermore, the obtained optimal decision threshold pairs minimized the total error rates, which considered the interests of the PU and SUs simultaneously.

Appendix
Proof of the Eqs. (4), (5), (6) and (7)

In order to obtain the expressions of sensing error rates under different hypotheses, the distributions of the test statistic $T_{\rm ED}$ have to be derived under the hypotheses $\mathcal{H}_{10}, \mathcal{H}_{00}, \mathcal{H}_{11}, \mathcal{H}_{01}$. When the total sample size of the received signal N is relatively large, these distributions could be modelled as normal distribution by using CLT. Therefore, the objective for this derivation is to derive the expectation and variance of $T_{\rm ED}$.

In non-time-slotted FD CR system, the PU may have two different states s1 and s2 within one periodic secondary sensing frame. Assuming the received sample sizes for the state s1, s2 are A, B respectively. Then, the expectation and variance of $T_{\rm ED}$ can be given by

$$\begin{aligned}\mathbb{E}[T_{\rm ED}] &= \frac{A}{N}\mathbb{E}[|y_i(n)|^2_{\rm s1}] + \frac{B}{N}\mathbb{E}[|y_i(n)|^2_{\rm s2}] \\ &= \frac{A}{N}\sigma^2_{y,{\rm s1}} + \frac{B}{N}\sigma^2_{y,{\rm s2}}, \qquad (23)\\ {\rm Var}[T_{\rm ED}] &= \frac{A}{M_{\rm s}N^2}{\rm Var}[|y_i(n)|^2_{\rm s1}] + \frac{B}{M_{\rm s}N^2}{\rm Var}[|y_i(n)|^2_{\rm s2}] \\ &= \frac{A}{M_{\rm s}N^2}\sigma^4_{y,{\rm s1}} + \frac{B}{M_{\rm s}N^2}\sigma^4_{y,{\rm s2}}. \qquad (24)\end{aligned}$$

Under $\mathcal{H}_{10}$, from the equation (3), we can obtain

$$\sigma^2_{y,{\rm s1}} = (\gamma_{\rm sp} + \chi^2\gamma_{\rm in} + 1)\sigma^2_u, \quad \sigma^2_{y,{\rm s2}} = (\chi^2\gamma_{\rm in} + 1)\sigma^2_u. \quad (25)$$

By substituting the equation (25) into (23) and (24), the expressions of $\mathbb{E}[T_{\rm ED}]$ and ${\rm Var}[T_{\rm ED}]$ under $\mathcal{H}_{10}$ can be obtained. Then, by using the CLT and $P_{{\rm fa},1}(x) = \Pr\{T_{\rm ED} > x|\mathcal{H}_{10}\}$, the equation (4) can be derived.

Meanwhile, the distributions under $\mathcal{H}_{00}, \mathcal{H}_{11}, \mathcal{H}_{01}$ can be obtained in the same way and equations (5), (6) and (7) can be obtained by taking similar steps.

References

[1] S. Haykin, "Cognitive radio: Brain-empowered wireless communications," *IEEE J. Sel. Areas Commun.*, vol. 23, no. 2, pp. 201–220, February 2005.

[2] M. Kiessling and J. Speidel, "Mutual information of MIMO channels in correlated Rayleigh fading environments−a general solution," in *IEEE ICC*, June 2004.

[3] J. I. Choi, M. Jain, K. Srinivasan, P. Levis, and S. Katti, "Achieving single channel, full duplex wireless communication," in *ACM MobiCom*, September 2010.

[4] A. S. *et al.*, "In-band full-duplex wireless: Challenges and opportunities," *IEEE J. Sel. Areas Commun.*, vol. 32, no. 9, pp. 1637–1652, September 2014.

[5] Y. He, T. Ratnarajah, E. H. G. Yousif, J. Xue, and M. Sellathurai, "Performance analysis of multi-antenna GLRT-based spectrum sensing for cognitive radio," *Signal Processing*, vol. 120, pp. 580–593, March 2016.

[6] Y. C. Liang, Y. Zeng, E. C. Peh, and A. T. Hoang, "Sensing-throughput tradeoff for cognitive radio networks," *IEEE Trans. Wireless Commun.*, vol. 7, no. 4, pp. 1326–1337, April 2008.

[7] J. Heo, H. Ju, S. Park, E. Kim, and D. Hong, "Simultaneous sensing and transmission in cognitive radio," *IEEE Trans. Wireless Commun.*, vol. 13, no. 4, pp. 1948–1959, April 2014.

[8] T. Wang, Y. Liao, B. Zhang, and L. Song, "Joint spectrum access and power allocation in full-duplex cognitive cellular networks," in *IEEE ICC*, June 2015.

[9] T. Riihonen and R. Wichman, "Energy detection in full-duplex cognitive radios under residual self-interference," in *IEEE CROWNCOM*, June 2014.

[10] W. Cheng, X. Zhang, and H. Zhang, "Full-duplex spectrum-sensing and MAC-protocol for multichannel nontime-slotted cognitive radio networks," *IEEE J. Sel. Areas Commun.*, vol. 33, no. 5, pp. 820–831, May 2015.

[11] D. C. Oh and Y. H. Lee, "Energy detection based spectrum sensing for sensing error minimization in cognitive radio networks," *International Journal of Communication Networks and Information Security*, vol. 1, no. 1, pp. 1–5, April 2009.

2015 IEEE 26th International Symposium on Personal, Indoor and Mobile Radio Communications - (PIMRC): Mobile and Wireless Networks

Optimization of Multi-antenna GLRT-Based Spectrum Sensing for Cognitive Radio

Yibo He †, T. Ratnarajah †, E. H. G. Yousif †, J. Xue † and M. Sellathurai §
† IDCOM, The University of Edinburgh, Kings Buildings, Edinburgh, EH9 3JL, U.K.
§ School of Engineering & Physical Sciences, Heriot-Watt University, U.K.

***Abstract*—This paper investigates the optimization of the generalized likelihood ratio test (GLRT) eigenvalue-based spectrum sensing detector in terms of decision thresholds and sensing time. In order to guarantee the interests of primary and secondary users simultaneously, the sensing performance is assessed using the total error rate, i.e., the summation of probabilities of false alarm and missed detection. Therefore, the generalized statistical distributions of the test statistic are derived under the absence and presence of primary users, assuming an arbitrary number of receive antennas. These distributions are necessary for the analyses of the total error rate performance and the optimization. The optimization consists of two parts. Firstly, the optimal decision threshold is numerically obtained, which can minimize the total error rate under the constraints of target probabilities of false alarm and missed detection. Secondly, the optimal sensing time is obtained when a target total error rate is guaranteed, so that the spectrum sensing process can be accelerated without the loss of sensing accuracy. Furthermore, the simulation and theoretical results reveal that the chosen optimal decision thresholds benefit the primary and secondary users simultaneously and the chosen optimal sensing time improves the speed of spectrum sensing.**

***Index Terms*—Complex Wishart matrices, generalized likelihood ratio test, optimization, spectrum sensing, total error rate.**

I. Introduction

Approaches for dynamic spectrum reuse has been widely investigated in order to cope with the problem of spectrum scarcity. One promising technology is cognitive radio (CR), which allows unlicensed/secondary users (SUs) to take advantage of spectrum holes. However, during exploitation of spectrum holes, licensed/primary users (PUs) should be protected from any harmful interference caused by SUs. Therefore, reliable spectrum sensing techniques are essential and crucial to the implementation of cognitive radio systems or other CR-based derivatives, such as licensed shared access (LSA) [1].

In particular, eigenvalue-based spectrum sensing can detect spectrum holes accurately without much prior knowledge about the primary signal and is robust to the noise uncertainty. In order to analyze the total error rate performance, the optimal decision threshold and the optimal sensing time for the GLRT eigenvalue-based detector, closed form expressions for the probabilities of false alarm and missed detection are both required. However, most literature, e.g., [2]–[5], have mainly focused on probability of false alarm only, which only considers from the perspective of SUs. Thus, the benefits of PUs were neglected in the literature work. In addition, the exact probability density function (PDF) of the test statistic assuming the presence of PUs, was derived in [5] for the GLRT detector. However, this result in [5] is only valid for the special case of 2 receive antennas. Also, the exact expression of the probability of false alarm provided in [5] is with high computational complexity. The optimization of the cooperative sensing with energy detector was studied in [6], but the energy detector was sensitive to noise uncertainty. Therefore, the aforementioned issues form our major motivation to investigate the generalized asymptotic behavior of the GLRT-based detector assuming an arbitrary number of receive antennas. A low probability of false alarm can make the SUs have more chances to access idle frequency bands. However, the benefits of PUs can not be guaranteed simultaneously, which is related to probability of missed detection. A low probability of missed detection can protect the PU from harmful interference. Meanwhile, according to the IEEE 802.22 standard for Wireless Regional Area Networks (WRANs), the SUs should vacate the licensed frequency band as soon as possible once the PU is active.

In this paper, the optimality of the decision threshold and sensing time for the GLRT detector is investigated, which guarantees the interests of PUs and SUs concurrently as well as the speed of spectrum sensing. we derive the asymptotic generalised closed form expressions of probabilities of false alarm and missed detection for the GLRT-based detector. Meanwhile, the expressions of the decision threshold with regard to the probabilities of false alarm and detection are also derived. Furthermore, in order to guarantee the interests of PUs and SUs simultaneously and accelerate the sensing process, we propose an efficient algorithm to obtain the optimal decision threshold and the optimal sensing time, which makes the minimum total error rate achieve the target value most speedily.

The remainder of this paper is organized as follows. Section II describes the considered system model. Section III derives the distributions of the test statistic for the GLRT detector. Section IV analyzes the optimality of the decision threshold and the sensing time. Section V presents simulation results and finally section VI concludes this paper.

II. System Model

Let us consider a spectrum sensing scenario which consists of a sensing node with m receive antennas. The PU is assumed to be equipped with single antenna, and each of the transmitted

This work is supported by the Seventh Framework Programme for Research of the European Commission under grant number ADEL-619647.

978-1-4673-6782-0/15/$31.00 ©2015 IEEE

2015 IEEE 26th International Symposium on Personal, Indoor and Mobile Radio Communications - (PIMRC): Mobile and Wireless Networks

signal is assumed to have a length of n samples, where $n > m$. The notations $\mathcal{H}_0$ and $\mathcal{H}_1$ denote the null hypothesis (PU is absent) and the alternate hypothesis (PU is present) respectively. During the sensing period, the matrix of received signal samples, $\mathbf{Y} \in \mathbb{C}^{m\times n}$, by the secondary receiver is

$$\mathcal{H}_0 : \mathbf{Y} = \mathbf{V}, \tag{1a}$$
$$\mathcal{H}_1 : \mathbf{Y} = \mathbf{h}\mathbf{x}^\dagger + \mathbf{V}, \tag{1b}$$

where $\mathbf{V} \in \mathbb{C}^{m\times n}$ represents the samples from a circular symmetric complex additive white Gaussian noise (AWGN) process and $\mathbf{V} \sim \mathcal{CN}\left(\mathbf{0}, \sigma_v^2\mathbf{I}_m \otimes \mathbf{I}_n\right)$, $\mathbf{x} \in \mathbb{C}^{n\times 1}$ consists of the transmitted signal samples which are assumed to be circularly symmetric complex Gaussian variables and $\mathbf{x} \sim \mathcal{CN}(\mathbf{0}, \sigma_x^2\mathbf{I}_n)$. Finally, $\mathbf{h} \in \mathbb{C}^{m\times 1}$ is the vector of channel gain. Henceforth, the covariance matrix of $\mathbf{Y}$, $\mathbf{R}_{yy} \triangleq \mathbb{E}[\mathbf{Y}\mathbf{Y}^\dagger]$, is given by

$$\mathcal{H}_0 : \quad \mathbf{R}_{yy} = \sigma_v^2\mathbf{I}_m, \tag{2a}$$
$$\mathcal{H}_1 : \quad \mathbf{R}_{yy} = \sigma_x^2\mathbf{h}\mathbf{h}^\dagger + \sigma_v^2\mathbf{I}_m. \tag{2b}$$

Within the sensing duration of n samples, the sample covariance matrix estimated from $\mathbf{Y}$ is $\widehat{\mathbf{R}}_{yy} = \frac{1}{n}\mathbf{Y}\mathbf{Y}^\dagger$. $\mathbf{W} \in \mathbb{C}^{m\times m}$ is the complex Wishart matrix given by $\mathbf{W} = n\widehat{\mathbf{R}}_{yy} = \mathbf{Y}\mathbf{Y}^\dagger$. $\hat{\lambda}_{\min} = \hat{\lambda}_m < \cdots < \hat{\lambda}_1 = \hat{\lambda}_{\max}$ are the ordered eigenvalues that are estimated from $\widehat{\mathbf{R}}_{yy}$. The decision statistic for the GLRT detector is given by

$$T_{\mathrm{GLRT}} = \frac{\hat{\lambda}_{\max}}{\sum_{i=1}^{m}\hat{\lambda}_i}. \tag{3}$$

For a predetermined decision threshold r, the probability of false alarm P_{fa} and the probability of missed detection P_{m} are defined as

$$P_{\mathrm{fa}}(r) = \mathrm{Prob}\big[T_{\mathrm{GLRT}} > r|\mathcal{H}_0\big] = \int_r^\infty f_0(t)\,\mathrm{d}t, \tag{4}$$
$$P_{\mathrm{m}}(r) = \mathrm{Prob}\big[T_{\mathrm{GLRT}} < r|\mathcal{H}_1\big] = \int_{-\infty}^r f_1(t)\,\mathrm{d}t, \tag{5}$$

where $f_0(t)$ and $f_1(t)$ denote the PDFs of the test statistic T_{GLRT} under the hypotheses $\mathcal{H}_0$ and $\mathcal{H}_1$. The total error rate is defined as the summation of the probabilities of false alarm and missed detection, i.e.,

$$P_{\mathrm{te}}(r) = P_{\mathrm{fa}}(r) + P_{\mathrm{m}}(r). \tag{6}$$

III. Distributions on The GLRT Detector

In order to investigate the total error rate and the optimality of decision thresholds and the sensing time, we derive the generalized closed form expressions of the PDF of T_{GLRT} and the probabilities of false alarm and missed detection when $n \gg m$ in this section.

A. Statistical Distributions Under the Hypothesis $\mathcal{H}_0$

Considering the null hypothesis $\mathcal{H}_0$, an asymptotic expression of the PDF of the test statistic T_{GLRT} is presented in the following theorem.

Theorem 1 (PDF of the Test Statistic of the GLRT Eigenvalue Detector under $\mathcal{H}_0$): Given the complex central uncorrelated Wishart matrix $\mathbf{W} \sim \mathcal{CW}_m(n, \sigma_v^2\mathbf{I}_m)$, where $m \ll n$, then the PDF of $T_{\mathrm{GLRT}} = \frac{\hat{\lambda}_{\max}}{\sum_{i=1}^{m}\hat{\lambda}_i}$ is given by

$$f_{\mathrm{GLRT}}^{(0)}(x) = \frac{\Gamma(mn)c^{1-mn}}{\Gamma(mn-d)\Gamma(d)}x^{d-1}(c-x)^{mn-d-1}, \tag{7}$$

where $\frac{1}{m} \le x \le 1$, $\Gamma(\cdot)$ denotes the Gamma function, c and d are given by

$$c = \frac{0.8132b^2}{a - 1.7711b}, \quad d = \frac{(a-1.7711b)^2}{0.8132b^2}, \tag{8}$$

where a and b are defined as

$$a = (\sqrt{m}+\sqrt{n})^2, \quad b = (\sqrt{m}+\sqrt{n})\left(\sqrt{\frac{1}{m}}+\sqrt{\frac{1}{n}}\right)^{\frac{1}{3}}. \tag{9}$$

Proof: The test statistic T_{GLRT} can be rewritten as

$$T_{\mathrm{GLRT}} = \frac{1}{m}\frac{m\hat{\lambda}_{\max}}{\sum_{i=1}^{m}\hat{\lambda}_i} = x. \tag{10}$$

Let $z = \frac{m\hat{\lambda}_{\max}}{\sum_{i=1}^{m}\hat{\lambda}_i}$ and $f_{\mathrm{S}}(z)$ denote the PDF of z, therefore $x = g(z) = \frac{z}{m}$ and the PDF of T_{GLRT} can be calculated by

$$f_{\mathrm{GLRT}}^{(0)} = \left.\frac{f_{\mathrm{S}}(z)}{\left|\frac{\mathrm{d}}{\mathrm{d}z}\left(g(z)\right)\right|}\right|_{z=mx}, \tag{11}$$

where the expression of $f_{\mathrm{S}}(z)$ is referred in [7]. After further calculations, the expression of (7) can be obtained. ■

By calculating the integral of equation (7) in the previous theorem and utilizing the definition in (4), the asymptotic expression of the probability of false alarm P_{fa} is given by

$$P_{\mathrm{fa}}(x) = 1 - \frac{\Gamma(mn)(mc)^{-d}}{d\Gamma(mn-d)\Gamma(d)}\left(\mathbf{\Delta}(x) - \mathbf{\Delta}\left(\frac{1}{m}\right)\right), \tag{12}$$

where $\frac{1}{m} \le x \le 1$ and $\mathbf{\Delta}(\cdot)$ is given by

$$\mathbf{\Delta}(y) = {}_2F_1\left(d, 1+d-mn; d+1; \frac{y}{c}\right)(my)^d, \tag{13}$$

where ${}_2F_1(.,.;.;.)$ denotes the Gaussian hypergeometric function.

Hence, for a complex Gaussian signal, the decision threshold r with respect to the probability of false alarm can be calculated from (14) (at the top of next page), where $I^{-1}(z,x,y)$ represents the inverse regularised incomplete Beta function $I_z^{-1}(x,y)$. The proof of (14) is omitted here because of the space limitation.

B. Statistical Distributions Under The Hypothesis $\mathcal{H}_1$

Assuming the system under the alternate hypothesis $\mathcal{H}_1$, we have $\mathbf{W} \sim \mathcal{CW}_m(n, \mathbf{\Sigma}_m)$, where $\mathbf{\Sigma}_m = \sigma_x^2\mathbf{h}\mathbf{h}^\dagger + \sigma_v^2\mathbf{I}_m$.

Theorem 2 (PDF of the Test Statistic of the GLRT Eigenvalue Detector under $\mathcal{H}_1$): Given the complex central correlated Wishart matrix $\mathbf{W} \sim \mathcal{CW}_m(n, \mathbf{\Sigma}_m)$, the PDF of the test statistic T_{GLRT} for GLRT detector is expressed as in (15)

2015 IEEE 26th International Symposium on Personal, Indoor and Mobile Radio Communications - (PIMRC): Mobile and Wireless Networks

$$r = cI^{-1}\left(\frac{\Gamma(mn)(mc)^{-d}}{d\Gamma(mn-d)\Gamma(d)}\left(\mathbf{\Delta}\left(\frac{1}{m}\right)+(1-P_{\rm fa})\frac{d\Gamma(mn-d)\Gamma(d)}{\Gamma(mn)(mc)^{-d}}\right), d, mn-d\right). \tag{14}$$

$$f^{(1)}_{\rm GLRT}(x) = \frac{(m-1)\left(1-\frac{1+m\gamma}{mn\gamma}\right)}{\sqrt{\frac{2\pi}{n}}(1+m\gamma)(1-x)^2}\exp\left(-\frac{n}{2}\left[\frac{x(m-1)}{1-x}\left(\frac{1}{1+m\gamma}-\frac{1}{mn\gamma}\right)-\left(1+\frac{m-1}{mn\gamma}\right)\right]^2\right), \tag{15}$$

$$r = \left(\frac{1}{2}\left(\sum_{k=0}^{\infty}\frac{C_k\sqrt{\beta}}{2k+1}\left[\frac{\sqrt{\pi}}{2}{\rm erf}\left(\alpha\sqrt{\beta}+\frac{1}{2(m-1)\beta}\right)+\sqrt{\pi}P_{\rm m}\right]^{2k+1}-\alpha\beta\right)^{-1}+1\right)^{-1}, \tag{20}$$

(at the top of this page), where $\gamma \triangleq \frac{\sigma_x^2\|\mathbf{h}\|^2}{m\sigma_v^2}$ is the average received SNR of the PU's signals at the secondary receiver.

Proof: The largest eigenvalue $\hat{\lambda}_{\max}$ of the sample covariance matrix follows a Gaussian distribution [8] under the hypothesis $\mathcal{H}_1$, which is given as $\hat{\lambda}_{\max} \sim \mathcal{N}\left(\lambda_{\max}+\frac{(m-1)\lambda_{\max}\sigma_v^2}{n(\lambda_{\max}-\sigma_v^2)}, \frac{\lambda_{\max}^2}{n}\right)$, where $\lambda_{\max}$ is the actual maximum eigenvalue of the actual covariance matrix $\mathbf{R}_{yy}$ under the hypothesis $\mathcal{H}_1$. Since the determinant of the actual covariance matrix $\det(\mathbf{R}_{yy}) = (\sigma_v^2)^{m-1}(\sigma_x^2\|\mathbf{h}\|^2+\sigma_v^2)$ and $\lambda_{\max}=\lambda_1>\lambda_2=\lambda_3=\cdots=\lambda_m$, it can be deduced that $\lambda_{\max}=\sigma_x^2\|\mathbf{h}\|^2+\sigma_v^2$.

The summation of the eigenvalues of the sample covariance matrix $\widehat{\mathbf{R}}_{\rm yy}$ excluding the maximum eigenvalue can be approximated as $\sum_{i=2}^{m}\hat{\lambda}_i \approx (m-1)\left(\sigma_v^2-\frac{\sigma_v^2\lambda_{\max}}{(\lambda_{\max}-\sigma_v^2)n}\right)=\psi$ [9]. The test statistic of the GLRT detector can be rewritten as

$$T_{\rm GLRT} = \frac{\hat{\lambda}_{\max}}{\sum_{i=1}^{m}\hat{\lambda}_i} = \frac{\hat{\lambda}_{\max}}{\hat{\lambda}_{\max}+\sum_{i=2}^{m}\hat{\lambda}_i} = x. \tag{16}$$

Thus, it can be obtained that $\hat{\lambda}_{\max}=\frac{x\psi}{1-x}$. Let $\hat{\lambda}_{\max}=z$ and $f_{\hat{\lambda}_{\max}}(z)$ denote the PDF of $\hat{\lambda}_{\max}$, then the generalized PDF of the test statistic $T_{\rm GLRT}$ under $\mathcal{H}_1$ can be derived through

$$f^{(1)}_{\rm GLRT}(x) = \left.\frac{f_{\hat{\lambda}_{\max}}(z)}{\left|\frac{\rm d}{{\rm d}z}\left(\frac{z}{z+\psi}\right)\right|}\right|_{z=\frac{x\psi}{1-x}}, \tag{17}$$

after further manipulations, the expression of the PDF of $T_{\rm GLRT}$ can be derived as (15). ■

By making use of the result from the previous theorem and the definition in (5), the asymptotic expression of the probability of missed detection $P_{\rm m}$ is derived as.

$$P_{\rm m}(x) = \frac{1}{2}\left[{\rm erf}\left(\alpha\sqrt{\beta}+\frac{x}{2\sqrt{\beta}(1-x)}\right) - {\rm erf}\left(\alpha\sqrt{\beta}+\frac{1}{2(m-1)\sqrt{\beta}}\right)\right], \tag{18}$$

where ${\rm erf}(y)=\frac{2}{\sqrt{\pi}}\int_0^y e^{-t^2}{\rm d}t$ denotes the error function, and α and β are given by

$$\alpha = n(m-1)\left(\frac{1}{mn\gamma}-\frac{1}{1+m\gamma}\right)\left(1+\frac{m-1}{mn\gamma}\right), \tag{19a}$$

$$\beta = \frac{1}{2n(m-1)^2}\left(\frac{1}{1+m\gamma}-\frac{1}{mn\gamma}\right)^{-2}. \tag{19b}$$

Besides, we also derive the expression for calculating the decision threshold in terms of the probability of missed detection, which is given by (20) (at the top of this page), where the coefficient $C_k = \begin{cases} 1, & k=0, \\ \sum_{i=0}^{k-1}\frac{C_iC_{k-1-i}}{(i+1)(2i+1)}, & \text{others.} \end{cases}$.

By utilizing the results derived in this section and the definition of total error rate in (6), the closed-form expression of total error rate is also obtained when the GLRT-based detector with an arbitrary number of receive antennas is employed.

IV. Optimization of The GLRT-Based Spectrum Sensing

By using the derived expressions of the decision threshold with regard to $P_{\rm fa}$ and $P_{\rm m}$, the decision threshold can be obtained for a target $P_{\rm fa}$ and $P_{\rm m}$, respectively. On the one hand, when a spectrum sensing system considers from the benefits of SUs, a constant false alarm rate (CFAR) is predetermined and the corresponding decision threshold can be obtained by (14). Under the CFAR requirement, the opportunities of accessing spectrum holes for SUs can be guaranteed. On the other hand, when the interests of PU are considered preferentially in demand, a constant detection rate (CDR) is assumed and the corresponding decision threshold can be calculated by (20). Under the CDR requirement, the PU can be well protected from harmful interference caused by SUs. However, in realistic applications, only considering each of the CFAR and CDR requirements is not comprehensive and fair enough, since the interests of PU and SUs can not be guaranteed simultaneously. Therefore, in this paper, we investigate the total error rate which considers the interests of PU and SUs together and this is of significance to the implementation of spectrum sensing.

In this section, we consider the optimization of the GLRT eigenvalue detector based on two criteria. First, we investigate the optimal decision threshold that can make the total error rate achieve the minimum value with constraints. Second, the optimal sensing time is analysed, which enables the minimum total error rate to achieve the desired value fast.

A. Optimal Decision Threshold Analysis

In this subsection, the optimal decision threshold is investigated in order to minimize the total error rate $P_{\rm te}$ with constraints. Specifically, the constraints are the desired probabilities of false alarm and missed detection. Let us assume

2015 IEEE 26th International Symposium on Personal, Indoor and Mobile Radio Communications - (PIMRC): Mobile and Wireless Networks

that the number of the receive antennas m, the width of the sensing windows n, and the average received SNR of the PU's signals measured at the secondary receiver γ are known. From the definition of the total error rate in (6), it can be seen that the total probability of error $P_{\rm te}(r)$ is a convex function and it has a global minimum value for r. Also, this implies that there exists one and only one value of r which minimizes $P_{\rm te}(r)$ with the target $P_{\rm fa}$ and $P_{\rm m}$ constraints. Therefore, the optimal decision threshold $r_{\rm opt}$ with constraints can be determined and is given by

$$r_{\rm opt} = \arg\min_{x} \; P_{\rm te}(x), \tag{21a}$$

$$\text{s.t.} \quad P_{\rm fa}(x) \le \xi_{\rm fa}, \tag{21b}$$

$$P_{\rm m}(x) \le \xi_{\rm m}, \tag{21c}$$

where $\xi_{\rm fa}$ and $\xi_{\rm m}$ are the desired values of $P_{\rm fa}$ and $P_{\rm m}$ respectively. When only each of the probability of false alarm $P_{\rm fa}$ and the probability of missed detection $P_{\rm m}$ achieves the desired value, the benefits of PUs and SUs can not be guaranteed concurrently. Therefore, in practical applications, it is essential to find an optimal decision threshold $r_{\rm opt}$ that minimizes the total error rate with target $P_{\rm fa}$ and $P_{\rm m}$ constraints. This can lead to the minimum total error rate and also make both $P_{\rm fa}$ and $P_{\rm m}$ meet the target values simultaneously.

The optimal decision threshold $r_{\rm opt}$ can be obtained numerically by utilizing the Karush-Kuhn-Tucker (KKT) conditions, then the optimization of the decision threshold can be reformulated as follow

$$(1+\eta_2) f^{(1)}_{\rm GLRT}(x) - (1+\eta_1) f^{(0)}_{\rm GLRT}(x) = 0, \tag{22a}$$

$$P_{\rm fa}(x) \le \xi_{\rm fa}, \tag{22b}$$

$$P_{\rm m}(x) \le \xi_{\rm m}, \tag{22c}$$

$$\eta_1 \left(P_{\rm fa}(x) - \xi_{\rm fa}\right) = 0, \tag{22d}$$

$$\eta_2 \left(P_{\rm m}(x) - \xi_{\rm m}\right) = 0, \tag{22e}$$

$$\eta_1, \eta_2 \ge 0, \tag{22f}$$

where η_1 and η_2 are the KKT multipliers.

B. Optimal Sensing Time Analysis

In this part, the optimal sensing time duration is investigated. Generally, a longer sensing time provides a larger number of received samples, which helps to achieve a better sensing performance to some extent. However, in real time, very long sensing periods may affect the speed of the spectrum sensing process. In order to address this issue, we propose an algorithm to get the optimal sensing time which can make the total error rate achieve the desired value speedily. Assuming that the average received SNR γ and the optimal decision threshold $r_{\rm opt}$ are known, the optimal sensing time $\tau_{\rm opt}$ can be determined, which can make the total error rate achieve the target bound, i.e., $P_{\rm te} \le \xi$.

For a given transmit signal, the sample frequency $f_{\rm s}$ is known. Due to the relationship between the sensing time and sample numbers, the optimal sample numbers should be determined first in order to obtain the optimal sensing time.

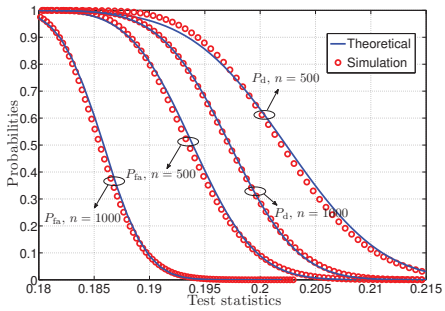

Fig. 1. The probabilities of false alarm and detection for the GLRT detector ($m = 6$) under various sample numbers ($n = 500, 1000$) and the received SNR is -15 dB

Let us define the objective function as a function of the number of samples n as

$$F(n, r_{\rm opt}) = P_{\rm te}(n, r_{\rm opt}) - \xi, \tag{23}$$

where $r_{\rm opt}$ is obtained by utilizing the method proposed in last subsection. The desired optimal number of samples $n_{\rm opt}$ should satisfy the conditions

$$F(n_{\rm opt}, r_{\rm opt}) \le 0, \tag{24}$$

$$F(n_{\rm opt} - 1, r_{\rm opt}) > 0, \tag{25}$$

where $n_{\rm opt}$ is the optimal sample size that enables $P_{\rm te}(n, r_{\rm opt}) \le \xi$. Hence, we get

$$n_{\rm opt} = \lceil n^* \rceil, \tag{26}$$

where $\lceil \cdot \rceil$ denotes the ceiling function and n^* is the first zero-crossing point of the curve $F(n, r_{\rm opt})$ with respect to n. By utilizing the relation between the sample size n and the sensing time τ, the desired sensing time can be obtained as $\tau_{\rm opt} = n_{\rm opt}/f_{\rm s}$. Therefore, the optimal sensing time $\tau_{\rm opt}$ can be used for a spectrum sensing process so that the speed of spectrum sensing can be improved and the desired total error rate can be also guaranteed at the same time.

V. Simulation and Theoretical Results

In this section, simulation and theoretical results are provided to validate the analyses on the considered detector. These results give an insight into the total error rate performance of the GLRT eigenvalue-based detector and also help to determine the optimal decision threshold and optimal sensing time investigated in last section.

Assuming that the SU is equipped with 6 receive antennas, i.e., $m = 6$, the closed form expressions of $P_{\rm fa}$ and $P_{\rm m}$ derived in this paper are verified in Fig. 1. It should be noted that the probability of detection $P_{\rm d} = 1 - P_{\rm m}$. The theoretical and Monte Carlo empirical curves are plotted for various cases of the sample size $n = \{500, 1000\}$. When the curves of $P_{\rm d}$ are presented, the average received SNR is assumed to be -15 dB. It can be seen from Fig. 1 that the theoretical results are matching the results from Monte-Carlo simulations. Therefore, we only show the theoretical results in the remaining part.

2015 IEEE 26th International Symposium on Personal, Indoor and Mobile Radio Communications - (PIMRC): Mobile and Wireless Networks

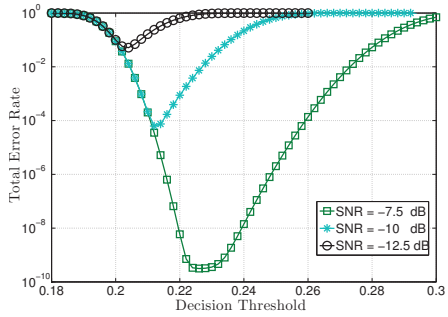

Fig. 2. The total error rate of the GLRT detector with multiple antennas under different received SNR: $m = 6, n = 500$.

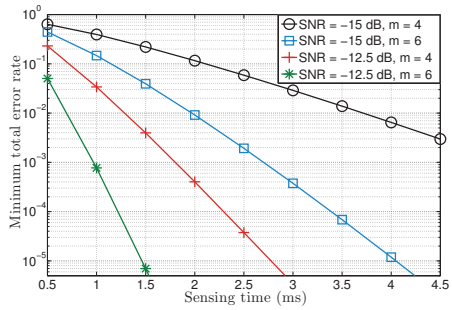

Fig. 3. The minimum total error rate versus sensing time of the GLRT detector with multi-antennas ($m = 4, m = 6$) under different values of the received SNR (γ = 15dB, γ = 12.5dB).

Fig. 2 depicts the total error rate versus the decision threshold under different received SNR scenarios when the number of receive antennas $m = 6$ and the sample size $n = 500$. It can be seen from this figure that the total error rate decreases first and then increases monotonously with the increasing decision thresholds. When the constraints of the target $P_{\rm fa}$ and $P_{\rm m}$ are given, the optimal decision thresholds can be obtained numerically by using the method described in Section IV-A. According to the IEEE 802.22 standard for WRANs [10], both $P_{\rm fa}$ and $P_{\rm m}$ should be under 0.1. Therefore, both the constraints of target $P_{\rm fa}$ and $P_{\rm m}$ are set at 0.1, i.e., $\xi_{\rm fa} = \xi_{\rm m} = 0.1$. Specifically, the optimal decision thresholds are $r_{\rm opt} = \{0.2034, 0.2127, 0.2259\}$ when the SNR is given by $\gamma = \{-12.5, -10, -7.5\}$ dB, respectively. It is found that the chosen decision thresholds obtained by our proposed algorithm can minimize the total error rate while $P_{\rm fa}$ and $P_{\rm m}$ are both under the target value 0.1. Therefore, the benefits of the PU and SUs are guaranteed concurrently even under very low SNR.

Fig. 3 presents the minimum total error rates with regard to different sensing time durations for the GLRT detector when $m = \{4, 6\}$ under very low SNRs $\gamma = \{-15, -12.5\}$ dB. It is found that the performance of the minimum total error rate tends to be better with the increasing number of receive antennas and the increasing sensing time. When the target minimum total error rate is set at 0.01, the optimal sensing time can be calculated by employing the algorithm introduced in Section IV-B. In detail, the optimal sensing time is $\tau_{\rm opt} = \{4.0, 2.0\}$ ms for $m = \{4, 6\}$ respectively when $\gamma = -15$ dB. Meanwhile, for $\gamma = -12.5$ dB, the optimal sensing time is $\tau_{\rm opt} = \{1.5, 1.0\}$ ms for $m = \{4, 6\}$ respectively. All these obtained optimal sensing time durations enable the minimum total error rates to achieve the target minimum total error rate speedily and efficiently.

VI. Conclusion

This paper investigated the total error rate and the optimization of the generalized case of the GLRT eigenvalue based detector with an arbitrary number of receive antennas. Initially, generalized asymptotic expressions of the probabilities of false alarm and missed detection were derived. Secondly, the optimal decision threshold was obtained by employing KKT conditions. The optimal decision threshold minimized the total error rate with the constraints of target probabilities of false alarm and missed detection, which could benefit primary and secondary users simultaneously. Finally, an algorithm was proposed to obtain the optimal sensing time for a target total error rate, which made the total error rate achieve the target value speedily. The results had shown that the chosen optimal decision thresholds minimized the total error rates while meeting the constraints on target probabilities of false alarm and missed detection. Meanwhile, the obtained optimal sensing time accelerated the spectrum sensing.

References

[1] CEPT-ECC, "Ecc report 205: Licensed shared access (LSA)," February 2014.

[2] T. Ratnarajah, C. Zhong, A. Kortun, M. Sellathurai, and C. B. Papadias, "Complex random matrices and multiple-antenna spectrum sensing," *IEEE International Conference on Acoustics, Speech and Signal Processing (ICASSP)*, May 2011.

[3] A. Kortun, T. Ratnarajah, M. Sellathurai, C. Zhong, and C. B. Papadias, "On the performance of eigenvalue-based cooperative spectrum sensing for cognitive radio," *IEEE Journal of Selected Topics in Signal Processing*, vol. 5, no. 1, pp. 49–55, February 2011.

[4] Y. Zeng and Y. C. Liang, "Eigenvalue-based spectrum sensing algorithms for cognitive radio," *IEEE Transactions on Communications*, vol. 57, no. 6, pp. 1784–1793, June 2009.

[5] A. Kortun, M. Sellathurai, T. Ratnarajah, and C. Zhong, "Distributionn of the ratio of the largest eigenvalue to the trace of complex Wishart matrices," *IEEE Transactions on Signal Processing*, vol. 60, no. 10, pp. 5527–5532, October 2012.

[6] W. Zhang, R. K. Mallik, and K. B. Letaief, "Optimization of cooperative spectrum sensing with energy detection in cognitive radio networks," *IEEE Transactions on Wireless Communications*, vol. 8, no. 12, pp. 5761–5766, December 2009.

[7] L. Wei and O. Tirkkonen, "Analysis of scaled largest eigenvalue based detection for spectrum sensing," *IEEE International Conference on Communications (ICC)*, June 2011.

[8] F. Haddadi, M. M. Mohammadi, M. M. Nayebi, and M. R. Aref, "Statistical performance analysis of MDL source enumeration in array processing," *IEEE Transactions on Signal Processing*, vol. 58, no. 1, pp. 452–457, January 2010.

[9] K. M. Wong, Q. Zhang, J. P. Reilly, and P. C. Yip, "On information theoretic criteria for determining the number of signals in high resolution array," *IEEE Transactions on Acoustics, Speech, And Signal Processing*, vol. 38, no. 11, pp. 1959–1971, November 1990.

[10] C. R. Stevenson, C. Cordeiro, E. Sofer, and G. Chouinard, "IEEE P802.22 wireless RANs functional requirements for the 802.22 WRAN standard doc.:IEEE 802.22-05/0007r46," pp. 1–49.

IEEE ICC 2015 - Workshop on Cooperative and Cognitive Networks (CoCoNet)

Cooperative Sensing Technique for Random Secondary Wireless Networks

Yibo He †, Jiang Xue †, Tharmalingam Ratnarajah † and Mathini Sellathurai §
† IDCOM, The University of Edinburgh, Kings Buildings, Edinburgh, EH9 3JL, U.K.
§ School of Engineering & Physical Sciences, Heriot-Watt University, U.K.

***Abstract*—This paper investigates the optimal number of collaborating secondary users which can minimize the total error rate (i.e., the summation of probabilities of missed detection and false alarm) for cooperative spectrum sensing when the secondary users follow Poisson point process (PPP). The received signal-to-noise ratios (SNRs) at secondary users can vary since the practical locations and the amount of secondary users are various. In order to cope with the diversity of received SNRs, a practical cooperative spectrum sensing system model is proposed based on the generalized likelihood ratio test (GLRT) detector. Firstly, the analytical expressions of the probabilities of false alarm and detection are derived. Secondly, an efficient cooperative spectrum sensing technique is proposed, which only requires the least amount of cooperative secondary users to achieve the minimum total error rate. Furthermore, the analytical results reveal the chosen optimal numbers of collaborating secondary users can achieve the best spectrum sensing performance.**

***Index Terms*—Cooperative spectrum sensing, generalized likelihood ratio test detector, optimization, Poisson point process.**

I. Introduction

The spectrum scarcity has been a major issue due to conflicts between the dramatic increase of the demand for the wireless communication services and the fixed spectrum allocation policy. One of the promising solutions to the spectrum scarcity is cognitive radio which allows the unlicensed/secondary users (SUs) to occupy the spectrum holes when licensed/primary users (PUs) are inactive. Meanwhile, during the exploitation of spectrum holes, SUs should not cause harmful interference to PUs. Therefore, a reliable spectrum sensing technique is essential and crucial to the implementation of cognitive radio system and other CR-based derivatives, such as licensed shared access (LSA) [1].

Cooperative spectrum sensing technique can improve the performance of the spectrum sensing system [2]. In this paper, we concentrate on the centralized cooperative spectrum sensing which makes a final decision on the status of the PU at a fusion center. Many different fusion strategies and sensing techniques were proposed to improve the performance of cooperative spectrum sensing [3]–[5]. The sensor selection method was investigated in [6] in order to obtain spatially independent sensors. In [7], the sensing throughput tradeoff of the secondary network was studied based on energy detector (ED). Meanwhile, PPP has been investigated [8] and applied to the random wireless network analysis [9].

This work is supported by the Seventh Framework Programme for Research of the European Commission under grant number ADEL-619647.

This paper investigates the optimization of cooperative spectrum sensing with the GLRT eigenvalue based detector assuming the SUs follow a PPP. Most of the previous work assume that the received SNRs at SUs are identical, but actually the received SNRs can vary depending on the locations of SUs in realistic situations. Meanwhile, the works in the literature mainly focus on the probability of false alarm, which only considers the interests of SUs. A low probability of false alarm can make SUs have more chances to access the spectrum holes, however, the benefits of PUs can not be guaranteed. It should be mentioned that the performance of the cooperative spectrum sensing with ED was investigated in [10] based on the constant detection rate (CDR) and the constant false alarm rate (CFAR) requirements when the SUs were distributed randomly. Besides, the optimization of cooperative spectrum sensing with ED was studied in [11] assuming the locations of SUs are identical and fixed. It is well-known that ED is affected seriously by the noise uncertainty, but the GLRT detector is robust. The aforementioned issues motivate us to investigate the total error rate performance and the optimality of cooperative spectrum sensing with the GLRT detector and random SUs, which considers the benefits of PU and SUs concurrently. The main contribution of this paper can be summarized as follows. Firstly, this paper derives the expressions of probabilities of false alarm and detection of the GLRT detector for each SU, which is required to analyse the total error rate. Secondly, an efficient cooperative spectrum sensing technique is proposed, which utilizes only a few, not all, SUs to achieve the minimum total error rate. Meanwhile, the optimal number of cooperating SUs is also studied, which enables the total error rate to achieve the minimum value.

The remainder of this paper is organized as follows. Section II describes the system model of cooperative spectrum sensing with PPP based on the GLRT detector. Section III derives the closed form expressions of the probabilities of detection and false alarm when utilizing the GLRT detector. Section IV investigates and finds the optimal number of collaborating SUs. Section V presents the analytical and simulation results and section VI concludes this paper.

II. System Model

We consider a centralised cooperative spectrum sensing system with decision fusion, which is shown as Fig. 1. The secondary users' base station (SBS) is the fusion center which is used to collect the decisions made by the SUs and make

978-1-4673-6305-1/15/$31.00 ©2015 IEEE

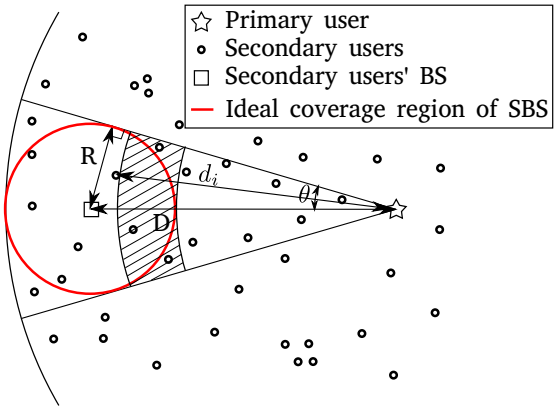

Fig. 1. The system model

a final decision. During the cooperative spectrum sensing process, each SU within the coverage radius of the SBS detects the status of the PU independently and then sends the detection result to the SBS. After that, the SBS gives a final decision on the status of the PU through an appropriate voting rule. The PU is assumed to be equipped with single antenna and each SU has multiple antennas.

A practical assumption is that the SUs are uniformly distributed on a 2-dimensional plane $\mathbb{R}^2$ based on a homogenous PPP with density ρ. According to Palm theory, the SUs located within the coverage radius of the SBS follow the same PPP. The coverage radius of the SBS is denoted by R and the distance between the SBS and the PU is represented by D. Since only the SUs within the coverage radius of the corresponding SBS can be collaborated together to detect the status of the PU, we only consider the SUs that are located within the area of interests in this paper. Assuming the transmitted signals between the PU and secondary network experience Rayleigh fading, the received signal power at ith SU can be given as

$$P_i = \frac{P_{\mathrm{T}}}{d_i^{\varepsilon}} h_i, \tag{1}$$

where h_i follows the Gamma distribution when maximal ratio combining (MRC) is used to achieve full diversity gain, i.e., $h_i \sim \Gamma(m,1)$, m is the number of receive antennas of each SU, P_{T} denotes the PU's signal power, d_i means the distance between the PU and the ith nearest SU from the PU and ε is the path loss exponent factor. The shadowing area in Fig. 1 is defined as the region whose distance is equal or greater than $D-R$ but less than $d_i - D + R$. The probability density function (PDF) of h_i can be written as

$$f_{h_i}(h) = \frac{h^{m-1} e^{-h}}{(m-1)!}. \tag{2}$$

The spectrum sensing between each SU and the PU is assumed to be a GLRT-based sensing system with m receive antennas. Let $\mathcal{H}_0$ (PU is absent) and $\mathcal{H}_1$ (PU is present) denote the null and the alternate hypotheses. During the sensing period, the matrix of received signal samples, $\mathbf{Y} \in \mathbb{C}^{m\times n}$, at the secondary receiver is

$$\mathcal{H}_0 : \mathbf{Y} = \mathbf{V}, \tag{3a}$$
$$\mathcal{H}_1 : \mathbf{Y} = \mathbf{h}\mathbf{x}^{\dagger} + \mathbf{V}, \tag{3b}$$

where n is the sample number, $\mathbf{V} \in \mathbb{C}^{m\times n}$ represents the samples of a complex additive white Gaussian noise, where $\mathbf{V} \sim \mathcal{CN}\left(\mathbf{0}, \sigma_v^2 \mathbf{I}_m \otimes \mathbf{I}_n\right)$, $\mathbf{x} = \mathbf{s} d^{-\frac{\varepsilon}{2}} \in \mathbb{C}^{n\times 1}$ (with mean $\mathbf{0}$ and variance $\sigma_x^2 \mathbf{I}_n$) consists of the transmitted signal samples $\mathbf{s}$ and path loss, $\mathbf{s} \in \mathbb{C}^{n\times 1}$ is assumed to be circularly symmetric complex Gaussian variable. Finally, $\mathbf{h} \in \mathbb{C}^{m\times 1}$ is the vector of channel gain. Henceforth, the covariance matrix of $\mathbf{Y}$, $\mathbf{R}_{yy} = \mathbb{E}[\mathbf{Y}\mathbf{Y}^{\dagger}]$, is given by

$$\mathcal{H}_0 : \quad \mathbf{R}_{yy} = \sigma_v^2 \mathbf{I}_m, \tag{4a}$$
$$\mathcal{H}_1 : \quad \mathbf{R}_{yy} = \sigma_x^2 \mathbf{h}\mathbf{h}^{\dagger} + \sigma_v^2 \mathbf{I}_m. \tag{4b}$$

Within the sensing duration of n samples, the sample covariance matrix estimated from $\mathbf{Y}$ is

$$\widehat{\mathbf{R}}_{yy} = \frac{1}{n}\mathbf{Y}\mathbf{Y}^{\dagger}. \tag{5}$$

Assuming $\mathbf{W} = n\widehat{\mathbf{R}}_{yy} = \mathbf{Y}\mathbf{Y}^{\dagger} \in \mathbb{C}^{m\times m}$ is a complex Wishart matrix. Also, let $\hat{\lambda}_{\min} = \hat{\lambda}_m < \cdots < \hat{\lambda}_1 = \hat{\lambda}_{\max}$ be the eigenvalues, in increasing order, estimated from $\widehat{\mathbf{R}}_{yy}$. The decision statistic for the GLRT-based eigenvalue detector is given by

$$T_{\mathrm{GLRT}} = \frac{\hat{\lambda}_{\max}}{\sum_{l=1}^{m} \hat{\lambda}_l}. \tag{6}$$

III. Distributions On The GLRT Detector

Both the probability of detection and the probability of false alarm of an individual SU are required to investigate the total error rate performance of the cooperative spectrum sensing system. Therefore, we derive the probability of detection $P_{\mathrm{d},i}$ and probability of false alarm $P_{\mathrm{fa},i}$ of the ith SU in this section.

Theorem 1: The closed-form expression of the probability of false alarm of ith SU using the GLRT detector with m receive antennas, i.e., $P_{\mathrm{fa},i}$, is given by

$$P_{\mathrm{fa},i}(r_i) = 1 - \frac{\Gamma(mn)(m\eta)^{-\omega}}{\omega\Gamma(mn-\omega)\Gamma(\omega)} \left(\mathbf{\Delta}(r_i) - \mathbf{\Delta}\left(\frac{1}{m}\right) \right), \tag{7}$$

where $\frac{1}{m} \le r_i \le 1$ denotes the decision threshold of ith SU and $\mathbf{\Delta}(\cdot)$ is defined by

$$\mathbf{\Delta}(y) = {}_2F_1\left(\omega, 1+\omega-mn; \omega+1; \frac{y}{\eta}\right)(my)^{\omega}, \tag{8}$$

where ${}_2F_1(.,.;.;.)$ denotes the Gaussian hypergeometric function. η and ω are given by

$$\eta = \frac{0.8132b^2}{a - 1.7711b}, \quad \omega = \frac{(a-1.7711b)^2}{0.8132b^2}, \tag{9}$$

$$r_i = \eta I^{-1}\left(\frac{\Gamma(mn)(m\eta)^{-\omega}}{\omega\Gamma(mn-\omega)\Gamma(\omega)}\left(\mathbf{\Delta}\left(\frac{1}{m}\right)+(1-P_{\mathrm{fa},i})\frac{\omega\Gamma(mn-\omega)\Gamma(\omega)}{\Gamma(mn)(m\eta)^{-\omega}}\right),\omega,mn-\omega\right). \quad (14)$$

$$f^{(1)}_{\mathrm{GLRT}}(x)=\frac{(m-1)\left(1-\frac{1+m\gamma_i}{mn\gamma_i}\right)}{\sqrt{\frac{2\pi}{n}}(1+m\gamma_i)(1-x)^2}\exp\left(-\frac{n}{2}\left[\frac{x(m-1)}{1-x}\left(\frac{1}{1+m\gamma_i}-\frac{1}{mn\gamma_i}\right)-\left(1+\frac{m-1}{mn\gamma_i}\right)\right]^2\right), \quad (20)$$

$$r_i=\left(\frac{1}{2}\left(\sum_{t=0}^{\infty}\frac{C_t\sqrt{\beta_i}}{2t+1}\left[\frac{\sqrt{\pi}}{2}\Phi\left(\alpha_i\sqrt{\beta_i}+\frac{1}{2(m-1)\beta_i}\right)+\sqrt{\pi}(1-P_{\mathrm{d},i})\right]^{2t+1}-\alpha_i\beta_i\right)^{-1}+1\right)^{-1}, \quad (21)$$

where a and b are defined as

$$a=\left(\sqrt{m}+\sqrt{n}\right)^2,\quad b=\left(\sqrt{m}+\sqrt{n}\right)\left(\sqrt{\frac{1}{m}}+\sqrt{\frac{1}{n}}\right)^{\frac{1}{3}}. \quad (10)$$

Proof: The test statistic T_{GLRT} can be rewritten as

$$T_{\mathrm{GLRT}}=\frac{1}{m}\frac{m\hat{\lambda}_{\max}}{\sum_{l=1}^{m}\hat{\lambda}_l}=x. \quad (11)$$

Let $z=\frac{m\hat{\lambda}_{\max}}{\sum_{l=1}^{m}\hat{\lambda}_l}$ and $f_{\mathrm{S}}(z)$ denote the PDF of z, therefore $x=g(z)=\frac{z}{m}$ and the PDF of T_{GLRT} can be calculated by

$$f^{(0)}_{\mathrm{GLRT}}(x)=\left.\frac{f_{\mathrm{S}}(z)}{\left|\frac{\mathrm{d}}{\mathrm{d}z}\left(g(z)\right)\right|}\right|_{z=mx}, \quad (12)$$

where the expression of $f_{\mathrm{S}}(z)$ is given in [12]. After further calculations, the expression of the PDF of the test statistic under $\mathcal{H}_0$ can be derived as

$$f^{(0)}_{\mathrm{GLRT}}(x)=\frac{\Gamma(mn)\eta^{1-mn}}{\Gamma(mn-\omega)\Gamma(\omega)}x^{\omega-1}(\eta-x)^{mn-\omega-1}, \quad (13)$$

where the parameters η and ω are obtained by utilizing Gamma distribution to approximate $\hat{\lambda}_{\max}$ [12]. After further integral calculation, the cumulative distribution function (CDF) of the decision threshold under the hypothesis $\mathcal{H}_0$ can be derived and the expression of (7) can be obtained. ■

Hence, for a complex Gaussian signal, the decision threshold r_i with respect to the probability of false alarm can be calculated from (14) at the top of this page, where $I^{-1}(.,.,.)$ represents the inverse regularised incomplete Beta function.

Theorem 2: The detection probability $P_{\mathrm{d},i}$ of the ith SU using the GLRT detector is derived as

$$P_{\mathrm{d},i}(r_i)=1-\frac{1}{2}\left[\Phi\left(\alpha_i\sqrt{\beta_i}+\frac{r_i}{2\sqrt{\beta_i}(1-r_i)}\right)-\Phi\left(\alpha_i\sqrt{\beta_i}+\frac{1}{2(m-1)\sqrt{\beta_i}}\right)\right], \quad (15)$$

where $\Phi(y)\triangleq\frac{2}{\sqrt{\pi}}\int_0^y e^{-t^2}\mathrm{d}t$ denotes the error function, α_i and β_i are given by

$$\alpha_i=n(m-1)\left(\frac{1}{mn\gamma_i}-\frac{1}{1+m\gamma_i}\right)\left(1+\frac{m-1}{mn\gamma_i}\right), \quad (16)$$

$$\beta_i=\frac{1}{2n(m-1)^2}\left(\frac{1}{1+m\gamma_i}-\frac{1}{mn\gamma_i}\right)^{-2}, \quad (17)$$

where γ_i denotes the average received SNR at the ith SU.

Proof: The test statistic in this paper is

$$T_{\mathrm{GLRT}}=\frac{\hat{\lambda}_{\max}}{\sum_{l=1}^{m}\hat{\lambda}_l}=\frac{\hat{\lambda}_{\max}}{\hat{\lambda}_{\max}+\sum_{l=2}^{m}\hat{\lambda}_l}=\frac{\frac{\hat{\lambda}_{\max}}{\sum_{l=2}^{m}\hat{\lambda}_l}}{\frac{\hat{\lambda}_{\max}}{\sum_{l=2}^{m}\hat{\lambda}_l}+1}. \quad (18)$$

Let $x=T_{\mathrm{GLRT}}$ and $z=\frac{\hat{\lambda}_{\max}}{\sum_{l=2}^{m}\hat{\lambda}_l}$, it can be obtained that $x=\frac{z}{z+1}$. The PDF of variable z, which is defined as $f_{\mathrm{G}}(z)$, is a Gaussian distribution [13]. Then the PDF of T_{GLRT} under $\mathcal{H}_1$ can be derived as

$$f^{(1)}_{\mathrm{GLRT}}(x)=\left.\frac{f_{\mathrm{G}}(z)}{\left|\frac{\mathrm{d}}{\mathrm{d}z}\left(\frac{z}{z+1}\right)\right|}\right|_{z=\frac{x}{1-x}}=(z+1)^2 f_{\mathrm{G}}(z)\big|_{z=\frac{x}{1-x}}, \quad (19)$$

after further manipulations, the expression for the PDF of T_{GLRT} for $n\gg m$ can be obtained assuming the alternate hypothesis $\mathcal{H}_1$ and we arrive at (20) at the top of this page. By calculating the integral of (20), the CDF of the decision threshold under $\mathcal{H}_1$ and the probability of detection can be derived as (15). ■

Meanwhile, we derive the analytical equation for calculating the decision threshold in terms of the probability of detection, which is given by (21) at the top of this page, where the coefficient C_t is given by

$$C_t=\begin{cases}1, & t=0,\\ \sum_{q=0}^{t-1}\frac{C_qC_{t-1-q}}{(q+1)(2q+1)}, & \text{others.}\end{cases} \quad (22)$$

IV. Optimization of the Cooperative Sensing

In this section, an efficient cooperative spectrum sensing technique is proposed while achieving the minimum total error rate of the final decision. Firstly, collaborating all the possible SUs to implement cooperative spectrum sensing can not always achieve the best performance due to the diversity of the SNRs received at SUs. An SU with very low received SNR can be classified as an unreliable node and may degrade the cooperative sensing performance. Secondly, combining all the local spectrum sensing decisions concurrently at the fusion center can lead to the high design complexity and the waste of bandwidth, such as sending local decisions on orthogonal frequency bands. Hence, sending different local

decisions in different time slots is chosen in this paper, but this may affect the sensing speed. However, according to the IEEE 802.22 standard for Wireless Regional Area Networks (WRANs) [14], the SUs should vacate the licensed frequency bands as soon as possible once the PU is active. Therefore, in order to address the two issues mentioned above, an efficient cooperative spectrum sensing technique using different time slots to receive local decisions is proposed to guarantee the accuracy and speed of the sensing process in this section. Furthermore, the statistical optimal number of the cooperating SUs $k_{\rm opt}$ is studied, which can make the total error rate achieve the minimum value, when the amount of available SUs is large enough compared with $k_{\rm opt}$.

A. Decision Fusion Rules

In the cooperative spectrum sensing system, the final decision on the status of the PU can be made through different techniques, including decision fusion and data fusion. In this paper, we apply decision fusion to investigate the performance of the system. During a decision fusion process, each SU processes the data individually and makes a local decision independently. Then, the final decision is made by fusing these individual decisions through a voting rule. Specifically, voting rules Logic-OR (OR) and Logic-AND (AND) are used in this paper in order to find out the optimal number of the collaborating SUs conveniently. Assuming there are k cooperating SUs, the mathematical characters of the OR and AND rules are as follows

- OR fusion rule: When at least one local decision among the k local decisions indicates the PU is present, the final decision declares the PU is present. The probabilities of detection $P_{\rm d}$ and false alarm $P_{\rm fa}$ of the final decision are given by

$$P_{\rm d} = 1 - \prod_{i=1}^{k}(1 - P_{{\rm d},i}), \tag{23}$$

$$P_{\rm fa} = 1 - \prod_{i=1}^{k}(1 - P_{{\rm fa},i}). \tag{24}$$

- AND fusion rule: Only when all local decisions indicate the PU is present, the final decision declares the PU is present. The corresponding probabilities of detection $P_{\rm d}$ and false alarm $P_{\rm fa}$ of the final decision are given by

$$P_{\rm d} = \prod_{i=1}^{k} P_{{\rm d},i}, \tag{25}$$

$$P_{\rm fa} = \prod_{i=1}^{k} P_{{\rm fa},i}. \tag{26}$$

The total error rate is defined to be the summation of the false alarm rate and missed detection rate, which can be given by

$$P_{\rm te} = P_{\rm fa} + P_{\rm m}, \tag{27}$$

where the probability of missed detection $P_{\rm m}$ is defined as

$$P_{\rm m} = 1 - P_{\rm d}. \tag{28}$$

B. Optimal Number of Cooperating SUs

The optimization of the cooperative spectrum sensing can be considered from three perspectives. Firstly, it can be considered under the constant detection rate (CDR) requirement, which aims to minimize the probability of false alarm for a given probability of detection. This guarantees the benefits of PU preferentially. Secondly, the probability of detection can be minimized for a desired constant false alarm rate (CFAR), which gives priority to the interests of the SUs. Thirdly, this issue can be considered to minimize the total error rate for a given constant decision threshold (CDT), which considers the interests of PU and SUs concurrently. In this paper, the optimization of cooperative spectrum sensing is investigated under the CDT requirement because of the space limitation. However, it should be noted that all the expressions and the research method proposed in this paper can also be applied to the CDR and CFAR cases.

Under the CDT requirement, the decision threshold is fixed and identical for every individual spectrum sensing period. Therefore, the individual probability of false alarm $P_{{\rm fa},i}$ for each SU is constant. However, the individual probability of detection varies depending on γ_i. From (15), it can be found that a higher received SNR helps to achieve a higher individual probability of detection $P_{{\rm d},i}$. Therefore, the SUs with higher received SNRs should be chosen first to implement the cooperative spectrum sensing. In order to study the received SNR at ith SU, the Euclidean distance d_i between the PU and the ith nearest SU within the coverage radius of SBS (shown as Fig. 1) should be investigated. The PDF of d_i is derived as the following theorem.

Theorem 3: In a PPP with density ρ on a 2-dimensional plane, the PDF of the distance d_i between the ith nearest SU within the coverage radius of SBS from the PU and the PU outside the region of interests is given by

$$\begin{aligned} f_{d_i}(d) =& 2\rho\theta(D-R)e^{-2\rho\theta(D-R)(d-D+R)} \\ &\times \frac{\big(2\rho\theta(D-R)(d-D+R)\big)^{i-1}}{\Gamma(i)}, \end{aligned} \tag{29}$$

where $\theta = \sin^{-1}\left(\frac{R}{D}\right)$ and $D \gg R$.

Proof: When the PU is far from the SUs within the coverage radius of SBS, the area S m^2 of the shadowing region in the Fig. 1 can be approximated as

$$\begin{aligned} S &= 2\pi(D-R)\frac{2\theta}{2\pi}\big(d-(D-R)\big) \\ &= 2\theta(D-R)(d-D+R). \end{aligned} \tag{30}$$

Since in a homogeneous 2-dimensional PPP with density ρ, the probability of having i nodes in a region $\mathcal{A}$ with the area S m^2 is given by

$$\mathbf{P}\{i \text{ nodes in } \mathcal{A}\} = e^{-\rho S}\frac{(\rho S)^i}{i!}. \tag{31}$$

The complementary CDF of d_i can be computed as the probability that there are less than i SUs within the shadowing

area (as defined in Section II and Fig. 1), which is given by

$$P_i = \mathbf{P}\{0, 1, \cdots, i-1 \text{ nodes between } D\text{–}R \text{ and } d_i\text{–}(D\text{–}R)\} = \sum_{j=0}^{i-1} e^{-\rho S_j} \frac{(\rho S)^j}{j!}, \quad (32)$$

By utilizing the relationship between the complementary CDF and the PDF, it can be derived that

$$\begin{aligned} f_{d_i}(d) =& -\frac{\mathrm{d}P_i}{\mathrm{d}d} \\ =& 2\rho\theta(D-R)e^{-\rho 2\theta(D-R)(d-D+R)} \\ & \times \left[\sum_{j=0}^{i-1} \frac{\left(\rho 2\theta(D-R)(d-D+R)\right)^j}{j!} \right. \\ & \left. - \sum_{j=1}^{i-1} \frac{\left(\rho 2\theta(D-R)(d-D+R)\right)^{j-1}}{(j-1)!} \right], \end{aligned} \quad (33)$$

after further manipulations, the expression of (29) can be obtained. ■

Hence, the average received SNR γ_i at the ith SU can be derived as

$$\begin{aligned} \gamma_i =& \int_{D-R}^{\infty} \int_0^{\infty} \frac{P_{\mathrm{T}} h}{\sigma_v^2 d^{\varepsilon}} f_{h_i}(h) f_{d_i}(d) \quad \mathrm{d}h\mathrm{d}d \\ =& \frac{P_{\mathrm{T}} m \left(2\rho\theta(D-R)\right)^{\varepsilon}}{\sigma_v^2 \Gamma(i)} e^{2\rho\theta(D-R)^2} \\ & \times \sum_{j=0}^{i-1} \binom{i-1}{j} \left(-2\rho\theta(D\text{–}R)^2\right)^j \Gamma\left(i-j-\varepsilon, 2\rho\theta(D\text{–}R)^2\right), \end{aligned} \quad (34)$$

where $\Gamma(\cdot,\cdot)$ denotes upper incomplete Gamma function. Therefore, by using the result above, $P_{\mathrm{fa},i}$ and $P_{\mathrm{d},i}$ can be computed under the CDT requirement. Also, the total error rate P_{te} can be obtained by using specific decision fusion rules.

Under the CDT requirement, when an additional SU is added into the cooperative spectrum sensing, the additional SU has the worst individual probability of detection, i.e. $P_{\mathrm{d},k}$, among the cooperating SUs. However, the individual probability of false alarm of the additional SU $P_{\mathrm{fa},k}$ is identical with other cooperating SUs. Meanwhile, the additional SU does not affect the performance of other SUs.

1) OR rule: The total error rate of the final decision P_{te} under OR rule can be given by

$$P_{\mathrm{te}} = 1 - \prod_{i=1}^{k} (1 - P_{\mathrm{fa},i}) + \prod_{i=1}^{k} (1 - P_{\mathrm{d},i}). \quad (35)$$

Because of the properties of $P_{\mathrm{fa},i}$ and $P_{\mathrm{m},i}$ mentioned above, it can be seen from (23) and (24) that the probability of false alarm of the final decision P_{fa} increases with the increase of the cooperating SUs' amount k, but the probability of missed detection of the final decision P_{m} falls down. Due to the monotonicity of the P_{m} and P_{fa}, it can be seen from (27) that collaborating all the SUs in the secondary network is not always the best option. The performance of the total error rate is determined by the changing speed of P_{fa} and P_{m} with the increase of k. Therefore, under two cases, collaborating all the available SUs can not achieve the minimum total error rate. Firstly, when the absolute values of the slope of P_{fa} and P_{m} are similar, the total error rate of the final decision will reduce initially and rise later with the increase of k. Secondly, when the absolute value of the slope of P_{fa} is larger the value of P_{m}, the total error rate should increase with the increasing k. By utilizing (7), (15) and (35), the total error rate can be calculated and the optimal number of the cooperating SUs k_{opt} can be obtained.

2) AND rule: Under the AND rule, the total error rate is given by

$$P_{\mathrm{te}} = 1 - \prod_{i=1}^{k} P_{\mathrm{d},i} + \prod_{i=1}^{k} P_{\mathrm{fa},i}. \quad (36)$$

On the contrary, it can be seen from (25) and (26) that P_{fa} is a decreasing function and P_{m} is an increasing function with regard to the number of the cooperating SUs k under the AND rule. From (27), the trend of the total error rate is also decided by the changing speed of P_{fa} and P_{m}. Hence, collaborating all the SUs in the network can not guarantee that the total error rate achieves the minimum value. By utilizing (7), (15) and (36), the total error rate when using AND rule under CDT requirement can be computed and the optimal number of the SUs can be obtained for a large k.

V. Simulation and Theoretical Results

In this section, simulation and theoretical results are provided to validate the derived expressions and analysis throughout this paper.

Fig. 2 verifies the expressions of the individual probabilities of false alarm and detection at the ith SU. Assuming each SU is equipped with 6 receive antennas, i.e., m = 6, the theoretical and Monte-Carlo results of $P_{\mathrm{fa},i}$ and $P_{\mathrm{d},i}$ are plotted for various cases of the received signal sample size n = $\{500, 1000\}$. Besides, $P_{\mathrm{d},i}$ is plotted under the received SNR = -15 dB. It can be observed that the theoretical results match the Monte-Carlo simulations.

Fig. 3 depicts the total error rate of the final decision versus the number of collaborating SUs under the CDT requirement by using OR and AND fusion rules, respectively. In the theoretical results, the coverage radius of the fusion center $R = 5$ km, the distance between the fusion center and PU is $D = 50$ km, the transmit power of PU is 5 w, the noise power is 10^{-12} w, the path loss exponent factor $\varepsilon = 3.1$, the preset decision threshold is 0.28 and the density in the considered PPP is $\rho = 10^{-7}$ nodes/m^2. Besides, each SU is assumed with 4 receive antennas ($m = 4$) and the sample size of received signal is $n = \{600, 800\}$. The total error rate of the final decision can be calculated as described in last section. Since the number of available SUs in PPP is random, it is impossible to show all the possible cases of different amount of SUs. However, The probability of over certain amount of SUs within the coverage radius of SBS can be calculated by using (31). For the PPP with the determined density ρ considered

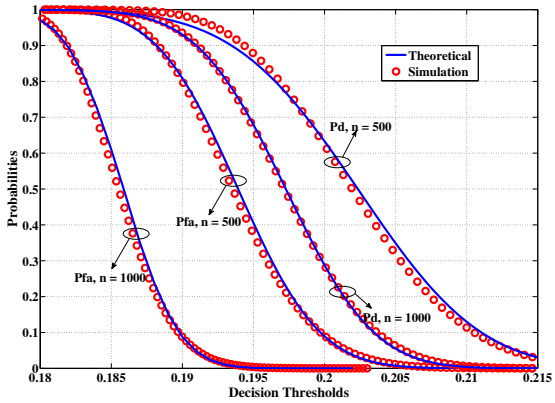

Fig. 2. The individual probabilities of false alarm and detection versus decision thresholds for various sample size n, $m = 6$ and SNR $= -15$ dB

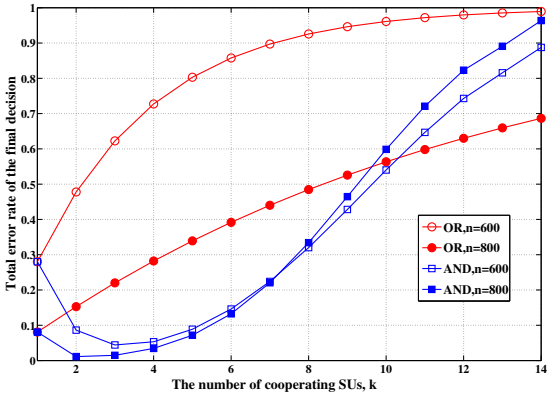

Fig. 3. The total error rate of the final decision versus the number of cooperating SUs k for various sample size n by using OR and AND fusion rules under the CDT requirement

in this paper, the probability of over 14 SUs located within the area of interests is under 0.05. Thus, Fig. 3 only shows the case of the number of available SUs up to 14, which is enough for analysis. It can be seen that the total error rate decreases first and then increases with the increase of the number of cooperating SUs, under the AND rule. The optimal numbers of cooperating SUs are $k_{\text{opt}} = \{3, 2\}$ which make the total error rates achieve the minimum values $\{0.04, 0.01\}$ for the cases of $n = \{600, 800\}$, respectively. Under the OR rule, the total error rate goes up with the increasing k. Hence, cooperating 1 SU can achieve the best sensing performance. Overall, cooperating all the available SUs can not always achieve the best sensing performance. When the amount of available SUs is large, cooperating SUs partially not only improves the accuracy of spectrum sensing, but also accelerates the cooperative spectrum sensing.

VI. Conclusion

This paper studied the efficient cooperative spectrum sensing technique by using the GLRT detector when SUs follow a Poisson point process with density ρ. Firstly, the analytical expressions of the individual probabilities of false alarm and detection were derived for the general case of the GLRT detector in order to analyse the total error rate performance of the cooperative sensing system. Secondly, the total error rate of the final decision was investigated when cooperating different amounts of SUs under OR and AND fusion rules, respectively. The analytical results indicate that collaborating all the SUs can not always achieve the best spectrum sensing performance and the obtained optimal numbers of cooperating SUs in this paper minimize the total error rates of the final decisions. It should be noted that the SUs with higher received SNRs should be collaborated to implement cooperative spectrum sensing preferentially.

References

[1] CEPT-ECC, "ECC report 205: Licensed shared access (LSA)," February 2014.

[2] S. M. Mishra, A. Sahai, and R. W. Broderson, "Cooperative sensing among cognitive radio," *Proc. IEEE International Conference on Communications*, June 2006.

[3] J. Unnikrishnan and V. V. Veeravalli, "Cooperative sensing for primary detection in cognitive radio," *IEEE Journal of Selected Topics in Signal Processing*, vol. 2, no. 1, pp. 18–27, February 2008.

[4] N. Nguyen-Thanh and I. Koo, "Optimal truncated ordered sequential cooperative spectrum sening in cognitive radio," *IEEE Sensors Journal*, vol. 13, no. 11, pp. 4188–4195, November 2013.

[5] A. Kortun, T. Ratnarajah, M. Sellathurai, C. Zhong, and C. B. Papadias, "On the performance of eigenvalue-based cooperative spectrum sensing for cognitive radio," *IEEE Journal of Selected Topics in Signal Processing*, vol. 5, no. 1, pp. 49–55, February 2011.

[6] Y. Selen, H. Tullberg, and J. Kronander, "Sensor selection for cooperative spectrum sensing," *3rd IEEE Symposium on New Frontiers in Dynamic Spectrum Access Networks*, October 2008.

[7] Y. C. Liang, Y. Zeng, E. C. Peh, and A. T. Hoang, "Sensing-throughput tradeoff for cognitive radio networks," *IEEE Transactions on Wireless Communications*, vol. 7, no. 4, pp. 1326–1337, April 2008.

[8] M. Haenggi, "On distances in uniformly random networks," *IEEE Transactions on Information Theory*, vol. 51, no. 10, pp. 3584–3586, October 2005.

[9] M. G. Khoshkholgh, K. Navaie, and H. Yanikomeroglu, "Outage performance of the primary service in spectrum sharing networks," *IEEE Transactions on Mobile Computing*, vol. 12, no. 10, pp. 1955–1971, October 2013.

[10] E. Peh and Y. C. Liang, "Optimization for cooperative sensing in cognitive radio networks," *IEEE Wireless Communications and Networking Conference*, March 2007.

[11] W. Zhang, R. K. Mallik, and K. B. Letaief, "Optimization of cooperative spectrum sensing with energy detection in cognitive radio networks," *IEEE Transactions on Wireless Communications*, vol. 8, no. 12, pp. 5761–5766, December 2009.

[12] L. Wei and O. Tirkkonen, "Analysis of scaled largest eigenvalue based detection for spectrum sensing," *IEEE International Conference on Communications (ICC)*, pp. 1–5, June 2011.

[13] A. Taherpour, M. Nasiri-Kenari, and S. Gazor, "Multiple antenna spectrum sensing in cognitive radios," *IEEE Transactions on Wireless Communications*, vol. 9, no. 2, pp. 814–823, February 2010.

[14] C. R. Stevenson, C. Cordeiro, E. Sofer, and G. Chouinard, "IEEE P802.22 wireless RANs functional requirements for the 802.22 WRAN standard doc.:IEEE 802.22-05/0007r46," *Submitted by Carl R. Stevenson, WK3C Wireless LLC*, pp. 1–49, September 2005.

2014 IEEE International Conference on Acoustic, Speech and Signal Processing (ICASSP)

OPTIMAL DECISION THRESHOLD FOR EIGENVALUE-BASED SPECTRUM SENSING TECHNIQUES

Yibo He [†], *Tharmalingam Ratnarajah* [†], *Jiang Xue* [†], *Ebtihal H. G. Yousif* [†] *and Mathini Sellathurai* [§]

[†] IDCOM, The University of Edinburgh, Kings Buildings, Edinburgh, EH9 3JL, UK
[§] School of Engineering & Physical Sciences, Heriot-Watt University, U.K

ABSTRACT

This paper investigates optimization of the sensing threshold that minimizes the total error rate (i.e., the sum of the probabilities of false alarm and missed detection) of eigenvalue-based spectrum sensing techniques for multiple-antenna cognitive radio networks. Four techniques are investigated, which are maximum eigenvalue detection (MED), maximum minimum eigenvalue (MME) detection, energy with minimum eigenvalue (EME) detection, and the generalized likelihood ratio test (GLRT) detection. The contribution of this paper is of four parts. Firstly, we present the derivative of the matrix-variate confluent hypergeometric function, which is required for the MED case. Secondly, we derive the probabilities of false alarm for both cases MME and EME detection. Thirdly, we derive the probability of missed detection for the GLRT detector. Finally, we provide the exact expressions required to obtain the optimal sensing thresholds for all cases. The simulation results reveal that for all the investigated cases the chosen optimal sensing thresholds achieve the minimum total error rate.

Index Terms— Cognitive radio, eigenvalue-based spectrum sensing, optimal decision threshold, matrix-variate confluent hypergeometric function

1. INTRODUCTION

The problem of efficient utilization of the frequency spectrum has become a major issue within the research community. This is due to the well-known fact that the available spectrum is an overcrowded natural shared resource, and the fact that there is an overgrowing demand for communication services. However, under the current spectrum management schemes, unlicensed (secondary) users are prohibited to access the frequency bands which are allocated exclusively to licensed (primary) users [1]. An efficient solution to spectrum scarcity is cognitive radio which allows secondary (or cognitive) users (SUs) to detect and exploit spectrum holes whenever the primary users (PUs) are absent. However, during exploitation of such spectrum opportunities, SUs should not cause harmful interference to PUs. Therefore, spectrum sensing is an essential and crucial part for the implementation of the cognitive radio technology. An efficient spectrum sensing scheme should allow detection of PUs even under very low SNR conditions. For instance, the IEEE 802.22 standard for Wireless Regional Area Networks (WRANs) requires detection of Digital Television (DTV) signals using minimum probabilities of false alarm $P_{\rm fa}$ and missed detection $P_{\rm m}$ of 0.1.

Among many spectrum sensing techniques, eigenvalue-based detection is highly accurate and can provide minimal probability of error without much prior knowledge of the PU signals [2]. Four methods exist for eigenvalue-based detection which include MED [3], MME detector [4], EME detector [2] and GLRT detector [5]. The major objective of spectrum sensing is finding an optimal threshold that minimizes sensing errors.

Maintaining a minimal probability of missed detection serves the interests of PUs, as it protects them from secondary interference. On the other hand, maintaining a minimal probability of false alarm creates more chances for the SUs to access more channels. Since studying $P_{\rm m}$ is more difficult and complicated, the previous work [2–6] on eigenvalue-based detection have mainly focused on minimizing $P_{\rm fa}$ to benefit secondary users only. The optimization of energy detector (ED) was studied in [7], but the ED was sensitive to noise uncertainty which had no influences on eigenvalue-based detectors. Therefore, in this paper we focus on $P_{\rm m}$ and the total error rate $P_{\rm te}$ of eigenvalue-based detection to benefit both PUs and SUs simultaneously. This enables protection of PUs from secondary interference, while SUs can have higher probability of accessing the available frequency bands. Therefore, in this study we investigate the optimization of eigenvalue-based detection by finding the optimal decision threshold that minimizes $P_{\rm te}$. Specifically, we derive the exact expressions of $P_{\rm te}$ for MED with arbitrary number of receive antennas and MME, EME and GLRT detectors with 2 receive antennas and find the optimal decision thresholds to minimize the $P_{\rm te}$.

The remainder of this paper is organized as follows. Section II describes the system model, section III investigates optimization of the sensing threshold for the four methods, Section IV presents the simulation results, and finally Section V concludes the paper.

2. MULTIPLE-ANTENNA SPECTRUM SENSING MODEL

Let us consider a generic spectrum sensing scenario within a MIMO system that consists of p transmit antennas and m receive antennas. The transmitted signals are assumed to have a length of n samples, where $n > m$. Let $\mathcal{H}_0$ (PU is absent) and $\mathcal{H}_1$ (PU is present) denote the null and the alternate hypotheses respectively. During the sensing period, the received signal $\boldsymbol{Y}$ is given by

$$\begin{aligned} \mathcal{H}_0 &: \mathbf{Y} = \mathbf{V}, \\ \mathcal{H}_1 &: \mathbf{Y} = \mathbf{H}\,\mathbf{X} + \mathbf{V}, \end{aligned} \tag{1}$$

where $\boldsymbol{Y} \in \mathbb{C}^{m\times n}$ is the matrix of the received signal samples at the secondary receivers, $\boldsymbol{H} \in \mathbb{C}^{m\times p}$ is a complex Gaussian channel matrix. The matrix $\boldsymbol{V} \in \mathbb{C}^{m\times n}$ represents an additive Gaussian white noise, which is independent of the channel, and the circularly symmetric complex Gaussian matrix of the transmitted signals $\boldsymbol{X} \in \mathbb{C}^{p\times n}$. Specifically, $\boldsymbol{V} \sim \mathcal{CN}(\mathbf{0}, \delta_v^2 \boldsymbol{I_m})$ and $\boldsymbol{X} \sim \mathcal{CN}(\mathbf{0}, \boldsymbol{\Sigma})$. Therefore, the received signals by the cognitive antennas should be an $m \times n$ complex Gaussian matrix. Henceforth, the matrix $\boldsymbol{W} = \boldsymbol{Y} \times \boldsymbol{Y}'$ is a complex central Wishart matrix, i.e.,

This work was supported by the Seventh Framework Programme for Research of the European Commission under grant number ADEL-619647.

978-1-4799-2893-4/14/$31.00 ©2014 IEEE

$\boldsymbol{W} \sim \mathcal{CW}_m(n, \boldsymbol{\Sigma_m})$, where the covariance matrix $\boldsymbol{\Sigma_m}$ is given by

$$\boldsymbol{\Sigma_m} = \begin{cases} \delta_v^2 \boldsymbol{I_m}, & \mathcal{H}_0, \\ \boldsymbol{H\Sigma H}^H + \delta_v^2 \boldsymbol{I_m}, & \mathcal{H}_1. \end{cases}$$

Let T denotes the test statistic used for eigenvalue-based spectrum sensing. The formulation of T can vary depending on the different types of eigenvalue-based detectors. Let $\lambda_{\max} = \lambda_1 > \cdots > \lambda_{\mathrm{m}} = \lambda_{\min}$ denote the eigenvalues of the matrix $\boldsymbol{W}$. Hence, the test statistics for MED, MME detection, EME detection and GLRT detection are given by: $T_{\mathrm{MED}} = \lambda_{\max}$, $T_{\mathrm{MME}} = \frac{\lambda_{\max}}{\lambda_{\min}}$, $T_{\mathrm{EME}} = \frac{\sum_{i=1}^{m} \lambda_i}{\lambda_{\min}}$ and $T_{\mathrm{GLRT}} = \frac{\lambda_{\max}}{\sum_{i=1}^{m} \lambda_i}$ respectively. The focus of this paper is to find the optimal sensing threshold r_{opt} that minimizes the total error rate P_{te} which is determined by

$$P_{\mathrm{te}} = P_{\mathrm{fa}} + P_{\mathrm{m}}, \tag{2}$$

where P_{fa} and P_{m} denote the probabilities of false alarm and missed detection respectively, and are given by

$$P_{\mathrm{fa}} = \mathrm{Prob}\left[T > r | \mathcal{H}_0\right] = \int_r^{\infty} f_0(t)\mathrm{d}t, \tag{3}$$

$$P_{\mathrm{m}} = \mathrm{Prob}\left[T < r | \mathcal{H}_1\right] = \int_{-\infty}^{r} f_1(t)\mathrm{d}t, \tag{4}$$

where $f_0(t)$ and $f_1(t)$ denote the probability distribution functions (PDFs) of the test statistic T under $\mathcal{H}_0$ and $\mathcal{H}_1$ respectively and r stands for the decision threshold.

An appropriate decision threshold r can achieve the desired value of probability of false alarm P_{fa}, but the corresponding probability of missed detection P_{m} may not meet an acceptable value concurrently. Therefore, in practical applications, it is essential to find an optimal decision threshold r_{opt} that minimizes the total error rate. This can make both P_{fa} and P_{m} meet the acceptable values simultaneously.

3. OPTIMIZATION OF THE DECISION THRESHOLD

In this section, we investigate the optimal sensing thresholds for the cases of MED (with arbitrary number of receive antennas) and MME, EME and GLRT detectors (with 2 receive antennas), and assuming the case of one PU with a single antenna, i.e., $p = 1$. For each type of the eigenvalue-based detectors, and in order to find the optimal decision threshold r_{opt} and the total error rate P_{te}, the exact cumulative distribution function (CDF) (or the PDF) of the corresponding test statistic is required for both cases of $\mathcal{H}_0$ and $\mathcal{H}_1$.

3.1. Optimal Threshold for the MED

In this subsection, we derive the exact expression of the total error rate P_{te} for MED assuming an arbitrary number of receive antennas. Also, the corresponding optimal decision threshold is analysed by using the derivative of the total error rate. However, in order to get the derivative of P_{te}, we have to solve the issue of finding the derivative of a confluent hypergeometric function with a matrix argument. This case was not studied in the literature and only the derivative of the confluent hypergeometric function with a scalar argument is studied before.

Firstly, let us start with the case of $\mathcal{H}_0$, where in this case $\boldsymbol{W} \sim \mathcal{CW}_m(n, \sigma_v^2 \boldsymbol{I_m})$. Hence, by making use of the CDF of the maximum eigenvalues of an uncorrelated complex central Wishart matrix, the probability of false alarm is given by [8]

$$P_{\mathrm{fa}}(x) = 1 - \frac{C\Gamma_m(m)}{C\Gamma_m(n+m)} x^{mn}\ {}_1F_1(n; n+m; -x\sigma_v^2 \boldsymbol{I}), \tag{5}$$

where ${}_1F_1\left(.;.;.\right)$ is the matrix-variate confluent hypergeometric function and

$$C\Gamma_m(a) = \pi^{\frac{m(m-1)}{2}} \prod_{k=1}^{m} \Gamma(a-k+1),$$

where $\Gamma(.)$ is the gamma function, $\Re(a) > (m-1) + k_1$, $k = k_1 + k_2 + \cdots + k_m$ and $k_1 \geq \cdots \geq k_m \geq 0$. On the other hand, considering the hypothesis $\mathcal{H}_1$, $\boldsymbol{W} \sim \mathcal{CW}_m(n, \boldsymbol{\Sigma_m})$. Therefore, the probability of missed detection is given by [8]

$$P_{\mathrm{m}}(x) = \frac{C\Gamma_m(m) x^{mn}\ {}_1F_1(n; n+m; -x{\boldsymbol{\Sigma_m}}^{-1})}{C\Gamma_m(n+m)(\det \boldsymbol{\Sigma_m})^n}. \tag{6}$$

Henceforth, the total error rate P_{te} for MED with an arbitrary number of receive antennas can be obtained by using (2). It can be seen that $P_{\mathrm{te}}(x)$ is a convex function, which indicates it has a global minimum value for x. Also, this implies that there exists one and only one value of x which minimizes $P_{\mathrm{te}}(x)$. Therefore, the optimal decision threshold r_{opt} is given by

$$r_{\mathrm{opt}} = \arg\min_x\ P_{\mathrm{te}}(x), \tag{7}$$

which can be achieved when the derivative of the total error rate is $\frac{\mathrm{d}P_{\mathrm{te}}(x)}{\mathrm{d}x} = 0$. The corresponding derivative is obtained as

$$\begin{aligned} \frac{\mathrm{d}P_{\mathrm{te}}(x)}{\mathrm{d}x} =& \frac{C\Gamma_m(m)\ {}_1F_1(n; n+m; -x{\boldsymbol{\Sigma_m}}^{-1})}{C\Gamma_m(n+m)(\det \boldsymbol{\Sigma_m})^n} \\ &\times \Big(mnx^{mn-1} + x^{mn} \Big(\mathrm{tr}(\boldsymbol{C}) - \mathrm{tr}(\boldsymbol{D}) \Big) \Big) \\ &- \frac{C\Gamma_m(m)\ {}_1F_1(n; n+m; -x\sigma_v^2 \boldsymbol{I_m})}{C\Gamma_m(n+m)} \\ &\times \Big(mnx^{mn-1} + x^{mn} \Big(\mathrm{tr}(\boldsymbol{A}) - \mathrm{tr}(\boldsymbol{B}) \Big) \Big), \end{aligned} \tag{8}$$

where the matrices $\boldsymbol{A}, \boldsymbol{B}, \boldsymbol{C}, \boldsymbol{D}$ are given by

$$\boldsymbol{A} = \Big((-x\sigma_v^2)^{k_j+m-j} \Big)^{-1} \Big(\sigma_v^2 (-k_j - m + j)(-\sigma_v^2 x)^{k_j+m-j-1} \Big),$$

$$\boldsymbol{B} = \Big((-x\sigma_v^2)^{m-j} \Big)^{-1} \Big(\sigma_v^2 (j-m)(-\sigma_v^2 x)^{m-j-1} \Big),$$

$$\boldsymbol{C} = \Big((x\beta_i)^{k_j+m-j} \Big)^{-1} \Big(\beta_i (k_j + m - j)(\beta_i x)^{k_j+m-j-1} \Big),$$

$$\boldsymbol{D} = \Big((x\beta_i)^{m-j} \Big)^{-1} \Big(\beta_i (m-j)(\beta_i x)^{m-j-1} \Big),$$

where $\beta_1, ..., \beta_m$ are the eigenvalues of the matrix $-{\boldsymbol{\Sigma_m}}^{-1}$. The solution to $\frac{\mathrm{d}P_{\mathrm{te}}(x)}{\mathrm{d}x} = 0$ can be evaluated numerically and represents the desired optimal decision threshold.

3.2. Optimal Threshold for the MME

In this subsection, we derive the exact expression of the total error rate for the MME detector assuming $m = 2$ and show the required steps to obtain the optimal decision threshold. Assuming $\mathcal{H}_0$, the PDF of the test statistic T_{MME} for the case of $m = 2$ is given by [4]

$$f_{\mathrm{MME0}}(x) = \frac{\Gamma(2n)}{\Gamma(n)\Gamma(n-1)} \Big(1 - \frac{1}{x}\Big)^2 \Big(\frac{1}{x}\Big)^n \Big(1 + \frac{1}{x}\Big)^{-2n}. \tag{9}$$

By making use of the previous equation, (9), we derive the probability of false alarm as

$$\begin{aligned} P_{\mathrm{fa}}(x) =& \frac{\Gamma(2n)}{\Gamma(n)\Gamma(n-1)} \Big[\Delta_1(2n, n-1, x) - 2\Delta_1(2n, n, x) \\ &+ \Delta_1(2n, n+1, x) \Big), \end{aligned} \tag{10}$$

$$f_{\mathrm{MME1}}(x) = \frac{(\delta_1\delta_2)^{1-n}}{(n-1)!(n-2)!(\delta_2-\delta_1)}\Big(\Delta_2(n-1,n-1,1/\delta_1,1/\delta_2,x) - \Delta_2(n-2,n,1/\delta_1,1/\delta_2,x) - \Delta_2(n-1,n-1,1/\delta_2,1/\delta_1,x) + \Delta_2(n-2,n,1/\delta_2,1/\delta_1,x)\Big), \quad x>1 \tag{22}$$

$$S(y) = \Delta_3(n-1,n-1,1/\delta_1,1/\delta_2,y) - \Delta_3(n-2,n,1/\delta_1,1/\delta_2,y) - \Delta_3(n-1,n-1,1/\delta_2,1/\delta_1,y) + \Delta_3(n-2,n,1/\delta_2,1/\delta_1,y) \tag{23}$$

where $\Delta_1(a,b,y) = \frac{y^{-b}}{b}\,{}_2F_1(a,b;b+1,-y^{-1})$, and ${}_2F_1(.,.;.;.)$ is the Gaussian hypergeometric function. Assuming $\mathcal{H}_1$, $\boldsymbol{W} \sim \mathcal{CW}_2(n,\boldsymbol{\Sigma_2})$, and making use of the results in [8] yields the PDF of the test statistic T_{MME} associated with $\boldsymbol{W}$ as given by (22), where

$$\Delta_2(a,b,c,d,y) = -(b-1)!\sum_{k=0}^{b-1}\frac{(a+k)!y^{k-1}(kd-c(a+1)y)}{k!c^{b-k}(cy+d)^{a+k+2}},$$

and $\delta_1 > \delta_2$ are the non-zero ordered eigenvalues of $\boldsymbol{\Sigma_2}$. The probability of missed detection of the MME detector can then be obtained by

$$P_{\mathrm{m}}(x) = \frac{(\delta_1\delta_2)^{1-n}}{(n-1)!(n-2)!(\delta_2-\delta_1)}\Big(S(x)-S(1)\Big), \tag{11}$$

where $x>1$, and $S(y)$ is given by (23) and Δ_3 is given by

$$\Delta_3(a,b,c,d,y) = (b-1)!\times\left(\frac{a!}{c^b d^{a+1}} - \sum_{k=0}^{b-1}\frac{(a+k)!y^k}{k!c^{b-k}(cy+d)^{a+k+1}}\right).$$

Thus, the exact expression of the total error rate P_{te} can be directly obtained from summing (10) and (11). In order to obtain the optimal decision threshold r_{opt}, the derivative $\frac{\mathrm{d}P_{\mathrm{te}}(x)}{\mathrm{d}x}$ is

$$\frac{\mathrm{d}P_{\mathrm{te}}(x)}{\mathrm{d}x} = \frac{\mathrm{d}(P_{\mathrm{fa}}(x)+P_{\mathrm{m}}(x))}{\mathrm{d}x} = f_{\mathrm{MME1}}(x) - f_{\mathrm{MME0}}(x).$$

The solution to $f_{\mathrm{MME1}}(x) - f_{\mathrm{MME0}}(x) = 0$ can be evaluated numerically and is the desired optimal decision threshold.

3.3. Optimal Threshold for the EME

In this subsection, the case of the EME detector is considered assuming 2 receive antennas. Since under $\mathcal{H}_0$, $\boldsymbol{W} \sim \mathcal{CW}_2(n,\sigma_v^2\boldsymbol{I_m})$ then the PDF of the test statistic T_{EME} is given by [9]

$$f_{\mathrm{EME0}}(x) = \frac{\Gamma(2n)x^{-2n}(x-1)^{n-2}(x-2)^2}{\Gamma(n)\Gamma(n-1)}, x \geq 2. \tag{12}$$

Hence, we derive the probability of false alarm P_{fa} as

$$P_{\mathrm{fa}}(x) = 1 - \frac{\Gamma(2n)}{\Gamma(n)\Gamma(n-1)}\sum_{k=0}^{n-2}\binom{n-2}{k}(-1)^{n-2-k} \times\Big(\frac{x^{k-2n+3}-2^{k-2n+3}}{k-2n+3} - 4\frac{x^{k-2n+2}-2^{k-2n+2}}{k-2n+2} + 4\frac{x^{k-2n+1}-2^{k-2n+1}}{k-2n+1}\Big). \tag{13}$$

Assuming $\mathcal{H}_1$, and using [10], the PDF of the threshold T_{EME}, that is associated with the dual correlated complex central Wishart matrix $\boldsymbol{W} \sim \mathcal{CW}_2(n,\boldsymbol{\Sigma_2})$ is given by

$$f_{\mathrm{EME1}}(x) = \frac{\Gamma(2n-1)(\delta_1\delta_2)^{1-n}(x-2)}{\Gamma(n)\Gamma(n-1)(\delta_1-\delta_2)}(x-1)^{n-2} \times\Big(\Delta_4(\delta_1,\delta_2,x)^{1-2n} - \Delta_4(\delta_2,\delta_1,x)^{1-2n}\Big), \tag{14}$$

where $x \geq 2$, $\Delta_4(\delta_1,\delta_2,x) = \frac{x-1}{\delta_1}+\frac{1}{\delta_2}$, $\Delta_4(\delta_2,\delta_1,x) = \frac{x-1}{\delta_2}+\frac{1}{\delta_1}$ and δ_1 and δ_2 are the non-zero ordered eigenvalues of $\boldsymbol{\Sigma_2}$, where $\delta_1 > \delta_2$. Hence, using the CDF in [10] , P_{m} is given by

$$P_{\mathrm{m}}(x) = \frac{\Gamma(2n-1)(\delta_1\delta_2)^{1-n}}{\Gamma(n)\Gamma(n-1)(\delta_1-\delta_2)} \times\left\{\Delta_5\left(\frac{\delta_1-\delta_2}{\delta_1},\frac{\delta_2}{\delta_1},\delta_2,x\right) - \Delta_5\left(\frac{\delta_2-\delta_1}{\delta_2},\frac{\delta_1}{\delta_2},\delta_1,x\right) - \Delta_5\left(\frac{\delta_1-\delta_2}{\delta_1},\frac{\delta_2}{\delta_1},\delta_2,2\right) + \Delta_5\left(\frac{\delta_2-\delta_1}{\delta_2},\frac{\delta_1}{\delta_2},\delta_1,2\right)\right\}, \tag{15}$$

where $x \geq 2$, and

$$\Delta_5(a,b,c,x) = \Big(\frac{c}{a}\Big)^{2n-1}\sum_{k=0}^{n-2}\binom{n-2}{k}(-1)^k \times\Big\{P(n-k-1,b,a,2n-1,x) - 2P(n-k-2,b,a,2n-1,x)\Big\}, \tag{16}$$

$$P(n,b,a,m,x) = \frac{x^{n+1}}{n+1}\,{}_2F_1\Big(m,n+1;n+2;-x\frac{b}{a}\Big). \tag{17}$$

Thus, the derivative of the total error rate P_{te} is $\frac{\mathrm{d}P_{\mathrm{te}}(x)}{\mathrm{d}x} = \frac{\mathrm{d}(P_{\mathrm{fa}}(x)+P_{\mathrm{m}}(x))}{\mathrm{d}x} = f_{\mathrm{EME1}}(x) - f_{\mathrm{EME0}}(x)$ and the solution to $f_{\mathrm{EME1}}(x) - f_{\mathrm{EME0}}(x) = 0$ is the desired optimal decision threshold.

3.4. Optimal Threshold for the GLRT

This subsection investigates the case of the optimal threshold for the GLRT detector with 2 receive antennas. Starting with the null hypothesis, and since in this case $\boldsymbol{W} \sim \mathcal{CW}_2(n,\sigma_v^2\boldsymbol{I_m})$, then using the PDF and CDF in [5], the PDF of the test statistic T_{GLRT} and the probability of false alarm are given by

$$f_{\mathrm{GLRT0}}(x) = \frac{\Gamma(2n)(2x-1)^2}{\Gamma(n)\Gamma(n-1)\left(x(1-x)\right)^{2-n}}, \tag{18}$$

$$P_{\mathrm{fa}}(x) = 1 - \frac{\Gamma(2n)\left(\Delta_6(n,x)-\Delta_6(n,\frac{1}{2})\right)}{\Gamma(n)\Gamma(n-1)}, \tag{19}$$

where $\frac{1}{2} \leq x \leq 1$ and

$$\Delta_6(n,y) = \sum_{k=0}^{n-2}\binom{n-2}{k}(-1)^{n-2-k} \times\Big\{\frac{y^{2n-k-3}}{2n-k-3} - 4\frac{y^{2n-k-2}}{2n-k-2} + 4\frac{y^{2n-k-1}}{2n-k-1}\Big\}. \tag{20}$$

Assuming $\mathcal{H}_1$, we have $\boldsymbol{W} \sim \mathcal{CW}_2(n,\boldsymbol{\Sigma_2})$, and therefore the PDF of T_{GLRT} is given by [5]

$$f_{\mathrm{GLRT1}}(x) = \frac{\left(x\delta_2+(1-x)\delta_1\right)^{1-2n} - \left(x\delta_1+(1-x)\delta_2\right)^{1-2n}}{\Gamma(n)\Gamma(n-1)(\delta_1-\delta_2)\left(x(1-x)\right)^{2-n}} \times\Gamma(2n-1)(\delta_1\delta_2)^n(2x-1), \quad \frac{1}{2} \leq x \leq 1, \tag{21}$$

$$P_{\rm m}(x) = C_{\rm g}\sum_{k=0}^{n-2}\binom{n-2}{k}(-1)^k\Bigg[2\Bigg(\Delta_7\left(\delta_1, 2n-1, k+n, \delta_1-\delta_2, x\right) - \Delta_7\left(\delta_1, 2n-1, k+n, \delta_1-\delta_2, \frac{1}{2}\right)\Bigg)$$
$$-2\Bigg(\Delta_7\left(\delta_2, 2n-1, k+n, \delta_2-\delta_1, x\right) - \Delta_7\left(\delta_2, 2n-1, k+n, \delta_2-\delta_1, \frac{1}{2}\right)\Bigg)$$
$$-\Bigg(\Delta_7(\delta_1, 2n-1, n+k-1, \delta_1-\delta_2, x) - \Delta_7\left(\delta_1, 2n-1, n+k-1, \delta_1-\delta_2, \frac{1}{2}\right)\Bigg)$$
$$+\Bigg(\Delta_7(\delta_2, 2n-1, n+k-1, \delta_2-\delta_1, x) - \Delta_7\left(\delta_2, 2n-1, n+k-1, \delta_2-\delta_1, \frac{1}{2}\right)\Bigg)\Bigg], \frac{1}{2} \le x \le 1. \quad (24)$$

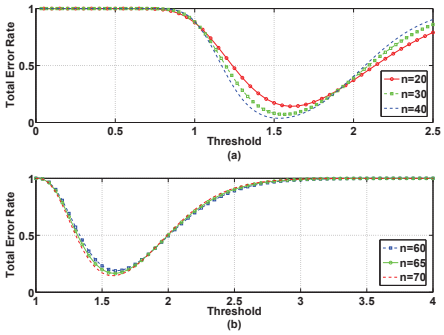

Fig. 1. The total error rate of MED (m=2, SNR=0 dB) (a) and MME detector (m=2, SNR=-5 dB) (b) vs decision threshold

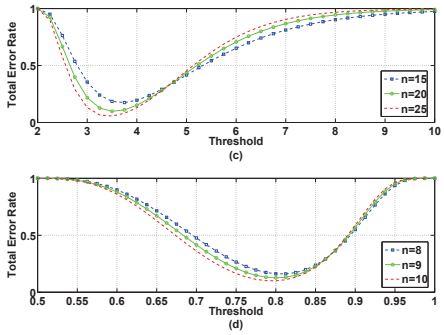

Fig. 2. The total error rate of EME (c) and GLRT (d) detector (m=2, SNR=0 dB) vs decision threshold

where $\delta_1 > \delta_2$ are the non-zero ordered eigenvalues of $\mathbf{\Sigma_2}$. By applying the binomial expansion and then integrating we derive the probability of missed detection as given by (24), where $C_{\rm g} = \frac{\Gamma(2n-1)(\delta_1\delta_2)^n}{\Gamma(n)\Gamma(n-1)(\delta_1-\delta_2)}$ and $\Delta_7(a,b,c,d,t) = \frac{a^{-b}t^c}{c}\ {}_2F_1(b,c;1+c;\frac{d}{a}t)$. Therefore, the derivative of the total error rate can be obtained as $\frac{{\rm d}P_{\rm te}(x)}{{\rm d}x} = \frac{{\rm d}(P_{\rm fa}(x)+P_{\rm m}(x))}{{\rm d}x} = f_{\rm GLRT1}(x) - f_{\rm GLRT0}(x)$ and the solution to $f_{\rm GLRT1}(x) - f_{\rm GLRT0}(x) = 0$ is the desired optimal decision threshold.

4. SIMULATION RESULTS

In this section, some simulation results are presented and discussed. For simplicity but without loss of generality, we assume a spectrum sensing scenario with 2 receive antennas and one transmit antenna. The calculation of matrix-variate confluent complex hypergeometric function utilizes the MATLAB codes provided by [11]. Starting with the case of MED, Figure (a) of Fig. 1 depicts the total error rate versus the decision threshold. The results are plotted for different cases of number of transmitted signal samples, $n = \{20, 30, 40\}$, and an SNR of 0dB using $\mathbf{\Sigma_m} = \left(\begin{smallmatrix} 2 & 0 \\ 0 & 1.3 \end{smallmatrix}\right)$. The results show the corresponding optimal decision threshold is $r_{\rm opt} = \{1.60, 1.57, 1.53\}$ with a total error rate of $P_{\rm te} = \{0.14, 0.07, 0.04\}$.

Figure (b) of Fig. 1 shows the total error rate of MME detection versus the threshold. The simulation parameters are $n = \{60, 65, 70\}$, SNR $= -5$dB and $\mathbf{\Sigma_m} = \left(\begin{smallmatrix} 1.7 & -0.3+0.2i \\ -0.3-0.2i & 1.2 \end{smallmatrix}\right)$. Here we can indicate the optimal decision threshold is $r_{\rm opt} = 1.6$, where $P_{\rm te} = \{0.19, 0.16, 0.15\}$. Figure (c) of Fig. 2 illustrates the total error rate of EME detection versus the threshold using $n = \{15, 20, 25\}$ when SNR $= 0$dB and $\mathbf{\Sigma_m} = \left(\begin{smallmatrix} 3.3 & -0.9+0.7i \\ -0.9-0.7i & 1.6 \end{smallmatrix}\right)$. Here we can find the optimal decision threshold is $r_{\rm opt} = 3.75$ for $n = 15$ and $r_{\rm opt} = 3.5$ for $n = \{20, 25\}$. The corresponding total error rates are $P_{\rm te} = \{0.17, 0.09, 0.06\}$. Finally, Figure (d) of Fig. 2 shows the total error rate of the GLRT detector versus the threshold, assuming $n = \{8, 9, 10\}$ when SNR $= 0$dB and $\mathbf{\Sigma_m} = \left(\begin{smallmatrix} 1.9 & 0.55+2.1i \\ 0.55-2.1i & 6.2 \end{smallmatrix}\right)$. Here it is found that the optimal decision threshold is $r_{\rm opt} = 0.82$ for $n = 8$ and $r_{\rm opt} = 0.80$ for $n = \{9, 10\}$, where the corresponding total error rates are $P_{\rm te} = \{0.17, 0.13, 0.10\}$. For all cases, it is clear that the proposed optimal decision thresholds minimize the total error rate which enables both $P_{\rm fa}$ and $P_{\rm m}$ achieving acceptable values simultaneously.

5. CONCLUSION

In this paper, the problem of finding the optimal decision threshold was considered for eigenvalue-based spectrum sensing. Specifically, we focused on the MED with arbitrary number of receive antennas, as well as the MME, EME and GLRT detectors with 2 receive antennas. The case of MED required finding the derivative of the matrix-variate confluent hypergeometric function. Also, for the cases of both the MME and EME detectors we presented accurate expressions for the probability of false alarm. Furthermore, for the case of the GLRT detector we derived an accurate expression for the probability of missed detection. For all cases, the exact total error rate was formulated and we presented the equations to numerically obtain the optimal decision thresholds which could minimize the total error rate.

6. REFERENCES

[1] Federal Communications Commission, "Spectrum policy task force," *ET Docket no. 02-135*, November 2002.

[2] Y. Zeng and Y. Liang, "Eigenvalue-based spectrum sensing algorithms for cognitive radio," *IEEE Transactions on Communications*, vol. 57, no. 6, pp. 1784–1793, June 2009.

[3] T. Ratnarajah, C. Zhong, A. Kortun, M. Sellathurai, and C. B. Papadias, "Complex random matrices and multiple-antenna spectrum sensing," *IEEE International Conference on Acoustics, Speech and Signal Processing (ICASSP)*, vol. 26, no. 2, pp. 3848–3851, May 2011.

[4] A. Kortun, T. Ratnarajah, M. Sellathurai, C. Zhong, and C. B. Papadias, "On the performance of eigenvalue-based cooperative spectrum sensing for cognitive radio," *IEEE Journal of Selected Topics in Signal Processing*, vol. 5, no. 1, pp. 49–55, February 2011.

[5] A. Kortun, M. Sellathurai, T. Ratnarajah, and C. Zhong, "Distributionn of the ratio of the largest eigenvalue to the trace of complex Wishart matrices," *IEEE Transactions on Signal Processing*, vol. 60, no. 10, pp. 5527–5532, October 2012.

[6] Y. Zeng, Y. Liang, A. T. Hoang, and R. Zhang, "A review on spectrum sensing for cognitive radio: Challenges and solutions," *EURASIP Journal on Advances in Signal Processing*, vol. 2010, pp. 1–15, 2010.

[7] W. Zhang, R. K. Mallik, and K. B. Letaief, "Optimization of cooperative spectrum sensing with energy detection in cognitive radio networks," *IEEE Transactions on Wireless Communications*, vol. 8, no. 12, pp. 5761–5766, December 2009.

[8] T. Ratnarajah, R. Vaillancourt, and M. Alvo, "Eigenvalues and condition numbers of complex random matrices," *SIAM J. Matrix Anal. Appl.*, vol. 26, no. 2, pp. 441–456, January 2005.

[9] C. Zhong, M. R. McKay, T. Ratnarajah, and K. Wong, "Distribution of the Demmel condition number of Wishart matrices," *IEEE Transactions on Communications*, vol. 59, no. 5, pp. 1309–1320, May 2011.

[10] M. Matthaiou, M. R. McKay, P. J. Smith, and J. A. Nossek, "On the condition number distribution of complex Wishart matrices," *IEEE Transactions on Communications*, vol. 58, no. 6, pp. 1705–1717, June 2010.

[11] P. Koev and A. Edelman, "The efficient evaluation of the hypergeometric function of a matrix argument," *Mathematics of Computation*, vol. 75, no. 254, pp. 833–846, January 2006.

References

[1] J. Ma, G. Y. Li, and B. H. Juang, "Signal processing in cognitive radio," *Proceedings of IEEE*, vol. 97, pp. 805–823, May 2009.

[2] A. Ghasemi and E. S. Sousa, "Spectrum sensing in cognitive radio networks: requirements, challenges and design trade-offs," *IEEE Communications Magazine*, vol. 46, pp. 32–39, Apr. 2008.

[3] S. M. Mishra, A. Sahai, and R. W. Broderson, "Cooperative sensing among cognitive radio," in *IEEE ICC*, Jun. 2006.

[4] J. Ma, G. D. Zhao, and G. Y. Li, "Soft combination and detection for cooperative spectrum sensing in cognitive radio networks," *IEEE Trans. Wireless Commun.*, vol. 7, pp. 4502–4507, Nov. 2008.

[5] D. Daley and D. V. Jones, eds., *An introduction to the theory of point processes*. New York: Springer, 1988.

[6] Y. Zeng, Y. C. Liang, A. T. Hoang, and R. Zhang, "A review on spectrum sensing for cognitive radio: Challenges and solutions," *EURASIP Journal on Advances in Signal Processing*, vol. 2010, pp. 1–15, Jan. 2010.

[7] Y. Zeng and Y. C. Liang, "Eigenvalue-based spectrum sensing algorithms for cognitive radio," *IEEE Trans. Commun.*, vol. 57, pp. 1784–1793, Jun. 2009.

[8] T. Ratnarajah, C. Zhong, A. Kortun, M. Sellathurai, and C. B. Papadias, "Complex random matrices and multiple-antenna spectrum sensing," in *IEEE International Conference on Acoustics, Speech and Signal Processing (ICASSP)*, May 2011.

[9] A. Kortun, T. Ratnarajah, M. Sellathurai, C. Zhong, and C. B. Papadias, "On the performance of eigenvalue-based cooperative spectrum sensing for cognitive radio," *IEEE J. Sel. Topics Signal Process.*, vol. 5, pp. 49–55, Feb. 2011.

[10] A. Kortun, M. Sellathurai, T. Ratnarajah, and C. Zhong, "Distributionn of the ratio of the largest eigenvalue to the trace of complex Wishart matrices," *IEEE Trans. Signal Process.*, vol. 60, pp. 5527–5532, Oct. 2012.

[11] A. Kortun, T. Ratnarajah, M. Sellathurai, Y. C. Liang, and Y. Zeng, "On the eigenvalue-based spectrum sensing and secondary user throughput," *IEEE Trans. Veh. Technol.*, vol. 63, pp. 1480–1486, Mar. 2014.

[12] W. Cheng, X. Zhang, and H. Zhang, "Full-duplex spectrum-sensing and MAC-protocol for multichannel nontime-slotted cognitive radio networks," *IEEE J. Sel. Areas Commun.*, vol. 33, pp. 820–831, May 2015.

[13] T. Wang, Y. Liao, B. Zhang, and L. Song, "Joint spectrum access and power allocation in full-duplex cognitive cellular networks," in *IEEE ICC*, June 2015.

[14] W. Zhang, R. K. Mallik, and K. B. Letaief, "Optimization of cooperative spectrum sensing with energy detection in cognitive radio networks," *IEEE Trans. Wireless Commun.*, vol. 8, pp. 5761–5766, Dec. 2009.

[15] E. Peh and Y. C. Liang, "Optimization for cooperative sensing in cognitive radio networks," in *IEEE WCNC*, Mar. 2007.

[16] J. Mitola and G. Q. Maguire, "Cognitive radio: making software radios more personal," *IEEE Personal Communications*, vol. 6, pp. 13–18, Aug. 1999.

[17] J. Mitola, "Cognitive radio: An integrated agent architecture for software defined radio," *Ph.D. dissertation, KTH, Stockholm, Sweden*, Dec. 2000.

[18] S. Haykin, "Cognitive radio: Brain-empowered wireless communications," *IEEE J. Sel. Areas Commun.*, vol. 23, pp. 201–220, Feb. 2005.

[19] I. F. Akyildiz, W.-Y. Lee, M. C. Vuran, and S. Mohanty, "NeXt generation/dynamic spectrum access/cognitive radio wireless networks: A survey," *Computer Networks*, vol. 50, pp. 2127–2159, Sep. 2006.

[20] F. C. Commission, "Notice of proposed rulemaking and order," *ET Docket no. 03-222*, Dec. 2003.

[21] A. Goldsmith, S. A. Jafar, I. Maric, and S. Srinivasa, "Breaking spectrum gridlock with cognitive radios: An information theoretic perspective," *Proceedings of the IEEE*, vol. 97, pp. 894–914, May 2009.

[22] V. Pla, J. R. Vidal, J. Martinez-Bauset, and L. Guijarro, "Modeling and characterization of spectrum white spaces for underlay cognitive radio networks," in *IEEE ICC*, May 2010.

[23] Q. Zhao and B. M. Sadler, "A survey of dynamic spectrum access," *IEEE Signal Process. Mag.*, vol. 24, pp. 79–89, May 2007.

[24] Y. C. Liang, K. C. Chen, G. Y. Li, and P. Mahonen, "Cognitive radio networking and communications: An overview," *IEEE Trans. Veh. Technol.*, vol. 60, pp. 3386–3407, Sep. 2011.

[25] S. Srinivasa and S. A. Jafar, "Cognitive radios for dynamic spectrum access - the throughput potential of cognitive radio: A theoretical perspective," *IEEE Communications Magazine*, vol. 45, pp. 73–79, May 2007.

[26] S. Sun, Y. Ju, and Y. Yamao, "Overlay cognitive radio ofdm system for 4g cellular networks," *IEEE Wireless Communications*, vol. 20, pp. 68–73, April 2013.

[27] E. Axell, G. Leus, E. G. Larsson, and H. V. Poor, "Spectrum sensing for cognitive radio : State-of-the-art and recent advances," *IEEE Signal Processing Magazine*, vol. 29, pp. 101–116, May. 2012.

[28] X. Kang, Y. C. Liang, H. K. Garg, and L. Zhang, "Sensing-based spectrum sharing in cognitive radio networks," *IEEE Transactions on Vehicular Technology*, vol. 58, pp. 4649–4654, Oct. 2009.

[29] "IEEE 802.22 working group on wireless regional area network," *http://www.ieee802.org/22/*.

[30] Y. C. Liang, A. T. Hoang, and H. H. Chen, "Cognitive radio on TV bands-a new approach to provide wireless connectivity for rural areas," *IEEE Wireless Commun.*, vol. 15, pp. 16–22, Jun. 2008.

[31] C. R. Stevenson, G. Chouinard, Z. Lei, W. Hu, S. J. Shellhammer, and W. Caldwell, "IEEE 802.22: The first cognitive radio wireless regional area network standard," *IEEE Commun. Mag.*, vol. 47, pp. 130–138, Jan. 2009.

[32] Z. Quan, S. Cui, H. V. Poor, and A. H. Sayed, "Collaborative wideband sensing for cognitive radios," *IEEE Signal Process. Mag.*, vol. 25, pp. 1053–5888, Nov. 2008.

[33] C. R. Stevenson, C. Corderio, E. Sofer, and G. Chouinard, "Functional requirements for the 802.22 WRAN standard," *IEEE 802.22-05/0007r46*, Sep. 2005.

[34] W. Lee and B. C. Jung, "Pricing-based distributed spectrum access for cognitive radio networks with geolocation database," *IET Communications*, vol. 11, pp. 733–738, Apr. 2017.

[35] B. Wild and K. Ramachandran, "Detecting primary receivers for cognitive radio applications," in *IEEE Int. Symp. DySPAN*, pp. 124–130, Nov. 2005.

[36] R. Zhang and Y. C. Liang, "Exploiting hidden power-feedback loops for cognitive radio," in *IEEE Int. Symp. DySPAN*, Oct. 2008.

[37] G. Zhao, G. Y. Li, C. Yang, and J. Ma, "Proactive detection of spectrum holes in cognitive radio," in *IEEE ICC*, Jun. 2009.

[38] G. Zhao, G. Y. Li, and C. Yang, "Proactive detection of spectrum opportunities in primary systems with power control," *IEEE Trans. Wireless Commun.*, vol. 8, pp. 4815–4823, Sep. 2009.

[39] A. Sahai, N. Hoven, and R. Tandra, "Some fundamental limits in cognitive radio," in *Proc. Allerton Conf. Commun., Control Comput.*, Oct. 2004.

[40] R. Tandra and A. Sahai, "SNR walls for signal detection," *IEEE J. Sel. Topics Signal Process.*, vol. 2, pp. 4–17, Feb. 2008.

[41] W. A. Gardner, "Exploitation of spectral redundancy in cyclostationary signals," *IEEE Signal Process. Mag.*, vol. 8, pp. 14–36, Apr. 1991.

[42] D. Cabric, S. M. Mishra, and R. W. Brodersen, "Implementation issues in spectrum sensing for cognitive radios," in *Proc. Asilomar Conf. Signals, Syst., Comput.*, Nov. 2004.

[43] P. D. Sutton, K. E. Nolan, and L. E. Doyle, "Cyclostationary signatures in practical cognitive radio applications," *IEEE J. Sel. Areas Commun.*, vol. 26, pp. 13–24, Jan. 2009.

[44] I. Jacobs, "Energy detection of Gaussian communication signals," in *Proc. 10th National Commun. Symp.*, Oct. 1965.

[45] Z. Ye, G. Memik, and J. Grosspietsch, "Energy detection using estimated noise variance for spectrum sensing in cognitive radio networks," in *IEEE WCNC*, Apr. 2008.

[46] S. M. Kay, *Fundamentals of statistical signal processing: detection theory*. Englewood Cliffs, NJ: Prentice Hall, 1998.

[47] Y. Zeng, C. L. Koh, and Y. C. Liang, "Maximum eigenvalue detection: Theory and application," in *IEEE International Conference on Communications (ICC)*, May 2008.

[48] Y. Zeng and Y. C. Liang, "Maximum-minimum eigenvalue detection for cognitive radio," in *IEEE International Symposium on Personal, Indoor and Mobile Radio Cummunications*, Sep. 2007.

[49] X. Yang, K. Lei, S. Peng, and X. Cao, "Blind detection for primary user based on the sample covariance matrix in cognitive radio," *IEEE Communications Letters*, vol. 15, pp. 40–42, Jan. 2011.

[50] A. Kortun, T. Ratnarajah, and M. Sellathurai, "Exact performance analysis of blindly combined energy detection for spectrum sensing," *2010 IEEE 21st International Symposium on Personal Indoor and Mobile Radio Cummunications*, pp. 560–563, 2010.

[51] P. Wang, J. Fang, N. Han, and H. Li, "Multiantenna-assisted spectrum sensing for cognitive radio," *IEEE Trans. Veh. Technol.*, vol. 59, pp. 1791–1800, May 2010.

[52] A. Ghasemi and E. S. Sousa, "Collaborative spectrum sensing for opportunistic access in fading environments," in *Proc. 1st IEEE Symp. New Frontiers Dyn. Spectrum Access Netw. (DySPAN)*, Nov. 2005.

[53] H. Arslan, ed., *Cognitive Radio, Software Defined Radio, and Adaptive Wireless Systems*. Springer, 2007.

[54] N. Noorshams, M. Malboubi, and A. Bahai, "Centralized and decentralized cooperative spectrum sensing in cognitive radio networks: A novel approach," in *IEEE 11th International Workshop on Signal Processing Advances in Wireless Communications (SPAWC)*, Jun. 2010.

[55] N. Ahmad and S. Keshav, "Guess: Gossiping updates for efficient spectrum sensing," in *Proc. International Workshop on Decentralized Resource Sharing in Mobile Computing and Networking*, Jul. 2006.

[56] H. Tang, "Some physical layer issues of wide band cognitive radio systems," in *IEEE Dynamic Spectrum Access Networks (DySPAN)*, Oct. 2005.

[57] G. Ganesan and Y. Li, "Cooperative spectrum sensing in cognitive radio, part i: Two user networks," *IEEE Trans. Wireless Commun.*, vol. 6, pp. 2204–2213, Jun. 2007.

[58] G. Ganesan and Y. Li, "Cooperative spectrum sensing in cognitive radio, part ii: Multiuser networks," *IEEE Trans. Wireless Commun.*, vol. 6, pp. 2214–2222, Jun. 2007.

[59] H. Guo, W. Jiang, and W. Luo, "Linear soft combination for cooperative spectrum sensing in cognitive radio networks," *IEEE Communications Letters*, vol. 21, pp. 1573–1576, July 2017.

[60] P. K. Varshney, *Distributed Detection and Data Fusion*. New York: Springer-Verlag, 1997.

[61] A. Ghasemi and E. S. Sousa, "Opportunistic spectrum access in fading channels through collaborative sensing," *J. Commun.*, vol. 2, pp. 71–82, Mar. 2007.

[62] M. Duarte, C. Dick, and A. Sabharwal, "Experiment-driven characterization of full-duplex wireless systems," *IEEE Trans. Wireless Commun.*, vol. 11, p. 42964307, Dec. 2012.

[63] Z. Zhang, K. Long, and J. Wang, "Self-organization paradigms and optimization approaches for cognitive radio technologies: A survey," *IEEE Wireless Communications Magazine*, vol. 20, pp. 36–42, April 2013.

[64] Z. Zhang, K. Long, A. V. Vasilakos, and L. Hanzo, "Full-duplex wireless communications: Challenges, solutions, and future research directions," *Proceedings of The IEEE*, vol. 104, pp. 1369–1409, July 2016.

[65] J. I. Choi, M. Jain, K. Srinivasan, P. Levis, and S. Katti, "Achieving single channel, full duplex wireless communication," in *ACM MobiCom*, September 2010.

[66] M. Duarte and A. Sabharwal, "Full-duplex wireless communications using off-the-shelf radios: Feasibility and first results," in *Asilomar Conf. Signals Syst.*, pp. 1558–1562, 2010.

[67] L. Wei, O. Tirkkonen, P. Dharmawansa, and M. McKay, "On the exact distribution of the scaled largest eigenvalue," in *IEEE International Conference on Communications (ICC)*, Jun. 2012.

[68] Y. C. Liang, Y. Zeng, E. C. Peh, and A. T. Hoang, "Sensing-throughput tradeoff for cognitive radio networks," *IEEE Trans. Wireless Commun.*, vol. 7, pp. 1326–1337, Apr. 2008.

[69] A. Sonnenschein and P. M. Fishman, "Radiometric detection of spread-spectrum signals in noise of uncertain power," *IEEE Transactions on Aerospace and Electronic Systems*, vol. 28, pp. 654–660, Jul. 1992.

[70] W. Jouini, "Energy detection limits under log-normal approximated noise uncertainty," *IEEE Signal Process. Lett.*, vol. 18, pp. 423–426, Jul. 2011.

[71] Y. Zeng, Y. C. Liang, A. T. Hoang, and E. C. Y. Peh, "Reliability of spectrum sensing under noise and interference uncertainty," in *IEEE International Conference on Communications (ICC) Workshops*, Jun. 2009.

[72] T. Ratnarajah, R. Vaillancourt, and M. Alvo, "Eigenvalues and condition numbers of complex random matrices," *SIAM J. Matrix Anal. Appl.*, vol. 26, pp. 441–456, Jan. 2005.

[73] C. Zhong, M. R. McKay, T. Ratnarajah, and K. Wong, "Distribution of the Demmel condition number of Wishart matrices," *IEEE Trans. Commun.*, vol. 59, pp. 1309–1320, May 2011.

[74] M. Matthaiou, M. R. McKay, P. J. Smith, and J. A. Nossek, "On the condition number distribution of complex Wishart matrices," *IEEE Trans. Commun.*, vol. 58, pp. 1705–1717, Jun. 2010.

[75] L. Wei and O. Tirkkonen, "Analysis of scaled largest eigenvalue based detection for spectrum sensing," in *IEEE ICC*, pp. 1–5, Jun. 2011.

[76] K. Johansson, "Shape fluctuations and random matrices," *Commun. Math. Phys.*, vol. 209, pp. 437–476, Feb. 2000.

[77] K. L. Majumder and G. P. Bhattacharjee, "Algorithm as 64: Inverse of the incomplete beta function ratio," *Applied Statistics*, pp. 411–414, 1973.

[78] F. Haddadi, M. M. Mohammadi, M. M. Nayebi, and M. R. Aref, "Statistical performance analysis of MDL source enumeration in array processing," *IEEE Trans. Signal Process.*, vol. 58, pp. 452–457, Jan. 2010.

[79] K. M. Wong, Q. Zhang, J. P. Reilly, and P. C. Yip, "On information theoretic criteria for determining the number of signals in high resolution array," *IEEE Trans. Acoust., Speech, Signal Process.*, vol. 38, pp. 1959–1971, Nov. 1990.

[80] D. C. Oh and Y. H. Lee, "Energy detection based spectrum sensing for sensing error minimization in cognitive radio networks," *International Journal of Communication Networks and Information Security*, vol. 1, pp. 1–5, Apr. 2009.

[81] A. W. Roberts and D. E. Varberg, *Convex Functions*. Academic Press, 1974.

[82] H. J. Greenberg and W. P. Pierskalla, "A review of quasi-convex functions," *Operations Research*, vol. 19, pp. 1553–1570, Nov.-Dec. 1971.

[83] Z. Luo and W. Yu, "An introduction to convex optimization for communications and signal processing," *IEEE Journal on Selected Areas in Communications*, vol. 24, pp. 1426–1438, Aug. 2006.

[84] H. Wu, "The karushkuhntucker optimality conditions in an optimization problem with interval-valued objective function," *European Journal of Operational Research*, vol. 176, pp. 46–59, Jan. 2007.

[85] M. Grant, S. Boyd, and Y. Ye, "CVX: Matlab software for disciplined convex programming," *[online] Available: http://www.stanford.edu/ boyd/cvx*, 2009.

[86] S. Boyd and L. Vandenberghe, *Convex Optimization*. Cambridge, U.K.: Cambridge Univ. Press, seventh ed., 2004.

[87] R. Andreani, J. M. Martinez, and M. L. Schuverdt, "On second-order optimality conditions for nonlinear programming," *Optimization*, vol. 56, no. 5-6, pp. 529–542, 2007.

[88] P. Koev and A. Edelman, "The efficient evaluation of the hypergeometric function of a matrix argument," *Mathematics of Computation*, vol. 75, pp. 833–846, Jan. 2006.

[89] J. Unnikrishnan and V. V. Veeravalli, "Cooperative sensing for primary detection in cognitive radio," *IEEE J. Sel. Topics Signal Process.*, vol. 2, pp. 18–27, Feb. 2008.

[90] J. Shen, T. Jiang, S. Liu, and Z. Zhang, "Maximum channel throughput via cooperative spectrum sensing in cognitive radio networks," *IEEE Trans. Wireless Commun.*, vol. 8, pp. 5166–5175, Oct. 2009.

[91] S. Xie, Y. Liu, Y. Zhang, and R. Yu, "A parallel cooperative spectrum sensing in cognitive radio networks," *IEEE Trans. Veh. Technol.*, vol. 59, pp. 4079–4092, Oct. 2010.

[92] H. Mu and J. K. Tugnait, "Joint soft-decision cooperative spectrum sensing and power control in multiband cognitive radios," *IEEE Trans. Signal Process.*, vol. 60, pp. 5334–5346, Oct. 2012.

[93] A. Mariani, A. Giorgetti, and M. Chiani, "Test of independence for cooperative spectrum sensing with uncalibrated receivers," in *IEEE GLOBECOM*, Dec. 2012.

[94] N. Nguyen-Thanh and I. Koo, "Optimal truncated ordered sequential cooperative spectrum sening in cognitive radio," *IEEE Sensors J.*, vol. 13, pp. 4188–4195, Nov. 2013.

[95] D. Hamza, S. Assa, and G. Aniba, "Equal gain combining for cooperative spectrum sensing in cognitive radio networks," *IEEE Trans. Wireless Commun.*, vol. 13, pp. 4334–4345, Aug. 2014.

[96] T. Q. Duong, T. T. Le, and H. J. Zepernick, "Performance of cognitive radio networks with maximal ratio combining over correlated Rayleigh fading," in *IEEE International Conference on Communications and Electronics (ICCE)*, pp. 65–69, Aug. 2010.

[97] Y. Selen, H. Tullberg, and J. Kronander, "Sensor selection for cooperative spectrum sensing," in *3rd IEEE Symp. on New Frontiers in DySPAN*, Oct. 2008.

[98] M. Haenggi, "On distances in uniformly random networks," *IEEE Trans. Inf. Theory*, vol. 51, pp. 3584–3586, Oct. 2005.

[99] M. Haenggi, J. Andrews, F. Baccelli, O. Dousse, and M. Franceschetti, "Stochastic geometry and random graphs for the analysis and design of wireless networks," *IEEE J. Sel. Areas Commun.*, vol. 27, pp. 1029–1046, Sep. 2009.

[100] X. Song, C. Yin, D. Liu, and R. Zhang, "Spatial throughput characterization in cognitive radio networks with threshold-based opportunistic spectrum access," *IEEE J. Sel. Areas Commun.*, vol. 32, pp. 2190–2204, Nov. 2014.

[101] S. A. R. Zaidi, M. Ghogho, D. C. Mclernon, and A. Swami, "Achievable spatial throughput in multi-antenna cognitive underlay networks with multi-hop relaying," *IEEE J. Sel. Areas Commun.*, vol. 31, pp. 1543–1558, Aug. 2013.

[102] J. Lee, J. G. Andrews, and D. Hong, "Spectrum-sharing transmission capacity," *IEEE Trans. Wireless Commun.*, vol. 10, pp. 3053–3063, Sep. 2011.

[103] M. G. Khoshkholgh, K. Navaie, and H. Yanikomeroglu, "Outage performance of the primary service in spectrum sharing networks," *IEEE Trans. Mobile Comput.*, vol. 12, pp. 1955–1971, Oct. 2013.

[104] M. Peng, S. Yan, and H. V. Poor, "Ergodic capacity analysis of remote radio head associations in cloud radio access networks," *IEEE Wireless Commun. Lett.*, vol. 3, pp. 365–368, Aug. 2014.

[105] C. Lee and M. Haenggi, "Interference and outage in Poisson cognitive networks," *IEEE Trans. Wireless Commun.*, vol. 11, pp. 1392–1401, Apr. 2012.

[106] L. T. Tan and L. B. Le, "Joint cooperative spectrum sensing and MAC protocol design for multi-channel cognitive radio networks," *EURASIP J. Wirel. Commun. Netw.*, vol. 2014, Dec. 2014.

[107] R. Zhang and Y. C. Liang, "Exploiting multi-antennas for opportunistic spectrum sharing in cognitive radio networks," *IEEE J. Sel. Topics Signal Process.*, vol. 2, pp. 88–102, Feb. 2008.

[108] Z. Quan, S. Cui, A. Sayed, and H. V. Poor, "Optimal multiband joint detection for spectrum sensing in cognitive radio network," *IEEE Trans. Signal Process.*, vol. 57, pp. 1128–1140, Mar. 2009.

[109] F. Li and Z. Xu, "Sparse bayesian hierarchical prior modeling based cooperative spectrum sensing in wideband cognitive radio networks," *IEEE Signal Process. Lett.*, vol. 21, pp. 586–590, May 2014.

[110] R. Zhang, T. J. Lim, Y. C. Liang, and Y. Zeng, "Multi-antenna based spectrum sensing for cognitive radios: A GLRT approach," *IEEE Trans. Commun.*, vol. 58, pp. 84–88, Jan. 2010.

[111] D. Stoyan, W. Kendall, and J. Mecke, eds., *Stochastic Geometry and Its Applications, 2nd Edition*. John Wiley and Sons, 1996.

[112] A. Sahai and D. Cabric, "A tutorial on spectrum sensing: Fundamental limits and practical challenges," in *IEEE Symp. New Frontiers DySPAN*, Nov. 2005.

[113] C. R. Stevenson, C. Cordeiro, E. Sofer, and G. Chouinard, "IEEE P802.22 wireless RANs functional requirements for the 802.22 WRAN standard doc.:IEEE 802.22-05/0007r46," *WK3C Wireless LLC*, pp. 1–49, Sep. 2005.

[114] S. Chaudhari, J. Lunden, V. Koivunen, and H. V. Poor, "Cooperative sensing with imperfect reporting channels: Hard decisions or soft decisions?," *IEEE Trans. Signal Process.*, vol. 60, pp. 18–28, Jan. 2012.

[115] I. S. Gradshteyn and I. M. Ryzhik, *Table of integrals, series, and products*. New York, USA: Academic Press, seventh ed., 2007.

[116] M. Kiessling and J. Speidel, "Mutual information of MIMO channels in correlated Rayleigh fading environments−a general solution," in *IEEE ICC*, June 2004.

[117] A. S. *et al.*, "In-band full-duplex wireless: Challenges and opportunities," *IEEE J. Sel. Areas Commun.*, vol. 32, pp. 1637–1652, September 2014.

[118] Y. He, T. Ratnarajah, E. H. G. Yousif, J. Xue, and M. Sellathurai, "Performance analysis of multi-antenna GLRT-based spectrum sensing for cognitive radio," *Signal Processing*, vol. 120, pp. 580–593, March 2016.

[119] J. Heo, H. Ju, S. Park, E. Kim, and D. Hong, "Simultaneous sensing and transmission in cognitive radio," *IEEE Trans. Wireless Commun.*, vol. 13, pp. 1948–1959, April 2014.

[120] T. Riihonen and R. Wichman, "Energy detection in full-duplex cognitive radios under residual self-interference," in *IEEE CROWNCOM*, June 2014.

[121] S. Huang, X. Liu, and Z. Ding, "Opportunistic spectrum access in cognitive radio networks," in *IEEE INFOCOM*, Apr. 2008.

[122] F. C. Commission, "Enabling innovative small cell use in 3.5GHz band," *Notice of Proposed Rulemaking and Order*, Dec. 2012.

[123] E. H. G. Yousif, M. C. Filippou, F. Khan, T. Ratnarajah, and M. Sellathurai, "A new LSA-based approach for spectral coexistence of MIMO radar and wireless communications systems," in *IEEE ICC*, May 2016.

[124] C. Shannon, "A mathematical theory of communication," *Bell System Technical Journal*, vol. 27, pp. 379–423,623–656, Oct. 1948.

[125] J. Guo, S. Durrani, X. Zhou, and H. Yanikomeroglu, "Outage probability of ad hoc networks with wireless information and power transfer," *IEEE Wireless Communications Letters*, vol. 4, pp. 409–412, Aug. 2015.

[126] G. Nigam, P. Minero, and M. Haenggi, "Coordinated multipoint in heterogeneous networks: A stochastic geometry approach," in *IEEE Globecom Workshops (GC Wkshps)*, Dec. 2013.

[127] D. Dominici, "Nested derivatives: a simple method for computing series expansions of inverse functions," *International Journal of Mathematics and Mathematical Sciences*, vol. 2003, pp. 3699–3751, Mar. 2003.